Studies of Laser Brazing with Regard to the Quality Influencing Parameters

by

Sabrina Ernst

A Doctoral Thesis

Submitted in partial fulfilment of the requirements for the award of Doctor of Philosophy of Loughborough University

March 2015

Acknowledgements

At first I would like to thank Prof. Dr. Robert Parkin and Prof. Dr. Michael R. Jackson for the opportunity to do my PhD project as well as for the support and feedback throughout the project.
Furthermore I would like to thank Prof. Dr. Horst Kreitlow for the inspiration to this project and for the help and guidance through all these years. It was a pleasure working for and with him.
I also would like to thank Dr.-Ing. Thomas Schüning for his support and the opportunity to use the diode laser at the Technologiepool GmbH.
My thanks also go to Arnold Terviel, who helped me with the mechanical constructions.
I would also like to thank my friends, especially, Tine for the nights of getting to know Word 2003 in detail, Isabella for the nights of taking thousands of pictures of brazed joints together, Nils for giving me support and making me delicious meals, Silvia for just being her and the good times we had together in Emden, Mareike -my pillar of strength- and David for the nice and technical chats during the past years and for teaching me how to use adverbs correctly.

Last but not least, I offer my greatest gratitude to **my family** - not only bond by blood but just by love - for their constant love and support.

Abstract

Laser joining processes, such as brazing and welding, are a common application in industry, especially in the automotive industry. These processes are the key to lightweight and efficient design with regard to the automotive industry. There, laser brazing is used mainly for visible joints due to the superior paint adhesion and surface roughness of brazed joints compared to welds. As laser brazing is applied in the automotive industry without using any fluxes or shielding gas, this leads to a difficulty in maintaining and ensuring the quality of brazed joints.

As the quality influencing parameters have not been thoroughly investigated so far, studies of laser brazing are needed to identify and understand the parameters that have an influence on the brazing result. Not only the influence on the brazing result is important to understand, but also the way these parameters interact and are dependent on each other.

Within this work, the parameters that have an influence on the brazing result are identified. They are subdivided into material characteristics, laser and process parameters. Moreover, their interactions and dependencies are shown based on the investigations made during the parameter studies. These parameter studies were carried out by using a Nd:YAG as well as a diode laser.

Furthermore, two key aspects are presented, which are important in order to obtain good quality joints. The first key aspect is the understanding of the importance of the correct wire positioning to the brazing process. The second aspect is the need for a pre-heating phase prior to brazing as well as its successful implementation to achieve a suitable operating temperature at the beginning of the brazing process. These key aspects are demonstrated and verified within this work, which represent the novelty of this thesis.

Keywords: Laser brazing, Nd:YAG, diode laser, pre-heating, wire positioning, laser parameters, process parameters

Contents

List of Figures

List of Tables

Glossary of terms

Symbol	Meaning	Units
α	Coefficient of linear expansion	K^{-1}
β	Image scaling ratio	
γ_H	Adhesion energy	$\frac{J}{m^2}$
γ_L	Liquid surface free energy	$\frac{J}{m^2}$
γ_{SL}	Solid/ Liquid interfacial free energy	$\frac{J}{m^2}$
γ_S	Solid surface free energy	$\frac{J}{m^2}$
κ	Imaginary part of the refractive index / extinction coefficient	
λ	Wavelength	m
ρ	Density	$\frac{kg}{m^3}$
σ_{el}	Electron conductivity	$\frac{A}{Vm}$
Θ	Full-width far-field divergence	rad
θ	Contact angle	$^\circ$
θ	Divergence	rad
ε	Emissivity	
ε_T	Thermal expansion strain	
2A	Spread diameter	μm
A	Absorption	
A_{strain}	Ultimate strain	%

c	Specific heat capacity	$\frac{J}{gK}$
c_p	Specific heat capacity at constant pressure	$\frac{J}{gK}$
c_v	Specific heat capacity at constant volume	$\frac{J}{gK}$
D	Alloy zone	μm
d	Spot size	m
d_0	Beam waist	m
D_{base}	Diffusion zone in base material	μm
$D_{brazingwire}$	Diffusion zone in brazing wire	μm
d_{gap}	Gap width	mm
d_k	Core diameter of fibre	m
$d_{Vickers}$	Arithmetic mean of the two diagonals of the indentation	μm
d_{x0} / d_{y0}	Beam waist in respective direction	m
d_x / d_y	Spot size in respective direction	m
F	Focal position	m
f_c	Focal length of the collimating lens	m
f_f	Focal length of the focussing lens	m
h	Height of the spherical cap	μm
h_c	Ceiling	m
H_m	Enthalpy of fusion	$\frac{J}{kg}$
I	Intensity	$\frac{W}{m^2}$
K	Heat conductivity	$\frac{W}{mK}$
k	Conductibility of temperature	$\frac{m^2}{s}$
l	Length	mm
m	Mass of material	kg
M^2	Beam propagation factor	
n	Real part of the refractive index	
P	Peak power	W

P_{abs}	Absorbed laser power	W
P_{av}	Average laser power	W
p_c	Capillary filling pressure	P
Q	Amount of heat gained or lost by material	J
Q_m	Heat of fusion	$\frac{J}{g}$
Q_v	Heat of vaporisation	$\frac{J}{g}$
R	Radius of the spherical cap	μm
R	Reflectivity	
r	Radius	m
R_a	Average surface finish	μm
R_e	Yield stress	$\frac{N}{mm^2}$
R_m	Tensile strength	$\frac{N}{mm^2}$
R_z	Average surface roughness	μm
T	Temperature	K
T	Transmittance	
T_m	Melting temperature, liquidus temperature	K
t_p	pulse length	ms
T_v	Evaporating temperature	$^\circ$C
v	Feed speed of base material	$\frac{m}{s}$
v_b	Feed speed of the brazing wire	$\frac{m}{s}$
WZD	Delay time	ms
WZL	Delay time	ms
z_R	Rayleigh length	m
$\vec{q}$	Heat flow density	$\frac{W}{m^2}$

Constants / Material constants

α_{steel}	Coeff. of linear expansion for steel at 25°C	$11 * 10^{-6}\ K^{-1}$

Acronyms

ALO	Adaptive Laser Optic	37
BPNN	Back Propagation Neural Network	32
BPP	Beam Parameter Product	14
CNC	Computerised Numerical Control	65
CO_2	Carbon dioxide	21
$CuSi_3$	Copper Silicon	23
cw	Continuous Wave	6
DPSSL	Diode Pumped Solid State Laser	19
FPGA	Field-Programmable Gate Array	37
FEM	Finite Element Method	181
GA	Genetic Algorithm	32
GMR	Giant Magneto-Resistance	36
HAZ	Heat Affected Zone	156
HB	Brinell hardness	75
HPDL	High Power Diode Laser	6
HV	Vickers Hardness	59
LPSSL	Lamp Pumped Solid State Laser	19
MIG	Metal Inert Gas	36
MPI	Message Passing Interphase	33
N_2	Nitrogen	128
Nd	Neodymium	6
NDT	Non-Destructive Testing	34
Q-Switch	Quality-switching	7
SEM	Scanning Electron Microscope	xi
SMD	Surface Mounted Devices	28
TE	Transverse Electric	12
TM	Transverse Magnetic	12

UT	Ultrasonic Testing	35
VCSEL	Vertical Cavity Surface Emitting Laser	11
YAG	Yttrium - Aluminium - Garnet	6
Zn	Zinc	23

Chapter 1.

Introduction

1.1. Project motivation and research objective

Laser joining processes, such as brazing and welding, are a common application in industry, especially in the automotive industry. These processes can be seen as the key to lightweight and efficient design (Graudenz and Heitmanek, 2012). Focusing on the process of laser brazing, it has a significant advantage compared to laser welding, as it is capable of joining mating materials that could not be joined by laser welding (Jacobson and Humpston, 2005). Furthermore, laser brazing is used especially for visible joints, as their surface condition is superior compared to the ones of laser welding with regard to paint adhesion and surface roughness (Hornig, 2000).

Figure 1.1.: Laser brazing applied to a zero-gap roof joint of a car (Graudenz and Heitmanek, 2012)

Transferring this aspect to the automotive industry, it can be seen in Figure 1.1 that laser brazing is applied to a zero-gap roof joint (Graudenz and Heitmanek, 2012). Furthermore, it is used for brazing a hatch car body shell (Hornig, 2000).
To ensure and maintain the quality of brazed joints is important. In automotive industry, laser brazing is carried out without using any fluxes and shielding gas. This aspect has a difficulty with regard to ensuring and maintaining the quality. Furthermore, the parameters that have an influence on the brazing result have not been thoroughly investigated so far. Research is still ongoing in order to ensure and maintain the quality of brazed joints.
For this reason, studies of laser brazing are needed to understand the parameters that have an influence on the brazing result and how they interact or are dependent on each other.
Within this thesis, parameters are identified that have an influence on the brazing result. These parameters are subdivided into laser, process parameters as well as material characteristics. Furthermore parameter studies are carried out with the common laser types used for brazing in the automotive industry: Nd:YAG and diode (Graudenz and Heitmanek, 2012).
The results of the parameter studies show the dependencies of parameters as well as their respective interactions. Moreover, this research demonstrates the importance of wire positioning as a key to good quality brazed joints. Another key aspect, presented in this thesis, is the successful implementation of a pre-heating phase prior to the actual laser brazing process. Good quality brazed joints are achieved due to this implementation of pre-heating.

1.2. Thesis outline

This thesis is subdivided into 9 chapters. In the following, a brief overview is given with regard to the chapters and their respective content.

Chapter 1 comprises the research motivation as well as the research scope of this thesis.

Chapter 2 gives an introduction to the lasers used within this research (Nd:YAG, diode) with regard to their working principle and their specific characteristics. Furthermore, it is an introduction to laser material processing in general with a specific emphasis on the laser joining process, laser brazing. Subsequently, an overview of the respective quality control methods is presented and exemplified on a respective area of application.

Chapter 3 identifies the parameters that have an influence on the brazing result. These parameters are subdivided into laser, process parameters and material characteristics. These parameters and their effect to the brazing result are described. Subsequently, quality measures are introduced for brazed joints as well as respective examination techniques.

Chapter 4 presents the experimental procedures and initial tests carried out. First, the design and implementation of the laser brazing setup including the required measurement equipment for temperature and wire feed are presented. Then the materials and their preparation used throughout this research are introduced. This is followed by the initial experiments carried out with the Nd:YAG laser. The observation made during these experiments highlight the aspects that are further investigated within the parameter studies. The two most significant aspects observed are pre-heating and wire positioning, as they seem to be essential in order to obtain a good quality brazed joint. Finally, a quality control system based on a laser triangulation sensor is presented for the Nd:YAG laser that is capable of measuring possible deformation over the length of the brazed joint.

Chapter 5 investigates the aspects by using the Nd:YAG laser. These aspects were identified during the initial experiments carried out, as they seem to have an influence on the brazing result. Within these parameter studies, carried out with the Nd:YAG laser, the aspects wire positioning itself as well as within the laser spot and the characteristics of disappearing gap width and deformation are further investigated. Furthermore, the influence of the repetition rate (f) to the surface condition of brazed joints is investigated.

Chapter 6 presents the parameter studies carried out with the diode laser. Within these parameter studies, the aspect of wire positioning is also investigated, since the beam profile of the diode laser differs from the Nd:YAG laser. As opinions deviate in literature with regard to the ratio of feed speeds for the same joint geometry, this aspect is further investigated with and without using shielding gas with regard to the quality of brazed joints. Furthermore, the successful implementation of a pre-heating phase is demonstrated and their influence to the brazing result is presented. Subsequently, the change in heat input to the brazing result is investigated. Moreover, quality investigations were carried out with regard to Vickers hardness, tensile testing and alloy zone formation.

Chapter 7 discusses the results obtained in chapter 5 and 6.

Chapter 8 summarises the investigations and concludes the research carried out.

Chapter 9 contains suggestions for future work.

Chapter 2.

Literature review

This chapter gives an overview of the state-of-the-art concerning the fields of this research. First, the lasers, Nd:YAG and diode, are introduced with regard to their working principle and characteristics. As these types of laser are commonly for material processing, especially for laser brazing, and therefore for this research. Subsequently, both laser sources are compared with each other concerning their efficiency, design, operational costs, beam characteristics and their areas of application.
Afterwards, the broader range of laser material processing is introduced. It is particularly focussed on the laser processes: laser soldering and brazing, since laser brazing is part of this research. These processes are defined and the conventional methods for these joining processes and their applications are named. Subsequently, the application areas of laser soldering and brazing are presented.
Quality control is of major concern in industry. Therefore several methods of quality control regarding the joining processes, especially laser brazing, are presented. These methods are subdivided into destructive and non-destructive testing methods, which are named and their area of application is explained. The explanations are concentrated on the non-destructive testing methods.

2.1. Lasers used for material processing

Several types of lasers exist that are used for material processing. For this research Nd:YAG lasers and High Power Diode Laser (HPDL) are used and therefore the emphasis is on these laser types. In the following subsections their respective working principles and characteristics are explained. Subsequently, both laser types are compared with each other concerning their efficiency, design, operational costs, beam characteristics as well as their areas of application.

2.1.1. Nd:YAG lasers

Within this section the working principle of Nd:YAG lasers, their different modes of operation, types of construction as well as their beam characteristics are going to be introduced and explained.

2.1.1.1. Working principle of Nd:YAG lasers

The Nd:YAG laser, which was first demonstrated by Geusic in 1964 (Geusic et al., 1964), belongs to the group of solid state lasers, as its laser active medium is a crystalline substrate. The substrate is the laser host doped with ions. This represents the actual laser medium. In the case of the Nd:YAG laser, the gain medium is made of Yttrium - Aluminium - Garnet (YAG), which is doped with Neodymium (Nd) ions. This combination, next to many others, has established itself for industrial laser applications.
As summarised by Poprawe the Nd:YAG medium is pumped optically, i.e. the excitation of the Neodymium ions occurs due to absorption of optical radiation in the energy bands. The emission of the typical wavelength of 1064 nm takes place, due to the electronic transition of the Nd ions from the upper laser level to the lower laser level (Poprawe, 2005).

2.1.1.2. Modes of operation

As outlined by Poprawe solid state lasers can be differentiated between their method of optical excitation (lamps, diode laser) and the geometrics of the laser active medium (rod, disk, slab, fibre) (Poprawe, 2005).
Furthermore, the mode of operation can either be Continuous Wave (cw) or pulsed. For the latter mode of operation two opportunities exist as Poprawe outlines. The first one is gain switching. There the optical pumping source is operated in pulsed mode.

The resulting laser pulses then follow the characteristic of the pumping pulse and have a pulse length from 50 μs up to 2000 μs with repetition rates of 4 kHz. The other opportunity is Quality-switching (Q-Switch), where shorter pulses with pulse lengths from 10 ns up to 500 ns with repetition rates of 100 kHz can be achieved (Poprawe, 2005).

2.1.1.3. Types of construction

As summarised by Poprawe one type of construction is a lamp pumped system, which is shown in 2.1. There, rod - shaped Nd:YAG crystals are used that have a typical diameter of 2 - 8 mm and are between 20 and 200 mm in length. The lamp(s) as well as the crystal is arranged in such a way that each is in one focal point of an elliptical shaped reflector. If more elliptical reflectors are used, e.g. two, then the crystal is positioned at the overlapping focal point of both elliptical reflectors (Figure 2.1). The lamps as well as the laser rod are placed into flow tubes for cooling, where deionised water is used as a coolant (Figure 2.1) (Poprawe, 2005).

Figure 2.1.: Cross-section of the cavity of a lamp pumped laser rod (Poprawe, 2005)

The optical axis of this type of construction is perpendicular to the polished, circular end facets (Figure 2.1). For this reason, such an arrangement is called transversally pumped.

According to Poprawe lamp pumped systems are industrially available with output powers from 50 W up to 800 W per laser rod which have a beam quality from M^2 = 15 up to M^2 = 150. Cascading the laser rods can achieve an efficient increase in output power up to 4 kW with a beam quality of M^2 = 70. For gain-switching, gas discharge flash lamps are used. They have typical average powers from 20 W up to 500 W. The

achievable pulse peak powers are in the range of 5 - 20 kW (Poprawe, 2005).
As summarised by Poprawe and Koechner gas discharge lamps have a very wide spectrum compared to the small absorption line of the Nd:YAG laser at 808 nm. Therefore, the pump efficiency of those gas discharge lamps is marginal. To avoid this disadvantage, AlGaAs diode lasers can be used as the pump source, due to the fact that their wavelength can be matched with the absorption line of the Nd:YAG crystal. In addition, they have the advantage of better optical formability and adaptation to the geometry of the crystal. For this reason, the achievable electrical - optical efficiencies range from 10 % to 25 %. Longitudinal and transversal pump adjustments are realised for rod - shaped Nd:YAG crystals (Figure 2.2) (Poprawe, 2005, Koechner, 1988).

Figure 2.2.: a) Longitudinal pumped laser rod; b) Transversal pumped laser rod (Poprawe, 2005)

At the longitudinal pumping, the laser rod is pumped through a polished circular surface behind a dichroic mirror (Figure 2.2 a). Such an approach enables fundamental mode laser (M^2= 1) with up to 20 W output power. Transversal diode pumped Nd:YAG lasers (Figure 2.2 b) that operate in cw mode are commercially available up to 6 kW through cascading of laser rods. Such systems have less heat loss and therefore, the thermal lens has significantly fewer aberrations, which results in a beam quality that is twice as good (M^2= 35) compared to identical lamp pumped systems. By operating these transversal diode pumped Nd:YAG laser systems in Q-switch mode, pulse peak powers of 10 MW with pulse repetition rates of 100 kHz can be reached according to Poprawe and Koechner (Poprawe, 2005, Koechner, 1988).

For further improvement of the beam quality of diode pumped lasers, three other concepts exist with different geometries of the laser active medium. These concepts aim for an improved cooling and consequently reduced aberrations and higher applicable pumping power densities. These concepts are called InnoSlab
(Du et al., 20. / 21. September 2007), Disk (Speiser, 2008) and Fibre laser (Speiser, 2008, Koester and Snitzer, 1964, Stone and Burrus, 1974, Melles Griot, 2005, Samson et al., 2008).
According to Poprawe and Koechner all systems mentioned above are available from 10 W up to several kilowatts with beam qualities of $M^2 = 1$ to $M^2 < 35$ depending on output power and concept (Figure 2.3) (Poprawe, 2005, Koechner, 1988).
More information regarding these concepts mentioned above can be found in respective literature stated above, which is offered in the references of this work.

Figure 2.3.: Comparison of concepts: InnoSlab, Disk, Fibre and laser rod laser (Poprawe, 2005)

2.1.1.4. Characteristics of Nd:YAG lasers

For characterising propagation of radiation, especially laser radiation, the Gaussian beam is used, which is a solution of the paraxial approximated Helmholtz - equation. The Helmholtz - equation represents the time - independent form of the wave equation, derived by applying the technique of separation of variables, in order to reduce

the complexity of analysis according to Bahaa and McQuarrie (Bahaa E. A. et al., 1991, McQuarrie, 2003). Siegman states that the usage of the Gaussian beam is approximately valid for angles of beam less than 30° (Siegman, 1986). For this reason, it can be used for Nd:YAG lasers due to having a divergence of less than 30°.
As summarised by Meschede and Hecht it is determined by its transversal and longitudinal profile, which is characterized by the Gaussian distribution and the latter by the Lorentz - profile (Meschede, 2005, Hecht, 2005).For further information on this subject, please refer to the literature which can be found in the references of this work.

2.1.2. Diode lasers

In this section the working principle, the development over the decades, its characteristics as well as construction principles of High Power Diode Laser (HPDL) is explained.

2.1.2.1. Working principle of diode lasers and their evolution

As summarised by Eichler, materials used for the production of diode lasers are based on semiconductors of group III-V compounds. By combining different semiconductor materials a small junction (p-n junction) develops. To achieve the necessary population inversion for stimulated emission, the p-n junctions are forward-biased. In doing so, electron transitions from the valency to the conduction band of doped semiconductors take place. When electrons of the conduction band recombine with the holes of the valency band a spontaneous and stimulated emission occurs. The emitted wavelength depends on the valence-conduction band gap. The condition for the emission of laser radiation is fulfilled, if the losses of photons, due to absorption and emission out of the active zone, are less than the increase of photons due to stimulated emission. In order to achieve this, a proper resonator is needed, which is formed by the two opposite facets of the semiconductor itself (Eichler and Eichler, 1998) - forming a Fabry-Perot lasing cavity (Lin, 2000), for amplification. Furthermore, as another condition for laser emission, the current source has to inject sufficient charge carriers into the p - n junction. This necessary current is called the threshold current.
In 1962, the first diode laser consisting of the semiconductor gallium arsenide (GaAs) with a homogeneous structure was demonstrated by Nathan et al.
(Nathan et al., 1962, Holonyak and Bevacqua, 1962). Such developed diode lasers could only be operated in pulsed mode at room temperature due to their homogeneous structure. Hall et al. realised an operation of diode lasers in cw mode by cooling

them down to low temperatures (77 K) (Hall et al., 1962).
In 1970, diodes with hetero structures were developed. They consist of a multilayered body of different semiconductor materials. Transferring this knowledge into action for diode lasers, the threshold current density was significantly reduced for laser mode and for this reason a cw-mode at room temperature was realised by Hayashi et al. (Hayashi et al., 1970, Doeldisson, 1999).
This invention was the precondition for the technical application of diode lasers and at the same time the starting point for a fast development in the field of diode lasers. Wide wavelength spectra were realised against the used semiconductor material from 400 nm (GaN; GaInN) up to 30 μm (lead salts laser). As summarised by Eichler and Doeldisson different kinds of structural shapes were realised such as edge emitting laser diodes (Dual hetero diode) or surface emitting diode lasers that are called Vertical Cavity Surface Emitting Lasers (VCSELs) (Eichler and Eichler, 1998, Doeldisson, 1999). This resulted in many areas of application for diode lasers with low output power, particularly in the field of telecommunication engineering and consumer goods industry (CD - player). Explaining the different structural shapes of diode lasers as well as their working principles, which were developed over the past 40 years, was renounced due to not extending this work. For more detailed information about this subject, please use the following literature (Eichler and Eichler, 1998, Winstel and Weyrich, 1981, Cheo, 1989, Koechner, 1988, Hiller, 1990, Schneider, 1988, Haag, 2000) which can be found in the references of this work.
The application of diode lasers in material processing started at the end of 1970s with the development of arrays of diodes, which permitted output powers in the range of Watts. These have wavelengths between 800 nm and 940 nm and that makes them suitable for the pumping of solid state lasers, since the different laser crystals have an absorption maximum within this wavelength range. The first experiments with diode pumped solid state lasers were published in the 1960sas summarised by Schneider (Schneider, 1988).
In the aftermath, the output power of those diode arrays was increased significantly and many research activities were carried out in the 1980s. But direct applications of High Power Diode Laser (HPDL)s in material processing were not reported until the beginning of the 1990s as outlined by Krause et al. (Krause and Treusch, 1992, Krause et al., 1992, Toenshoff et al., 1993).

2.1.2.2. Characteristics of diode lasers

One of the characteristics of a diode laser is the linear dependence of the output power on the driving current above the lasing threshold. Due to power loss, the diode laser self-heats which results in a change of the temperature dependent diode laser parameters as summarised by Poprawe (Poprawe, 2005). One of these parameters is the emitted wavelength. Furthermore, it is dependent on the band gap energy, the cavity length and the refractive index of the semiconductor material used. For this reason, it is material, temperature and driving current dependent. The wavelength of a diode laser can be tuned via temperature control (up to 0.4 nm / °C) (Melles Griot, 1996). Wavelength changes can also occur by varying the laser power via the driving current. For instance, the wavelength typically changes 0.025 nm / mA for AlGaAs lasers (Melles Griot, 1996).

Another characteristic is the large beam divergence due to diffraction of the emitted radiation at the narrow p-n junction region (typically 1 - 3 μm). The half angle of the beam divergence can be up to 45° perpendicular to the p-n junction (fast axis) (Das, 1991) and 2.5 - 6 times less parallel to the p-n junction (slow axis) (Haag et al., 1997) due to the non-circular cross section of the active zone.

For this reason, the emitted radiation is very asymmetrical. This results in astigmatism, i.e. the radiation in the two perpendicular directions does not come from one waist location (Lin, 2000).

This asymmetry also leads to an unequal beam quality of the axis, since the slow axis is very multimodal compared to the fast axis (Dueckminor and Frede, 2006). The fast axis has a maximum beam quality of $M^2 = 1$ due to the small height of the active zone, whereas the slow axis only achieves a poor beam quality, compared to the fast axis, of $M^2 = 20 - 30$. As outlined by Poprawe, this is due to the large width of the active zone (typically 100 - 200 μm) in relation to the emitted wavelength and non-linear effects within the diode laser itself (Poprawe, 2005). Furthermore, it needs to be mentioned that the emitted beam of a diode laser is linearly polarised, either Transverse Electric (TE), i.e. the electric field polarisation vector is parallel to the x-axis (plane of the diode junction), or Transverse Magnetic (TM), which means that the electric field vector is perpendicular to the x - axis (plane of the diode junction) and the magnetic field vector is parallel to it (Apter, 2005).

Due to the missing conversion from electrical to optical pumping power compared to solid state lasers, diode lasers achieve higher electrical - optical efficiency of about

$< 50\,\%$ as summarised by Poprawe (Poprawe, 2005).

2.1.2.3. High power diode laser systems

The achievable output power of a single emitting diode laser is limited due to the damage threshold of the end-facets forming the resonator. Depending on the material, the damage threshold can be up to $18\,MW / cm^2$ (Erbert, 14./15. September 2000). The output power can be increased through optimal cooling, e.g. microchannel coolers (Beach and et. al., 1992, Krause and et. al., 1994, Goodson et al., 1997), and widening of the emitting surface of the active zone. However, Poprawe outlines that only a maximum of a few Watts of output power can be reached. Therefore, the output power of a single diode laser is in general not sufficient for a reasonable use in laser material processing. For this reason, between 10 and 60 single emitters (laser diodes) are arranged in a line on a common substrate with a little gap between each of them. Such an arrangement is called 1D- diode array (diode bar). Its dimensions are typically $140\,\mu m$ thick (single emitter), about 1 mm deep and 10 mm wide (Figure 2.4) (Poprawe, 2005). An important factor concerning diode bars is the fill factor.

Figure 2.4.: Schematic diagram of a diode bar (adapted from (Poprawe, 2005))

It corresponds to the percentage of the bar that is covered by emitters and equals the width of one emitter divided by the center-to-center spacing between emitters. For instance, a typical bar might have 19 emitters, each 150 μm wide with a center-to-center spacing of 500 μm. These dimensions result in a fill factor of 30 %. Depending on the cooling mechanism, output powers of up to 40 W cw (conduction cooled) with a fill factor of 30 % (Apter, 2005, Osram Opto Semiconductors GmbH, 2007) as well as water - cooled versions with output powers of 100 W accw with a fill factor of 80 % are commercially available (Apter, 2005).

The emitted beam of a laser diode bar is the result of the incoherent interference of the multiple beamlets of all single emitters. This results in a significant decrease in beam quality as well as in a very asymmetric beam profile (Loosen et al., 1997).

Although the beamlet of a single emitter is almost diffraction-limited, the beam quality parallel to the emitter line decreases as the laser power increases, i. e. the Beam Parameter Product (BPP) increases to the n-times value of a single emitter (n: Number of single emitters). Hence, both axis of the beam have a very different beam quality, where the fast axis has a beam quality of $M^2 = 1$ and the slow axis one of $M^2 > 1{,}000$ (Loosen et al., 1997). A typical beam profile of a laser diode bar is shown in Figure 2.5. The slow axis (right, Figure 2.5) has a similar profile as a top - hat due to the lateral expansion of the emitter line and the interference of the beamlets of the single emitters, whereas the fast axis (left, Figure 2.5) has a Gaussian profile. These

Figure 2.5.: Typical beam profile of a laser diode bar: in direction of fast axis (left) and slow axis (right) (Poprawe, 2005)

beam characteristics require a special collimation. For direct application a fast axis collimation is required, especially to prevent a decrease in beam quality for material processing. This can be realized via optical elements, such as a micro cylindrical lens, with a very small focal length. The optical properties of the fast axis collimation have a huge influence on the achievable beam quality and therefore of the possible beam waist (Loosen et al., 1995). The positioning accuracy of the used optical elements is also very important as research studies show (Haag, 2000, Loosen et al., 1997).
After fast axis collimation, the divergence of the laser diode bar is reduced to 5 - 10 mrad (Dorsch et al.). The propagation along the slow axis is not influenced. However, in most applications an almost rotation - symmetric beam is required. For this special beam shaping optics are needed, such as a stairs - mirror (Poprawe, 2005).
The beam characteristics of laser diode bars are not only influenced by the dimensions of the single emitters, but also by the production process. Due to the production process the near field of the emitters is non-linear, the so-called "smile" - effect. This effect occurs as a result of a mismatch of thermal expansions coefficients of the used materials within production, which leads to a curvature in the laser diode bar , e.g. a convex or concave curvature ("smile" or "cry" respectively) (Jingwei Wang et al., 2009).
Jingwei Wang et al. showed that the "smile" - effect can be reduced for GaAs based laser bars if different materials for die bonding are used e.g. gold - tin alloy instead of Indium, since the mismatch of the thermal expansion coefficients is less compared to Indium - GaAs. Due to exchanging the mentioned materials for this packaging process they showed that the smile can be reduced from $< 1\,\mu m$ to less than $0.2\,\mu m$ (Jingwei Wang et al., 2009).
Furthermore, they demonstrated that the smile can be reduced by increasing the thickness of the sub-mount heatsink as well as by using different materials for the pick-up tools that are used within the die bonding process, e.g. using tungsten instead of stainless steel (Jingwei Wang et al., 2009).
Except for the single emitter, the laser diode bar is the basic module for high power diode lasers used in material processing. In the following section, different technical realisations for a further increase in output power are introduced.

Technical realisations for increasing output power of HPDLs

Stacking

Several diode bars that are each mounted onto a heat sink are densely arranged either next to or on top of each other. As outlined by Poprawe, such an arrangement is called diode laser stack. Typically stacks consist of up to 15 diode laser bars, but as a matter of principle larger quantities can be utilised. Thus, the output power is scaled to the number of diode laser bars in a stack. By doing so, the beam quality decreases with the increase of output power due to enlargement of the emitting surface (Poprawe, 2005).

Polarisation coupling

Due to the fact that the emitted diode laser bar / stack radiation is linearly polarised, it can be interfered with the emitted radiation of another diode laser bar / stack via a polarisation beam splitter, as summarised by Poprawe. By doing so, the emitted output power is almost doubled without any loss in beam quality (Poprawe, 2005).

Wavelength coupling

Wavelengths of different diode laser bars / stacks can be interfered with each other via wavelength selective mirrors or similar methods. Technically an interference of four wavelengths can be realised. Therefore, the emitted output power can almost be quadrupled without any loss in beam quality, as outlined by Poprawe
(Poprawe, 2005). It has to be mentioned that power losses as well as reduction of the beam quality occur at the technical realisation of the polarisation or wavelength coupling due to additional optical components. For this reason, the given factors should be regarded as theoretical limiting values (Poprawe, 2005).

With the techniques described above, high power diode laser systems have been realised.

2.1.3. Comparison of Nd:YAG with high power diode lasers

Within this section Nd:YAG lasers are compared to the high power diode lasers regarding design, efficiency, operational costs, beam characteristics and its areas of application.

2.1.3.1. Design, efficiency and operational costs

When comparing the designs of both lasers with each other, it is obvious that an HPDL unit with cooling is much more compact than an Nd:YAG laser unit. Due to this, it is possible to have portable HPDLs.
Furthermore, lamp pumped Nd:YAG lasers have high losses in electrical to optical conversion. This is caused by the wide spectral range emitted by the lamps and the small absorption line of the Nd:YAG crystal (see section 2.1.1.3) (Poprawe, 2005). For this reason, the efficiency of lamp pumped Nd:YAG lasers is very low (about 1 - 5 %). Even if they are diode pumped, only a small increase in efficiency can be realised of about 8 - 12 %. However, efficiency is almost doubled compared to the lamp pumped ones. Nevertheless, HPDLs have higher electrical to optical conversion efficiency than Nd:YAG lasers due to the missing losses caused by optical pumping. Therefore, HPDLs can reach efficiencies from 20 % up to 50 % (Lin, 2000, WEKA FACHMEDIEN GmbH, 2009).
Another factor that has to be regarded is the maintenance intervals of both units and therefore their service life. Lamp pumped Nd:YAG lasers have to be maintained every few hundred hours (approx. 800 h) due to replacing lamps, whereas diode pumped Nd:YAG lasers as well as HPDLs can be described as almost maintenance free, because of their long service life of about 10,000 h. The service life is very much dependent on degradation in conjunction with output power and thermal loss with respect to temperature, i.e. the respective output power has an influence on the amount of thermal loss of HPDLs, which in turn influences the temperature and the degradation is again dependent on temperature (Lin, 2000, WEKA FACHMEDIEN GmbH, 2009).
Regarding all the factors mentioned above, it is obvious that the operational costs of HPDLs are less than those of the Nd:YAG lasers in respect of electrical to optical efficiency (Haag, 2000).
HPDLs are commercially available with output powers of up to 10 kW cw (Laserline GmbH, 2009) and lamp pumped Nd:YAG lasers with output powers of up to 4.4 kW cw (TRUMPF GmbH + Co. KG (Holding), 2009).

2.1.3.2. Beam characteristics

The beam of an Nd:YAG laser can be described as a Gaussian beam, because of having a divergence less than 30° (see section 2.1.1.4). Its Beam Parameter Product (BPP) of a lamp pump system ranges from 0.3 up to 30 mm$*$mrad compared to

one of a HPDL that has a range of 3 - 1,000 mm∗mrad (Figure 2.3). The BPP quantifies the beam quality of the emitted radiation and is a measure for the focusability of a beam, i.e. how well it can be focussed to one spot (Haag, 2000).
For this reason, it is obvious that the focusability of Nd:YAG lasers is a lot better than that of HPDLs, which results in a higher achievable intensity on material and a significantly higher working distance for Nd:YAG lasers (Haag, 2000).
Furthermore, research has been done in the field of improving the beam quality of HPDLs, for instance with different structures of diode bars such as tapered ones (DILAS Diodenlaser GmbH and Osram Opto Semiconductors GmbH & Co, 2005) or by using an off - axis external cavity (Zhouping et al., 2007).
Although, the beam profile of Nd:YAG lasers can be described as a Gaussian beam due to the less divergence, their profile does not exactly comply with the one of a Gaussian beam as the M^2 - values show. The M^2 value, which is called the beam propagation factor, is also a measure for beam quality. It is defined as the ratio of the BPP of an actual beam to the one of an ideal Gaussian beam at the same wavelength (DIN EN ISO 11146-1, 2005-04), i.e. an ideal Gaussian beam has a value of $M^2 = 1$. Nd:YAG lasers have M^2 values in the range of 15 - 150 compared to the ones of HPDLs from $>$ 1,000 (in direction of the slow axis) up to 1 (in direction of the fast axis). Therefore, the beam profile of HPDLs can also be described as a Gaussian beam due to $M^2 = 1$ along the latter mentioned axis. However, the beam profile corresponds to a top hat in the direction of the slow axis (see section 2.1.2.3).
Regarding all mentioned beam characteristics, it can be stated that the beam quality of Nd:YAG lasers is better than that of HPDLs. Furthermore, the ability of Q-switching is another characteristic that needs to be mentioned. Hence, Nd:YAG lasers can be Q-switched compared to HPDLs which cannot (Lin, 2000).

2.1.3.3. Application areas of Nd:YAG and high power diode lasers in material processing

At first, an insight should be taken into the laser market concerning market share and sales revenues of different laser types in order to get an impression of the main areas of application regarding Nd:YAG lasers as well as HPDLs.
The market share of lasers used in material processing in respect to overall revenues corresponded to 29 % in 2008 (Figure 2.6a). Although, the market share of diode lasers (Figure 2.6b) was 58 % in 2008 compared to Solid state lasers
(Diode Pumped Solid State Laser (DPSSL), Lamp Pumped Solid State Laser (LPSSL)) that had a market share of 6 % and 9 % respectively, the main area of application of HPDLs can be seen in optical storage and telecommunication as sales figures show (Figure 2.6a) (Overton and Anderson, 2009).

(a) Laser applications segmented into overall percentage of revenues in 2008

(b) Laser technologies segmented into overall percentage of revenues in 2008

Figure 2.6.: a) Laser applications as well as b) laser technologies are segmented into the overall percentage of revenues in 2008 (Overton and Anderson, 2009)

Although, the worldwide sales of diode lasers in the market of material processing are significantly low (Figure 2.7a) compared to the worldwide sales of non-diode lasers, which also include the Nd:YAG lasers (Figure 2.7b), HPDLs are trying to enter the market (Steele and Strategies unlimited, 2007, Kincade and Anderson, 2008).

The limiting factor for the usage of HPDLs in material processing is their beam characteristics, such as focusability. However, important characteristics for material processing are the achievable power density as well as the output power, since the power density determines the interaction between laser beam and material, e.g. keyhole welding $> 106\,W/cm^2$, and the heated volume is dependent on the output power (Huegel, 1992). Figure 2.8 shows the established application areas in material

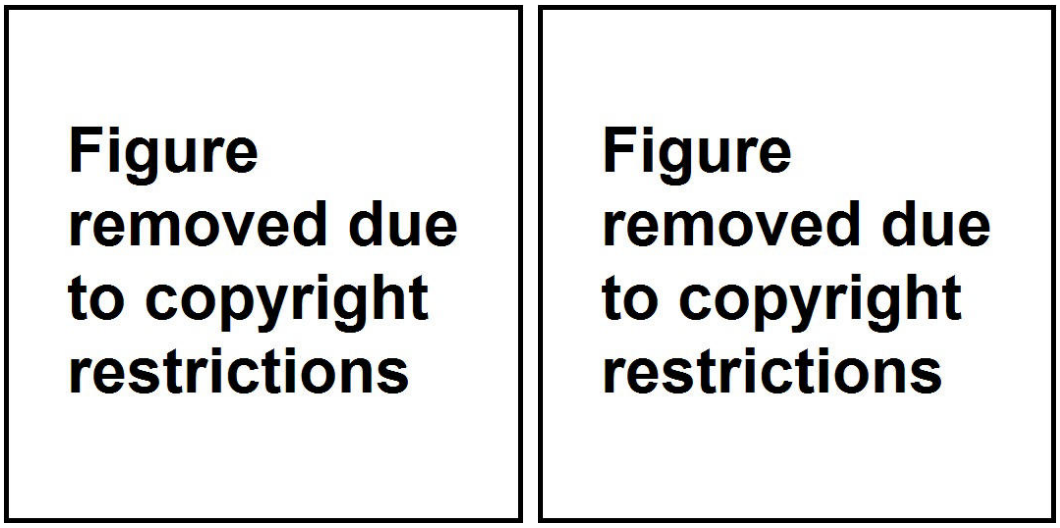

(a) Worldwide diode lasers sales by application in 2006 - 2007

(b) Worldwide non-diode lasers sales by application in 2007 - 2008

Figure 2.7.: a) Worldwide diode laser sales by application in 2006 - 2007 (Steele and Strategies unlimited, 2007) as well as b) worldwide non-diode laser sales by application in 2007 - 2008 (Kincade and Anderson, 2008)

processing depending on BPP and laser power. The BPP can be used as an indication of the focusability of a laser beam and therefore, it is a measure for the achievable power density. Furthermore, the limit of HPDLs (in 2000) regarding power and power density is shown in Figure 2.8. In this respect, HPDLs are used for applications such as soldering, hardening, welding and brazing.

One of the earliest reported applications of HPDLs in material processing was soldering (Polijanczuk and Whitehead, 18.04.1991). For instance, surface mount soldering has often been achieved by means of 10 W - 25 W air-cooled HPDL fibre guided beams (Loosen et al., 1997, Gilbert, 1995). Those HPDLs within this power range are more compact and more reliable than other lasers, such as Nd:YAG lasers. In addition, the radiation of HPDLs can be better absorbed to a certain extent by the mate-

Figure 2.8.: Parameter fields for laser material processing in 2000) (Bachmann, 2003)

rials used compared to Carbon dioxide (CO_2) and Nd:YAG lasers, due to their shorter wavelength.

Furthermore, the usage of HPDLs in surface treatments, with required power densities of 10^3 - 10^5 W/cm^2, is of interest due to the characteristic line-shaped spot and higher absorption in metals. For this, they have advantages concerning process efficiency compared to other laser types. For instance, the homogenous power distribution has a positive effect on work geometry for hardening, remelting and coating (Schuermann et al., 1999). For example, HPDLs are used for hardening of controller shafts fabricated from 100Cr6 steel, with an output power of 300 W and a flat-top rectangular beam. For this application, good uniformity of the hardened depth was found (Haag et al., 1997). For instance, transformation hardening of tool steels by means of a 1.5 kW diode laser having a Gaussian beam profile in one direction and a rectangular one in the other direction was demonstrated. There, it was shown that the HPDL achieved better results in hardness and wider track width due to increased absorption as a result of the shorter wavelength compared to a 2 kW Nd:YAG laser with a Gaussian beam (Schneider, 1988).

Another application area is welding that can be subdivided into conduction, polymer and deep penetration welding. Most welding applications are limited to conduction welding due to the achievable power density. For instance, conduction welding was

demonstrated for welding of thermocouple wires by using a fibre - coupled beam of an HPDL (Triantafyllidis et al., 1999). The results showed a superior weld quality concerning bead and porosity compared to the existing plasma arc - welded thermocouples. The same work was carried out with an Nd:YAG laser that resulted in a marginally worse weld compared to the HPDL (Lin, 2000). Another application of conduction welding is, the welding of tailored blanks (Bonss, 14 / 15. October 1999). Reasons for this application area are the features of HPDLs, such as the quiet weld pool as a result of a time - constant beam characteristic (Brandner et al., 1999), no plasma and the lack of the circulation effect due to the absent capillary tube. These features lead to a very smooth weld bead.

Furthermore, HPDLs require less edge preparation than CO_2 or Nd:YAG lasers and gaps up to a few tenths of an mm can definitely be bridged. Polymer and plastics welding was reported by Haensch et al. (Haensch et al., 16-19.11.1998). A much greater beam transmission was found for the HPDL (5 % - 75 %), although absorption of polymer at the near IR is similar to that at the far IR spectrum (10 % - 15 %). To vary the beam absorptivity various pigments were used. In this work, it was found that green - coloured polymer has the highest absorption coefficient (70 %) followed by red, blue, natural and yellow coloured ones. The absorption length can be reduced to 0.1 mm. A special feature of such an arrangement is that the surface absorption can lead to deep penetration because of the high transmission or absorption length of the HPDLs. These techniques are applied to welding of e.g. car seat belt holders and sun glasses (Lin, 2000).

Deep penetration welding, as it can be seen in Figure 2.8, could not be carried out via HPDLs due to their low power density. However, proof of this concept was given by e.g. Bliedtner et al. (Bliedtner et al., 2000), who reported successful keyhole welding of stainless steels that were up to 3.9 mm thick at a welding rate of 1,000 mm/min. This was done with a 2.5 kW Jenoptik diode laser delivered with 1.5 mm optical fibre that gave a power density of $2.6 \cdot 10^5$ W/cm^2 on the workpiece. To prevent the weld plume from damaging the processing head that was 34 mm away from the surface of the workpiece, a cross gas jet was used.

HPDLs with sufficient power density and low BPP of about 22 mm$*$mrad were launched from LIMO (Naumer et al., 2007). Furthermore, Trumpf developed a high-brightness fibre-coupled diode module that delivers 100 W at a numerical aperture of less than 0.12 from a fibre with a diameter of 100 μm. Due to the small diameter of the fibre, multiple fibres can be close-packed together to produce an increased power output, which can then be coupled into a delivery fibre. For instance, 19 mod-

ules can be coupled together reaching an output power of 1,900 W with a BPP of 25 mm∗mrad (Wallace, 2009).

These developed concepts can open the market of deep penetration welding and marking for HPDLs due to the significantly reduced BPP at sufficient output power. In future, non-diode lasers such as Nd:YAG lasers might have to give way to HPDLs in these areas of application. However, the required BPP depending on output power for processes such as cutting of metals has not been reached so far.

For brazing, Nd:YAG lasers are still the conventionally ones used, although, as experiments show, HPDLs obtain the same results as Nd:YAG lasers. For instance, brazing of Zinc (Zn) - coated steel (0.9 mm) with Copper Silicon ($CuSi_3$) brazing wire (1 mm in diameter) led to very smooth seams. For this, a HPDL with an output power of 2.5 kW was used and the brazing speed was 2 - 4 m/min (Bachmann, 2003). The material used within the mentioned example is typical for the automotive industry, which is one of the main application areas of brazing (Ribolla et al., 2005).

2.2. Laser material processing

Nowadays lasers are commonly used in material processing. They are implemented in many processes such as forming, joining, machining and surface engineering. Figure 2.9 gives an overview about the processing of materials with lasers.

Figure 2.9.: Classification of laser material processing (Dutta Majumdar and Manna, 2003)

In the following, it is focused on the joining process especially soldering and brazing. Both of these joining methods are introduced, defined and transferred to laser soldering and brazing and its areas of applications within the next subsections.

2.2.1. Soldering and brazing

The joining technology of soldering has been known for thousands of years. In 4000 B.C. jewellery was made by soldering gold and silver. Also weapons, chain mail as well as household articles, from Roman times were found at excavations, which were soldered (Zaremba, 1988). In the 19th century soldering lost its alchemical character due to metallurgical research (Wuich, 1972). Since this time soldering techniques have been permanently enhanced.

2.2.1.1. Definition of soldering and brazing

Soldering is defined as processing a coalescence of materials by heating them to a suitable temperature and by using a filler metal that has a liquidus temperature which is below or equal to 450°C. Furthermore, the solidus temperature of the base materials used is not allowed to be reached. Brazing is similar to soldering except for the temperature range used. A process is defined as brazing, if the temperature exceeds 450°C (Jacobson and Humpston, 2005, Brandner, 2003).
During the process of soldering / brazing diffusion takes place, i.e. atoms of the solder diffuse into the base material to achieve a positive joint. This area of diffusion is called diffusion zone (Fritz and Schulze, 2006).
In contrast to soldering / brazing, welding is defined as melting both materials to form a weld pool, where both materials are mixed. After cooling, an inter-metallic phase forms, which is the positive joint (Britannica, 2009).

2.2.1.2. Conventional methods

Soldering and brazing are differentiated in several types regarding the heat source used. In the following, the main conventional methods are introduced (Jacobson and Humpston, 2005, Manko, 2001, DIN ISO 857-2, 2007-3).

Soldering:

- Soldering via solid body
  - Hand soldering with soldering irons, e.g. assembly of electronic circuit boards
- Soldering via fluids
  - Dipping solder bath, e.g. assembly of electronic circuit boards
- Soldering via gas
  - Flame soldering, e.g. plumbing
- Soldering via radiation
  - Infrared soldering, e.g. electronics
- Soldering via electrical current
  - Resistance soldering, e.g. assembly of electronic circuit boards
- Furnace soldering
  - Furnace soldering, e.g. semiconductor device joining

Brazing:

- Brazing via fluids
  - Salt bath brazing, e.g. joining of aluminium parts (Dip Braze Inc., 2009)
- Flame brazing
  - Flame brazing, e.g. plumbing (joining of pipes)
- Electric arc brazing
  - Electric arc brazing, e.g. joining of metallic components (Svarkainfo, 2009)
- Brazing via radiation
  - Laser brazing, e.g. automotive industry
- Brazing via electrical current
  - Induction brazing, e.g. joining of metallic or ceramic materials (TWI Ltd., 2009)

The methods of soldering and brazing via radiation are introduced in more detail in the subsequent section. For radiation, the laser beam is used. Therefore, the methods are called laser soldering and laser brazing respectively.

2.2.2. Laser soldering and brazing

In the following different areas of application concerning laser soldering and brazing and its advantages are introduced.

2.2.2.1. Laser Soldering

New requirements evolve on joining technologies due to the fast developing miniaturisation of components in electronics with regard to the increasing packing density on e.g. circuit boards as well as the incremental complexity.
For instance, electronic or semiconductor components become more and more powerful and effective and the number of connections / ports increases, whereas the size of these connections / ports decreases as well as the pitches between each of them (Klein Wassink, 1991). But, conventional mass - soldering methods such as vapour phase soldering are constrained to pitches not smaller than 400 μm (Verguld, 1992). Therefore, these methods cannot fulfil the new requirements, since pitches decrease and the danger of solder - bridging increases in the same manner.
For this reason, smaller pitches can only be realised via selective soldering operations such as hot bar or laser soldering. Although, hot bar soldering is mainly used in electronic manufacture, the productivity is relatively low, the range of solderable component types is limited and an even heating of the hot bar cannot be guaranteed (Norwalk, CT : Reed Exhibition Companies, 1997, Lish, 1986). Hence, laser soldering is an alternative, where pitches down to 50 μm can be soldered (Krause and Treusch, 1992). The advantages of using a laser as a contact - free tool evolve out of its special characteristics. Since it is precise and results in locally narrow energy input with a good capability of automation, several advantages accrue (Semerad et al., 1993, Alavi et al., 1990):

- Individual adjustment of the heat input to the specific requirements of soldering tasks

- Soldering of temperature - sensitive components and connections is possible close to plastic components, due to the locally narrow heat input at the soldering point

- Opportunity of soldering pressure - sensitive components, since the laser does not strain the components mechanically

- Formation of brittle inter - metallic phases is inhibited due to the quick soldering time in conjunction with its high cooling rates. For this reason, a fine - grained structure develops, which can be highly loaded.

- The soldering process results in low stress joints due to the low thermal load of the components and the whole printed board (Verguld, 1992, Lish, 1986).

In spite of these advantages mentioned above, laser soldering did not really enter industrial manufacture, except for niche applications, where the technological advantages of laser soldering pander to its usage, e.g. temperature - sensitive components. Reasons for this behaviour can be found in the high investment costs and low productivity due to the sequential method.
However, the usage of laser soldering is indicated due to advancing miniaturisation of components as well as the introduction of 3D - printed boards in industrial manufacture (Krause and Treusch, 1992).
The main area of application for laser soldering is the joining of Surface Mounted Devices (SMD) on printed board manufacture. The disadvantages of laser soldering also account for this application. Therefore, several approaches are considered for simultaneous soldering to increase productivity such as the division of one laser beam from one source into four beamlets by means of a beam splitter (Dorn et al., 1992).

2.2.2.2. Laser brazing

The advantage of the locally narrow energy input mentioned above is also used for brazing of precision parts (Witherell, 1981). In such a case, brazing is preferred instead of welding to join those parts due to the low working temperature. Conventional methods cannot keep up with laser brazing, because of several disadvantages such as overheating, strong distortion, degradation and destruction of the join parts. There, the danger exists of destroying the join partners due to the relatively long process time of the solder. For this reason, laser brazing is a promising alternative (Witherell, 1981).
Laser brazing is also used in optical industry e.g. for the realisation of specific creative-visual criteria such as joining a hinge from glasses consisting of copper alloy with an earpiece out of alpaca (Klein and Abram, 1996). This method is also applied to the manufacture of premium frames as well as laser welding, due to the advantages compared to conventional methods (Dorn et al., 1998). However, in this area of application laser brazing competes against laser welding.
In the 1990s, the development concerning joining large - scale metal sheets was advanced due to a problem in the automotive industry. There, the problem was the production tolerances of metal sheets in bodywork that partly result in large gaps. If these joints were located in the car body shell or were designed as reparation sites,

they were predominantly joined via manual hand - flame brazing. Therefore, the quality of the brazed joint was strongly dependent on the qualification of the worker. This circumstance in conjunction with an undefined condition of joint, due to a lack of joint preparation, led to variations in quality of brazed joints and thermal damages of the component, which resulted in an extensive and cost intensive reworking (Geiger et al., 1994).

In this respect, automation of the brazing process produces constant and high quality results by application of a laser as first investigations with a CO_2 laser show (Haferkamp et al., 1993). The biggest potential of this method can be seen with the reduction of reworking (Geiger et al., 1994). The basics of laser brazing were acquired through many researches (VDI Technologiezentrum Physikalische Technologien, 1996). Several materials ranging from non - alloyed, high - alloyed or galvanised steels as well as lightweight construction material as titanium and aluminium alloys can be joined via laser brazing. Formation of brittle inter - metallic phases is diminished due to the quicker brazing times compared to the conventional methods. Researches for spatial work show that laser brazing is possible in every forced position (overhead, perpendicular, tray position) with an appropriate process control (Hanebuth, 1996).

3D-brazing was demonstrated with an industrial robot and an Nd:YAG laser for car C-pillar (Keitel and Orlick, 1996). Nd:YAG lasers are predominantly used as a laser source, since they have advantages compared to CO_2 lasers such as a more flexible beam guidance due to glass fibres, which can easily be implemented into production facilities, and better absorption in metals. The laser beam is adjusted according to the requirements of the geometry of the joint and its gap. It must be considered that the heating of the joint partner is attuned to the wetting behaviour of the solder via a defined temperature-profile without excessive thermal stressing of the component. Optimal adjusting of the temperature-profile to each joint geometry can be reached, if two laser sources are used (Geiger et al., 1994). A temperature control is used to prevent brazing failures as partial melting of base material, overheating of the solder and wetting failures, respectively. This matters especially in the 3D-work of defined contours (Hanebuth, 1996).

Based on basic researches, many automobile manufacturers investigated laser brazing of car body components. The first transfer into serial production was realised by Audi AG with the manufacture of the Audi TT Coupe. There, the side panel frame is brazed externally on the side with the C-pillar. Volkswagen AG uses brazing, for instance, on the hatch of a VW Bora (Larsson, 1999). Researches at BMW verified brazing

of a hatch car body shell that was based on basic researches concerning brazing of galvanised steels (Hornig, 2000). There, very good brazing results were obtained with excellent paint adhesion. Furthermore, it was shown that HPDLs obtain comparable results as Nd:YAG lasers (Bachmann, 2003).
For this reason, there is a huge potential for the application of HPDLs for brazing in automotive industry, in addition to their advantages concerning e.g. costs and service life.
Riedelsberger, from the Scansonic IPT GmbH, summarises the advantages of laser brazing for the automotive industry as follows (Riedelsberger, 30th October 2006):

- Saving costs in the long run
- Smoother car design
- Elimination of distortion due to low heat input
- No additional sealing
- High productive
- Higher car body stiffness.

Koltsov et al. defined a specific methodology to reproduce the conditions of laser brazing and to understand the $CuSi_3$ wetting behaviour on different zinc coated and bare steel sheets. For this they used the dispensed-drop technique in a vertical furnace with Argon atmosphere at normal pressure. The controlled melting of the brazing wire is realised by induction melting and the spreading behaviour of the droplets onto steel is acquired by a CCD camera. Experiments showed that a limited drop spreading onto bare steel occurs that can be related to the partial surface deoxidation when the brazing wire reacts with the steel, since bare steel has a thin oxide layer (Koltsov et al., 2010). This finding amongst others is transferred to the actual laser brazing process. There, Koltsov et al. names three main parameters that have an influence on the quality of brazed joints, which are the laser power, the feed speed of the base material and the feed speed of the brazing wire. According to Koltsov et al. the robustness of the laser brazing process can be evaluated by defining a processing range as shown in Figure 2.10 (Koltsov et al., 2010).

Figure 2.10.: Laser brazing processing range of bare steel, electro-galvanised (EG) steel with a zinc coating thickness of 8 μm and hot-dip-galvanised steel with a zinc coating thickness of 8 μm; brazing wire is preheated by Jules effect at an electric current of 110 A (Koltsov et al., 2010)

The narrow process window of bare steel (see Figure 2.10) is related to the presence of the oxide layer mentioned above. This oxide layer can only be partially removed during laser brazing operation, since the contact time of the molten brazing wire to the bare steel is too short. The process windows of the zinc coated steels are broader as the zinc coating suppresses oxide layers (Koltsov et al., 2010).
Furthermore, the initial temperature of the brazing wire has an influence on the spreading kinetics and interfacial reactivity. If the initial temperature of the brazing wire is decreased it leads to a decrease in spreading rate. Therefore the brazing energy (brazing temperature) has an influence on the width of the process window (Koltsov et al., 2010). Unfortunately, no information was presented regarding exact material type used or if the process windows presented in Figure 2.10 account for every joint geometry. Based on the figures presented in his work, only flanged seams were considered as joint geometry (see Figure 1.1) (Koltsov et al., 2010).
Li et al. demonstrated for laser brazing that the shape of the laser beam has an influence on the joint interface formation (LI et al., 2008). For their experiments they used zinc coated steel as base material, $CuSi_3$ as brazing wire and a 3 kW CO_2 slab laser. The influence of Gaussian, dual-spot and rectangular beam shapes were investigated on the joint interface formation. Results showed that no obvious intermetallic compound layer at the joint interface was formed using a Gaussian beam. The interface formation occurred using the other two beam shapes. Li et al. conclude based on

their findings that the interface reaction in galvanized steel sheets can be controlled by selection of the laser beam shape with its respective power density distribution (LI et al., 2008).

Heitmanek et al. presented an approach to increase process stability and joint quality of laser brazing by using the dynamic beam shaping system LASSY from Fraunhofer IWS, which is based on scanning mirror optics (Heitmanek et al., 2014). They used one dimensional scanning in feed direction to change the spot geometry from circular to elliptical. As materials they used zinc coated steel as base material and $CuSi_3$ as brazing wire. Experiments showed that the usage of beam scanning leads to a higher connection width of flanged seams compared to the static laser brazing process without dynamic beam shaping, if laser power, feed speed of base material and feed speed of brazing wire are kept constant (Heitmanek et al., 2014). This can be reasoned by the better pre-heating and therefore better wetting behaviour of the brazing wire with regard to the elliptical spot geometry. Furthermore, they demonstrated that the scanning frequency has a positive influence on the quality of the brazed joint. For instance, they observed, if the scanning frequency is above 100 Hz, the laser brazing process is stable and homogeneous, since the wetting frequency of the melt pool follows the frequency of LASSY. This leads to a better and smoother surface condition of the brazed joints (Heitmanek et al., 2014).

Kai et al. investigated the influence of the feed speed of the brazing wire to the quality of brazed overlap joints (Kai et al., 2015). They used zinc coated steel as base material and $CuSi_3$ as brazing wire for their studies laser. Experiments showed that the feed speed of the brazing wire influences the thickness of the interface layer of the joint; increasing the feed speed of brazing wire results in an increase in thickness of the interface layer of the joint. Furthermore, intermetallic compounds are formed, which are able to reinforce the joint as tensile tests indicate (Kai et al., 2015).

Rong et al. demonstrated an approach to optimise laser brazing process parameters with regard to joint geometry by using the Back Propagation Neural Network (BPNN) methodology in combination with Genetic Algorithm (GA) (Rong et al., 2015). This approach was verified by respective laser brazing experiments of flanged joints. Results showed that the average prediction error is below 15 % of the BPNN combined with GA methodology. For this reason, the presented approach is valid tool for optimising the process parameters for brazing flanged joints (Rong et al., 2015).

The research, presented above, have in common that they identify the laser power, the feed speed of base material and brazing wire as the important quality influenc-

ing parameters of the brazing process (LI et al., 2008, Heitmanek et al., 2014, Kai et al., 2015, Rong et al., 2015). Opinions deviate, regarding the ratio of feed speed of brazing wire to feed speed of base material for the same joint geometry, as Table 2.1 show (LI et al., 2008, Heitmanek et al., 2014, Kai et al., 2015, Rong et al., 2015). This could be reasoned by lack of information with regard to parameter set applied for researches concerning e.g. focal position, beam shape, gap and shielding gas.

Table 2.1.: Overview of both feed speeds used for laser brazing in researches, where (P)is the laser power, (v) is the feed speed of base material and (v_b)is the feed speed of the brazing wire

P (kW)	v ($\frac{m}{min}$)	v_b ($\frac{m}{min}$)	$\frac{v_b}{v}$	joint geometry	Reference
3	0.96 - 1.70	0.96 - 1.70	1	flanged seam	(LI et al., 2008)
3.00 - 3.80	3.00	3.20	1.07	flanged seam	(Heitmanek et al., 2014)
3.20	0.8 - 1.6	2.6 - 3.4	2.13 - 3.25	flanged seam	(Rong et al., 2015)
3.50	0.4	1.7 - 2.3	4.25 - 5.75	overlap joint	(Kai et al., 2015)

Furthermore, further literature research was carried out with regard to laser brazing of butt joints and quality issues of brazed joints, e.g. gap disappearance and deformation, albeit not found.

2.3. Quality control of joining processes

In this section, quality and process control are focussed on joining processes, especially regarding the brazing process.

The brazing process is dependent on an optimal adjustment of the process parameters. If this is not obtained, failures can occur such as pore formation, cracking of brazed joints, bad wetting behaviour, rough surfaces of brazed joints and danger of corrosion (Hornig, 2006). Therefore, a continuous process and / or quality control is necessary to ensure good quality and minimisation of possible rework.

For instance, BMW reported the following about the application of a laser brazing process control. This process control, called Message Passing Interphase (MPI), controls the heat input, where the brazing speed is the command variable and dependent on its value laser power and feed speed of the wire are set (Hornig, 2006).

Quality control can be separated into destructive and non-destructive quality control.

Destructive quality control is carried out amongst others in industrial production, e.g. the automotive industry. There, random samples from production are taken and investigated regarding micro-structure, tensile strength and toughness. For this, standardized test methods exist to gain the needed information.
For example, polished micrograph sections of brazed joints are produced to investigate the microstructure, possible cracks (weak adhesion) / pores, possible grain size changes due to heat input, thickness of diffusion zone and wetting behaviour.
Tensile testing of brazed joints is used to determine yield, ultimate and breaking strength of the joint (Gedney, 2005). From these results, the Young's modulus can be determined, which is a measure for the elasticity of the joint (metalinfo, 2009).
To determine the toughness of brazed joints, impact testing is executed (Higgins, 1983, S. 45f).
Receiving all information from these test methods, a good measure for the quality of brazed joints is achieved. However, these destructive test methods are only carried out on random samples in production. For this, they are a measure for the general quality of brazed joints, but failures during the production can still occur and might remain undiscovered.
For this reason, non-destructive quality control, so-called Non-Destructive Testing (NDT), gains more and more importance due to the opportunity of implementing this in the production with least amount of disturbance of the production process concerning required time and reduced production of scrap.
The non-destructive quality control can be subdivided into online and offline control, where offline means that the control is carried out after the process and online directly during the process. In the following, several non-destructive testing methods are introduced as well as their applications, which are used for the investigation of joints.
For instance, camera based methods in conjunction with image processing are used in offline mode for the investigation of brazed and welded joints regarding flaws such as pores (Muessigmann et al., 2003). However, Fraunhofer ILT (Dahmen and Kaierle, 2006) demonstrated the in process quality control, process monitoring respectively, of welded joints with a camera based system and its limitations.
Furthermore, Fraunhofer ILT (Mann, 2001) developed a model based predictive process control for laser deep penetration welding, since one criterion of welded seams is the penetration depth that is dependent on laser power and welding speed. For this, laser power was used as the actuating variable, whereas penetration depth should be the controlled process variable. However, penetration depth cannot normally be

measured. Therefore, plasma emission is used instead, since plasma emission and penetration depth are proportional to each other over a wide range. This developed process control for joining 3D components via laser welding with changing welding speeds was successfully tested.

Another technique of non-destructive testing is thermography. In general, a source heats the sample and if subsurface defects are within it, a temperature contrast will occur at the surface. This approach is called active and is used for investigation of materials. For this testing method, optical, mechanical, electromagnetic or other sources can be used. Optical energy is normally delivered externally, i.e. heat is produced at the surface of the sample and then travels through it to the subsurface anomaly (defect) and back to the surface. Mechanical energy can be considered as an internal way of stimulation, since heat is generated at the defect interface and then travels to the surface. In electromagnetic excitation, Eddy currents are externally induced to the material (electro-conductor), and heat is produced internally from the circulation of these currents in the material (Ibarra-Castanedo et al., 2006). In general, two approaches are used to carry out active thermography: either in reflection mode, i.e. excitation (source) and data acquisition are on the same side or in transmission mode, i.e. excitation and data acquisition are on opposite sides (Ibarra-Castanedo et al., 2008).

Chaudhuri et. al. (Chaudhuri et al., 2006), for instance, demonstrated the investigation of brazed joints between cooling tube and a heat sink via IR - thermography. There, it was determined that defects cause a slower temperature response on the surface during transient (Chaudhuri et al., 2006).

Ultrasonic Testing (UT) is also a very common method for the inspection of materials and joints concerning flaws. By now, this NDT method is over 55 years old. So far, the basis of flaw evaluation with UT is the processing of the A - scan, i.e. echo amplitude as a function of distance, which is still a very common evaluation procedure and described by many national and international standards. Typically, such A - scans are performed by trained personnel that have to interpret the obtained results. Therefore, flaw or volume imaging, which already exists in medical sector, are good enhancements to the obtained results, since the test results of the sample or at least parts of it are visualised and can be understood by non-trained personnel too. However, these techniques require more sophisticated hard and software, which is now available, even in portable and battery operated instruments. One example for the imaging ultrasonic testing is phased array technology (Berke, 2006).

Berke, for instance, (Berke, 2006) compared the conventional standard technique, i.e. a single emitter probe, with the phased array probe for the inspection of a weld. Results showed that the phased array inspection is faster, allows direct flaw imaging and has an increased probability of detection due to variable focussing and steering compared to the conventional technique. On the one hand, to mention a few disadvantages, phased array testing requires a higher surface quality than the conventional one, since the contact area is larger and unevenness impedes phasing. Furthermore, the investment costs of the phased array testing are higher and additional software for further data processing might be needed. On the other hand, the main advantage of phased array testing is the imaging including possible detected flaws in real time (Berke, 2006).

Furthermore, Rivas et. al. (Rivas et al., 2005) reported the development and testing of an automated spot weld inspection in the automotive industry. Motivation for this project was the circumstance that spot welds are manually tested by trained personnel, which investigate random samples during production. However, not all spot welds can be investigated without having a huge and non-realistic time delay of the production process. Therefore, a system was developed that can automatically investigate and classify at least 70 % of the spot welds made during the actual fabrication process in a fabrication cell with little time delay. As a next step, it is planned to implement this developed system into real production for field testing. X-raying also found its application within the NDT of joints (Rivas et al., 2005).

For instance, Hans Waelischmiller GmbH (Simon et al., 2006) developed an advanced computer tomography system for the investigation of large aluminium car bodies and its different joints, which was tested in cooperation with Audi AG. This developed system can scan parts from 3 mm up to 5000 mm with a resolution of up to 3 μm. It is capable of inspecting joints produced via Metal Inert Gas (MIG)-welding, laser welding, riveting and gluing even within complex structures of investigated parts (Simon et al., 2006).

An NDT method, mainly used for inspection of pipes (Vacher et al., 2006), metal sheets (Murner and Hansen, 25-28 Oct) as well as of rivet joints of aircraft components (Yashan et al., 2006) regarding flaws and cracks, is the eddy - current based method with Giant Magneto-Resistance (GMR) probes. Furthermore, a newly developed probe using the eddy current principle was introduced by Deltatest, which is able to detect flaws within austenitic weld seams of pipes (Heutling, 2008).

Another application of non - destructive testing is commercially available from the

company Vitronic. One of their products is, amongst others, a 3D soldering seam inspection system using a 500 Hz light - section sensor. This system automatically checks the existence of the seam, its length and width regarding e.g. seam interruptions and position relative to visible component edges. It can be directly implemented within production without any time delay in the actual process time. If any failures are detected, they are automatically marked via red chalk, so that it can be quickly optimised by personnel (Vitronic, 2008a). Another product of Vitronic is a system that recognises faults and inspects electronic - beam welded seams in automotive bodywork using a 2000 Hz light - stripe sensor. It investigates welds concerning existence, cracks, shape and length, and it is adjusted in such a way, including the robots of the production cell, so that it is able to detect failures > 1 mm (Vitronic, 2008b).
Scansonic IPT GmbH developed the Adaptive Laser Optic (ALO) which is capable of seam tracking. This is done by using the brazing wire as a tactile sensor as well as a server motor for the y-direction and a spring load for the z-direction. Furthermore, the ALO has an integrated auto focus system and it can operate within tolerances of ± 10 mm in y and ± 5 mm in z-direction. Due to the design of the ALO a very precise seam tracking has been realised, which can even handle small radii and it is not surface dependent as optical sensors (Riedelsberger, 30th October 2006).
Ungers et al. demonstrated an approach for controlling the laser power and the feed speed of the brazing wire according to the measured brazing velocity in real-time (Ungers et al., 2013). For this, they modified the Adaptive Laser Optic (ALO) mentioned above in cooperation with the company Scansonic IPT GmbH by coaxially implementing a CMOS camera into the existing ALO3. The measurement of the actual brazing velocity is realised via image processing by using the Field-Programmable Gate Array (FPGA) technology with respective algorithms (Ungers et al., 2013).
Furthermore, Lui et.al. introduced an approach for real-time monitoring of the laser hot-wire welding process. They monitored the welding process with the aid of a spectrometer. This spectrometer captured the emission spectrum of the laser-induced plasma plume. There, it was found that the plasma plume gets instable due to spattering, if a voltage above 9 V is applied to the wire. Furthermore they investigated the correlation between the electron temperature and the weld-bead shape. During welding, the molten pool was visualised by using a high-speed charge-coupled device (CCD) camera assisted by a green laser as an illumination source. They found out that the electron temperature of the plasma plume can be used for real-time monitoring with regard to variations of the weld-bead features as well as the formation of

weld defects (Liu et al., 2014).

2.4. Summary

Within this chapter an introduction is given to the lasers used for these parameter studies: Nd:YAG and diode with regard to their working principle and their respective characteristics.
The joining processes soldering and brazing are defined and distinguished. The brazing process is defined as processing a coalescence of materials by heating them to a suitable temperature and by using a filler metal that has a liquidus temperature which is higher than 450 °C. Furthermore, the solidus temperature of the base materials used is not allowed to be reached.
The research presented in the field of laser brazing indicate that maintaining and controlling the quality of laser brazing is of great interest and therefore investigated. They identify the laser power, the feed speed of base material and brazing wire as the important quality influencing parameters of the brazing process. However, opinions, found in literature, deviate with regard to the ratio between feed speed of brazing wire and feed speed of base material for the same joint geometry.
Literature research was carried out with regard to laser brazing of butt joints and quality issues of brazed joints, e.g. gap disappearance and deformation, albeit not found. Quality control is an important issue, therefore an overview is presented with significant emphasis on joining processes and non-destructive testing.

Chapter 3.

Quality influencing parameters

As it was shown in the literature review (see chapter 2), literature agrees upon that laser power, the feed speed of base material and brazing wire are the important quality influencing parameters of the brazing process.
This chapter presents and describes the parameters that influence the brazing result with regard to quality. These parameters are subdivided into laser and process parameters as well as material characteristics.
To measure the quality of a brazed joint, measures and examination techniques are needed. For this reason, quality measures for brazed joints are introduced as well as respective examination techniques presented, which are used for this research.

3.1. Influencing parameters

The influencing parameters, which may affect the quality of brazed joints, can be subdivided into laser, process parameters as well as material characteristics. Figure 3.1 presents an overview of these influencing parameters.

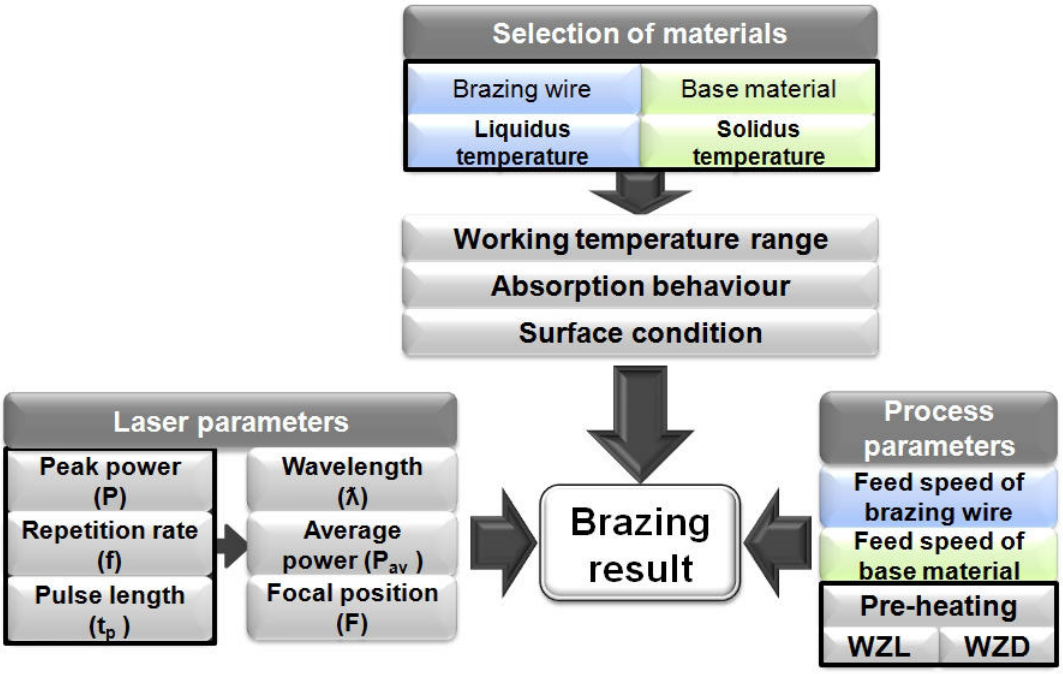

Figure 3.1.: Overview of influencing parameters: material characteristics, laser and process parameters

From Figure 3.1 it can be seen that the selection of the materials determine the operating temperature range for laser brazing due to its definition (see section 2.2.1.1 and 4.2.1.1 respectively). The absorption behaviour of these materials varies depending on the wavelength and therefore the laser type used. Furthermore, the surface condition of the materials used can have an influence on the brazing result, as summarised by Poprawe (Poprawe, 2005).

The laser parameters in Figure 3.1 consider both laser modes Continuous Wave (cw) and pulsed. For the latter mode the average laser power (P_{av}) is determined by the peak power (P), repetition rate (f) and the pulse length (t_p), as it can be seen in Figure 3.1 in contrast to the cw mode that only has the average laser power (P_{av}). In addition to the average laser power, the focal position and the wavelength of the laser have an influence on the brazing result. The influence of the latter mentioned

corresponds to the wavelength dependent absorption behaviour of the selected materials (Prokhorov et al., 1990).
As presented in Figure 3.1, three process parameters are considered, which also have an influence on the brazing result. On the one hand there are the feed speeds of the base material and of the brazing wire (see section 2.2.2.2) and on the other hand the pre-heating, which is done prior to the actual brazing process. This pre-heating phase is determined by the two delay times (WZD) and (WZL).
The material characteristics surface condition and physical properties, the laser and process parameters mentioned above are described in the following subsections.

3.1.1. Laser parameters

3.1.1.1. Influencing parameters of the Nd:YAG laser HL204P

For laser brazing the pulsed HL204P, Nd:YAG laser, is used. The technical data of this laser is shown in Table 3.1.

Table 3.1.: Technical data of the HL204P Nd:YAG laser

	HL204P	Unit
Wavelength of laser beam	1064	nm
Average Power by 10 ms pulse duration	190	W
Min. pulse power	300	W
Max. pulse power	7000	W
Pulse duration by reduced pulse power	0,3...20	ms
Pulse duration by max. pulse power	0,3...10	ms
Max. pulse energy	75	J
Max. pulse sequence frequency	600	Hz
Beam parameter product (BPP)	16	mm * mrad

In the following the laser parameters considered for the parameter studies are introduced.

3.1.1.1.1. Laser beam power

The Nd:YAG laser used is a pulsed laser. Therefore, two parameters regarding the laser beam power have to be differentiated: average laser power (P_{av}) and peak power (P). The average laser power is dependent on the repetition rate (f), the pulse length (t_p) and the peak power (P) used. The relation is as follows:

$$P_{av} = P * f * t_p \tag{3.1}$$

The peak power indicates the maximum power per pulse.
The heat input into the brazing wire as well as the base material can be influenced by the average laser power. Therefore, a high average laser power causes a large heat input, which corresponds to high rise in temperature within the materials and vice versa. The peak power of the HL204P Nd:YAG laser can be varied between 300 W - 7000 W per pulse (see Table 3.1).
Since the selected peak power as well as average laser power corresponds to a certain heat input and therefore temperature, it should be regarded that the solidus temperature of base material is not reached for laser brazing (see section 2.2.1.1).

3.1.1.1.2. Pulse length (t_p)

The duration of a laser pulse corresponds to the pulse length, which determines the average beam power emitted by the laser, in this case delivered to the surfaces of brazing wire and base material. Increasing the pulse length corresponds to an increase of the average beam power if the other parameters are kept constant. The pulse length of the Nd:YAG laser can be varied from 0.3 ms - 20 ms (see Table 3.1).

3.1.1.1.3. Repetition rate (f)

This parameter determines how many times a defined laser pulse is repeated. Therefore, it is the frequency of how often the laser beam is emitted per second. For this reason, it has also an effect on the heat input into the materials.
Furthermore, the repetition rate is dependent on the laser beam power and the pulse

length. If these two parameters are given the repetition rate can only be varied to some extend due to the capacity of the laser. For the beam powers and pulse lengths used, the repetition rate is limited from 10 Hz - 70 Hz, although the technical data of the Nd:YAG laser states that the repetition rate can be set up to 600 Hz. But this is only valid for a low beam power such as 300 W (see Table 3.1).

3.1.1.1.4. Focal Position (F)

The focal position (F) determines the size of the laser spot, i.e. if the focus of the laser beam is on the surface of the base material the focal position is zero and the laser spot has its minimum diameter, the so-called beam waist (d_0). By relatively moving the focus either above or beyond the surface of the base material, indicated as "+" and "-" respectively, the so-called defocusing, the spot size (d) changes accordingly (Hecht, 2005). The focal position corresponds to the displacement of the beam waist with regard to the surface of the base material. To obtain a sufficient laser spot size for laser brazing, the laser beam has to be defocused, so that the brazing wire as well as part of the base material is covered by the spot.

A reasonable spot size (d) can be determined for laser brazing by using the characteristics of a Gaussian beam (see section 2.1.1.4). To calculate the spot size (d), the beam waist (d_0) and the Rayleigh length ((z_R) have to be determined first, as the following equation shows (Steen, 1998):

$$d(F) = d_0 \cdot \sqrt{1 + \left(\frac{F}{z_R}\right)^2} \tag{3.2}$$

With: d(F): Spot size (beam diameter) on the surface of the base material at a focal position F
d_0: Beam waist
F: Focal position with regard to the surface of the base material
z_R: Rayleigh length

Beam waist (d_0)

For calculation of the beam waist (d_0) the optical system within the laser head needs to be considered (Figure 3.2). Therefore, the image scaling ratio (β) has to be determined.

It is defined as

$$\beta = \frac{f_f}{f_c} \tag{3.3}$$

With: f_f: Focal length of the focussing lens
f_c: Focal length of the collimating lens (collimator)

The focal lengths of the implemented focussing lens and collimator are $f_f = 150\,mm$ and $f_c = 200\,mm$ (Figure 3.2). Due to this, an image scaling ratio of

$$\beta = \frac{150\,mm}{200\,mm} = 0.75 \tag{3.4}$$

is determined.

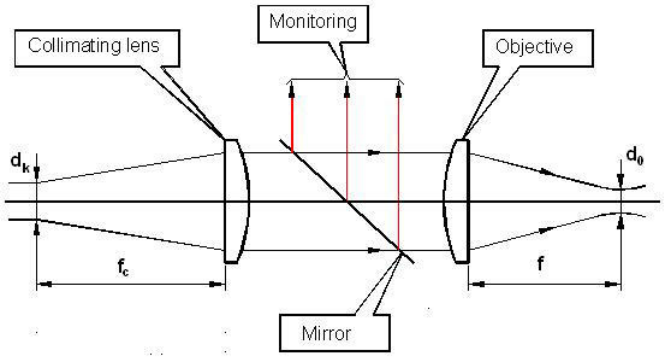

Figure 3.2.: Optical system (collimator) of the used laser head

Since the laser beam is fibre guided to the laser head, the diameter (d_k) in Figure 3.2 corresponds to the core diameter of the fibre, which is d_k = 0.400 mm. To actually calculate the beam waist (d_0) behind the optical system, the following equation is used.

$$\begin{aligned} d_0 &= d_k \cdot \beta \\ \Rightarrow d_0 &= 0.400\,mm \cdot 0.75 \\ \Rightarrow d_0 &= 0.300\,mm \end{aligned} \tag{3.5}$$

With: β: Image scaling ratio
d_k: Core diameter of the fibre

The beam waist (d_0) has a diameter of 0.300 mm.

Rayleigh length (z_R)

The Rayleigh length (z_R) is defined as the displacement between the beam waist (d_0) and the point where the cross-sectional area of the beam doubles compared to the cross-sectional area of the beam waist (Steen, 1998). To calculate the Rayleigh length (z_R), the following equation is used (Steen, 1998):

$$z_R = \frac{\frac{d_0}{2}}{\frac{\theta}{2}} \tag{3.6}$$

With: d_0: Beam waist
θ: Divergence

As defined in equation (3.6), the divergence (θ) has to be determined first, since this value is not given (see Table 3.1). To calculate the divergence, the Beam Parameter Product (BPP) can be used (see Table 3.1), as it is constant for a laser beam (Struve, 2001, RP Photonics Consulting GmbH, 2008).

$$BPP = \frac{\theta}{4} \cdot d_0 \tag{3.7}$$

By using equation (3.7), the divergence (θ) is $0.106\bar{6}$ rad. The divergence is transformed into degrees for further calculation: 0.1066 rad corresponds to 6.11°. After calculating the divergence (θ), the Rayleigh length (z_R) can be determined by using the equation (3.6). The Rayleigh length (z_R)corresponds to 1.401 mm .

Spot size (d)

To obtain a appropriate spot size (d) for laser brazing, an initial focal position (F) of +10 mm above the base material is considered. Then the spot size corresponds to by using equation (3.2):

$$\begin{aligned} d(10) &= 0.300\,mm \cdot \sqrt{1 + \left(\frac{10\,mm}{1.401\,mm}\right)^2} = 2.162\,mm \\ d(10) &= 2.162\,mm \end{aligned}$$

These theoretically determined values were verified by using the laser the beam profiler Laserscope UFF 100 from Prometec GmbH. The whole verification approach including results and discussion can be found in Appendix A.1.

3.1.1.2. Influencing parameters of the diode laser LDL 40-150

The diode laser used, an LDL 40-150 from Laserline GmbH is a Continuous Wave (cw) direct diode laser with a maximum output power of 150 W and a wavelength of 808 nm. As mentioned in subsection 2.1.2.2, the output power of the diode laser is linearly dependent on the driving current above the lasing threshold. The correspondent diagram for this laser can be found in Appendix A.3.
The diode laser used has a rectangular laser spot which results from the dimensions of the active zone of a single emitter and its correspondent collimation (see subsection 2.1.2.2). The rectangular laser spot means that the beam widths (d_x) and (d_y) are not equal (Laserline GmbH, 2003).
The spot diagram of the diode laser for the focussing lens with a focal length of 100 mm is provided within the manual, which is shown in Figure 3.3. The approximated beam parameter products for the slow (x) and the fast axis (y-direction) were provided by Laserline GmbH, which are as follows:

- BPP_x = 60 mm*mrad
- BPP_y = 40 mm*mrad

Figure 3.3.: Spot diagram of the diode laser LDL 40-150 for the focussing lens with a focal length of 100 mm (Laserline GmbH, 2003)

3.1.1.2.1. Laser beam power (P)

The diode laser is a (cw) direct laser. The laser beam power influences the heat input into the brazing wire as well as the base material.

Therefore, a high beam power causes a large heat input, which corresponds to high rise in temperature within the materials and vice versa. The beam power of the diode

laser LDL 40 -150 can be varied up to 150 W.
For the selection of laser beam power for laser brazing, it has to be regarded that the beam power corresponds to a certain heat input and therefore temperature increase, which should be lower than the solidus temperature of the base material (see section 2.2.1.1).

3.1.1.2.2. Focal Position (F)

As described in section 3.1.1.1, the focal position (F) determines the size of the laser spot, as (F) corresponds to the displacement of the beam waist (d_0) with regard to the surface of the base material.
To obtain a suitable spot size for laser brazing, the laser beam has to be defocused, so that the brazing wire as well as part of the base material is covered by the spot.
Since the LDL 40-150 has a simple astigmatic beam (see verification in Appendix A.4), the following equation can be used to determine the spot sizes for both directions by just interchanging (x) with (y) (Neubert and Scharfe, 2007):

$$d_x(F) = d_{x0}\sqrt{1 + \frac{(M_x^2)^2}{d_{x0}^4}\frac{16\lambda^2}{\pi^2}F^2}. \tag{3.8}$$

With: $d_x(F)$ Spot size (beam diameter) on the surface of the base material at a focal position F
d_{x0}: Beam waist
M_x^2: Beam propagation factor
λ: Wavelength

To actually calculate the spot sizes (d_x) and (d_y) respectively, the beam propagation factor M^2 has to be determined first for each direction. The beam propagation factor M_x^2 is defined as follows (Neubert and Scharfe, 2007):

$$M_x^2 = \frac{BPP_x \cdot \pi}{\lambda}, \tag{3.9}$$

Inserting the respective given BPPs (see above) and the wavelength into equation (3.9), results in beam propagation factors of $M_y^2 = 155.524$ and $M_x^2 = 233.287$.
Inserting the respective beam propagation factor in equation (3.8) the diameters of a +5 mm defocused laser spot (d_x) and (d_y) can be calculated with the given beam

waists (d_{x0}) and (d_{y0}) (width (x) and width (y) in Figure 3.3):

$$\begin{aligned} d_x(5) &= 0.5042\,mm\sqrt{1+\frac{(233.287)^2}{0.5042\,mm^4}\frac{16(0.808*10^{-3}mm)^2}{\pi^2}5^2} \\ d_x(5) &= 2.43\,mm \end{aligned}$$

$$\begin{aligned} d_y(5) &= 0.2177\,mm\sqrt{1+\frac{(155.524)^2}{0.2177\,mm^4}\frac{16(0.808*10^{-3}mm)^2}{\pi^2}5^2} \\ d_y(5) &= 3.68\,mm \end{aligned}$$

A photo-sensitive paper[1] is used to verify the theoretical determined spot sizes (d_x(F)) and (d_y(F)) respectively. The verification approach including the results can be found in Appendix A.5.

3.1.2. Process parameters

3.1.2.1. Feed speed of base material (v)

The feed speed of base material determines the duration of the process, because it states how fast the axes of the work station are moved. Therefore, this parameter influences the heat input into the materials and hence the temperature rise in them.

3.1.2.2. Feed speed of brazing wire (v_b)

This parameter determines the amount of brazing wire that is brought to the brazing process. A slow feed speed causes less brazing wire being melted during brazing process, which results in a low quality joint. Whereas a high feed speed causes a lot of brazing wire to be melted, which also can result in a joint with less quality, due to too much absorption of the heat input by the wire, so that the base material is not enough heated to get a qualitatively good brazed joint.

3.1.2.3. Pre-heating

Pre-heating means that an actual pre-heating time is introduced before the actual laser brazing process starts. It is needed, because the base material has to be heated appropriately, so that the brazing wire can wet properly onto the surface of the base

[1] The photo-sensitive paper used has been exposed to global irradiation, i.e. daylight, before usage

material due to sufficient operating temperature directly at the start of the brazing process. This pre-heating time is defined by two delay times (WZD) and (WZL), which are explained in the following subsections.

3.1.2.3.1. Delay time (WZD)

The delay time (WZD) introduces a delay between starting the temperature measurement, which is started when the incident laser radiation exceeds the threshold temperature, and starting the wire feed. This delay time is used to influence the heat input into the base material, so that it gets sufficiently heated before the wire feed starts to obtain a proper wetting.

3.1.2.3.2. Delay time (WZL)

Due to the delay time (WZD), a delay is also needed between starting the laser and starting brazing the joint, the so-called delay time (WZL). This also influences, as delay time (WZD), the heat input into the base material to obtain a proper wetting.

3.1.3. Material characteristics

3.1.3.1. Physical properties

The physical properties of a material determine its behaviour under specific circumstances e.g. temperature increase, incident laser radiation. A material can be characterised by its physical properties (Poprawe, 2005). In the following the most important physical properties of materials are named (Hornbogen, 1983, Poprawe, 2005):

- Index of refraction n,
- Absorption index κ
- Susceptibility ξ
- Electric conductivity σ
- Heat conductivity K and
- Specific heat c
- Density
- Solidus and liquidus temperature

For this reason, the operating temperature, process speed and laser power are dependent on the materials used for laser brazing.

3.1.3.2. Surface condition

The surface condition of the materials used for brazing can have also an influence on the brazing result and therefore on the selection of suitable parameters for laser brazing. For example, Figure 3.4 shows the result of a measurement of the reflectivity for two different steels. For polished surfaces measured and calculated values correspond to each other as summarised by (Poprawe, 2005). The variations at the technical surfaces are noticeable. The diffuse part of reflectivity is about 10 % except for polished surfaces. With increasing process gases, the directed reflectivity of sand blasted samples decreases, whereas the diffuse one increases according to (Poprawe, 2005).

Figure 3.4.: Measured degree of reflection for intensities (I) $\ll$ (I_p) ((I_p): Process intensity) of different metals (Wissenbach, 1985); (Poprawe, 2005)

With increasing temperature, a decrease of reflectivity is observed for metals (see section 4.2.1.1). At high temperatures, the increased reactivity of metals can cause irreversible changes of the reflectivity characteristics by chemical changes of the surface. For instance, if a hot metal has contact with air oxidation occurs (Poprawe, 2005).
In general, an oxide layer increases the absorption. This is particularly important for processes which form a molten bath, since oxides stay within the melt. On the contrary, the original process gases do not influence the absorption of the sample anymore, since the laser radiation hits the relatively smooth melt (Poprawe, 2005).

3.2. Quality measures and examination techniques of brazed joints

3.2.1. Quality measures

3.2.1.1. Adhesion energy γ_H and gap width

The adhesion energy (γ_H) is a measure for the ability of the melt of the brazing wire to wet surfaces and to extend on them. The wetting ability of the brazing wire can be described as extending on surfaces and filling the normally small gap widths of the base material against gravity. This property of the melted brazing wire within a small

gap is described by the capillary filling pressure (p_c) or by the ceiling (h). For gaps up to 0.3 mm in width it can be approximately said (Fritz and Schulze, 2006):

$$h_c \sim p_c \sim \frac{\gamma_H}{d_{gap}} \tag{3.10}$$

With: h_c: Ceiling
p_c: Capillary filling pressure
γ_H: Adhesion energy
d_{gap}: Gap width

Therefore, the ceiling (h) is dependent on the surface condition of the base materials, the brazing wire used, the adhesion energy (γ_H) as well as the gap width (d_{gap}) (Figure 3.5).

Figure 3.5.: Capillary filling pressure (p_c) against gap width (d_{gap}) (adapted from (Müller and Müller, 1995))

For gap widths (d_{gap}) larger than 0.5 mm the capillary filling pressure (p_c) is too small, so that the gap is not fully filled by the melted brazing wire anymore. For free-hand brazing, gap widths between 0.2 - 0.5 mm are used. For laser brazing gap widths between 0.05 - 0.2 mm are optimal, because then the brazing wire is "sucked" into the gap due to the capillary filling pressure (p_c) (Fritz and Schulze, 2006).

3.2.1.2. Contact angle

The wetting and expanding of the melted brazing wire on the surface of the base material can be described by surface free energies (γ) (Figure 3.6).

Figure 3.6.: Relation between surface free energies at the surface base material - melted brazing wire (Kyowa Interface Science Co., 2008)

The relation between the surface free energies (γ) are shown in the following (Kyowa Interface Science Co., 2008).

$$\gamma_S = \gamma_{SL} + \gamma_L \cdot \cos\theta \tag{3.11}$$

$$\gamma_S = \gamma_{SL} - \gamma_L \cdot \cos\theta = \gamma_H \tag{3.12}$$

With:
- γ_S: Solid surface free energy
- γ_L: Liquid surface free energy
- γ_{SL}: Solid/ Liquid interfacial free energy
- γ_H: Adhesion energy
- θ: Contact angle

The value of the contact angle (θ) is determined by the base and filler material used as well as the kind of the ambient medium (air, vacuum, protective gas). It is a measure for the wetting of a surface. For (θ) = 0°, theoretically a thin film would form, which is never reached in reality. Qualitatively good brazed joints are produced, if the contact angle (θ) is less than 30° (Fritz and Schulze, 2006).
An important parameter for a good wetting is the working temperature. If the working temperature is reached, the brazing wire wets the surface and expands on it. Normally, the actual used brazing temperature is above the working temperature. But it needs to be ensured that this brazing temperature does not exceed a certain value, because then the brazing wire and / or base material can be damaged (Fritz and

Schulze, 2006).

A sufficient wetting is one of the most important requirements for a qualitatively good brazed joint. Wetting occurs if the brazing wire and the base material can form solid solutions or intermediate compounds, whereas the solubility can be very small. For absolute insolubility of base and filler material, no wetting of the surface takes place (Fritz and Schulze, 2006).

The wetting and therefore the contact angle (θ) are also dependent on the cleanliness of the surface (Figure 3.7). A clean surface can result in a good wetting, whereas a contaminated surface decreases the wetting (Kyowa Interface Science Co., 2008).

Figure 3.7.: Behaviour of a drop due to cleanness of surface (Kyowa Interface Science Co., 2008)

The relation between contact angle, wettability, adhesiveness and solid surface free energies are shown in Figure 3.8.

Figure 3.8.: Relation between parameters that determine the quality of a brazed joint with respect to wetting (Kyowa Interface Science Co., 2008)

To derive the equation for contact angle determination, the following ideal conditions

are preconditioned (Jacobson and Humpston, 2005):

- the original brazing wire pellet is in the form of a spherical bead of radius (r)

- while brazing the droplet spreads on the base material as a spherical cap of radius (R) and height (h) and resolidifies subsequently (see Figure 3.9)

- the interface between the resolidified droplet and the base material has a diameter of (2A), the so-called spread diameter (see Figure 3.9)

- the volume of the original brazing wire pellet and of the resolidified droplet are the same, i.e. volatilisation of the molten brazing wire as well as reaction with the base material are neglected

With regard to these ideal conditions and by using the Pythagorean Theorem the following expressions can be derived from Figure 3.9 (Jacobson and Humpston, 2005):

$$A^2 + (R - h)^2 = R^2 \tag{3.13}$$

Solving equation 3.13 for (R)

$$R = \frac{A^2 + h^2}{2h} \tag{3.14}$$

the contact angle can be described as follows:

$$\theta = \arcsin\left(\frac{2}{\frac{A}{h} + \frac{h}{A}}\right) \tag{3.15}$$

Figure 3.9.: Schematic diagram of the dimensions from the solidified brazing wire for contact angle determination (adapted from (Jacobson and Humpston, 2005))

3.2.1.3. Diffusion

The area, in which the compound brazing wire-base material is formed, is an extremely thin alloy zone (D) (Figure 3.10) due to the very limited change of functional location of the atoms within the solid base material (Fritz and Schulze, 2006).

Figure 3.10.: Formation of an alloy zone between brazing wire and base material (adapted from (Fritz and Schulze, 2006))

$$D = D_{base} + D_{brazingwire} \tag{3.16}$$

With: D: Alloy zone
D_{base}: Diffusion zone in base material
$D_{brazingwire}$: Diffusion zone in brazing wire

A brazed joint can fail due to the properties of the formed alloy zone and by the non-optimal selection of base and filler material (Jacobson and Humpston, 2005). In general, the possibility of failing of a brazed joint is influenced by the working temperature of the brazing wire. The lower the working temperature of the brazing wire is, the lower the possibility of failing, since the change of functional atoms occurs slower at lower working temperatures (Fritz and Schulze, 2006). Therefore, the thickness of the alloy zone reduces, which corresponds to a reduction of the possibility of failing. Depending on working temperature, alloy zones with a thickness between 0.5 μm - 20 μm form (Fritz and Schulze, 2006).
A qualitatively good brazed joint is produced, if the alloy zone consists of primary crystals or solid solutions. Brazed joints, which consist of steel as base material and copper as filler material, often tend to brazing wire-brittleness by temperatures above 900 °C (Fritz and Schulze, 2006). This happens due to the fast diffusion of the copper along the grain boundaries in the steel. Therefore, intercrystalline material separations take place within the tensioned material as long as the brazing wire is melted (Fritz and Schulze, 2006).

3.2.2. Examination techniques

3.2.2.1. Polished micrograph sections

To investigate the microstructure of a brazed joint, polished micrograph sections are carried out for quality control. The preparation of the micrograph sections is described in Appendix A.7.
The microstructure or grain size of both materials brazing wire and base materials can be changed depending on the heat input (heat affected zone) (Fritz and Schulze, 2006). Therefore, polished micrograph sections give information about the heat input as well as the quality of joining these two materials due to possible pores and thickness of alloy zone. Furthermore the contact angle can also be determined from the polished micrograph sections (see section 3.2.1.2). An explanation of the basics of microstructure with regard to the iron - iron carbide (Fe-FeC_3) phase diagram can be found in Appendix A.9. The optical inspection of those polished micrograph sections

is carried out by the aid of a microscope. If the microscope used did not provide an analysis software to measure e.g. the width or the height of the brazed joint, these measurements are carried out as described in Appendix A.8.
The preparation of polished micrograph sections (Appendix A.7) as well as their subsequent investigation (Appendix A.8) applies for all polished micrograph sections carried out.

3.2.2.2. Vickers hardness (HV)

Investigation of the hardness across a brazed joint is important due to hardness change across this joint. It is also a destructive quality control method. A description of the measurement approach can be found in Appendix A.10. To determine the Vickers Hardness (HV), the two diagonals (d1) and (d2) of the indentation are measured (see Figure 3.11) and the arithmetic mean is calculated (University of Tennessee, 2008). After calculating the arithmetic mean (d) of the two diagonals, the Vickers hardness

Figure 3.11.: Determination of the Vickers hardness (University of Tennessee, 2008)

(HV) can be calculated with the following equation (University of Tennessee, 2008):

$$HV = \frac{2 \cdot F \cdot \sin(\frac{136^\circ}{2})}{d^2_{Vickers}} \tag{3.17}$$

With: F: Applied force (1kgf corresponds to 9.807 N)
136°: Angle between opposite faces of the indenter
$d_{Vickers}$: Arithmetic mean of the two diagonals of the indentation

These calculations are carried out by the Vickers hardness testing machine automatically, so that the Vickers hardness is presented on a screen. Figure 3.12 shows examplarily how the measured values are correctly stated.

Figure 3.12.: Example for the correct statement of the Vickers hardness value

As it can be seen in Figure 3.12, the testing period has only to be stated, if it differs from the common one, which is between 10 to 15 s. For instance, if the testing period corresponds to 20 s in this example, it has to be stated as follows: 100 HV 1/20.
The measurements across a brazed joint should be at least 3 * $d_{Vickers}$ apart from each other to ensure no influences of the previous measurement (Kubik, 2010), since this type of measurement is based on material displacement, which leads to an increase in hardness measurement and therefore to a falsification of the respective hardness value if the minimum distance is not kept (Kubik, 2010).

3.2.2.3. Tensile testing

The tensile testing belongs to the group of destructive quality control. By the aid of this test, stress-strain curves can be obtained and the respective characteristics, such as e.g. Young's modulus, yield strength and ultimate strength, can be determined. For a detailed description regarding this topic, please use the continuative literature e.g. (Bargel and Schulze, 2012, Gobrecht et al., 1975), which can be found in the bibliography of this work.
The tensile testing device used is shown in Figure 3.13 and its specifications can be found in Appendix D.8.

Figure 3.13.: Tensile testing machine Instron 3367

3.3. Summary

Within this chapter, the parameters that have an influence on the brazing result were presented. They can be subdivided into material characteristics, laser and process parameters. Figure 3.14 is presented again as it summarises the parameters introduced.

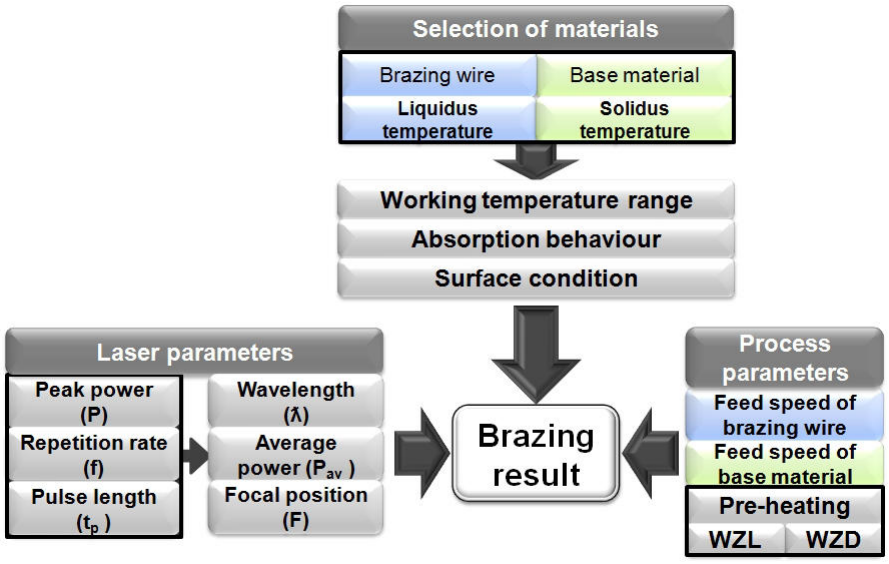

Figure 3.14.: Overview of influencing parameters: material characteristics, laser and process parameters

Furthermore, the quality measures adhesion energy and gap width, contact angle and alloy zone were explained, which are used within this research. Along with these quality measures, the examination techniques polished micrograph section, Vickers Hardness (HV) and tensile testing were presented that are used within this research as well.

Chapter 4.

Experimental procedures and initial tests

To investigate the correlations between the parameters influencing the brazing process, which were introduced in the previous chapter, a laser brazing test rig was designed which can be implemented into the Nd:YAG laser work station and in the diode laser work station. This test rig consists of the laser brazing setup and measurement equipment. For carrying out parameter studies of laser brazing, measurement equipment is needed with regard to wire feed and temperature. The design and implementation of test rig is presented within this chapter.
Furthermore, the materials and their preparation, used for laser brazing, are introduced. These materials are used throughout this research.
Subsequently, initial experiments, carried out with the Nd:YAG laser, are presented that identify the aspects, which are further investigated in the parameter studies.
Moreover a non-destructive quality control system, based on a laser triangulation sensor, is presented. Due to the measurement accuracy of the sensor it is supposed to be capable of e.g. measuring deformation in base material due to the heat induced tensions.

4.1. Laser brazing setup

To investigate the parameters influencing the laser brazing process, a setup for laser brazing needs to be constructed for both laser working stations: Nd:YAG and diode. For this, a clamping device for joining the base materials and a wire feeder are constructed and incorporated into the existing laser working stations. The following requirements were defined for the clamping device and the wire feeder, which they need to fulfil:

Clamping device:

- Easy adjustment for different sizes of metal plates
- Even clamping over the full plate length
- Easy adjustment of gap width

Wire feeder:

- Adjustable wire speed
- Adjustable incidence angle of the wire
- Usage of a tube, with a diameter that is a little bit larger than the wire, for wire guidance to prevent oscillation of the wire during the brazing process

The latter requirement for the wire feeder, mentioned above, is needed for an appropriate wire feed. Since early tests showed that brazing wire oscillations occur during brazing, if the brazing wire is not guided properly to the brazing process, due to the pulling of the wire by the stepper motor. These oscillations result in no brazed joints at all. Figure 4.1 shows an example of such a brazed joint.

Figure 4.1.: Example of brazed joint without wire guidance; Laser type: Nd:YAG, parameters used: P = 4900 W, f = 50 Hz, t_p = 0.6 ms, P_{av} = 147 W, F = -13 mm, v = 95 $\frac{mm}{min}$, v_b = 177.54 $\frac{mm}{min}$, d_{gap} = 0.1 mm

The realisation of both devices is shown in Figure 4.2 and the implementation in both working stations is presented in Figure 4.3 and 4.4. A detailed description of both devices and their technical drawings can be found in Appendix B.1 and E.1 respectively.

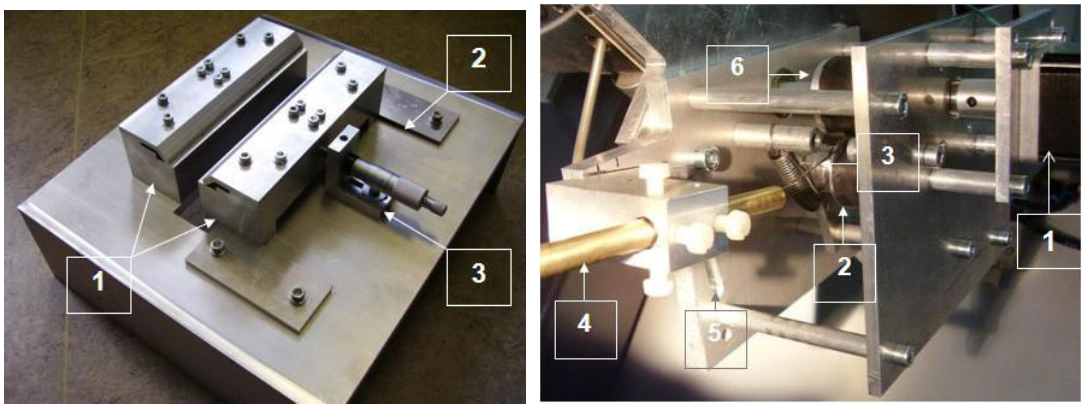

(a) Clamping device **(b)** Wire feeder

Figure 4.2.: Design (a) Clamping device: 1) Clamping brackets; 2) Dovetail; 3) Micrometer gauge for gap adjustment (b) Wire feeder: 1) Stepper motor; 2) Tensioner with guidance groove; 3) Wire; 4) Wire guidance; 5) Adjustment of the incidence angle of the wire; 6) Drive roll

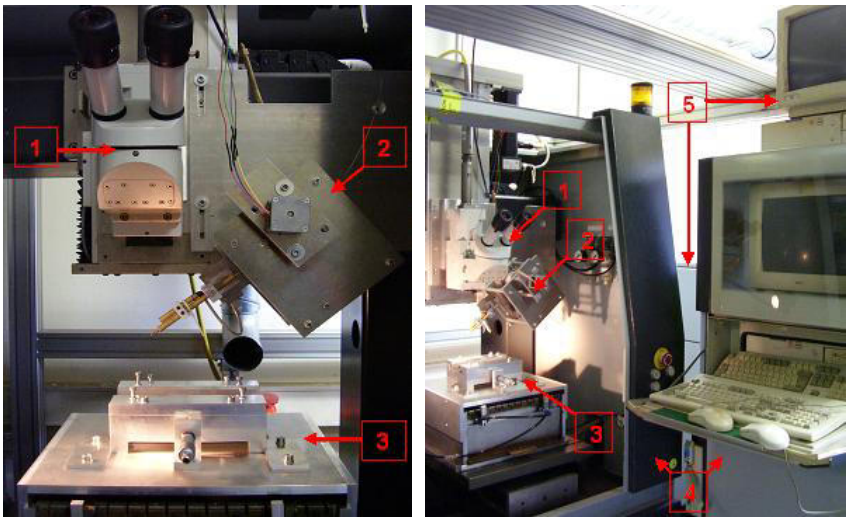

Figure 4.3.: Completion of Nd:YAG laser brazing setup; 1) Laser head; 2) Wire feeder; 3) Clamping device; 4) Working station with Computerised Numerical Control (CNC)-unit; 5) Nd:YAG laser (bottom) and its laser control (right)

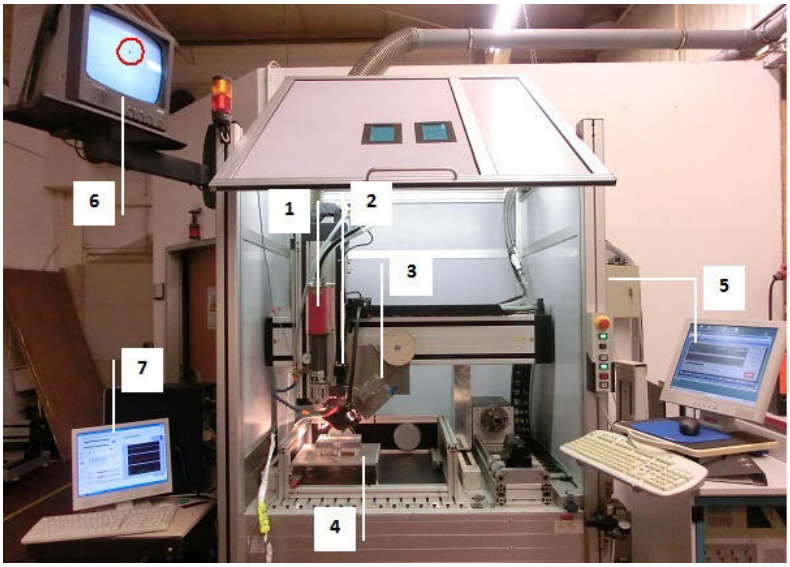

Figure 4.4.: Completion of diode laser brazing setup; 1) Diode laser; 2) Camera; 3) Wire feeder; 4) Clamping device; 5) Working station with CNC-unit; 6) Monitor that displays the enlarged view of the camera (red circle indicates the location of the laser spot); 7) Designed program for wire feed control and temperature measurement

4.2. Measurement equipment

For carrying out laser brazing parameter studies, a temperature measurement setup as well as a wire feed control is needed to ensure a appropriate operating temperature and wire feed. In the following subsections, the realisation of both temperature measurement setup and wire feed control are explained.

4.2.1. Temperature measurement setup

4.2.1.1. Importance of temperature measurement

Temperature measurement is very important for the brazing process due to exceeding the liquidus temperature of the filler material and not crossing the solidus temperature of the base material. Therefore, only a small temperature range can be used for the brazing process. For this reason it is important to control the temperature during the process.

The temperature within the workpiece is dependent on the absorbed energy of the incident laser radiation. The absorption (A) can be understood as the ratio of power that is coupled into the workpiece (P_{abs}) and the power that hits the workpiece (P) (Poprawe,

2005):

$$A = \frac{P_{abs}}{P} \tag{4.1}$$

The value of (A) can be between 0 and 1. In general, the absorbed energy of radiation is transformed into heat. This energy transformation can take place over several steps which might be used for material processing. For instance, laser radiation can dissociate molecules; before this non - equilibrium state reaches the equilibrium state, i.e. the energy of the absorbed laser radiation is transformed into heat, the dissociated molecule components are separated (ablation) (Poprawe, 2005).
The absorption is a global parameter, since it generally gives no information about where the energy of radiation is deposited and transformed into heat respectively. In metals the process of absorption takes place within a thin layer close to the surface, i.e. the process of absorption is localised. However, this information is not indicated in (A) (Poprawe, 2005).
If the radiation that is coupled into the workpiece is absorbed by the workpiece, then it follows for conductors (Poprawe, 2005)

$$A = 1 - R \tag{4.2}$$

With: R: Reflectivity

The absorption is no pure material characteristic as for instance, index of refraction, specific heat and electric and heat conductivity. It is, amongst others, dependent on (Poprawe, 2005)

- physical characteristics of the material (n, κ, etc) and of the laser beam (wavelength, polarisation, etc)
- environmental conditions (process gas, materials surrounding the workpiece, etc)
- surface characteristics (roughness, morphology, etc)
- geometry of the workpiece (thickness of the workpiece, limitations, etc)
- changes of the workpiece and of the environment due to the absorbed energy (localised heating, phase transformations, laser - induced plasma).

It was determined that the absorptivity increases approximately linearly with temperature as long as the temperature is below the liquidus temperature (T_m) of the metal used (Figure 4.5) (Rubahn, 1996, Yilbas et al., 1996). If the temperature increases above the liquidus temperature, the absorptivity increases faster and it becomes independent of the wavelength of the incident radiation (Figure 4.5) (Yilbas et al., 1996). For this reason, the temperature of vaporisation can be reached quickly, where a part of the material evaporates. Due to evaporation, a vapour and plasma cloud forms above the heated material, which absorbs a huge part of the laser radiation. Therefore, the absorptivity within this range, the so-called *abnormal absorption* is strongly dependent on the intensity of the incident radiation and only marginally increases with the temperature (Rubahn, 1996, Yilbas et al., 1996).

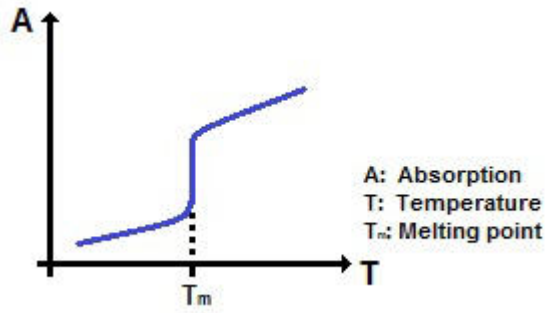

Figure 4.5.: Sketch of the absorption behaviour against temperature

Prokhorov et al (Prokhorov et al., 1990) showed the behaviour of absorptivity at the phase change solid-liquid of several pure metals by using the Drude model of apsorption[2]. They determined that the absorptivity increases linearly with the temperature up to the melting point (T_m). At the melting point the absorptivity increases almost instantaneously by a factor of 1.5 up to 2 and for temperatures above the melting point the absorptivity shows again a linear behaviour. Figure 4.6 shows this described behaviour of absorptivity.

[2] Poprawe presents a detailed description of this model as well as to the theory of temperature distribution in solids, which can be found in the references of this work (Poprawe, 2005)

Figure 4.6.: Computations carried out for absorptivity dependent on temperature for pure metals and CO_2 laser radiation by using the Drude model of absorption (Prokhorov et al., 1990)

4.2.1.2. Temperature measurement setup

As already mentioned in section 4.2.1.1 temperature measurement is important, since the valid temperature range for the brazing process is limited by the liquidus temperature of the filler material and the solidus temperature of the base material. The materials used set the temperature range from 1025°C up to 1490°C. Several applications have been developed and tested for measuring within this temperature range, such as using a pyrometer (Ignatiev et al., 1996) or thermography (Mathieu et al., 2006a).
Due to cost reasons thermocouples of type K were chosen for temperature measurement. They consist of a Chromel wire (90% nickel and 10% chromium) and an Alumel wire (approximately 95% nickel, 2% manganese, 2% aluminium and 1% silicon) and they can measure within a temperature range of -200°C up to 1250°C (TRINOS Vakuum-Systeme GmbH, 2008).
In the following the implementation of the temperature measurement setup is explained. It should be noted that the implementation of the thermocouples is exemplified on the implementation into the Nd:YAG laser work station, which is comparable to the implementation into the diode laser work station.
The thermocouples are used for temperature measurement on the one hand and as a trigger for the wire feed on the other hand. To connect the thermocouples to the Labview© program, which will be explained in section 4.2.3, their signal output is too small so that it has to be amplified. For this the measurement amplifier AD 595 from

Analog Devices is used.

To ensure the simultaneous temperature measurement at different places during the laser brazing process a 10 bit analogue - digital converter from H - Tronic with eight input ports is used. The data sheets for the amplifier and for the analogue-digital converter can be found in appendix D.1 and D.2 respectively.

At first, three thermocouples were implemented into the Nd:YAG laser work station as shown in Figure 4.7. One thermocouple was positioned in front of the actual brazing process (leading) and the other two were positioned at the side of the brazing process.

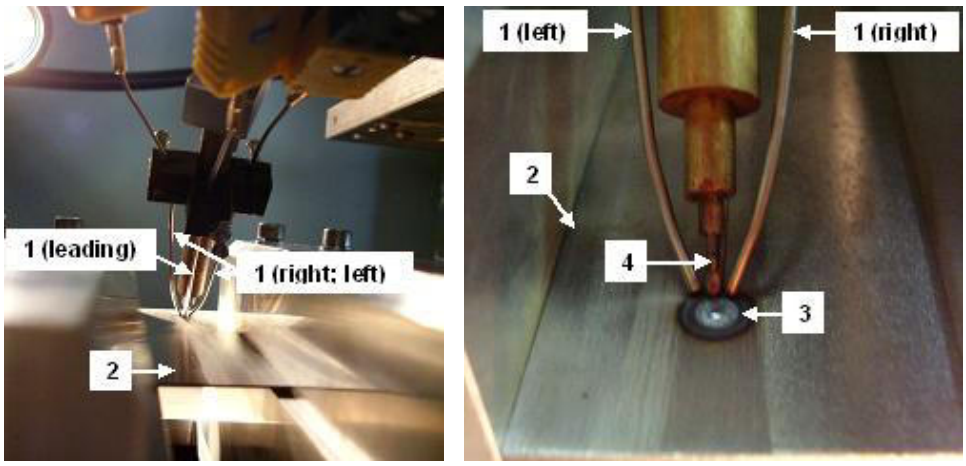

Figure 4.7.: Implementation of the thermocouples into the laser brazing setup; 1) Thermocouples and their position relative to the point of impact of the laser beam (right, left, leading) ; 2) Base material; 3) Point of impact of the laser beam; 4) Brazing wire

Early tests of the temperature measurement setup showed that the contact to the surface of the base material as well as remaining in the adjusted position was not always maintained. Thus, the temperature measurement setup has to be optimised, especially the positioning and mounting of the thermocouples.

During testing it was determined that thermocouples have a better and more stable contact to the surface of the base material if their incidence angle is between 75° - 90°, since the measurement tip of those thermocouples is the actual measurement point (Perrin, 1999). For this reason, a new thermocouples holder and positioner were developed that fulfils these requirements and can be implemented into the existing

laser work station. Due to this required incidence angle of 75° - 90°, only two thermocouples can be implemented in the existing setup. They are directly mounted to the laser head of the work station.

For the optimised temperature measurement setup, the range of the adjustable incidence angle of the thermocouple behind the laser head corresponds to approximately 30° for lack of space (Figure 4.8), whereas the one in front of the laser head has a range of about 70°.

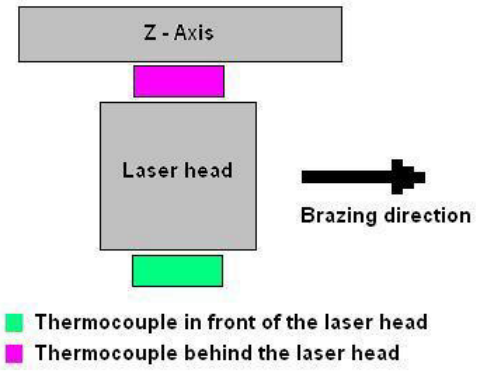

Figure 4.8.: Schematic diagram of thermocouple positions

The implementation of the thermocouples into the Nd:YAG laser work station is shown in Figure 4.9.

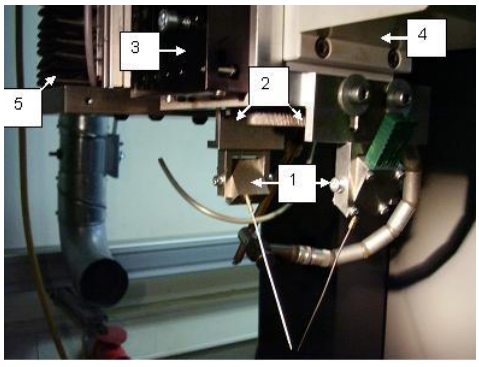

Figure 4.9.: Implementation of the temperature measurement setup into the laser work station; 1) Thermocouples in aluminium case; 2) Plates for height adjustment; 3) Joint plate for the implementation of the quality control measurement setup (see section 4.5); 4) Laser head; 5) Z - Axis

The respective technical drawings for the optimised temperature measurement setup can be found in Appendix E.2 and the testing of the optimised temperature measurement setup can be found in Appendix B.2.1.
This temperature measurement setup was verified by means of the SC640 IR camera from FLIR Systems. A detailed description of the verification approach as well as its respective results and discussion can be found in Appendix B.2.2.

4.2.2. Wire feed control

The wire feed control is needed to check if the wire is fed properly and the requested amount of wire is delivered to the brazing process. To realise such a control the optical encoder HEDM 5500 B11 from the company Agilent technologies is used. The data sheet of this device can be found in the Appendix D.3. This encoder is implemented onto the axis of the drive roll in the wire feed as it can be seen in Figure 4.10. The encoder is connected to the 32 bit counter of the National Instruments USB 6009 card (see Appendix D.4), which is again connected to the in LabView© program that is described in section 4.2.3.

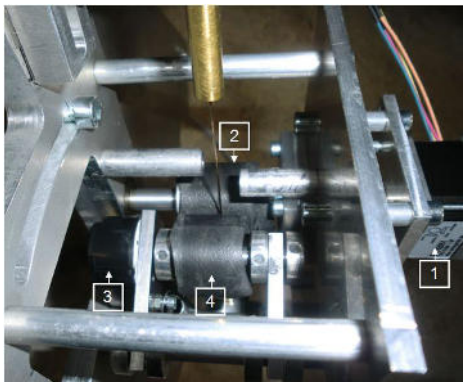

Figure 4.10.: Implementation of the encoder onto the axis of the tensioner in the wire feed; 1) Stepper motor; 2) Drive roll; 3) Encoder; 4) Tensioner

The verification of the wire feed control, including approach and results, can be found in Appendix B.2.3. As the verification shows, the encoder delivers a proper estimation of the fed wire even if the direction of movement cannot be determined.

4.2.3. Designed Program for wire feed control and temperature measurement

A program in Labview© was designed to control and set the wire feed as well as to measure the temperature. The user interface of this program is shown in Figure 4.11.

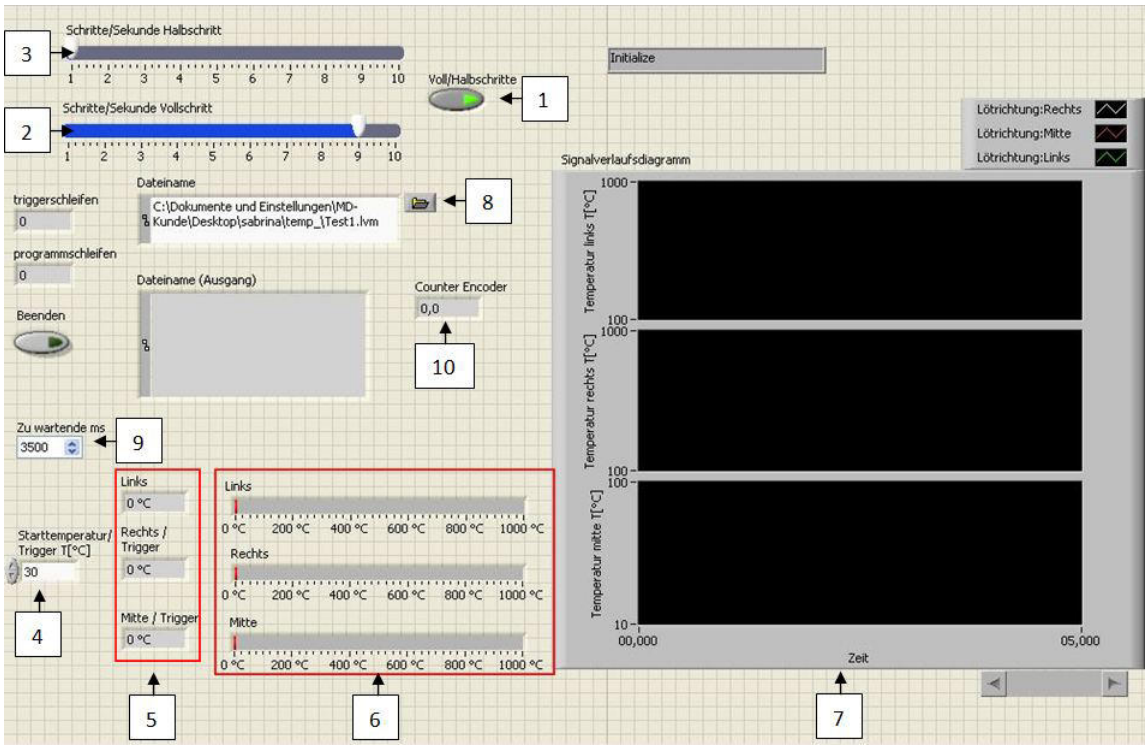

Figure 4.11.: User interface of the designed program for wire feed control and temperature measurement;1) Selection between mode of operation for the stepper motor;2) Control unit for speed of wire feed in full-step mode; 3) Control unit for speed of wire feed in half-step mode; 4) Selection of threshold temperature for trigger; 5) Display of the instantaneous value as a number; 6) Display of the instantaneous value as a bar graph; 7) Display of measurement signal against time; 8) Selecting path for automatic saving of measurement data; 9) Selection of delay time WZD; 10) Display of counts of the encoder

Via button No.1 it can be selected between the modes of operation of the stepper motor: Either full or half-step. By means of the control unit, shown in No. 2 (full-step) and No. 3 (half-step) respectively, the speed of the wire feed can be set in steps per second by adjusting the controller.

The temperature measurement setup is used as a trigger for starting the wire feed. The

threshold temperature for the trigger can be set by using button No. 4. While measuring, the current temperature of each thermocouple is displayed as a number (No.5) and via scale bar (No. 6) as well as a graph (No. 7). Even though the user interface indicates that three thermocouples are used, only two of them are implemented into the work station (see section 4.2.1.2). The third one is only used for testing the wire feed. Each temperature measurement is automatically saved. The path where the data is supposed to be saved can be adjusted by clicking No. 8.
Furthermore a delay time (WZD) is introduced (see section 3.1.2.3.1). (WZD) introduces a delay between starting the temperature measurement, which is started when the incident laser radiation exceeds the threshold temperature, and starting the wire feed. This delay time can be set by using button No. 9.
No. 10 displays the counts of the encoder that correspond to a certain wire length (see Appendix B.2.3).

4.3. Materials and their preparation for the parameter studies

The materials and their preparation, which are described in the following, are used throughout this work.

4.3.1. Base material: mild cold - rolled steel DC01

Mild cold - rolled constructional steel DC01 (steel 1.0330)[3] was used as a base material. This steel has a thickness of 0.8 mm and its material and physical properties are shown in Table 4.1 and Table 4.2 respectively.

Table 4.1.: Material properties of DC01 (Württemberger, 1987)

Material number	Tensile strength R_m (N / mm^2)	Yield stress R_e (N / mm^2)	Ultimate strain A_{strain} (%)
1.0330	270 - 410	280	28

[3]Material number according to EN 10027 - 2

Table 4.2.: Physical properties of iron[4] (Iffländer, 1990)

Material	ρ (g/cm^3)	c (J/gC)	K (W/cmC)	T_m (°C)	T_v (°C)	Q_m (J/g)	Q_v (J/g)	1-R
Iron	7.85	0.46	0.75	1537	2735	274	6365	0.35

DC01 consists of 0.12 % Carbon, 0.60 % Manganese, 0.045 % Phosphorus and 0.045 % Sulphur (Becker Stahl Service GmbH, 2008). Due to its carbon content, this steel belongs to the group of structural steels, which are normally used for screws and machine parts (Higgins, 1983). Furthermore DC01 is classified as an unalloyed steel based on its contents (Higgins, 1983). Its hardness is in the range of 90 - 120 Brinell hardness (HB) (Franz Gysi AG, 2008).

As this steel consists mainly of iron, the solidus temperature of iron is used for a Carbon content of 0.12 %, which is approx. 1,490 °C (see Figure A.12).

DC01 was chosen, because this type of steel is also used in automotive industry with the only difference that it is additionally zinc galvanised there.

For laser brazing, the absorption behaviour of the base material has to be approximately known for the wavelength used This behaviour determines the absorbed energy of the incident laser radiation and therefore the temperature within the workpiece (Prokhorov et al., 1990) (see section 4.2.1.1). Since the base material mainly consists of iron, it is a valid approximation to use its value of absorptance for the base material. Figure 4.12 shows the absorptance dependent on the wavelength for iron.

For Nd:YAG laser radiation ($\lambda = 1{,}064$ nm) the absorptance of iron corresponds to approximately 40 % and for diode laser radiation ($\lambda = 808$ nm) to approximately 50 % (see Figure 4.12).

[4]

- ρ: Density
- c: Specific heat capacity
- K: Heat conductivity
- T_m Liquidus temperature
- T_v: Evaporating temperature
- Q_m: Heat of fusion
- Q_v: Heat of vaporisation
- 1-R: Absorption at $\lambda = 1\mu$m (at room temperature)

Figure 4.12.: Absorptance of iron dependent on the wavelength (Bergström et al., 2003)

Furthermore, the surface roughness (R_z) of the base material was measured. The measurement approach including the results can be found in Appendix B.3. The mean of (R_z) over the length of the base material corresponds to $5.65 \pm 0.155\,\mu$m and the mean of (R_z) across the base material is $5.48 \pm 0.23\,\mu$m.

4.3.2. Brazing wire: $CuSi_3$

As a filler material $CuSi_3$ is used. This brazing wire has a diameter of 0.8 mm and its material properties are shown in Table 4.3.

Table 4.3.: Material properties of $CuSi_3$ (Metall Svetsmaterial KB, 2008)

As described in section 4.3.1, the absorption behaviour of the material is dependent on the wavelength used (Prokhorov et al., 1990). Therefore this dependency has to be known to estimate the required heat input. Figure 4.13 shows the reflectivity of copper dependent on the wavelength. Since the brazing wire mainly consists of copper, this shown behaviour is a valid approximation. As stated in section 4.2.1.1 and by using equation 4.2 the absorptance of the brazing wire can be estimated to 4% for both lasers used.

Figure 4.13.: Reflectivity of several metals dependent on the wavelength (Layertec GmbH, 2014)

4.3.3. Base material preparation

For all parameter studies, the dimensions used for the base material were 0.8 mm * 30 mm * 110 mm. The base materials were prepared as follows to remove possible dirt and grease and to avoid any influences caused by this soiling:
the base material is cleaned first with 96 % denatured ethanol and subsequently put into a ultrasonic bath for three minutes that is filled with distilled water. Afterwards, the base material is cleaned again with the denatured ethanol to remove any remaining water residuals.

4.4. Initial experiments

These initial experiments were carried out with the Nd:YAG laser. For these experiments, the materials were used and prepared as described in section 4.3. For all experiments, a joint of 100 mm is produced and subsequently investigated and furthermore only compressed air[5] is used to prevent pollution of the optics. Even if it is not always stated, several tests were carried out.
As presented in section 3.1, material characteristics, laser and process parameters have an influence on the brazing result. Prior to carrying out the parameter studies, considerations have to be done with regard to required heat input, suitable spot size,

[5]The usage of shielding gas is neglected due to cost reasons

ratio between feed speed of brazing wire and feed speed of base material.

4.4.1. Preliminary considerations

Estimation of heat input

The required heat for proper heating of the base metal and melting of the brazing wire has to be roughly estimated. For the following estimations losses regarding heat transport are neglected and only losses due to reflection at the surface are considered. For this the following equations can be used (Baehr and Stephan, 2009):

$$Q = m * c * (T_2 - T_1) \tag{4.3}$$

$$with$$

$$m = \rho * V$$

With:
- Q: Amount of heat gained or lost by material (J)
- m: Mass of material (kg)
- c: specific heat capacity ($\frac{J}{kg*^\circ C}$)
- T_2: Final temperature (°C)
- T_1: Initial temperature (°C)
- ρ: Density ($\frac{kg}{m^3}$)
- V: Volume of the material (m^3)

The considered volume (V) in equation 4.3 is dependent on thickness of the material, the focal position (F) and therefore the spot size (d) of the laser. As stated in section 4.3.1, the base material has a thickness of 0.8 mm and the brazing wire has a diameter of 0.8 mm. In section 3.1.1.1.4, it was shown that a reasonable spot size of 2.162 mm in diameter is obtained, if the laser is defocused by + 10 mm (= F). This spot size seems to be appropriate to heat the base material and melt the brazing wire. For volume calculation of the brazing wire, the considered length of the brazing wire corresponds to the radius of the spot size.
The specific heat capacity and density for the base material is stated in Table 4.2. For the brazing wire, its density can be found in Table 4.3, but its specific heat capacity is not known. However, as the brazing wire mainly consists of copper, its specific heat capacity is used instead. It corresponds to 382 $\frac{J}{kg*^\circ C}$ (Baehr and Stephan, 2009). The temperature range considered for proper heating of the base material starts from a

minimum of 800 °C up to a maximum 1,100 °C for the final temperature (T_2). For the brazing wire, the minimum temperature corresponds to the liquidus temperature of $CuSi_3$, which is 1,025 °C (see Table 4.3). The maximum temperature considered for the brazing wire corresponds to the one of the base material. The initial temperature (T_1) is set to 20 °C for these estimations.
Using the information stated above with equation 4.3, this results in a required heat range of the brazing wire from $Q_{wire_{min}} = 2.985\,J$ up to $Q_{wire_{max}} = 3.208\,J$ and for the base material the required heat ranges from $Q_{base_{min}} = 8.471\,J$ up to $Q_{base_{max}} = 11.729\,J$.
To estimate the heat input (Q_{input}), at first an average power (P_{av}) of 150 W and a feed speed of the base material (v) of 120 $\frac{mm}{min}$ are assumed, which leads to a heat input of

$$\begin{aligned} Q_{input} &= \frac{P_{av}}{v} \\ Q_{input} &= \frac{150W}{\frac{120mm}{60s}} \\ Q_{input} &= 75\frac{J}{mm}. \end{aligned} \tag{4.4}$$

Furthermore the losses due to reflection of the laser beam at the surface of the base material and brazing wire have to be considered. As explained in section 3.1.3.2, the surface condition of the base material also influences the reflectivity. If a technical surface for the base material is assumed the losses due to reflection can be roughly approximated to 60 % (see Figure 3.4 and Figure 4.12 respectively). For this reason the first estimation of the heat input of 75 $\frac{J}{mm}$ seems to be sufficient for carrying out the brazing process, even if 60% of the heat input are lost, it satisfies the maximum required thermal energy demand of 14.749 J.

Ratio of feed speeds

As in section 2.2.2.2 presented, opinions deviate in literature with regard to the ratio of feed speed of brazing wire to feed speed of base material for the same joint geometry (see Table 2.1). This ratio is in the range of 1 up to 3.25 for a flanged seam. As mentioned in section 2.2.2.2, no literature could be found with regard to the ratio of feed speeds for brazing butt joints. For this reason, as a rule of thumb, the ratio of feed speed of brazing wire to feed speed of base material can be approximated by 2:1 for a butt joint.

Gap width

For these initial experiments, the gap width (d_{gap}) is set to 0.1 mm, as this width is supposed to be within the optimal range for laser brazing (see section 3.2.1.1).

Average laser power

As described in section 3.1.1.1.1, the average laser power of the pulsed Nd:YAG laser is dependent on the laser peak power (P), the repetition rate (f) and the pulse length (t_p). Based on the estimation of the required heat input, an average laser power (P_{av}) of 150 W is needed. The repetition rate (f) is set to 50 Hz and kept constant throughout these experiments. Hence, the peak power and the pulse length have to be selected respectively to reach the average laser power of 150 W according to equation (3.1). For a start, the peak power (P) is set to 5,000 W and the pulse length (t_p) to 0.6 ms.

The considerations carried out are summarised in the following for clarity.

- Focal position (F) of +10 mm leads to a spot size (d) of 2.162 mm (see section 3.1.1.1.4)
- Average laser power (P_{av}) of 150 W fulfils the required heat input by using a feed speed of the base material (v) of 120 $\frac{mm}{min}$
- The average laser power of 150 W is obtained by setting
  - the pulse length (t_p) to 0.6 ms
  - the repetition rate (f) to 50 Hz
  - the peak power (P) to 5,000 W
- The ratio of feed speed of brazing wire to feed speed of base material is estimated to approximately 2:1
- Gap width (d_{gap}) is set to 0.1 mm

4.4.2. Experiments

Based on these preliminary considerations carried out in section 4.4.1, the first tested parameter set is shown in Table 4.4.

Table 4.4.: First tested parameter set for brazing[6]

P (W)	t_p (ms)	f (Hz)	P_{av} (W)	F (mm)	v_b ($\frac{mm}{min}$)	v ($\frac{mm}{min}$)	d_{gap} (mm)
5000	0.6	50	150	+10	210	120	0.1

From this brazed joint a polished micrograph section was carried out. For this the joint was cut at 55 mm and investigated. The polished micrograph section is shown in Figure 4.14. The greyish areas within the base material are flash rust, which rapidly develops after etching.

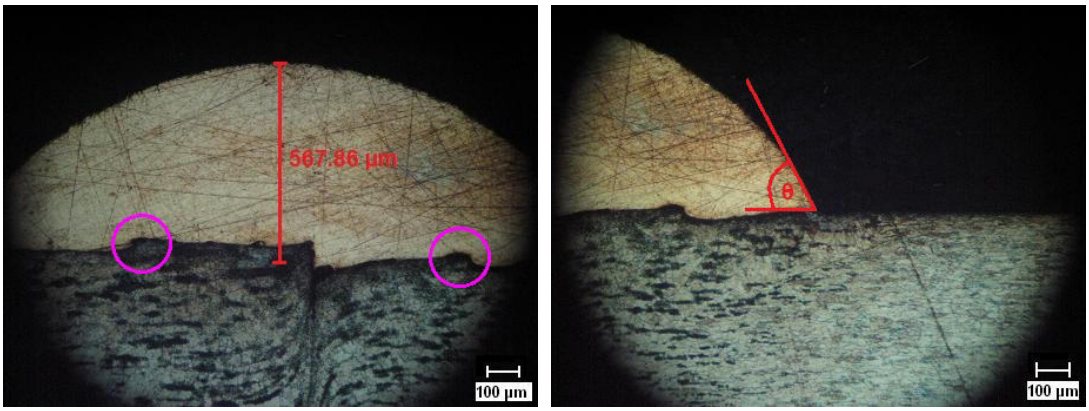

(a) Polished micrograph section of brazed butt joint from the first tested parameter set

(b) Polished micrograph section of the brazed butt joint showing the contact angle

Figure 4.14.: Parameters for brazing: P = 5,000 W, t_p = 0.6 ms, f = 50 Hz, P_{av} = 150 W, F = -10 mm, v = 120 $\frac{mm}{min}$, v_b = 210 $\frac{mm}{min}$, d_{gap} = 0.1 mm; a) Polished micrograph section of brazed butt joint from the first tested parameter set where the height (h) of 567.86 μm is indicated; the spread diameter (2A) could not be fully displayed and therefore not indicated, but (2A) is measured to 1741 μm ; b) With the height (h) and the spread diameter (2A) the contact angle corresponds to 66.24° by using equation 3.15

As it can be seen in Figure 4.14a and 4.14b respectively the wetting of the brazing wire onto the surface of the base material does not seem to be sufficient. To use the quality measure contact angle, which is introduced in section 3.2.1.2, the height (h)

6

P: Peak power
t_p: Pulse length
f: Repetition rate
P_{av} Average laser power
F: Focal position
v_b: Feed speed of brazing wire
v: Feed speed of base material
d_{gap}: Gap width

of the spherical cap as well as the spread diameter (2A) are determined[7].
However, the spread diameter is not indicated in Figure 4.14, since it was not possible to take a picture of the whole micrograph section. Using equation 3.15 the contact angle corresponds to 66.24°. Brazed joints are evaluated as qualitatively good, if the contact angle is less than 30° (see section 3.2.1.2). For this reason the measured contact angle of the first tested parameter set indicates a poor wetting and therefore a poor quality.
In addition to the poor wetting another measure that shows a poor quality is the fusing or ablation of the base material which is indicated by the pink circles in Figure 4.14. This fusing or ablation shows that the temperature rise within the base material exceeded at least 1537 °C up to 2735 °C (see Table 4.2). This temperature rise is too much and violates the definition of brazing, because the solidus temperature of the base material is not allowed to be exceeded (see section 2.2.1.1). The solidus temperature of the base material can be obtained from the Fe-Fe_3C phase diagram (see Figure A.12 in Appendix A.9), since the carbon content of the base material is known (see section A.9). The solidus temperature approximately corresponds to 1490 °C.
At this point it should be noted that the described temperature measurement set up in chapter 4.2.1.2 is not yet implemented. However, the implementation was completed just before the adapted parameter set was tested.
As previously mentioned the polished micrograph section was obtained by cutting the brazed joint at 55 mm. The initial gap width (d_{gap}) between the base materials was 0.1 mm. However, as it can be seen in Figure 4.14a the gap disappeared at the location of 55 mm and the base materials seem to be deformed due to thermal expansion. The base materials are not only deformed across the joint but also over the length of the joint. This behaviour indicates, as well, that the parameter set stated in Table 4.4 is not appropriate.
Furthermore Figure 4.14 shows that there is an offset of approximately 80 μm between the two base materials to be joined. This indicates that the layout of the clamping device is not yet optimal. Therefore the clamping device is adapted to diminish this offset. The adapted clamping device has already been introduced in section 4.1.
Considering the results mentioned above, of the first tested parameter set, adaptations have to be derived for improving the quality of the brazed joint.
Based on these results, the following conclusions can be reached:

[7] Further information regarding how the spread diameter as well as the height are determined can be found in Appendix A.8

- The peak power (P) is too high, as ablation or fusing of the base material occurs, which violates the definition of brazing
- The heat input, which is determined by (P_{av}) and (v), is not optimal as the wetting of the brazing wire is poor (contact angle greater than 30°)
- The gap disappeared due to thermal expansion and deformation of the joint occurred, which also indicates that the parameter set is not appropriate

The two aspects, mentioned first, indicate that the peak power (P) has to be decreased by increasing the average laser power (P_{av}) to avoid ablation and to achieve a better wettability. For this the repetition rate (f) is kept as constant and the laser peak power (P) is decreased and the pulse length t_p increased respectively to obtain an increase in the average laser power (P_{av}) of 30 W. Furthermore both feed speeds are exactly adapted to the previously mentioned ratio of 2:1. The adapted parameter set is shown in Table 4.5.

Table 4.5.: Adapted parameter set for brazing

P (W)	t_p (ms)	f (Hz)	P_{av} (W)	F (mm)	v_b ($\frac{mm}{min}$)	v ($\frac{mm}{min}$)	d_{gap} (mm)
4000	0.9	50	180	+10	200	100	0.1

After brazing the joint is cut at 55 mm and a polished micrograph section is carried out, which is shown in Figure 4.15.

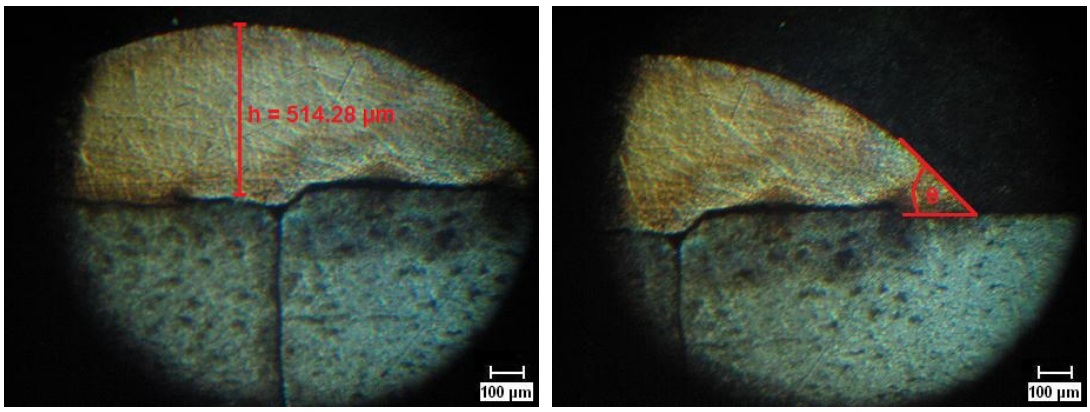

(a) Polished micrograph section of brazed butt joint from the adapted parameter set

(b) Polished micrograph section of the brazed butt joint showing the contact angle

Figure 4.15.: Parameters for brazing: P = 4,000 W, t_p = 0.9 ms, f = 50 Hz, P_{av} = 180 W, F = -10 mm, v = 120 $\frac{mm}{min}$, v_b = 200 $\frac{mm}{min}$, d_{gap} = 0.1 mm; a) Polished micrograph section of brazed butt joint from the adapted parameter set where the height (h) of 514.28 μm is indicated; the spread diameter (2A) could not be fully displayed and therefore not indicated, but (2A) is measured to 2178.57 μm ; b) With the height (h) and the spread diameter (2A) the contact angle corresponds to 50.55° by using equation 3.15

As it can be seen in Figure 4.15a the spherical cap height (h) decreased to 514 μm and the spread diameter (2A) is 2178.57 μm. By using equation 3.15 the contact angle corresponds to 50.55° (see Figure 4.15b). With regard to the contact angle, of the first test, the contact angle of this brazed joint improved, but it is not still appropriate and does not fulfill the quality measure of $< 30°$.

Furthermore Figure 4.15a clearly shows that the ablation or fusing is eliminated. Therefore the assumption that the ablation or fusing, caused by the high peak power, is verified.

As indicated in Table 4.5 the initial gap width (d_{gap}) is 0.1 mm. But at the location of 55 mm the gap disappeared as well due to thermal expansion. However the thermal expansion decreased compared to the first test, since no deformation of the base materials across the joint can be recognised (see Figure 4.15a). But deformation still occurred over the length of the joint.

Comparing the result of the adapted parameter set with the first one an improvement is clearly recognisable, even if the quality standards are not yet fulfilled.

In addition it is observed during these tests that the wetting of the brazing wire onto the base material increases over the length of the brazed joint. This behaviour indicates that the heating is improper at the beginning of the brazing process. Since

the temperature measurement set up implementation is complete for the testing of the adapted parameter set, Figure 4.16[8] shows a typical temperature profile of the adapted parameter set.

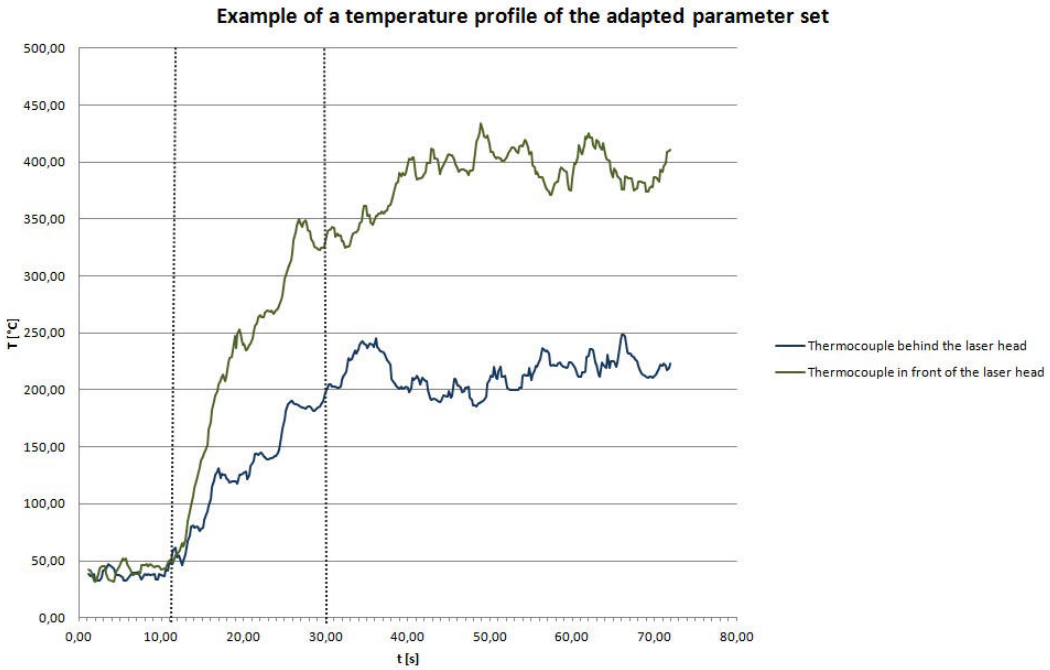

Figure 4.16.: Example of a typical temperature profile of a brazed joint based on the adapted parameter set (P = 4,000 W, t_p = 0.9 ms, f = 50 Hz, P_{av} = 180 W, F = -10 mm, v = 120 $\frac{mm}{min}$, v_b = 200 $\frac{mm}{min}$, d_{gap} = 0.1 mm); the first dotted line indicates when the brazing process started and the second dotted line indicates when a more sufficient operating temperature for brazing is reached; displacement of thermocouples from the joint: behind the laser app. 1.5 mm, in front of the laser approx. 4 mm

The first dotted line (t = 10 s) in Figure 4.16 indicates when the brazing process actually started and the second dotted line (t = 30 s) indicates when a proper operating temperature for the brazing process is reached. For this reason Figure 4.16 clearly shows that the heating at the beginning of the joint is inadequate, since the correct operating temperature for the brazing process is reached at 30 s. This corresponds to the observed wetting behaviour of the brazing wire, as the wetting of the brazing wire onto the base material increases over the length of the brazed joint. This time frame of

[8] It should be regarded that the duration of the temperature profiles do not always correlate exactly with the used feed speeds, since the temperature measurement is manually stopped. Furthermore for all presented temperature profiles a moving average of 5 values is used.

20 s corresponds to a distance of approximately 33 mm with regard to the feed speed of the base material (v) (see Table 4.5). Next to the reasons stated in chapter 4.2.1.1 for the importance of a temperature measurement set up, it can be added that it is also important to achieve and ensure a constant operating temperature over the length of the brazed joint.
From these initial experiments, the following conclusions can be made that have to be further investigated:

1. The heat input, which is determined by (P_{av}) and (v), is not optimal as the wetting of the brazing wire is poor (contact angle greater than 30°)

2. An appropriate operating temperature should be obtained at the beginning of the laser brazing process

3. The gap disappeared due to thermal expansion and deformation of the joint occurred, which also indicates that the parameter set is not appropriate

To point 1.:
The insufficient wettability can be originated from too high process speeds (v, v_b), i.e. that the material flow (brazing wire and base material) that is supposed to be melted, or heated respectively, is too high for the respective average power. This described cause can be summarised by an insufficient heat input, as the heat input is dependent on both the average laser power and the feed speed of the base material (see equation (4.4)).
Furthermore the selected laser spot size can also have an influence on the wettability with regard to the feed speeds, since the brazing wire can only wet onto the area of the heated base material (Jacobson and Humpston, 2005). If the temperature gradient between melted brazing wire and base material is too high, poor or no wetting of the brazing wire occurs.
To point 2.:
To achieve an appropriate operating temperature at the beginning of the brazing process, a pre-heating is needed. This pre-heating is realised by the introduction of two delay times (WZD) and (WZL) (see section 3.1.2.3). This pre-heating was implemented into the setup (see section 4.2.3).
To point 3.:
The characteristic of disappearing gap width and deformation of the joint indicate

that the laser brazing process itself might be too slow. However, as this matter contradicts point 1., these characteristics are neglected at this point and further investigated in the parameter studies.

Further testing was carried out with regard to point 1., while the pre-heating was implemented into the setup. For all tests carried out the gap width and the repetition rate were kept constant to d_{gap} = 0.1 mm and f = 50 Hz.
These tests showed that the spot size (d) has to be increased by increasing the focal position (F) to +13 mm. This leads to a spot size (d) of 2.8 mm by using equation (3.2). The increase in spot size is needed due to the disappearing gap width, so that the brazing wire has enough space to wet properly onto the surface of the base material. Along with this increase in spot size, the heat input has to be increased as well, since more material has to be heated. The adaptation was realised by decreasing both the average laser power and the feed speed of the base material. It was found by these tests that an average power of 144 W and a feed speed of the base material of 95 $\frac{mm}{min}$ result in an adequate heat input.
Moreover, the implementation of pre-heating, mentioned above, refers to the implementing of the delay time (WZD). The delay time (WZL), which introduces a delay between starting the laser and starting the brazing process, could be directly implemented into the respective NC-program. Therefore, testing was carried out as well with regard to (WZL). Results showed that a delay time (WZL) of 3.5 s seems to be appropriate for pre-heating.
The parameters determined by these tests are presented in Table 4.6.

Table 4.6.: Initial experiments: summary of appropriate parameters

P (W)	t_p (ms)	f (Hz)	P_{av} (W)	F (mm)	v_b ($\frac{mm}{min}$)	v ($\frac{mm}{min}$)	d_{gap} (mm)	WZL (s)
3600	0.8	50	144	-13	178	95	0.1	3.5

After completion of the pre-heating implementation, the parameters stated in Table 4.6 were used and the delay time (WZD) was tested by varying its value. As an example, Figure 4.17 shows the temperature measurement profiles of brazed joints with a (WZD) of 0.7 s, 2.5 s and 2.8 s. The dotted line in Figure 4.17 indicates when the delay time (WZL) ended.

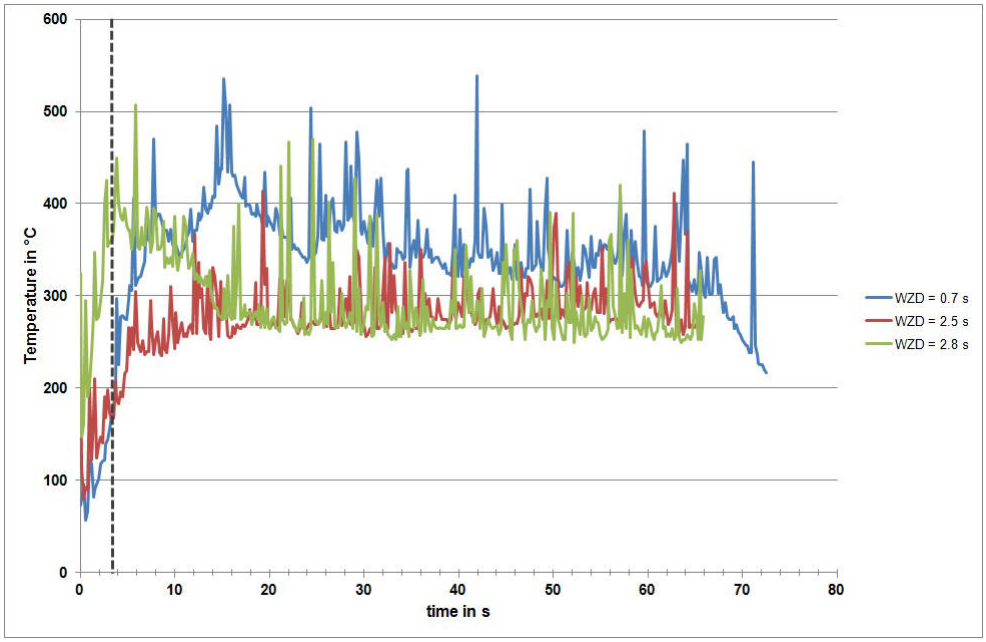

Figure 4.17.: Testing of the delay time (WZD): temperature measurement results presented from the thermocouple placed in front of the laser head; the dotted line indicates when (WZL) ended;Parameters for brazing: P = 3,600 W, t_p = 0.8 ms, f = 50 Hz, P_{av} = 144 W, F = -13 mm, v = 95 $\frac{mm}{min}$, v_b = 178 $\frac{mm}{min}$, d_{gap} = 0.1 mm , WZL = 3.5 s

As it can be seen in Figure 4.17, an appropriate operating temperature is achieved at the beginning of the brazing process and maintained throughout the process, if (WZD) is set to 2.8 s. The parameter set, stated in Table 4.6, is extended by this value of (WZD) (see Table 4.7).

Table 4.7.: Appropriate parameter set for laser brazing

P (W)	t_p (ms)	f (Hz)	P_{av} (W)	F (mm)	v_b ($\frac{mm}{min}$)	v ($\frac{mm}{min}$)	d_{gap} (mm)	WZL (s)	WZD (s)
3600	0.8	50	144	-13	178	95	0.1	3.5	2.8

Figure 4.18 shows a joint brazed with the parameter set stated in Table 4.7.

Figure 4.18.: Example of a brazed joint with pre-heating;Parameters for brazing: P = 3,600 W, t_p = 0.8 ms, f = 50 Hz, P_{av} = 144 W, F = -13 mm, v = 95 $\frac{mm}{min}$, v_b = 178 $\frac{mm}{min}$, d_{gap} = 0.1 mm, WZL = 3.5 s, WZD = 2.8 s

This brazed joint was cut at 55 mm and a polished micrograph section was carried out, which is shown in Figure 4.19.

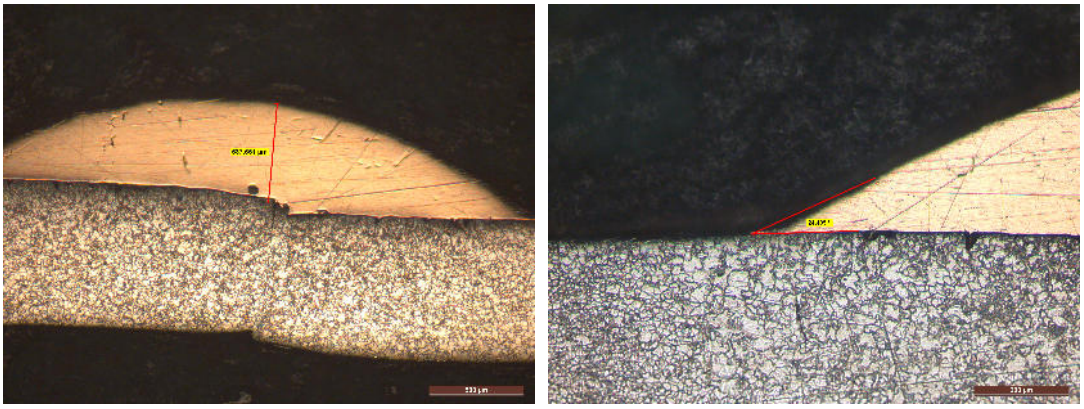

(a) Polished micrograph section of the brazed butt joint with an appropriate operating temperature

(b) Polished micrograph section of the brazed butt joint showing the contact angle

Figure 4.19.: Parameters for brazing: P = 3,600 W, t_p = 0.8 ms, f = 50 Hz, P_{av} = 144 W, F = -13 mm, v = 95 $\frac{mm}{min}$, v_b = 178 $\frac{mm}{min}$, d_{gap} = 0.1 mm, WZL = 3.5 s, WZD = 2.8 s; a) Polished micrograph section of brazed butt joint where the height (h) of 537.65 μm is indicated; the spread diameter (2A) could not be fully displayed and therefore not indicated, but (2A) is measured to 3416.29 μm ; b) With the height (h) and the spread diameter (2A) the contact angle corresponds to 34.94 $^\circ$ by using equation 3.15; the contact angle is also measured with the provided software tool of the microscope and corresponds to 24.41 $^\circ$ by considering the total spread of the brazing wire

In Figure 4.15a the spherical cap height (h) is shown as 537.65 μm and the spread diameter (2A) is 3416.29 μm. By using equation 3.15 the contact angle is calculated to be 34.94 $^\circ$ (see Figure 4.19b). The contact angle is also measured with the software tool provided with the microscope and corresponds to 24.41 $^\circ$. The deviation between the calculated and the measured contact angle can be reasoned by the assumptions made for equation 3.15 with specific regard to the spherical cap and the approach of the Pythagorean Theorem (see section 3.2.1.2). For this reason the measured value for the contact angle is taken as adequate quality. Therefore this parameter set presented fulfils the quality standard regarding the contact angle, since it is less than 30 $^\circ$. In Figure 4.19b "pegs" of brazing wire into the base material can be seen (for an enlarged view see Figure 4.20).

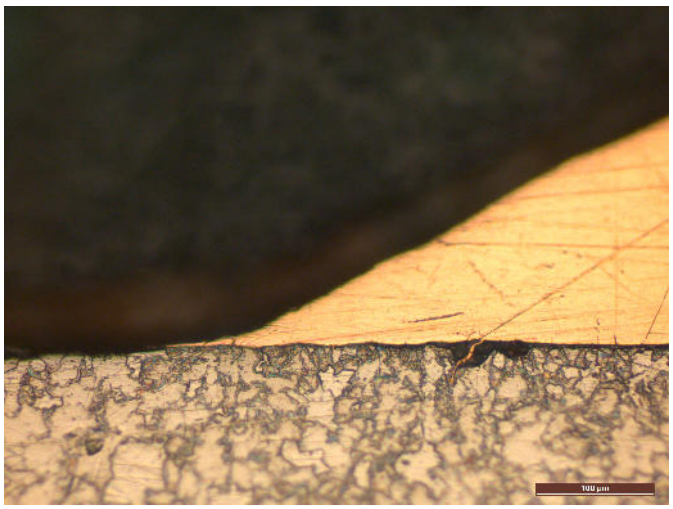

Figure 4.20.: Polished micrograph section of brazed butt joint with an appropriate operating temperature - enlarged view of Figure 4.19b; Parameters for brazing: P = 3,600 W, t_p = 0.8 ms, f = 50 Hz, P_{av} = 144 W, F = -13 mm, v = 95 $\frac{mm}{min}$, v_b = 178 $\frac{mm}{min}$, d_{gap} = 0.1 mm, WZL = 3.5 s, WZD = 2.8 s

These pegs develop during the brazing process due to the fast diffusion of the copper along the grain boundaries of the steel base material. This leads to intercrystalline material separations in the tensioned material as long as the brazing wire is melted, the so-called brazing wire-brittleness (see section 3.2.1.3) (Fritz and Schulze, 2006). Due to this brazing wire-brittleness, small parts of the base material miss (see blackish surrounding of the peg), since they broke as the brazed joint was manually cut for the preparation of a polished micrograph section. The very thin line between the base material and the brazing wire is assumed to be the alloy zone consisting of primary crystals, since it was verified that it did not correspond to cracks, when the focal position of the microscope was changed. These last mentioned aspects also need to be further investigated.

While carrying out these initial experiments, it was observed that the wire positioning can have an influence on the brazing result. Figure 4.21 also shows a joint brazed with the parameter set stated in Table 4.7.

Figure 4.21.: Example of brazed joint regarding wire positioning; Parameters for brazing: P = 3,600 W, t_p = 0.8 ms, f = 50 Hz, P_{av} = 144 W, F = -13 mm, v = 95 $\frac{mm}{min}$, v_b = 178 $\frac{mm}{min}$, d_{gap} = 0.1 mm, WZL = 3.5 s, WZD = 2.8 s

This example indicates that depending on the initial wire positioning a brazed joint is obtained either as shown in Figure 4.21 or as presented in Figure 4.18. This aspect also needs to be further investigated.

4.5. Quality control system

Quality control is subdivided into destructive and non-destructive methods. The destructive quality control comprises methods such as tensile testing, impact testing and polished micrograph sections.
Receiving all information of these test methods, a good measure for the quality of brazed joints is achieved. However, these destructive test methods are only carried out on random samples in production. For this, they are a measure for the general quality of brazed joints, but failures during production can still occur and might be undiscovered.
For this reason, non-destructive quality control gains more and more importance, since it can be implemented within the production with little disturbance of the production process concerning time needed and reduced production of scrap (see section 2.3).
Therefore, a non-destructive quality control system using a laser-triangulation sensor was implemented within the Nd:YAG laser work station.
Laser-triangulation sensors are commercially available for different measurement ranges ranging from micrometres up to a few meters. For this setup a laser-triangulation sensor M7L/0,5 of the company MEL Mikroelektronik is used.
The laser-triangulation sensor M7L/0,5 used has a measurement range of 250 μm and a resolution of 0.2 μm. More technical details can be found in the data sheet in Appendix D.5.
It should be mentioned that the accuracy of measurement is dependent on the reflectivity of the workpiece (Hochschule Hof, 2009). For this reason a test rig was designed to test if the laser triangulation sensor is capable of detecting useful measurement signals from technical surfaces.
These tests clearly showed that a continuous measurement signal is detected throughout the measurement. Therefore, the laser triangulation sensor is evaluated positively and will be used for the quality control system and implemented into the Nd:YAG laser work station.
The realisation regarding adaptation of an existing software program and implementation into the work station is described in the following subsections.

4.5.1. Adaptation of the software program “LNS_QS_V2“

The existing program "LNS_QS_V2" was adapted to the new application for quality control. However, before going into detail regarding adaptation, the original application for which it was designed is introduced.
With the aid of "LNS_QS_V2" surface finishes of measurement samples are detected by means of an optical sensor. These collected data are transferred to the program, evaluated regarding voltage correspondent distance and displayed.
Depending on the selection of the user, the measurement can start via manual triggering or automatically. After each measurement, either single or continuous, the measurement signal is displayed on screen (Figure 4.22).
A detailed description of this software program can be found in the diploma thesis of Frank Buchmueller (Buchmüller, 2005). In the following, the requirements of the software program for the new application are described and its realisation can be found in Appendix B.4.

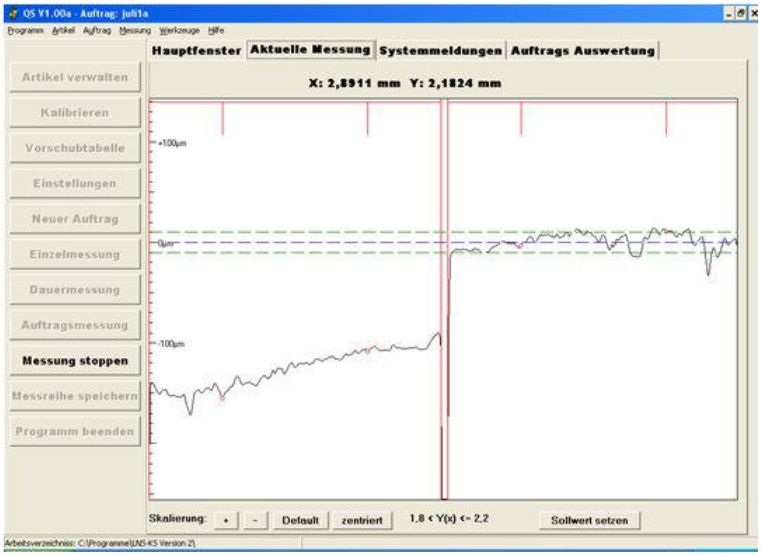

Figure 4.22.: Display of the measurement signals from, e.g. an autofocus sensor

Requirements for the software program to be adapted

In the following, the features that need to be implemented into the existing software program "LNS_QS_V2" are introduced.

The software is supposed to collect the transferred data from the laser-triangulation sensor, evaluate the data concerning the voltage correspondent distance and display the surface finish of the base materials. The base materials used are 30 mm x 110 mm in size, which are fixed via the specially designed clamping device (Figure 4.23).

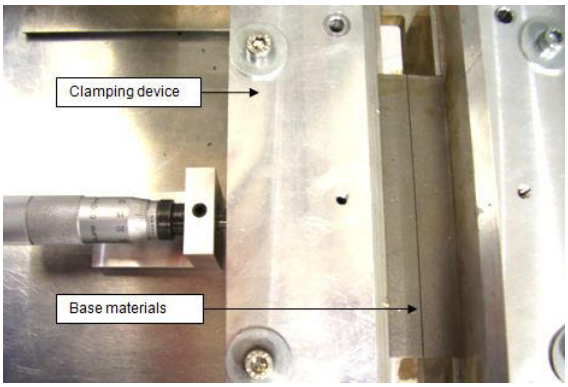

Figure 4.23.: Base materials fixed via clamping device

Since the size of the base materials can vary, the length of the samples shall be possible to enter in the program.
To detect the edges of the scanned base material, a length in front of the sample as well as behind the sample shall be entered which are then added to the whole measurement length (Figure 4.24). With this approach it is possible to display the measurement signal in the middle of the screen.

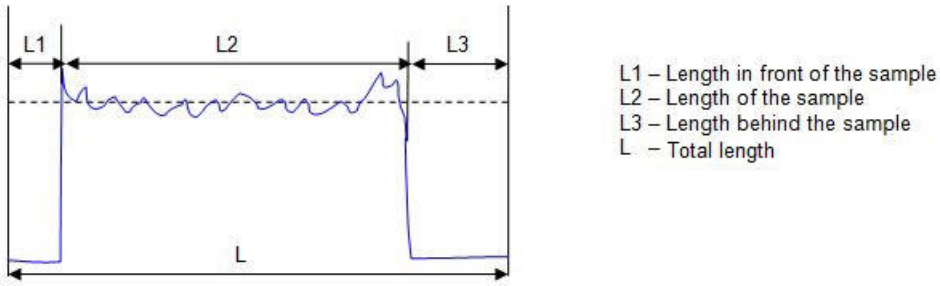

Figure 4.24.: Definition of the lengths to be entered into the software program

Furthermore, the quality control setup will be implemented within the Nd:YAG laser work station. The laser-triangulation sensor is supposed to be mounted to the z-axis. The base material to be scanned is then moved below the sensor, since the clamping device is mounted onto the x-axis. The axes can be moved via the CNC unit. There the velocity can be entered in mm/min. For this reason, the program needs to be adjusted regarding the entry of the velocity with which the base materials are moved instead of the entry of measurement time, because it is more users friendly. If the lengths and the velocity can be entered, the measurement time can be calculated, which is needed for further internal processing.
Moreover, the measurement shall either start automatically or by the usage of the above mentioned trigger sensor.
Additionally it should be possible to store and load the carried out measurement with its corresponding settings regarding settings of the filters, entered length and velocity.
For further processing of the measurement data (just detected or reloaded) an export of the data to Excel shall be realised.
In the following the requirements of the software to be adapted are summarized for clarity:

- Entry of lengths
- Entry of scanning velocity
- Start of measurement: either automatically or via trigger
- Storage and loading of the measurement data and its corresponding settings
- Export to Excel

The software is adapted according to the requirements stated above. The realisation of this adaptation can be found in Appendix B.4.

4.5.2. Implementation into the Nd:YAG - laser work station

To implement the laser triangulation sensor into the work station the following requirements have to be fulfilled:

- Independent adjustment of the sensor along the z - axis
- Fine adjustment along the z - axis as well as along the y - axis

The sensor is mounted to the z-axis of the work station. To protect it during the brazing process due to the high temperatures an independent adjustment along the z-axis is needed. This is realised via two slot holes, which corresponds to a coarse adjustment. For realising also a fine adjustment of the z-axis a linear axis is mounted onto the coarse adjustment. This is needed for calibrating the sensor onto the surface of the base material. To scan at different positions along the y-axis, e.g. at both base materials, brazed joint, a linear axis is used for an easy adjustment. The fixture of the laser triangulation sensor is shown in Figure 4.25a before the implementation into the work station. To apply the fixture to the z-axis a connection plate is needed to implement the sensor into the work station, which can be seen in Figure 4.25b.

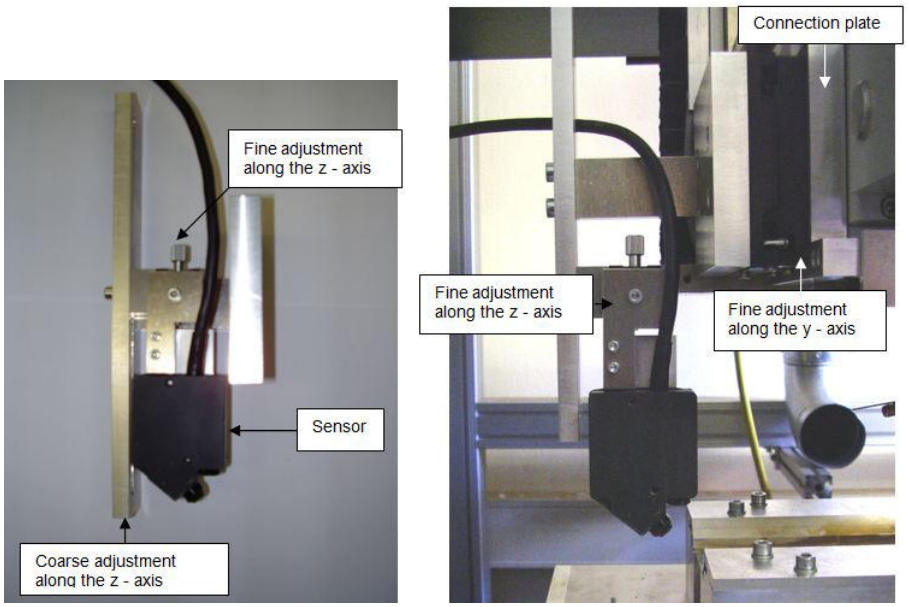

(a) Fixture of the laser - triangulation sensor

(b) Implementation of the laser - triangulation sensor into the Nd:YAG laser work station

Figure 4.25.: a) Fixture of the laser - triangulation sensor; b) Implementation of the laser - triangulation sensor into the laser work station

The mechanical drawings of this fixture can be found in the appendix D.5. Figure 4.26 shows a typical example of a measured profile of the base material after the brazing.

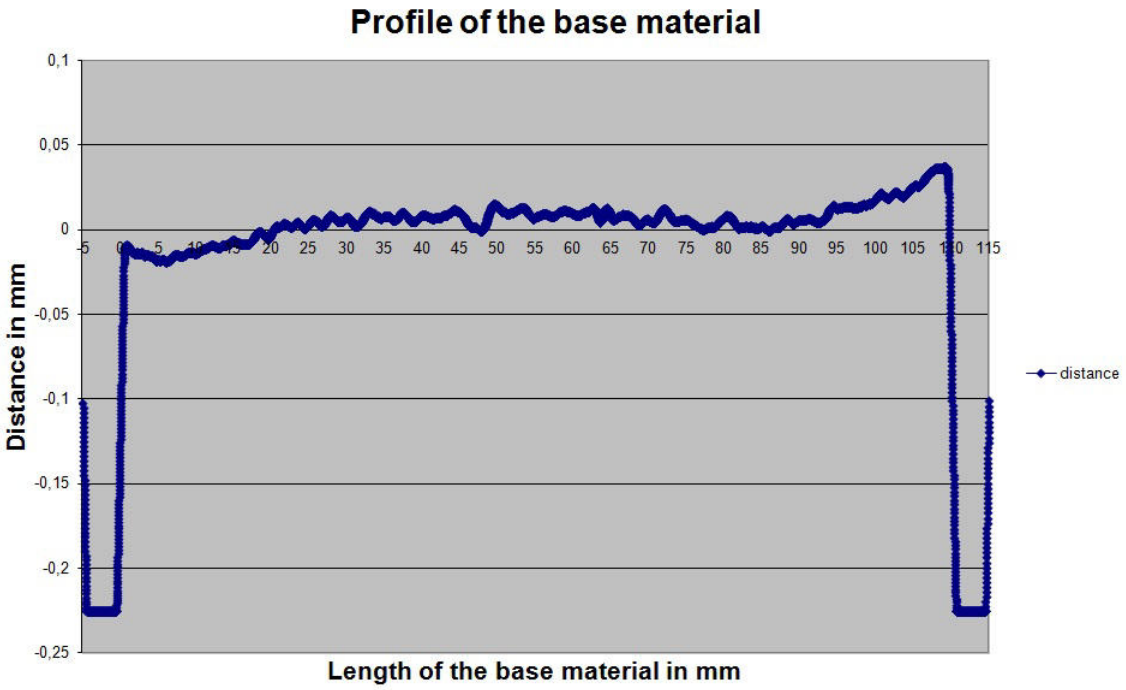

Figure 4.26.: Typical measured profile of a joint brazed with P = 2000 W, t_p = 2 ms, f = 50 Hz, v = 120 $\frac{mm}{min}$, v_b = 120 $\frac{mm}{min}$; this profile was measured with a speed of 600 $\frac{mm}{min}$ and a measurement frequency of 1000 Hz; the respective filters (median and mean) are set to 100 measurement values; the measurement time corresponds to 12 s

As it can be seen, the base material deforms due to the heat induced tensions. This is especially recognisable at the end of the base material, since there the heat accumulation takes place.

4.6. Summary

A test rig consisting of a laser brazing setup as well as a temperature measurement and wire feed control, was designed, so that it can be implemented into both laser work stations: diode and Nd:YAG.

Furthermore, the materials used for laser brazing were presented. As base material the mild cold-rolled steel DC01 was used. Throughout this research its dimensions were 0.8 mm * 30 mm * 110 mm. $CuSi_3$ was used as brazing wire with a diameter of 0.8 mm. The base material was cleaned for all experiments, as described in section 4.3.3. For all experiments carried out within this research, a joint of 100 mm was produced.

The initial experiments, carried out with the Nd:YAG laser, showed that pre-heating is necessary to obtain a qualitatively good brazed joint and led to the following aspects that need to be further investigated:

- The wire positioning, as it was observed to have an influence on the brazing result
- The characteristics of the disappearing gap width and deformation
- the ratio between feed speed of brazing wire and feed speed of base material, as opinions deviate in literature. For these tests this ratio was set to 2:1
- The influence of the pre-heating phase, which is defined by the two delay times (WZL) and (WZD), to the brazing result.
- Alloy zone formation, as it could not be clearly identified by the optical inspection of polished micrograph sections via a microscope.

The parameter set that results in a qualitatively good brazed joint for Nd:YAG laser brazing is presented in Table 4.8.

Table 4.8.: Appropriate parameter set for Nd:YAG laser brazing

P (W)	t_p (ms)	f (Hz)	P_{av} (W)	F (mm)	v_b ($\frac{mm}{min}$)	v ($\frac{mm}{min}$)	d_{gap} (mm)	WZL (s)	WZD (s)
3600	0.8	50	144	-13	178	95	0.1	3.5	2.8

A quality control system, based on a laser triangulation sensor, was designed and implemented into the Nd:YAG laser work station. Tests showed that deformation over the length of the joint can be measured with this device.

Chapter 5.

Parameter studies with the Nd:YAG laser

Based on the observations made during the initial experiments, carried out with the Nd:YAG laser (see section 4.4), 5 aspects were identified that need to be further investigated, as they seem to have an influence on the brazing result. Within this chapter the first two aspects are further investigated with regard to their influence on the brazing result, which are:

- The wire positioning, as it was observed to have an influence on the brazing result
- The characteristics of the disappearing gap width and deformation

Furthermore, the influence of the repetition rate (f) is investigated with regard to the surface condition of brazed joints. For all experiments carried out within these parameter studies, the materials were used and prepared as described in section 4.3 and studies, the materials were used and prepared as described in section 4.3 and a brazed joint,100 mm long, was always used. The appropriate parameter set used for investigating the wire positioning as well as the characteristics of gap width and deformation can be found in Table 4.8.

5.1. Influence of the wire position also within the laser spot

During the initial experiments that were carried out (see section 4.4) it was observed that the wire position, as well as within the laser spot, can have an influence on the brazing result. For this reason, this aspect is further investigated within this section by using the parameter set stated in Table 4.8.

5.1.1. Influence of the wire position itself

For the brazing setup in the Nd:YAG laser work station a front wire feed was realised. The principle of front feeding is shown in Figure 5.1a.

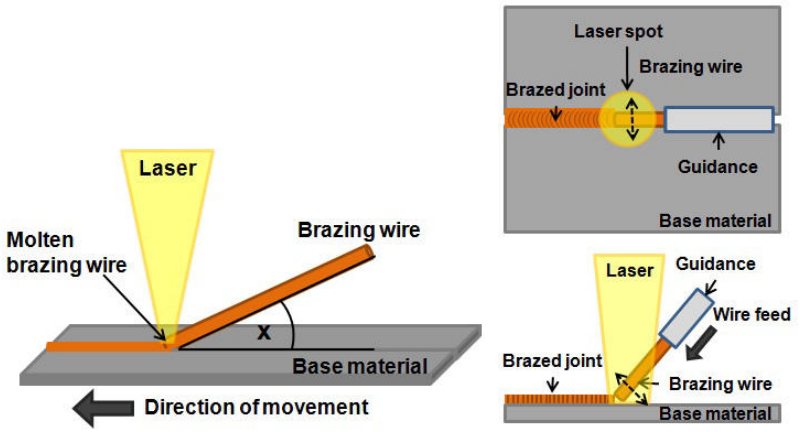

(a) Laser brazing with front feed

(b) Occurrence of wavy brazed joints for large incidence angles of the brazing wire

Figure 5.1.: a) Schematic diagram of laser brazing with front feed; "x" corresponds to the incidence angle of the brazing wire; b) Top and lateral view for the occurrence of wavy brazed joints for large incidence angles of the brazing wire due to oscillations of the wire, which are indicated by the dotted arrows

For front feeding, the brazing wire is fed from ahead of the laser beam into the laser spot with regard to the direction of movement. There the brazing wire encloses an incidence angle with the base material, which is marked with an "x" in Figure 5.1a. As mentioned in section 4.1, one requirement for the wire feeder is the adjustment of the incidence angle for the brazing wire. Therefore several incidence angles of the brazing wire were tried prior to testing the wire position within the laser spot. The incidence angle is adjustable in the range of approximately 40° up to 55°. This is because

of the dimensions of the wire feeder and the distance between it and the clamping device. This distance is also significantly dependent on the required focal position (F) and therefore spot size: The larger the spot size the smaller the distance between clamping device and wire feeder. Since a focal position (F) of -13 mm is required (see Table 4.8) the adjustment of the incidence angle is limited to the above stated range. Testing was carried out over this range, beginning with maximum incidence angle and then subsequently decreased. For large incidence angles (above app. 47°) it was observed that, depending on the wire position within the laser spot (see section 5.1.2), the surface of the brazed joint was visibly wavy instead of smooth. This was when the brazing wire was placed loosely onto the base material (see Figure 5.2 (Left)). The waviness could be caused by the occurrence of the following aspects: improper heating as well as oscillations of the brazing wire.

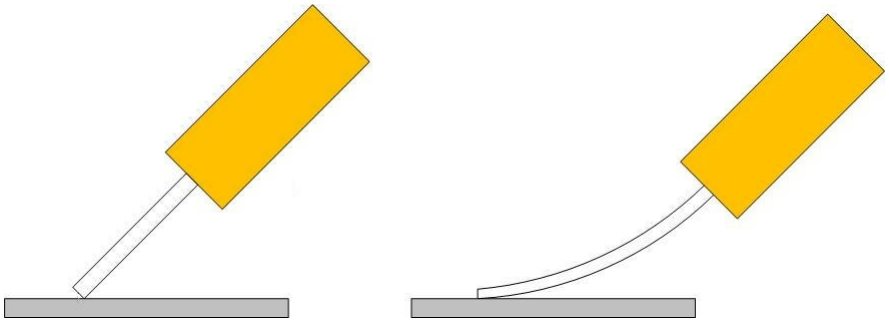

Figure 5.2.: Principle of wire positioning onto the base material; Left: Wire is loosely placed onto the base material; Right: Wire is slightly pressed onto the base material, so that it bends a little

Improper heating occurs, when the brazing wire encloses an incidence angle with the base material (see Figure 5.2 (Left), or Figure 5.1a respectively). Therefore the brazing wire only has minor contact with the base material. It covers the base material to its point of impact from the incident laser radiation. This gap between brazing wire and base material, as well as the coverage, can lead to improper heating. This also depends upon the wire positioning within the laser spot. For detailed information regarding this aspect, please refer to section 5.1.2.

With regard to the oscillations, the brazing wire is fed via the wire guidance tube to the brazing process (see section 4.1) and this guidance ends approximately 10 mm - 12 mm in front of the brazing process. This can lead to slight oscillations of the brazing

wire for every step of the wire feed, if the brazing wire is placed loosely onto the base material (see Figure 5.2 (Left)) and the brazing wire is not guided over the distance of up to 12 mm. The incident oscillating brazing wire reaches the brazing process, where the brazing wire is already molten. There it takes portions of the molten brazing wire and distributes it according to its oscillatory action resulting in a visibly wavy brazed joint (see Figure 5.1b).
Figure 5.3 shows a typical example of a brazed joint, with a loose wire placement.

Figure 5.3.: Typical example of a brazed joint with a loose wire placement onto the base material; Figure 5.4 shows an enlarged view of the white rectangle; Parameters for brazing: P = 3,600 W, t_p = 0.8 ms, f = 50 Hz, P_{av} = 144 W, F = -13 mm, v = 95 $\frac{mm}{min}$, v_b = 189.2 $\frac{mm}{min}$, d_{gap} = 0.1 mm, WZL = 3.5 s, WZD = 2.8 s

The white rectangle in Figure 5.3 indicates the part of the joint which is shown in enlarged in Figure 5.4.

Figure 5.4.: Enlarged view of the white rectangle shown in Figure 5.3; Parameters for brazing: P = 3,600 W, t_p = 0.8 ms, f = 50 Hz, P_{av} = 144 W, F = -13 mm, v = 95 $\frac{mm}{min}$, v_b = 189.2 $\frac{mm}{min}$, d_{gap} = 0.1 mm, WZL = 3.5 s, WZD = 2.8 s

The waviness of the brazed joints can be decreased or completely eliminated, if the incidence angle is decreased to approximately 45° or less depending on how the brazing wire is placed onto the base material in the first place. If the wire is placed

loosely onto the base material as shown in Figure 5.2 (Left), the waviness can be decreased, since the fed in brazing wire is partially guided via the gap between the base materials, which diminishes the oscillations. However, if the wire is slightly pressed onto the base material, so that it bends a little (see Figure 5.2 (Right)), the waviness can be completely eliminated. Using this guidance technique the brazing wire is controlled by the gap and therefore no oscillations can occur. Furthermore, this approach ensures that the wire is fed in under a very small angle at the beginning of the brazing process. While brazing the wire is fed into the brazing area at the beginning of the molten brazing wire resulting in a visibly smooth brazed joint.

5.1.2. Influence of the wire position within the laser spot

For laser brazing the wire is manually placed onto the base material. This is done by first giving a single laser shot onto the base material for orientation purposes and subsequently using the implemented microscope of the Nd:YAG laser work station for positioning the wire.
After clarifying a suitable incidence angle of less than 45° as well as the wire positioning itself (see Figure 5.2 right), the influence of the wire position within the laser spot is investigated. For this, three positions can be differentiated as shown in Figure 5.5: trailing, center and leading, which are examined in the following.

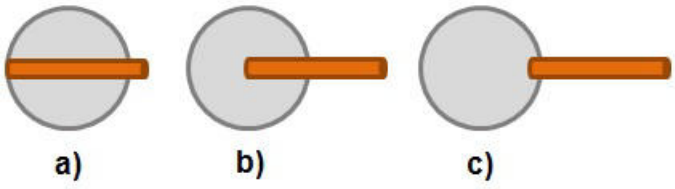

Figure 5.5.: Top view of brazing wire positioning within the laser spot: a) Wire position at the trailing edge of the laser spot; b) Wire is positioned at the center of the laser spot; c) Wire position at the leading edge of the laser spot

Trailing position

If the wire is placed exactly at the trailing edge (see Figure 5.5 (a)) of the laser spot, it was observed that no actual brazed joint is obtained with the parameter set stated

in Table 4.8. Figure 5.6 shows two typical examples of the brazing result, if the brazing wire is placed at the trailing edge of the laser spot.

Figure 5.6.: Typical brazing result for positioning the wire at the trailing edge; Parameters for brazing: P = 3,600 W, t_p = 0.8 ms, f = 50 Hz, P_{av} = 144 W, F = -13 mm, v = 95 $\frac{mm}{min}$, v_b = 189.2 $\frac{mm}{min}$, d_{gap} = 0.1 mm, WZL = 3.5 s, WZD = 2.8 s

This result, presented in Figure 5.6, can be reasoned by improper heating. The brazing wire has a diameter of 0.8 mm (see section 4.3.2) and the focal position (F) is -13 mm, which corresponds to a spot size (d) of 2.8 mm by using equation 3.8. As the brazing wire is placed centrally across the laser spot by enclosing an incidence angle with the base material, it has on the one hand no contact with the base material at the center of the laser spot and on the other hand it covers the base material across the laser spot. Therefore the main part of laser radiation hits the brazing wire and only a minor part reaches the base material with regard to the Gaussian intensity distribution of the laser beam. This gap between brazing wire and base material, in combination with the coverage of the base material at the center of the laser spot, results in improper heating.

This improper heating is also influenced by the reflection losses of the laser radiation at the brazing wire. The brazing wire has an an absorptance of approximately 4 % for Nd:YAG laser radiation (see section 4.3.2). For this reason major parts of the laser radiation are reflected, especially if the brazing wire is positioned at the trailing edge of the laser spot. This description explains what happens at the beginning of the brazing process. When the pre-heating phase ends, the base material is heated insufficiently and the brazing wire is molten. At this point it cannot wet properly onto the base material due to the high temperature gradient between brazing wire and base material (Jacobson and Humpston, 2005).

Center position

If the wire is placed at the center of the laser spot (see Figure 5.5 (b)) it was observed that it results in an appropriate brazed joint (see Figure 5.7).

Figure 5.7.: Example of a brazed joint with correct wire positioning; Parameters for brazing: P = 3,600 W, t_p = 0.8 ms, f = 50 Hz, P_{av} = 144 W, F = -13 mm, v = 95 $\frac{mm}{min}$, v_b = 189.2 $\frac{mm}{min}$, d_{gap} = 0.1 mm, WZL = 3.5 s, WZD = 2.8 s

This brazing wire positioning within the laser spot results in proper heating of both: brazing wire and base material. Due to the placement of the brazing wire at the center of the laser spot, it only covers half of the base material within the laser spot. Furthermore the brazing wire has contact with the base material at the center of the laser spot due to the wire positioning itself (see Figure 5.2 (Right)). For this reason the base material is heated properly, since approximately half of the incident laser radiation reaches it and the other half reaches mainly the brazing wire during the pre-heating phase. After this phase ends, the base material is heated sufficiently and the brazing wire is molten, which results in a brazed joint as presented in Figure 5.7.

Leading position

If the brazing wire is placed at the leading edge of the laser spot (see Figure 5.5 (c)) it was observed that no actual brazing process takes place with the parameter set stated in Table 4.8. This can be reasoned by improper heating, as explained in section 5.1.2 (Trailing position), only the other way around. If the brazing wire is positioned at the trailing edge of the laser spot, it does not reach the center of the laser spot, where the incident laser radiation is at its highest intensity due to the Gaussian distribution. Therefore, the main part of the incident laser radiation reaches the base material and only a minor part reaches the brazing wire. This leads to an improper heating during the pre-heating phase, since the base material is molten, which is a violation of the definition of brazing (see section 2.2.1.1), and the brazing wire does not reach its liquidus temperature (see Table 4.3). After the pre-heating phase, the base material is

partially welded and the brazing wire is not molten, so that no actual brazing result is obtained.

5.2. Characteristics of disappearing gap width and deformation

5.2.1. Characteristics of gap width in dependence on the location at the brazed joint

During the initial tests carried out with the Nd:YAG laser (see section 4.4), it was observed that the initial gap disappeared at the location of 55 mm, where the joint was cut to prepare a polished micrograph section.
The disappearance of the gap is an unfavourable characteristic as the sense of brazing is to join, for instance, two base materials by the aid of a filler metal to produce a strong joint if the gap is well filled (Jacobson and Humpston, 2005).
For this reason, this occurrence of disappearing gap width is further investigated. For the initial experiments, the gap width (d_{gap}) was set to 0.1 mm, since this is understood to be within the optimal range for laser brazing (see section 3.2.1.1). However, it was observed during these initial experiments that the gap disappears over the length of the brazed joint. Figure 5.8 (Left) shows a polished micrograph section of a joint brazed with the appropriate parameter set stated in Table 4.8. For this micrograph section, the joint was cut at the location 55 mm.

As it can be seen in Figure 5.8 (Left) the initial gap width of 0.1 mm is not recognisable anymore at this location. The enlarged view of the polished micrograph section (see Figure 5.8 (Right)) shows that the gap still exists at the upper part of the joined base materials and it disappears over the thickness of the base material. The existing gap is approximately 4 μm wide at this location. Furthermore, Figure 5.8 (Right) shows that the brazing wire is sucked into the gap due to the capillary filling pressure as described in section 3.2.1.1.
By visual inspection of a brazed joint with an initial gap width of 0.1 mm, the gap disappears approximately at the location of 10 mm to 15 mm. To better investigate this circumstance of the disappearing gap, the gap width (d_{gap}) is increased significantly into the area 0.5 mm and above, so that the brazed joints can be inspected optically by the aid of the Casio Exilim Ex-ZR100 12.1MPixel camera.

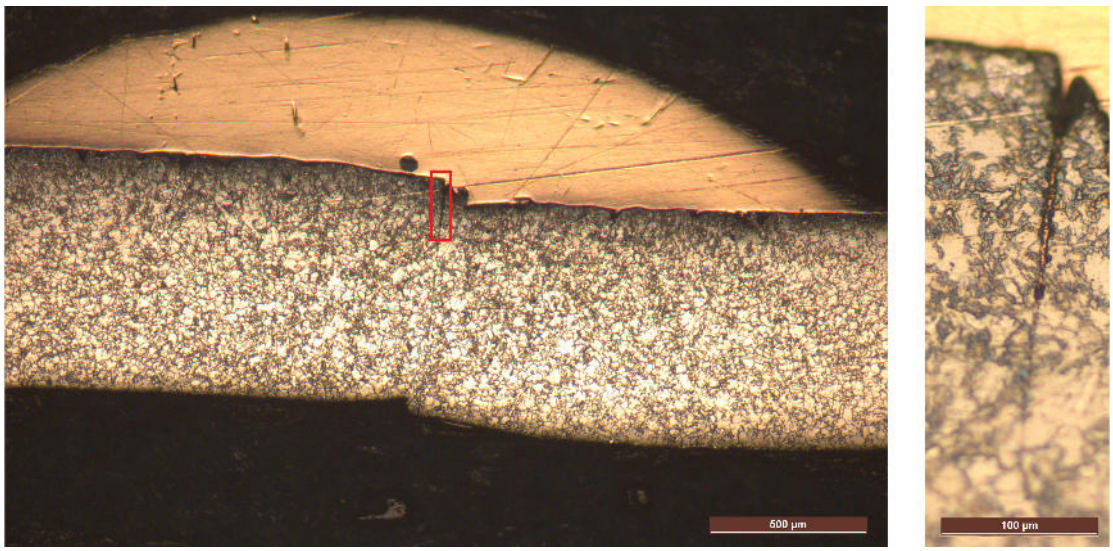

Figure 5.8.: Parameters for brazing: P = 3,600 W, t_p = 0.8 ms, f = 50 Hz, P_{av} = 144 W, F = -13 mm, v = 95 $\frac{mm}{min}$, v_b = 189.2 $\frac{mm}{min}$, d_{gap} = 0.1 mm, WZL = 3.5 s, WZD = 2.8 s; Left: Polished Micrograph section of the brazed joint; Right: Enlarged view of the red rectangle in the left image showing the gap and the sucked in brazing wire

For this, joints were brazed by using the parameter set stated in Table 4.8 with the following gap widths: 0.5 mm, 0.6 mm, 0.7 mm and 0.75 mm. To adjust the respective gap width a thickness gauge was used. Subsequently, each brazed joint was placed onto an even surface and a ruler was positioned onto the joint with a scale division of 0.5 mm. Then a close-up picture is taken of the respective joint with the camera. The scale division of the ruler was used to determine the relation between the unit length and pixel in the image.

Afterwards, the gap width was measured in 5 mm steps starting from the beginning of the brazed joint to where the gap width was not clearly recognisable anymore. Figure 5.9 shows typically the measurement locations of the gap width for the brazed joint with an initial gap width (d_{gap}) of 0.5 mm.

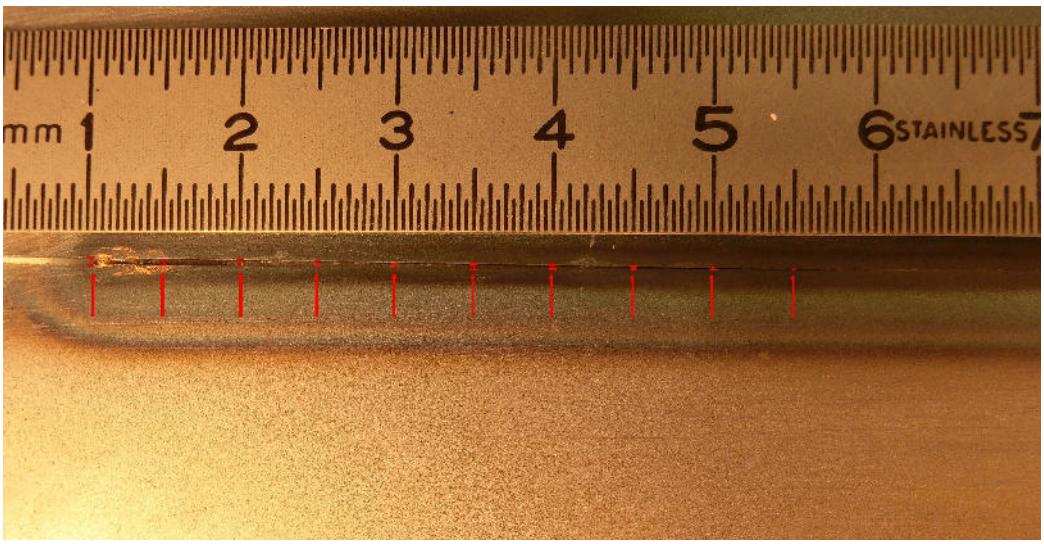

Figure 5.9.: Example of measuring the gap width dependent on its location at the brazed joint. The initial gap width of this joint is 0.5 mm; Parameters for brazing: P = 3,600 W, t_p = 0.8 ms, f = 50 Hz, P_{av} = 144 W, F = -13 mm, v = 95 $\frac{mm}{min}$, v_b = 189.2 $\frac{mm}{min}$, d_{gap} = 0.1 mm, WZL = 3.5 s, WZD = 2.8 s

A measurement tolerance of $\pm$ 4 pixel is taken into account for each measurement, which is transformed into the respective unit length. Figure 5.10 shows the measurement results of the gap width dependent on the location at the brazed joint.

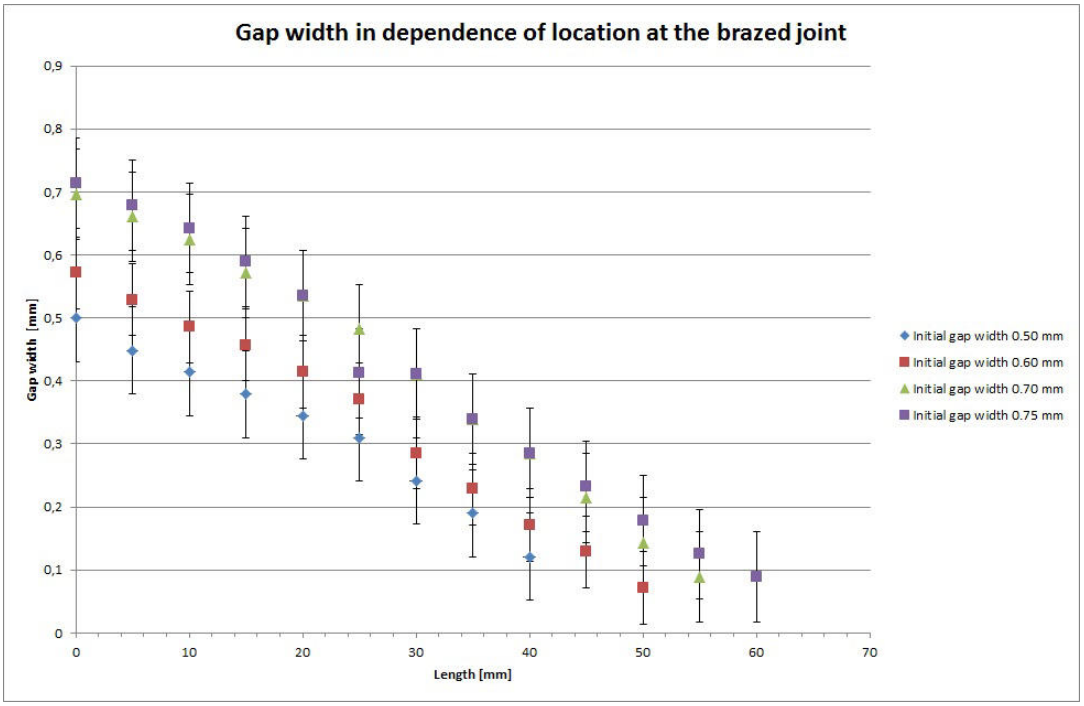

Figure 5.10.: Gap widths of brazed joints depending on their location at the brazed joint

As it can be seen in Figure 5.10, the gap width decreases linearly over the length of the brazed joint. This behaviour can be reasoned by the thermal expansion of the base materials due to heat conduction (Hornbogen, 1983). Since the spot size of the incident laser radiation is large compared to the heat penetration depth and the base material is assumed to be isotropic, the thermal expansion can be regarded one-dimensionally (Poprawe, 2005). The measurement of the gap widths (see Figure 5.10) clearly indicates a linear behaviour of the thermal expansion. For this reason the linear thermal expansion of the base materials can be estimated by (Stöcker, 2000):

$$\Delta l = l_0 \, \alpha \, \Delta T \tag{5.1}$$

With: Δl: Change in length
l_0: Initial length
α: Coefficient of linear expansion
ΔT: Temperature difference

with the assumption that the coefficient of linear expansion (α) is independent of temperature. Solving equation 5.1 for (ΔT), the temperature difference can be calculated, as the initial length is known (30 mm, see section 4.3.3) and the change in length (Δl) can be determined from the decrease in gap width. The coefficient of linear expansion for the base material (α_{steel}) corresponds to 11 * 10^{-6} K^{-1} at 25 °C (Stöcker, 2000). This calculation is exemplified for the brazed joint with an initial gap width of 0.75 mm, because for this joint the most measurements could be taken. The measured gap width at the location of 5 mm corresponds to 0.68 mm (see Figure 5.10). The change in length (Δl) of the base material is therefore:

$$\begin{aligned} \Delta l &= \frac{0.75\,mm - 0.68\,mm}{2} \\ \Delta l &= 0.035\,mm \end{aligned}$$

Using this change in length with equation 5.1, the temperature difference (ΔT) corresponds to 106.06 °C. These calculations are carried out for each measurement point of the brazed joint with an initial gap width of 0.75 mm. In Figure 5.11 the result is presented. Furthermore, the new length of base material for each measurement point is also included in Figure 5.11.

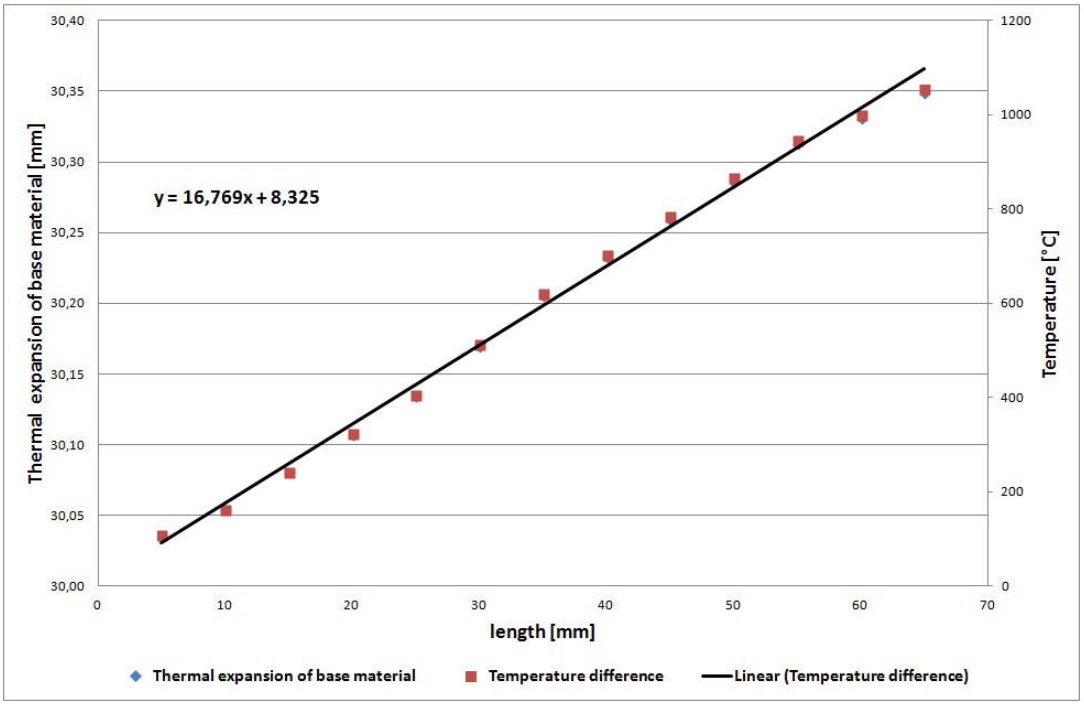

Figure 5.11.: Change in length of the base material as well as the temperature difference over the length of the brazed joint with an initial gap width of 0.75 mm

Figure 5.11 shows the constant increase in temperature over the length of the brazed joint due to heat conduction. This results in the thermal expansion of the base materials and therefore in a decrease in gap width.

To verify this method of optical inspection, the brazed joint, which has a total length of 100 mm and an initial gap width of 0.75 mm, was cut every 10 mm beginning at 15 mm up to 95 mm length of the brazed joint. For each cut a polished micrograph section was carried out and the respective gap width according to its location at the brazed joint was measured by using the microscope. Figure 5.12 shows the respective polished micrograph sections of the brazed joint.

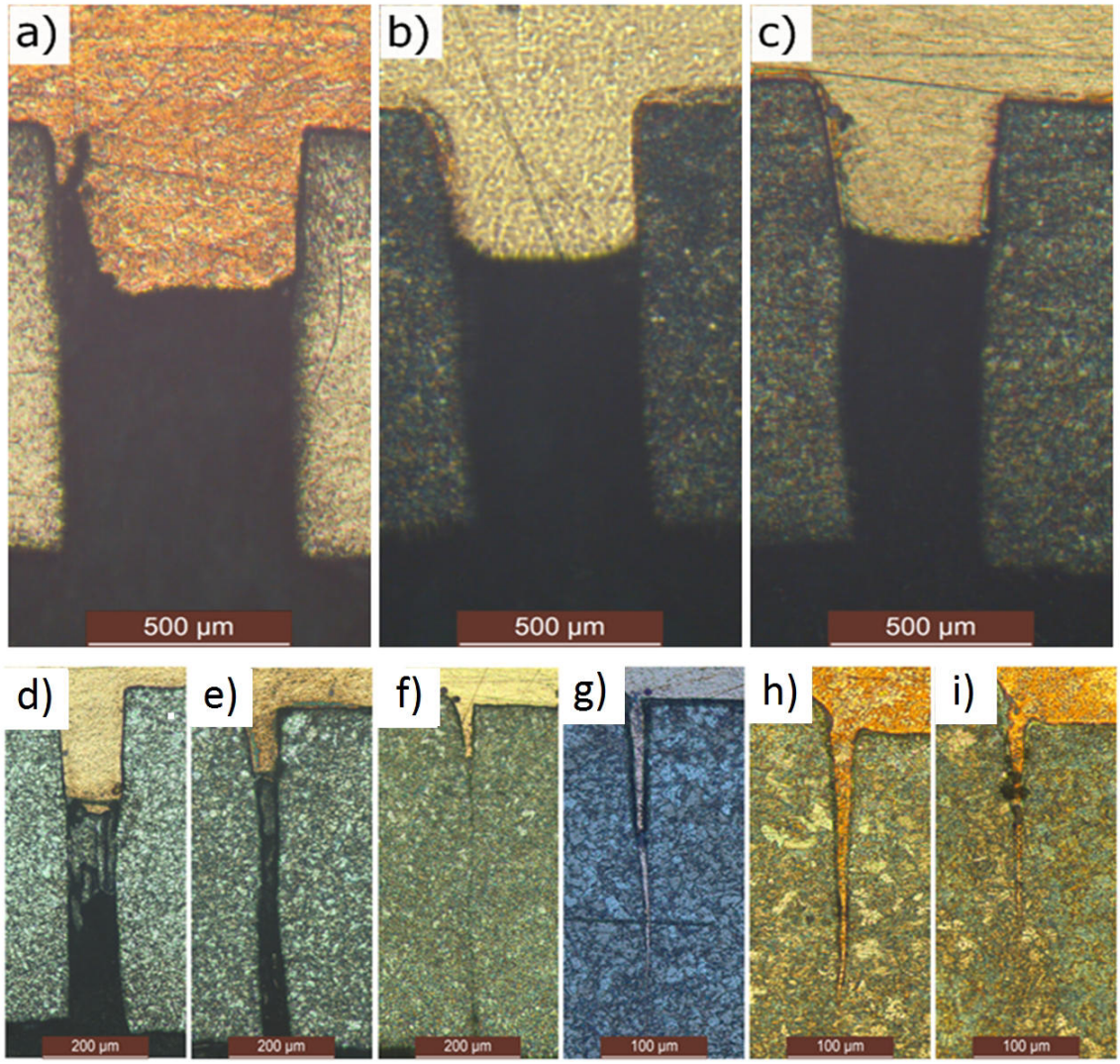

Figure 5.12.: Polished micrograph sections of the brazed joint with an initial gap width of 0.75 mm: a) Location: 15 mm, gap width: 0.525 mm; b) Location: 25 mm, gap width: 0.349 mm; c) Location: 35 mm, gap width: 0.275 mm; d) Location: 45 mm, gap width: 0.167 mm; e) Location: 55 mm, gap width: 0.084 mm; f) Location: 65 mm, gap width: 0.042 mm; g) Location: 75 mm, gap width: 0.021 mm; h) Location: 85 mm, gap width: 0.017 mm; i) Location: 95 mm, gap width: 0.025 mm; Parameters for brazing: P = 3,600 W, t_p = 0.8 ms, f = 50 Hz, P_{av} = 144 W, F = -13 mm, v = 95 $\frac{mm}{min}$, v_b = 189.2 $\frac{mm}{min}$, d_{gap} = 0.1 mm, WZL = 3.5 s, WZD = 2.8 s

At this point, it should be noted that the crack in Figure 5.12 a) occurred while manually cutting the brazed joint into pieces. The measured gap widths from the polished micrograph sections, as well as those of the inspection via the camera, are presented in Figure 5.13.

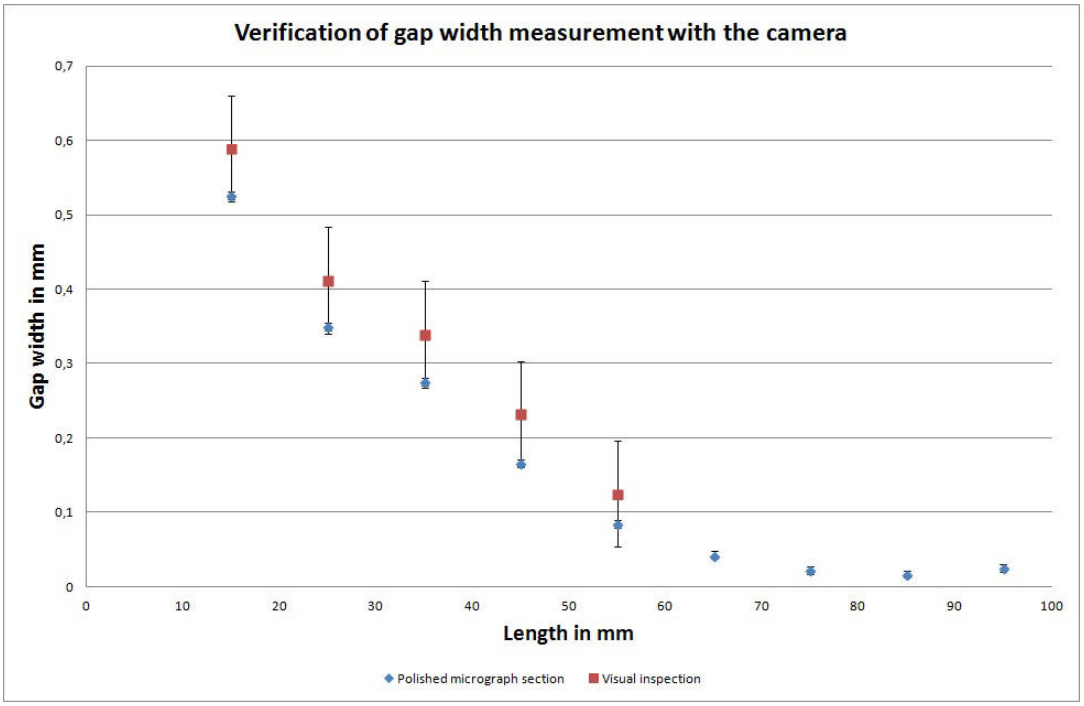

Figure 5.13.: Verification of gap width measurement with the camera: Polished micrograph section and inspection via the camera exemplified on a brazed joint with an initial gap width of 0.75 mm

For the gap widths measured at the polished micrograph sections a measurement tolerance of ± 0.005 mm is taken into account and the measurement tolerance of the inspection with the camera corresponds to ± 0.071 mm ($\pm$ 4 pixels). As it can be seen in Figure 5.13, the gap widths measured at the polished micrograph sections also decrease linearly over the length of the brazed joint up to the location of 55 mm. These gap width measurements up to 55 mm are compared to those measurements done with the camera. There, it can be noted that the gap widths measured at the polished micrograph sections are in general approximately 0.05 mm smaller than those measured via the inspection with the camera. But they are within the stated tolerance of the gap widths measured via inspection with the camera. Therefore the approach of gap width measurement via inspection with the camera is verified.

As mentioned in section 3.2.1.1, the optimal gap width for laser brazing is in the range of 0.05 mm up to 0.2 mm, since then the melted brazing wire is "sucked" into the gap due to the capillary filling pressure. Comparing this statement to the polished micrograph sections carried out (see Figure 5.12), it is clearly visible in Figure 5.12 a) to c) that the gap is too wide or the capillary filling pressure too less respectively, so that the melted brazing wire cannot fill the gap anymore. Even if the gap width is in the

above stated range (see Figure 5.12 (d) , (e)) the melted brazing wire does not fully fill the gap due to the capillary filling pressure; although an increase in filling the gap is recognisable (Figure 5.12 (a) to (e)) . This behaviour might be either an indicator that the parameter set used is not optimal with regard to "filling" the gap or that the laser used might not be sufficient.
However, at the length of 65 mm up to 95 mm the melted brazing wire is completely "sucked" into the gap due to the capillary filling pressure (Figure 5.12 (f) to (i)) , since there the gap is significantly diminished by thermal expansion.

5.2.2. Tests to maintain gap width

As the gap disappears over the length of the joint (see section 5.2.1), tests were carried out to maintain the gap width over the length of the joint. These tests and their outcome are presented in the following.
It was tested to maintain the gap width over the length of the brazed joint by using pieces of spring steel with a thickness that corresponds to the gap width. Those pieces were placed at the beginning and at the end of the base materials to be joined (see Figure 5.14).

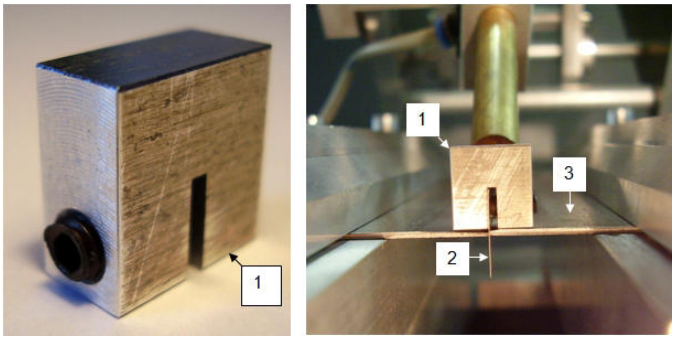

Figure 5.14.: Holder for the spring steel pieces (Left); Positioning of spring steel pieces (Right): 1) Holder; 2) Pieces of spring steel; 3) Clamped base materials

These tests resulted in no improvement with regard to maintaining the gap width as well as enhancing the existence of the gap width over the length of the joint.
As these tests showed no improvement and the gap width still disappears due to thermal expansion, it is tested to maintain the gap width by placing each base material

1.6 mm apart from the clamping block, as the base material expands in both directions. For this a piece of wire with a diameter of 1.6 mm was used. The base materials were placed onto the clamping brackets and the wire was put between the clamping bracket and the base material. Then the base materials were clamped and the wire was removed before the brazing process started. An initial gap width of 0.75 mm was used, because there changes in gap width are easiest to recognise. For brazing, the parameter set stated in Table 4.8) was used. After brazing and before releasing the brazed joint out of the clamping, the distance between base material and the clamping block was measured via a calliper. The gap between the left base material and the clamping block corresponds to 1.35 mm and the gap on the other side to 1.5 mm. Figure 5.15 shows a typical result, where the white marks indicate the point where the gap is not recognisable anymore.

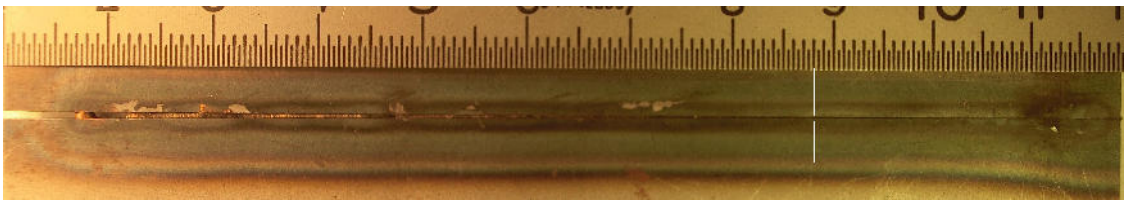

Figure 5.15.: Typical example of a brazed joint for trying to maintain the gap by leaving space between the clamping block and the base material; Parameters for brazing: P = 3,600 W, t_p = 0.8 ms, f = 50 Hz, P_{av} = 144 W, F = -13 mm, v = 95 $\frac{mm}{min}$, v_b = 189.2 $\frac{mm}{min}$, d_{gap} = 0.1 mm, WZL = 3.5 s, WZD = 2.8 s

The length of the brazed joint to the white mark corresponds to 71 mm (see Figure 5.15). Comparing this length of gap existence to the joint brazed without this gap between base material and clamping block (see Figure 5.10) but with the same initial gap width, it is apparent that this type of preparation shows an improvement with regard to length of gap existence over the brazed joint. Since the normal brazed one has an existing gap length of 60 mm, whereas the other one has an existing gap length of 71 mm. This increase in the length of gap existence can be reasoned by the available space in both directions for the base material with regard to thermal expansion.
Furthermore, it was tested to maintain the gap width by the aid of tacking the base materials at the beginning, in the middle and at the end of the base materials to be joined. The middle was chosen as well, since the usage of spring steel pieces had no effect on the brazing result. It was tested with an initial gap width of 0.75 mm and after tacking the gap width corresponds to 0.25 mm. Then the joint was brazed with

the parameter set stated in Table 4.8. Figure 5.16 shows the result of this brazed joint, where the white arrows indicate the tacking points.

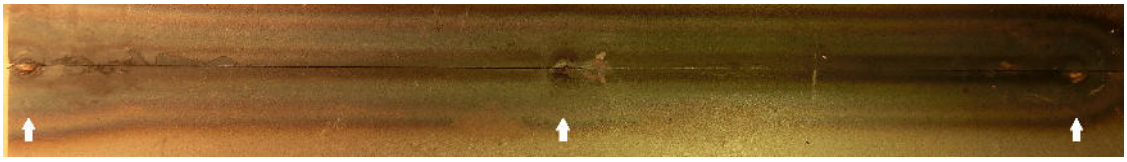

Figure 5.16.: Joint brazed with prior tacking of base materials to maintain gap width; Parameters for brazing: P = 3,600 W, t_p = 0.8 ms, f = 50 Hz, P_{av} = 144 W, F = -13 mm, v = 95 $\frac{mm}{min}$, v_b = 189.2 $\frac{mm}{min}$, d_{gap} = 0.1 mm, WZL = 3.5 s, WZD = 2.8 s

As it can be seen in Figure 5.16, the gap between the first and middle tacking point shows no gradient compared to normal brazed ones, but the gap between the middle and end tacking point is not recognisable anymore. For this reason the option of tacking the base material first eliminates the gradient of disappearing gap up to the middle, however, it does not maintain the gap over the length of the brazed joint.
To overcome this characteristic of disappearing gap width, the process of laser brazing has to be faster, so that the influence of heat conduction and therefore thermal expansion can be diminished.

5.2.3. Deformation

As mentioned in section 4.4, deformations of the joint occur due to the heat input of the laser. Figure 5.17 shows an example of a typical deformed joint.

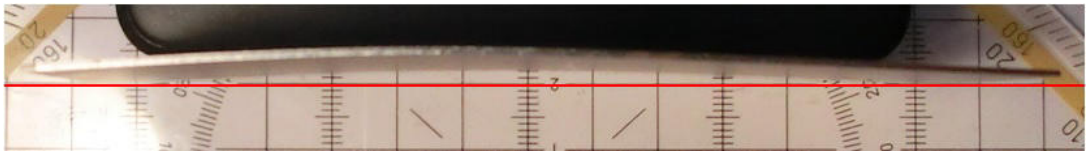

Figure 5.17.: Deflection measurement of brazed joint, where the rear side of the brazed joint reaches the red line; Parameters for brazing: P = 3,600 W, t_p = 0.8 ms, f = 50 Hz, P_{av} = 144 W, F = -13 mm, v = 95 $\frac{mm}{min}$, v_b = 189.2 $\frac{mm}{min}$, d_{gap} = 0.1 mm, WZL = 3.5 s, WZD = 2.8 s

It can be seen that the joint has a curvature over the length of the joint, where both ends of the rear side of the brazed joint reach the red line. This curvature is caused by

the heating induced thermal expansion strains, which can be calculated as follows for a uniform temperature rise or decrease respectively (ΔT) (Usmani et al., 2001):

$$\varepsilon_T = \alpha \Delta T \tag{5.2}$$

With: ε_T: Thermal expansion strain
α: Coefficient of linear expansion
ΔT: Temperature difference

The uniform temperature rise within the base material was proven for the gap disappearance over the length of the joint (see Figure 5.11 in section 5.2.1), which can be expressed by the trend line function

$$T = 16.769l + 8.325$$

With: T: Temperature
l: length

This equation was obtained by applying a linear trend line to the measurement results of the thermal expansion of the base materials (see Figure 5.11). Using this equation, (ΔT) can be determined as follows between two neighbouring measurement points:

$$\begin{aligned} \Delta T &= T_2 - T_1 \\ with & \\ T_2 &> T_1 \end{aligned}$$

This results in a uniform temperature rise (ΔT) of 83.845 °C. Inserting the value (ΔT) in equation (5.2), together with the coefficient of linear expansion for the base material (α_{steel}) of $11 * 10^{-6}$ K^{-1} (Stöcker, 2000), the thermal expansion strain (ε_T) corresponds to $0.922 * 10^{-3}$. This thermal expansion strain leads the to deformation, shown in Figure 5.17, as soon as the joint is released from clamping. Since the joint has a uniform curvature over the length of the joint, the deflection of the joint can be approximated by (Usmani et al., 2001)

$$\delta = \frac{2l}{\pi}\sqrt{\varepsilon_T + \frac{\varepsilon_T^2}{2}}. \tag{5.3}$$

With: ε_T: Thermal expansion strain
l: length

Therefore, the deflection of the base material is estimated to 2.13 mm with the length of 110 mm.
To measure the deflection of the brazed joint, the joint was placed onto a set square, as shown in Figure 5.17, and a picture was taken by the aid of the Casio Exilim Ex-ZR100 12.1MPixel camera.
Figure 5.18 shows an enlarged view of the measurement location for the deflection (red arrow). Furthermore, the black arrows in Figure 5.18 indicate the even curvature of the joint with respect to the scale of the set square.

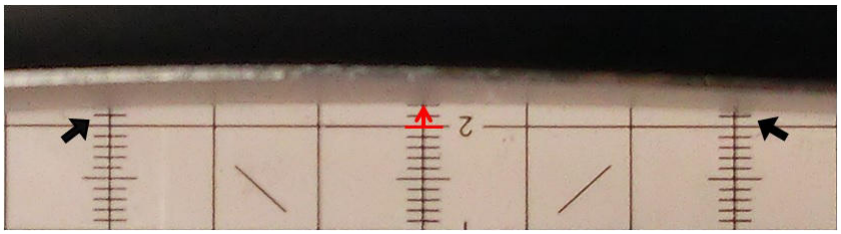

Figure 5.18.: Curvature of brazed joint; Parameters for brazing: P = 3,600 W, t_p = 0.8 ms, f = 50 Hz, P_{av} = 144 W, F = -13 mm, v = 95 $\frac{mm}{min}$, v_b = 189.2 $\frac{mm}{min}$, d_{gap} = 0.1 mm, WZL = 3.5 s, WZD = 2.8 s

For measuring the deflection, the pixels are counted and then converted to unit length. For this measurement, a tolerance of ± 2 pixels was taken into account. The deflection is measured to 2.25 mm $\pm$0.14 mm. As the estimated deflection is within the tolerance of the measured one, the estimation is verified.

5.3. Influence of the repetition rate (f) on the brazed joint

During the parameter studies carried out so far, the repetition rate (f) of the Nd:YAG laser was kept constant to the value of 50 Hz. However, the question arose if the repetition rate (f) has an influence on the brazing result with specific regard to the surface roughness. For this reason, the repetition rate (f) was supposed to be varied from 10 Hz to 70 Hz with 5 Hz steps by using the parameter set stated in Table 4.8. To maintain the average laser power (P_{av}) of 144 W stated in Table 4.8, the peak power (P) was kept constant and the pulse length (t_p) was adapted according to the equation (3.1).

The pulse length (t_p) was selected to be adapted, since the initial experiments carried out showed that high peak powers (P) affect the base material regarding melting and/or ablating (see section 4.4).
However, the repetition rate (f) could only be varied from 10 z to 40 z, as the laser set itself always to error-state for a repetition rate (f) of 45 z and higher with the parameter set stated in Table 4.8.
The joints were brazed with the respective repetition rate (f) and the adapted pulse length (t_p). The surface roughness of the brazed joints was measured with the stylus instrument Perthometer S5P from Perthen GmbH. This instrument has a measurement range of 50 μm and the radius of the measurement tip corresponds to 5 μm. The measurement distance is set to 4.8 mm, whereas the distance of 0.8 mm corresponds to the forward measurement distance, which is not included in the actual measurement.
To measure the average surface roughness (R_z), the brazed joints were placed onto an even measurement table and were fixed with small weights to keep them in place. Subsequently, the measurement tip was placed manually at the center of the spherical cap of the brazed joint. The average surface roughness (R_z) was measured at four locations (20 mm, 40 mm, 60 mm, 80 mm) for each brazed joint. Each measurement was repeated once for every location to minimise the influence of the manual placement.
The arithmetic mean was calculated for (R_z) out of all measurement values from each brazed joint. The result of these measurements is presented in Figure 5.19, where the average surface roughness (R_z) is plotted against the repetition rate (f).

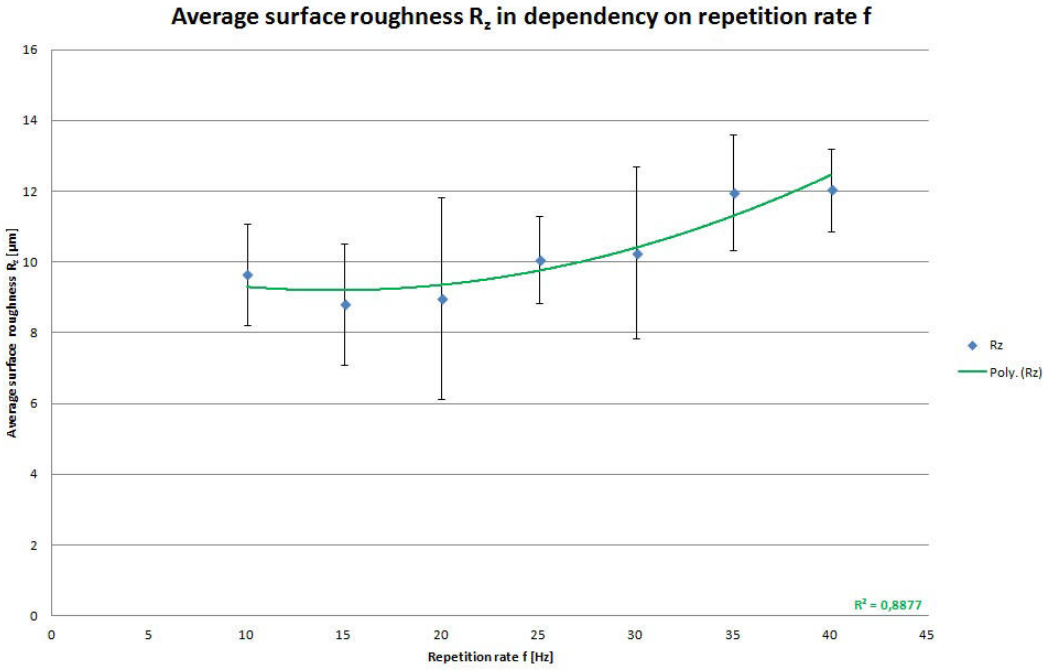

Figure 5.19.: Arithmetic mean of the measured average surface roughness (R_z) of the brazed joint in dependency on the repetition rate (f); the indicated tolerance corresponds to the standard deviation of (R_z)

The indicated tolerance corresponds to the standard deviation of (R_z). It should be noted that the relatively large values of the standard deviation from (R_z) for the repetition rates (f) 20 Hz and 30 Hz originate from the measurement at the location 80 mm, where the average surface roughness (R_z) has a significant increase of approximately 4 μm compared to the other measurements of the respective brazed joint. As it can be seen in Figure 5.19, the average surface roughness (R_z) decreases from 9.65 μm to 8.80 μm for the repetition rate (f) 10 Hz to 15 Hz. Then (R_z) increases from 8.98 μm to 12.04 μm for the repetition rates (f) from 15 Hz to 40 Hz.

This relation between the average surface roughness (R_z) and the repetition rate (f) can be approximated by a second order polynomial fit as indicated by the green trend line in Figure 5.19. The increase of (R_z) with the repetition rate (f) can be explained by the adaptation of the pulse length (t_p). Since the peak power (P) as well as the average laser power (P_{av}) were kept constant for this parameter study, the pulse length (t_p) and the repetition rate (f) are inversely related to each other, i.e. if the repetition rate (f) is decreased, the pulse length (t_p) is increased and vice versa (see equation (3.1)). An increase in pulse length means that the duration of a laser pulse is extended. This fact, in connection with a low repetition rate, approximates a quasi-continuous behaviour of the laser radiation more effectively than a high repetition rate

in connection with a short pulse length with respect to the surface condition (see Figure 5.19).

The brazed joints were also inspected visually. There it is recognised that ablation of base material occurred for the repetition rates (f) 10 Hz and 15 Hz. For example, Figure 5.20 a) shows the joint brazed with 15 Hz. The right image of Figure 5.20 a) presents an enlarged view of an part of the brazed joint, where the red arrow indicates the ablation. This ablation disappears for 20 Hz, as it can be seen in Figure 5.20 b).

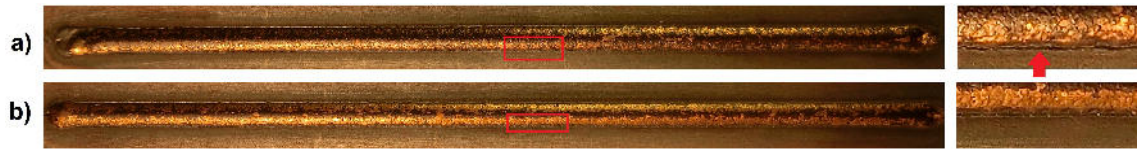

Figure 5.20.: Brazed joints with the repetition rates (f) 15 Hz and 20 Hz; a) Left: brazed joint with the repetition rate (f) 15 Hz, Right: Enlarged view of part of the brazed joint indicated by the red rectangle; the red arrow points at the affected base material; b) Left: brazed joint with the repetition rate (f) 20 Hz, Right: Enlarged view of part of the brazed joint indicated by the red rectangle; Parameters for brazing: P = 3,600 W, P_{av} = 144 W, F = -13 mm, v = 95 $\frac{mm}{min}$, v_b = 189.2 $\frac{mm}{min}$, d_{gap} = 0.1 mm, WZL = 3.5 s, WZD = 2.8 s

For this reason the joint brazed with a repetition rate (f) of 20 Hz seems to be the most effective with regard to surface condition.

5.4. Summary

These investigations carried out with the Nd:YAG laser showed that the wire positioning itself as well as within the laser spot has a significant influence on the brazing result. It was determined that wire oscillations occur if the wire itself has an incidence angle larger than 45°. These oscillations can be decreased if the incidence angle is decreased below 45°. To prevent the wire from oscillating, it has to be slightly pressed onto the base material, so that it bends a little. Using this technique, the wire is controlled by the gap and no oscillations can occur. Furthermore, the wire is fed under a very small angle to the brazing process due to this positioning described above. The experiments, carried out with regard to the wire positioning within the laser spot, showed that only the positioning at the center of the laser spot resulted in good quality brazed joints. The positioning of the wire at the leading or trailing edge of the laser spot resulted in low quality brazed joints or non at all.

The observed characteristic of disappearing gap width over the length of the joint (see section 4.4) was further investigated. The tests showed that the gap disappears over the length of the joint due to thermal expansion of the base materials. The correspondent measurements agree well with theory of linear expansion with regard to a uniform temperature change.

Tests were carried out for maintaining the gap over the length of the joint, e.g. using spring steel of respective thickness as a spacer, tacking of base materials prior to the brazing process and leaving space between the clamping bracket and base material. However, non of them led to a satisfactory result.

Along with the disappearance of gap width, deformation occurs in the form of deflection over the length of the brazed joints. This deformation is caused by heating induced thermal expansion strains. The deflection of the brazed joints was measured and agreed well with the theoretical values.

As the repetition rate (f) was kept constant throughout these parameter studies, investigations were carried out with regard to its influence on the surface condition of brazed joints. It was determined that a decrease of repetition rate (f) leads to a decrease in surface roughness by having its optimal value at $f = 20\,Hz$.

Chapter 6.

Parameter studies with the diode laser

Based on the observations made during the initial experiments, carried out with the Nd:YAG laser (see section 4.4), 5 aspects were identified that need to be further investigated, as they seem to have an influence on the brazing result. The first two aspects wire positioning, characteristics of disappearing gap width and deformation were investigated within the parameter studies with the Nd:YAG laser. Within this chapter, the other aspects are further investigated, which are:

- the ratio between feed speed of brazing wire and feed speed of base material, as opinions deviate in literature. For these tests this ratio was set to 2:1
- The influence of the pre-heating phase duration, which is defined by the two delay times (WZL) and (WZD), to the brazing result.
- Alloy zone formation, as it could not be clearly identified by the optical inspection of polished micrograph sections via a microscope.

Next to these aspects mentioned above, the change in heat input to the brazing result and wire positioning are also investigated. The latter mentioned is repeated for the diode laser, as its beam profile differs from the one of the Nd:YAG laser (see section 3.1.1). For all experiments carried out within these parameter studies, the materials were used and prepared as described in section 4.3 and a brazed joint,100 mm long, was always used.

6.1. Preliminary considerations

Prior to carrying out the parameter studies with the diode laser, considerations have to done with regard to the influencing parameters of the laser brazing process (see section 3.1) in order to determine a parameter set for laser brazing with the diode laser. For this, considerations were carried out with respect to the required heat input, a suitable laser spot size, ratio of feed speeds, pre-heating and gap width.

Estimation of heat input

As presented in section 4.4.1, the required heat for laser brazing can be estimated by equation (4.3). To determine the volume, a suitable laser spot size has to be determined first. The diode laser has a rectangular beam shape (see section 3.1.1.2) that can be described by its two beam width (d_x) and (d_y) respectively. By using equation (3.8), it was determined that a suitable laser spot size is achieved if the focal position (F) corresponds to +5 mm. This leads to beam widths of 2.43 mm in x-direction ($d_x(5)$) and 3.68 mm in y-direction ($d_y(5)$) (see section 3.1.1.2.2). The considered minimum and maximum temperature range for the base material are 20 °C - 800 °C and 20 °C - 1,100 °C respectively. For the brazing wire the minimum required temperature range is determined by its liquidus temperature 1,025 °C. Hence, the minimum required temperature range corresponds to 20 °C - 1,025 °C and the maximum one is the same as for the base material. Accumulating the minimum and maximum required heat of both materials, this leads to a needed heat for brazing in the range of 22.194 J up to 30.113 J.

To estimate the heat input, the laser power (P) and the feed speed of the base material (v) are needed (see equation (4.4)). Although the initial experiments with the Nd:YAG laser showed that an laser power of 144 W is appropriate, it is set to the maximum output power 150 W of the diode laser (see section 3.1.1.2), as the spot size of the diode laser is larger compared to the one of the Nd:YAG laser. The feed speed of base material (v) is adopted from the initial experiments with the Nd:YAG laser (see Table 4.8), which is 95 $\frac{mm}{min}$. Inserting these values in equation (4.4) results in a heat input of 94.74 $\frac{J}{mm}$.

This heat input should be sufficient for laser brazing, even if the absorption is considered, which corresponds to approx. 40 % for the base material and 4 % for the brazing wire for the wavelength 808 nm (see section 4.3).

Ratio of feed speeds ($\frac{v_D}{v}$)

As described in section 4.4.1, opinions deviate with regard to the ratio between feed speeds of brazing wire to feed speed of base material for the same joint geometry (see section 2.2.2.2 and Table 2.1). As no literature could be found concerning butt joints, the ratio can be approximated by 2:1 as a rule of thumb.

Laser power (P)

As mentioned in section 3.1.1.2, the diode laser is a cw direct diode laser with a maximum output power of 150 W. For estimation of the heat input, it was shown that an laser power of 150 W is appropriate.

Gap width (d_{gap})

The parameter studies carried out with the Nd:YAG laser showed that the gap disappears over the length of the joint (see section 5.2.1). There, the decrease in gap width shows a linear behaviour. Therefore, an initial gap width of 0.4 mm is chosen for these parameter studies with the diode laser. As this initial gap width is assumed to cover the optimal range of 0.05 mm up to 0.2 mm for laser brazing close to beginning of the brazed joint with regard to the relation between gap width and capillary filling pressure (see section 3.2.1.1).

Pre-heating

The initial experiments carried out with the Nd:YAG laser demonstrated that a pre-heating phase is essential for laser brazing in order to obtain a qualitatively good joint (see section 4.4.2). As the pre-heating phase is defined by the two delay times (WZL) and (WZD) (see section 3.1.2.3), these two delay times have to be estimated.
For this, (WZL) is going to be estimated in the following and (WZD) is adapted accordingly. During the initial experiments with the Nd:YAG laser, an appropriate (WZL) was determined to 3.5 s (see section 4.4.2) for a spot size (d) of 2.8 mm. Using this information, (WZL) can be approximated by the rule of three. For this, the area of both laser spots have to be calculated for the respective focal position first. As the laser spot of the Nd:YAG laser has a circular shape with a diameter of 2.8 mm, the area corresponds to 6.16 mm^2. The diode laser has a rectangular beam shape, which is described by its

two spot sizes (d_x) and (d_y) respectively (see section 3.1.1.2). For the focal position (F) of +5 mm, the spot sizes correspond to 2.43 mm for (d_x(5)) and 3.68 mm (d_y(5)) resulting in a laser spot area of 8.94 mm^2.
Applying the rule of three, (WZL) for the diode laser can be estimated to

$$\begin{aligned} 6.16\,mm^2 &= 3.5\,s \\ 8.94\,mm^2 &= WZL \\ \Longrightarrow WZL &= 5.08\,s \end{aligned}$$

As this is an estimation for (WZL), the value of (WZL) is increased slightly to 5.5 s to ensure a proper pre-heating.
The value of the delay time (WZD) is based upon the observations made during the initial experiments with the Nd:YAG laser (see section 4.4.2). It was observed if the difference in time between both delays (WZL) and (WZD) was too large, no appropriate operating temperature was reached at the beginning of the brazing process. This was caused by too much fed wire, if (WZD) was significantly shorter than (WZL). However, if (WZD) and (WZL) approximately correspond to each other, a repetitive brazing process could not always be obtained. This can be explained by the manual start of both delay times with regard to the human error on the one hand. On the other hand, the wire feed has to start a bit earlier than the brazing process, so that enough wire is fed and the brazing wire does not loose contact to melt as observations showed. Hence, (WZD) is set to 4.7 s with regard to these mentioned aspects.
The considerations carried out are summarised in the following for clarity.

- Focal position (F) of +5 mm leads to a spot size of 2.43 mm in x-direction (d_x(5)) and 3.68 mm in y-direction (d_y(5))(see section 3.1.1.2.2)

- Laser power (P) of 150 W fulfils the required heat input by using a feed speed of the base material (v) of 95 $\frac{mm}{min}$

- The ratio of feed speed of brazing wire to feed speed of base material is estimated to approximately 2:1

- Gap width (d_{gap}) is set to 0.4 mm to achieve an optimal gap width in the range of 0.05 mm up to 0.2 mm at the beginning of the brazing process

- For an appropriate pre-heating, (WZL) and (WZD) were estimated to 5.5 s and 4.7 s respectively

6.2. Influence of the wire position also within the laser spot

During the parameter studies carried out with the diode laser, almost the same observations were made with regard to the wire positioning as with the Nd:YAG laser (see section 5.1). The wire positioning itself can have a significant influence on the brazing result. Next to the loose positioning of the brazing wire at the gap with its correspondent consequences (see section 5.1), it was observed that if the wire was placed at the gap with a bit of pressure, but the incidence angle was not correct, it also resulted in low quality brazed joints. Figure 6.1a shows such an insufficient positioning. The black mark in Figure 6.1a indicates the approximate location of the laser spot with regard to its center.

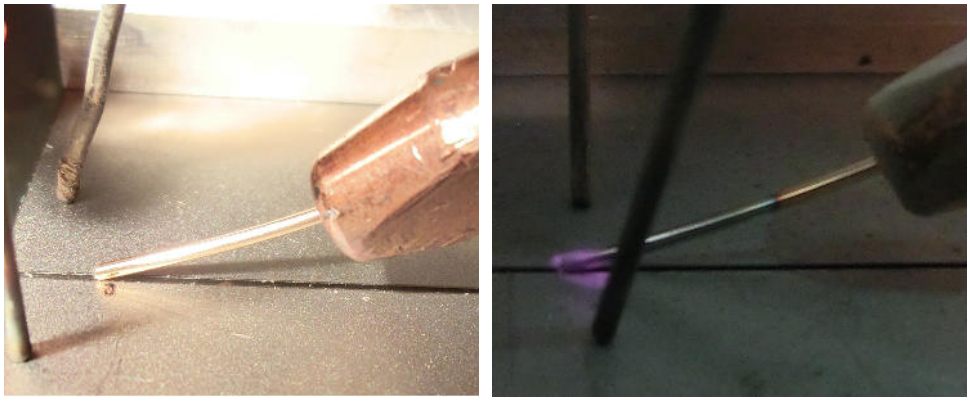

(a) Incorrect positioning of the brazing wire **(b)** Correct positioning of the brazing wire

Figure 6.1.: Example for brazing wire positioning: a) incorrect positioning; b) correct positioning

As it can be seen in Figure 6.1a, the brazing wire encloses an angle with the base material, which results in no contact at the center of the laser spot. Since the brazing wire is forced into the gap by a bit of pressure, the oscillations, as described in section 5.1, cannot occur. However, the pressure is not enough, which leads to an increased incidence angle of the brazing wire and to no contact with the base material at the center of the laser spot.
Figure 6.2 shows a joint brazed with an initial incorrect wire positioning. As it can be

seen, this brazed joint is low in quality. The joint looks stitched due to the incidence angle of the brazing wire.

Figure 6.2.: Bad example of a joint brazed with incorrect wire positioning; Parameters for brazing: P_{av} = 150 W, F = +5 mm, v = 76.00 $\frac{mm}{min}$, v_b = 161.4 $\frac{mm}{min}$, d_{gap} = 0.4 mm, WZL = 5.5 s, WZD = 4.7 s

Figure 6.1b shows the correct positioning of the brazing wire. The laser spot corresponds to the purplish spot in Figure 6.1b. As it can be seen there, the wire is guided by the gap and has contact with the base material within the laser spot. All brazed joints presented in these diode laser parameter studies had an initial wire positioning as shown in Figure 6.1b.
Furthermore, it was observed during these studies that the brazing wire positioning within the laser spot is not as crucial as for the Nd:YAG laser parameter studies. This can be explained by the top hat profile of the laser beam (see section 3.1.1.2) in direction of brazing.

6.3. Comparison of ratios of feed speeds ($\frac{v_b}{v}$) with and without shielding gas

As opinions vary in literature, with regard to the ratio of feed speeds (see section 2.2.2.2) for the same joint geometry, this ratio is further investigated for brazing butt joints.
Initially, as a rule of thumb, the ratio of feed speeds was approximately set and kept to 2:1 for the initial experiments carried out with the Nd:YAG laser (see section 4.4). Even the ratio of feed speeds of the appropriate parameter set presented for brazing with the Nd:YAG laser (see Table 4.8) corresponds to the rule of thumb with 1.99:1.
Therefore, tests were carried out to investigate the change in ratio with regard to the quality of the brazed joints. To start testing, the feed speeds of base material and brazing wire were taken from the parameter set of the Nd:YAG laser (see Table 4.8). Subsequently, the feed speed of brazing wire was decreased by one step of the stepper motor and the feed speed of base material was adjusted to the ratio of 2:1. Then the feed speed of base material was increased and decreased until an insufficient

brazed joint was obtained. This was inspected visually with regard to wetting and ablation of the base material.
These tests were carried out once with the aid of shielding gas Nitrogen (N_2) and once without and subsequently compared.
The feed speed of the base material can be adjusted in very small steps due to the CNC - unit of the diode laser. As the feed speed of base material that is entered in the NC - program corresponds to 100 % and this feed speed can be adapted by changing the percentage.
The parameters used for laser brazing can be found in Table 6.1 according to the preliminary considerations carried out in section 6.1.

Table 6.1.: Parameters used for the ratios of feed speed experiments with shielding gas

P (W)	WZD (s)	WZL (s)	F (mm)	d_{gap} (mm)
150	4.7	5.5	+5	0.4

6.3.1. Ratios of feed speeds ($\frac{v_b}{v}$) with shielding gas

For these tests, all joints were brazed by the aid of shielding gas N_2. The flow speed of the shielding gas could not be measured, since the shielding gas flow meter is insensitive to the slow flow speeds needed for these studies [9], the shielding gas flow speed can be compared to the wind speed of a whistle.
The feed speeds of the brazing wire that were tested as well as the initial feed speeds of the base material for the respective feed speed of the brazing wire can be found in Table 6.2.

Table 6.2.: Initial feed speeds tested with shielding gas

Test number	v_b ($\frac{mm}{min}$)	v ($\frac{mm}{min}$)
1	189.2	95.00
2	161.4	80.75
3	109.2	55.10

[9] it did not recognise that shielding gas was used at all

Test number (1)

For the first tests, the ratio of feed speeds is set according to the appropriate ratio of feed speeds obtained during the initial experiments carried out with the Nd:YAG laser (see Table 6.2, No.1). The feed speed of the brazing wire was kept constant and the feed speed of the base material was varied in the range of 93.1 $\frac{mm}{min}$ up to 96.9 $\frac{mm}{min}$. Figure 6.3 shows the joints brazed with the respective feed speed of the base material.

Figure 6.3.: Ratio of feed speeds with shielding gas: brazed joints of test number (1) with the respective feed speeds of the base material: starting from lowest (at the top) to fastest feed speed (at the bottom); Parameters for brazing: P_{av} = 150 W, F = +5 mm, v_b = 189.2 $\frac{mm}{min}$, d_{gap} = 0.4 mm, WZL = 5.5 s, WZD = 4.7 s

The joint brazed with a feed speed of 95 $\frac{mm}{min}$ can be seen in the middle of Figure 6.3. This joint shows a poor wetting behaviour onto the surface of the base material, even if it looks smooth with regard to surface condition. An increase in feed speed leads to even poorer wetting behaviour. This can be seen at the joint brazed with 96.9 $\frac{mm}{min}$ at the bottom of Figure 6.3, since the wetting is not continuous over the length of the brazed joint.

A decrease in feed speed shows a continuous wetting compared to the faster ones brazed, but also a slight decrease in wetting with regard to the width of wetting onto

the surface. The latter one mentioned means that the spherical cap of the brazed joint is slightly higher and thinner compared to the joint brazed with a feed speed of 95 $\frac{mm}{min}$.
Next to the poor wetting onto the surface, which accounts for brazed joints presented in Figure 6.3, their existing gap is not filled by the brazing wire, as it can be seen in Figure 6.4, where this behaviour is exemplified on the joint brazed with 95 $\frac{mm}{min}$.

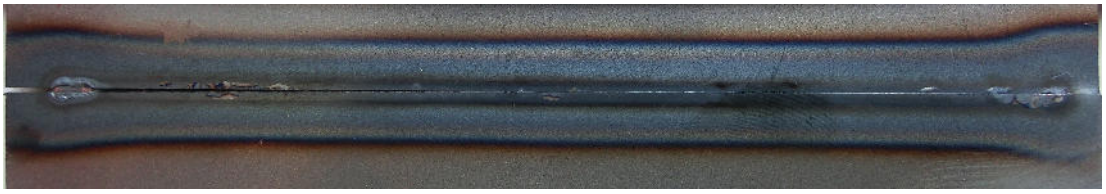

Figure 6.4.: Typical rear side of the above joints brazed exemplified on the joint brazed with 95 $\frac{mm}{min}$; Parameters for brazing: P_{av} = 150 W, F = +5 mm, v_b = 189.2 $\frac{mm}{min}$, d_{gap} = 0.4 mm, WZL = 5.5 s, WZD = 4.7 s

Therefore, it is apparent that either the speed of the process itself is too fast or the heat input too low for brazing with the diode laser. This results in insufficient brazed joints with regard to poor wetting and an unfilled gap.

Test number (2)

For these tests the feed speed of brazing wire was decreased by one step to 161.4 $\frac{mm}{min}$ and the initial feed speed of the base material was adapted according to the rule of thumb (see Table 6.2, No.2). The feed speed of the base material was varied in the range of 78.85 $\frac{mm}{min}$ to 81.70 $\frac{mm}{min}$. Figure 6.5 shows the brazed joints with the respective feed speed of the base material.

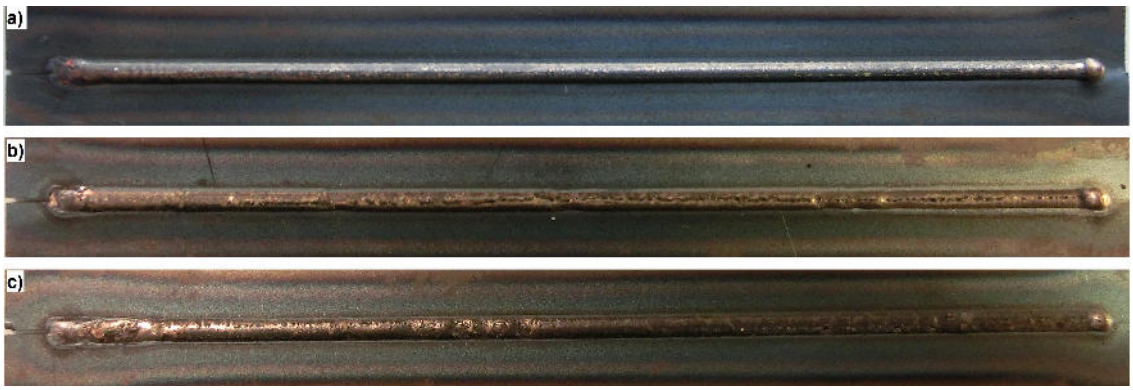

Figure 6.5.: Ratio of feed speeds with shielding gas: brazed joints of test number (2) with the respective feed speeds of the base material: a) 78.85 $\frac{mm}{min}$; b) 80.75 $\frac{mm}{min}$; c) 81.70 $\frac{mm}{min}$; Parameters for brazing: P_{av} = 150 W, F = +5 mm, v_b = 161.4 $\frac{mm}{min}$, d_{gap} = 0.4 mm, WZL = 5.5 s, WZD = 4.7 s

As it can be seen in Figure 6.5, the joints brazed are comparable to those brazed with the higher feed speeds (see Figure 6.3) of test number (1). The brazing wire insufficiently wets the base materials with regard to contact angle and the width of wetting onto each base material. Furthermore the existing gap is not filled by the brazing wire; the filling behaviour is comparable to the one of the higher feed speeds (see Figure 6.4) of test number (1).
These results clearly indicate that the heat input is too low due to the improper heating and melting of the brazing wire.

Test number (3)

Based on the results of test number (1) and 2, the feed speed of the brazing wire was significantly reduced to 4 steps per second, which corresponds to 109.2 $\frac{mm}{min}$ (see Appendix B.2.4). The feed speed of the base material was adapted according to the rule of thumb with an initial value of 55.10 $\frac{mm}{min}$. For these tests, the feed speed of base material was varied in the range of 51.30 $\frac{mm}{min}$ up to 62.70 $\frac{mm}{min}$. Figure 6.6 and 6.7 shows the joints brazed with the respective feed speeds of the base material.

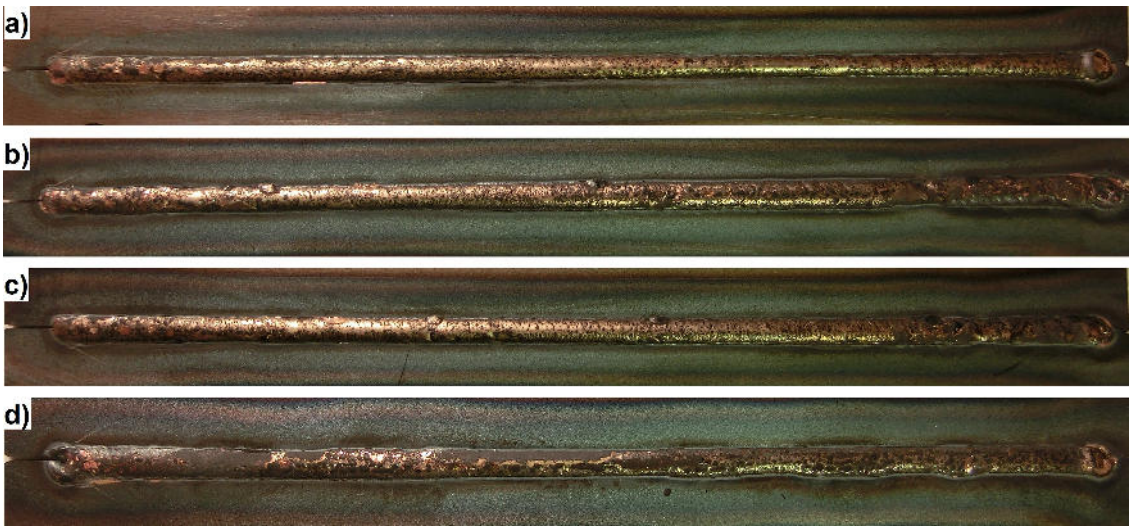

Figure 6.6.: Ratio of feed speeds with shielding gas: brazed joints of test number (3): a) 51.30 $\frac{mm}{min}$; b) 52.25 $\frac{mm}{min}$; c) 55.10 $\frac{mm}{min}$; d) 56.05 $\frac{mm}{min}$; Parameters for brazing: P_{av} = 150 W, F = +5 mm, v_b = 109.2 $\frac{mm}{min}$, d_{gap} = 0.4 mm, WZL = 5.5 s, WZD = 4.7 s

As it can be seen in Figure 6.6 a slight increase in width of the brazed joints is recognisable in a) to d) . This can be understood by the lesser feed speed of the base material compared to the feed speed of the brazing wire (Figure 6.6 (a)). This is because too much wire was fed, for the feed speed of the base material. Then more material had to be melted, which led to an improper heating of the base material and therefore led to an insufficient wetting of the brazing wire onto the base material. The mentioned increase in width results from the increase of the feed speed of the base material (Figure 6.6 (c) and (d)), since both feed speeds are more balanced with regard to material to be melted and heated respectively.

However, the wetting onto the base material significantly increased compared to the joints brazed with the higher feed speeds of both: brazing wire and base material (see Figure 6.3 and 6.5 respectively). The joints brazed with the lower feed speeds are wider, but they violate the definition of brazing (see section 2.2.1.1). As the base material close to the joint is ablated at its surface, due to too much heat input (Figure 6.6 (a) and (b)). The joints brazed with an increased feed speed, in the range of 57.00 $\frac{mm}{min}$ to 62.70 $\frac{mm}{min}$, are shown in Figure 6.7. There, a slight decrease in wetting, with regard to the width of the brazed joint, is recognised in a) to d). However, the joints brazed with a feed speed of base material of 57.00 $\frac{mm}{min}$ and 58.90 $\frac{mm}{min}$ still show a sufficient wetting.

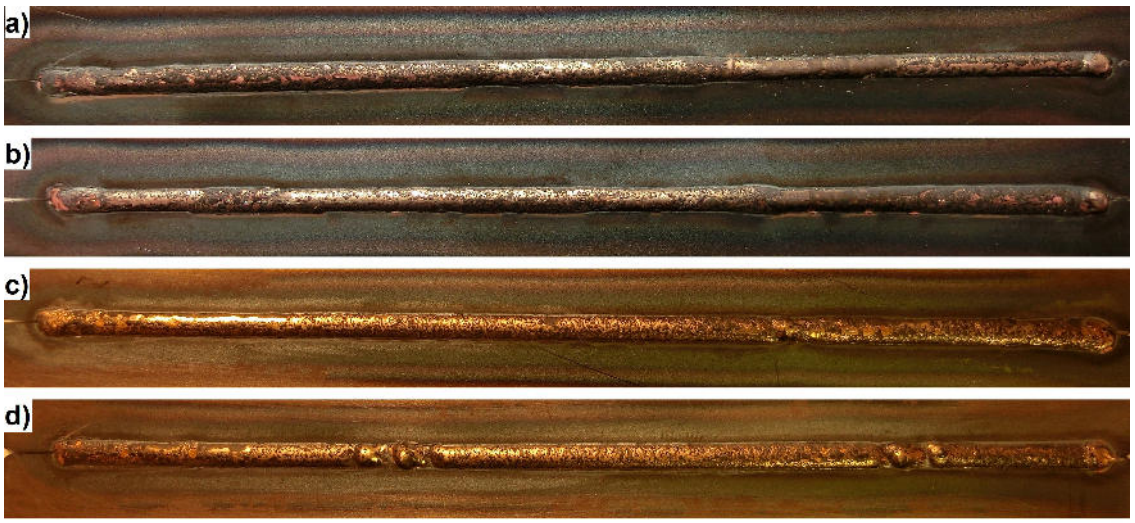

Figure 6.7.: Ratio of feed speeds with shielding gas: brazed joints of test number (3) with the following feed speeds of the base material a) 57.00 $\frac{mm}{min}$; b) 58.90 $\frac{mm}{min}$; c) 60.80 $\frac{mm}{min}$; d) 62.70 $\frac{mm}{min}$; Parameters for brazing: P_{av} = 150 W, F = +5 mm, v_b = 109.2 $\frac{mm}{min}$, d_{gap} = 0.4 mm, WZL = 5.5 s, WZD = 4.7 s

Not only the wetting of the brazing wire onto the surface is important, also the existing gap has to be filled by the brazing wire (Jacobson and Humpston, 2005). For this, the rear sides of the joints were also visually inspected. Figure 6.8 shows the rear side of the joint brazed with 55.10 $\frac{mm}{min}$ and 62.70 $\frac{mm}{min}$ respectively. As it can be seen in Figure 6.8 a), the existing gap is completely filled by the brazing wire. There, the white arrow indicates, when the existing gap is not recognisable anymore by visual inspection. For the higher feed speed of 62.70 $\frac{mm}{min}$, the existing gap is not completely filled by the brazing wire (Figure 6.8 (b)).

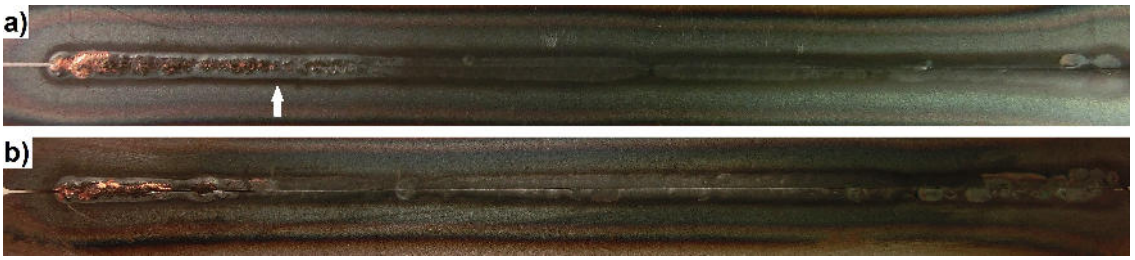

Figure 6.8.: Ratio of feed speeds with shielding gas test number 3: rear side of joints brazed with the following feed speed of base materials: a) 55.10 $\frac{mm}{min}$ and b) 62.70 $\frac{mm}{min}$; Parameters for brazing: P_{av} = 150 W, F = +5 mm, v_b = 109.2 $\frac{mm}{min}$, d_{gap} = 0.4 mm, WZL = 5.5 s, WZD = 4.7 s

To ensure that this filling behaviour is common for the respective feed speed, these joints were repeated three times. All repetitions show the same behaviour as pre-

sented in Figure 6.6, 6.7 and 6.8, i.e. the gap is completely filled for the feed speeds 55.10 $\frac{mm}{min}$ and 56.05 $\frac{mm}{min}$. A completely filled gap could not always be obtained for the other feed speeds due to the improper heat input (see Figure 6.8 (b)). Joints brazed with the respective feed speed of 55.10 $\frac{mm}{min}$ and 56.05 $\frac{mm}{min}$ were further visually inspected with regard to wetting, gap filling and base material influence. There, it was found that the joints brazed with the feed speed of 55.10 $\frac{mm}{min}$ are better than those brazed with the feed speed of 56.05 $\frac{mm}{min}$ with respect to the above mentioned aspects.
For this reason a polished micrograph section of the joint brazed with the feed speed of 55.10 $\frac{mm}{min}$ was carried out by cutting the joint at a length of 15 mm. Figure 6.9 shows the polished micrograph section.

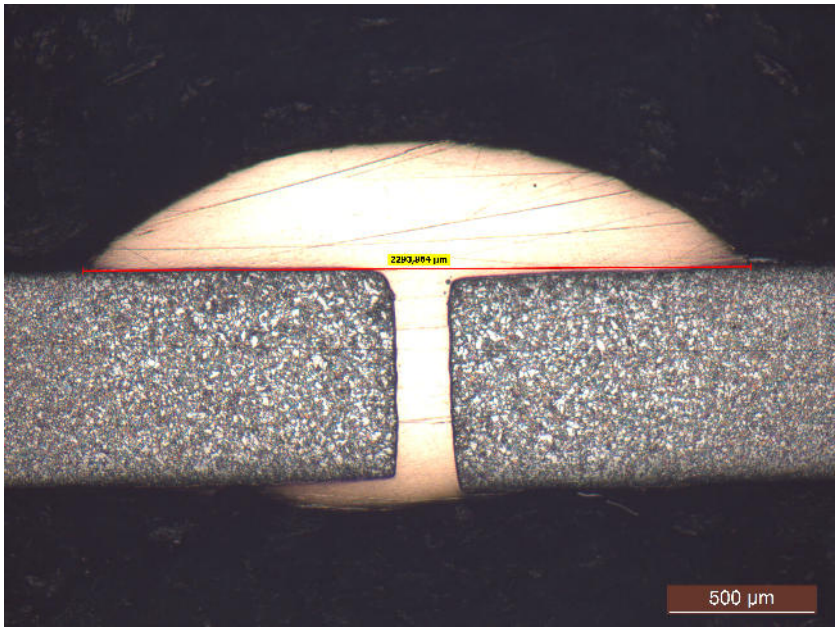

Figure 6.9.: Polished micrograph section of the joint brazed with (v) 55.10 $\frac{mm}{min}$; the height of the spherical cap is 437.653 μm and the width of the brazed joint corresponds to 2293.864 μm, which results in a theoretical contact angle of 41.77° by using equation 3.15. The measured contact angles correspond to: left: 43.709° and right: 41.822°; Parameters for brazing: P_{av} = 150 W, F = +5 mm, v_b = 109.2 $\frac{mm}{min}$, d_{gap} = 0.4 mm, WZL = 5.5 s, WZD = 4.7 s

There, it can be seen that the gap is completely filled by the brazing wire, which has even leaked through the joint. The visual inspection, prior to carrying out this polished micrograph section was correct, since no base material is affected concerning material ablation. Furthermore, the estimated range of gap width for this location mentioned in section (see section 6.1) was also correct, since the gap width seen in

Figure 6.9 corresponds to approximately 0.2 mm. As described in section 3.2.1.1, this gap width is within the optimal range for laser brazing, because there the capillary filling pressure is sufficient to fill the gap with the molten wire. However, the brazed joint does not fulfil the quality measure contact angle, since this angle should be less than 30° and the measured ones correspond to 43.709° (left) and 41.822° (right), whereas the theoretically determined contact angle is 41.77° by using equation 3.15.

These tests carried out with shielding gas showed that for test number (1) and (2) the process speed itself was too fast for the laser brazing with the diode laser. Test number 3 with a feed speed of brazing wire of $v_b = 109.2 \frac{mm}{min}$ showed that appropriate brazed joints are obtained for the feed speeds of base material 55.10 $\frac{mm}{min}$ and 56.05 $\frac{mm}{min}$. The respective ratio of feed speeds is in the range of 1.94 up to 1.98 for (v_b) to 1 (v). These results correspond almost exactly to the rule of thumb of 2:1.
Compared to the parameter studies carried out with the Nd:YAG laser, only slow process speeds for laser brazing could be achieved with shielding gas. This can be reasoned by the usage of shielding gas, as it was observed that the measured temperature was approximately 100° C to 250° C less for the same initial position of the thermocouples. Therefore, these tests are repeated without shielding gas. The results are presented in the following.

6.3.2. Ratios of feed speeds ($\frac{v_b}{v}$) without shielding gas

For these tests, all joints were brazed without using shielding gas. Only compressed air was used to prevent the optics from polluting. For this, the air supply was adjusted in such a way that it flows parallel to the optics.
Based on the results of section 6.3.1, the tests started with slow feed speeds of both, which were then increased. The feed speeds of the brazing wire that were tested as well as the initial feed speeds of the base material for the respective feed speed of the brazing wire can be found in Table 6.3.

Table 6.3.: Initial feed speeds tested without shielding gas

Test number	v_b ($\frac{mm}{min}$)	v ($\frac{mm}{min}$)
A	109.2	55.10
B	138.4	80.75

Test number (A)

For these tests, both feed speeds were initially set to the values of test number (3) with shielding gas (see Table 6.3, No.A). The feed speed of brazing wire was kept constant and the feed speed of base material was varied in the range of 51.30 $\frac{mm}{min}$ up to 70.30 $\frac{mm}{min}$.

Figure 6.10 shows the joints brazed with feed speeds of the base material in the range of 51.30 $\frac{mm}{min}$ (Figure 6.10 (a)) up to 55.10 $\frac{mm}{min}$ (Figure 6.10 (c)). The white arrows in Figure 6.10 indicate where significant material ablation at the surface of the base material took place.

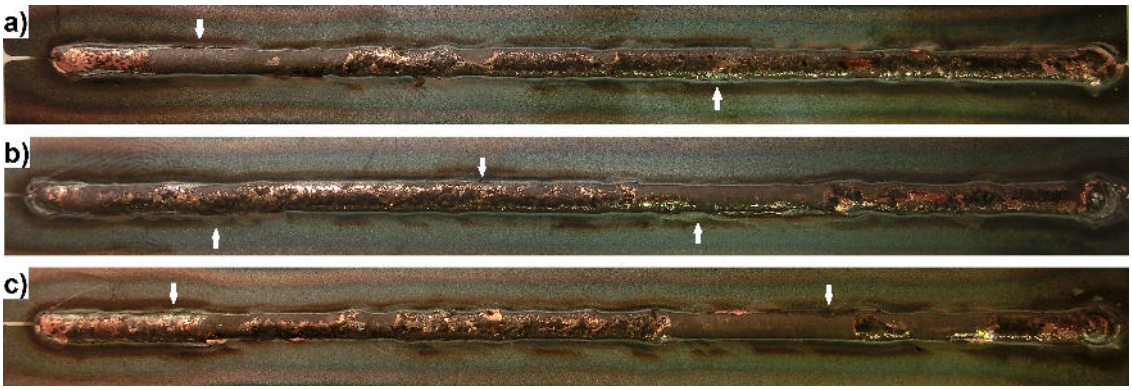

Figure 6.10.: Ratio of feed speeds without shielding gas: brazed joints of test number (A) with the following feed speeds of the base material a) 51.30 $\frac{mm}{min}$; b) 53.20 $\frac{mm}{min}$; c) 55.10 $\frac{mm}{min}$; Parameters for brazing: P_{av} = 150 W, F = +5 mm, v_b = 109.2 $\frac{mm}{min}$, d_{gap} = 0.4 mm, WZL = 5.5 s, WZD = 4.7 s

As this kind of base material change violates the definition of brazing (see section 2.2.1.1), the feed speed of the base material was further increased. Figure 6.11 shows the joints brazed with feed speeds from 58.90 $\frac{mm}{min}$ up to 64.60 $\frac{mm}{min}$. In Figure 6.11, the white marks indicate the locations where base material was effected by melting and/or ablation.

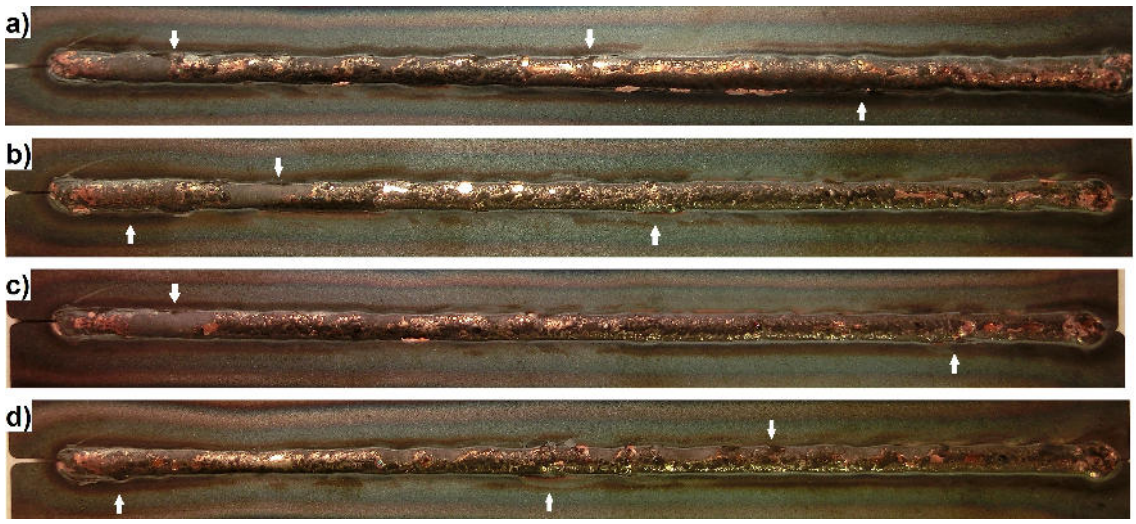

Figure 6.11.: Ratio of feed speeds without shielding gas: brazed joints of test number (A) with the following feed speeds of the base material a) 58.90 $\frac{mm}{min}$; b) 60.80 $\frac{mm}{min}$; c) 62.70 $\frac{mm}{min}$, d) 64.60 $\frac{mm}{min}$; Parameters for brazing: P_{av} = 150 W, F = +5 mm, v_b = 109.2 $\frac{mm}{min}$, d_{gap} = 0.4 mm, WZL = 5.5 s, WZD = 4.7 s

Figure 6.12 shows the joints brazed with feed speed of base material in the range of 66.50 $\frac{mm}{min}$ up to 70.30 $\frac{mm}{min}$. The white arrows indicate base material change with regard to melting or ablation.

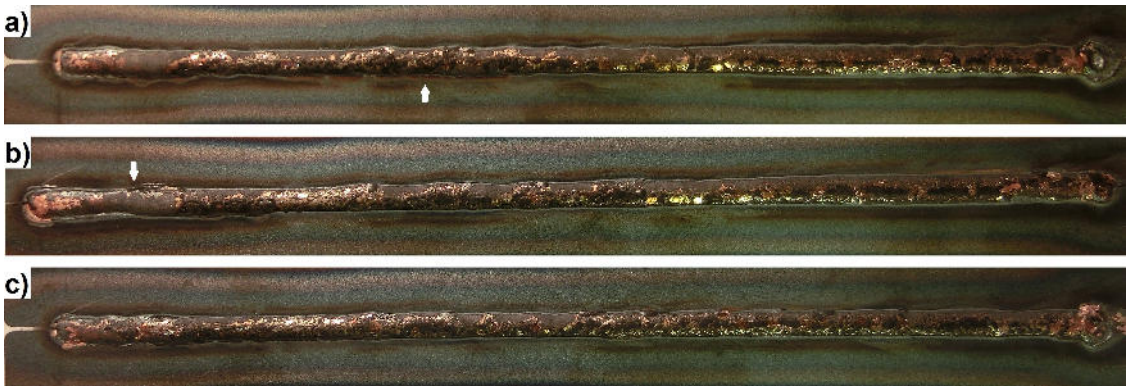

Figure 6.12.: Ratio of feed speeds without shielding gas: brazed joints of test number (A) with the following feed speeds of the base material a) 66.50 $\frac{mm}{min}$; b) 68.40 $\frac{mm}{min}$; c) 70.30 $\frac{mm}{min}$; Parameters for brazing: P_{av} = 150 W, F = +5 mm, v_b = 109.2 $\frac{mm}{min}$, d_{gap} = 0.4 mm, WZL = 5.5 s, WZD = 4.7 s

Comparing the brazed joints presented in Figure 6.11 and 6.10 to the ones presented in Figure 6.12, it can be seen that the grade of base material being effected decreased with increasing feed speed of base material. For the feed speed of base material of 70.30 $\frac{mm}{min}$, no base material change was recognised. The existing gap of these brazed

joints, shown in Figure 6.12, was always filled by the brazing wire. As an example, Figure 6.13 shows the rear side of the joint brazed with 70.30 $\frac{mm}{min}$.

Figure 6.13.: Typical rear side of the above joints brazed exemplified on the joint brazed with a feed speed of 70.30 $\frac{mm}{min}$; Parameters for brazing: P_{av} = 150 W, F = +5 mm, v_b = 109.2 $\frac{mm}{min}$, d_{gap} = 0.4 mm, WZL = 5.5 s, WZD = 4.7 s

Furthermore, it was recognised by the visual inspection of the brazed joints with the respective feed speeds presented in Figure 6.12, that the height of the joints significantly decreased, especially in the area where the gap still exists, which is approximately the first quarter of the joint with respect to its length (see Figure 6.12 (c)). This decrease in height is caused by the decrease in the ratio of feed speeds. The corresponding ratio of both feed speed ranges from 1.64 : 1 (Figure 6.12 (a)) to 1.55 : 1 (Figure 6.12 (c)).

Test number (B)

As the decrease in height of the joint is significant in test number (A), the feed speed of the brazing wire was increased by one step to 138.4 $\frac{mm}{min}$ and the initial feed speed of the base material corresponded to 70.30 $\frac{mm}{min}$ (see Table 6.3, No.(B)). The feed speed of the base material was then varied in the range of 70.30 $\frac{mm}{min}$ up to 79.80 $\frac{mm}{min}$. The feed speed of 70.30 $\frac{mm}{min}$ was repeated with this feed speed of brazing wire in order to compare it to the one with the lower feed speed of the brazing wire (test number (A)). Figure 6.14 shows the joints brazed with the feed speeds of base material in the range of 70.30 $\frac{mm}{min}$ up to 74.10 $\frac{mm}{min}$.

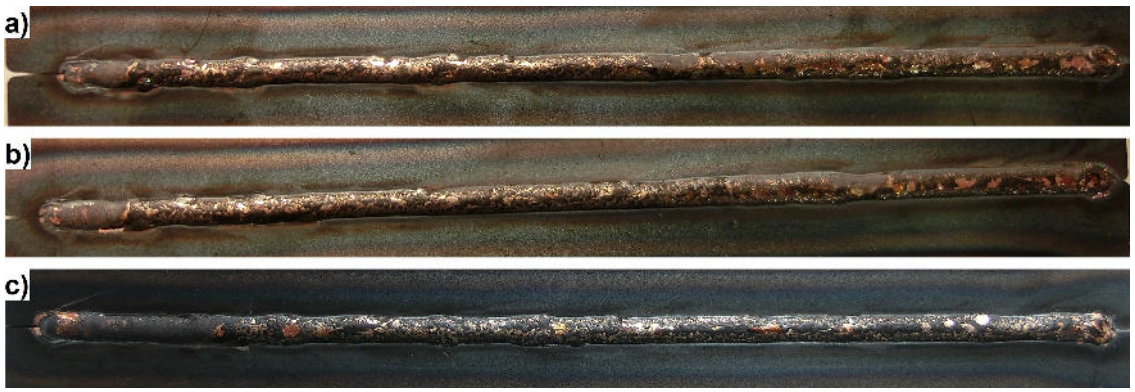

Figure 6.14.: Ratio of feed speeds without shielding gas: brazed joints of test number (B) with the following feed speeds of the base material a) 70.30 $\frac{mm}{min}$; b) 72.20 $\frac{mm}{min}$; c) 74.10 $\frac{mm}{min}$; Parameters for brazing: P_{av} = 150 W, F = +5 mm, v_b = 138.4 $\frac{mm}{min}$, d_{gap} = 0.4 mm, WZL = 5.5 s, WZD = 4.7 s

For all brazed joints presented in Figure 6.14, the existing gap was always completely filled by the brazing wire. Figure 6.15 shows a typical rear side of a brazed joint.

Figure 6.15.: Ratio of feed speeds without shielding gas: brazed joints of test number (B): typical rear side exemplified on the joint brazed with a feed speed of 74.10 $\frac{mm}{min}$; Parameters for brazing: P_{av} = 150 W, F = +5 mm, v_b = 138.4 $\frac{mm}{min}$, d_{gap} = 0.4 mm, WZL = 5.5 s, WZD = 4.7 s

The joint brazed with a base material speed of 70.30 $\frac{mm}{min}$ and a brazing wire speed of 138.4 $\frac{mm}{min}$ (Figure 6.14 (a)), was compared with, the one brazed with the same base material feed speed and a brazing wire speed of 109.2 $\frac{mm}{min}$. It can be seen that the one with the faster brazing wire feed speed looks smoother, with regard to wetting onto the base material, as the one brazed with the slower feed speed. Since no base material ablation and / or melting was recognisable by visual inspection, a polished micrograph section was carried out for both joints by cutting each at 15 mm. Figure 6.16 shows the respective polished micrograph sections.

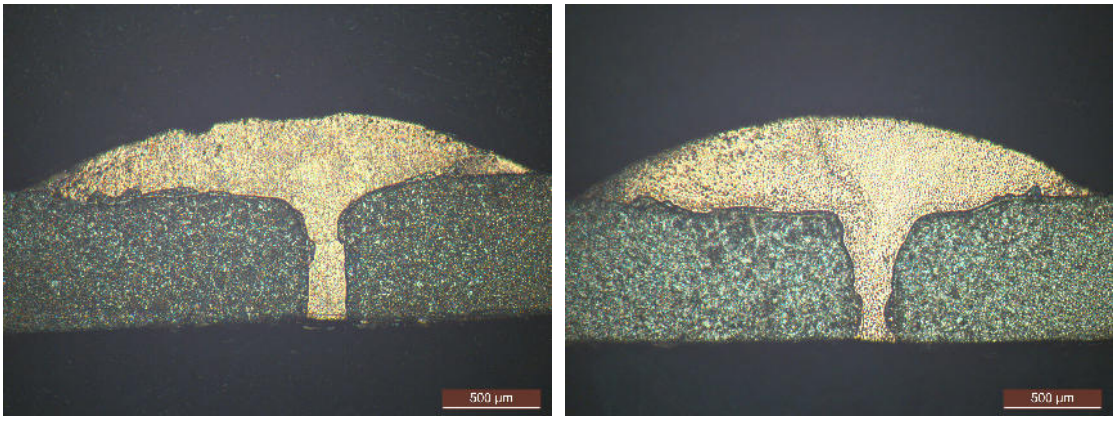

(a) Polished micrograph section of the joint brazed with a feed speed of base material 70.30 $\frac{mm}{min}$ and brazing wire 109.2 $\frac{mm}{min}$ respectively

(b) Polished micrograph section of the joint brazed with a feed speed of base material 70.30 $\frac{mm}{min}$ and brazing wire 138.4 $\frac{mm}{min}$ respectively

Figure 6.16.: Comparison of joints brazed with the same feed speed of base material 70.30 $\frac{mm}{min}$ and different feed speeds of brazing wire a) 109.2 $\frac{mm}{min}$; b) 138.4 $\frac{mm}{min}$ via polished micrograph sections; Parameters for brazing: P_{av} = 150 W, F = +5 mm, d_{gap} = 0.4 mm, WZL = 5.5 s, WZD = 4.7 s

There, it can be seen that base material was ablated within both brazed joints. Furthermore, it can be recognised that the laser spot was not centered to the gap for brazing both joints, since the material ablation as well as the spherical cap of the joint is slightly shifted to the left.

The surface condition of the spherical cap, of the joint brazed with the slower feed speed of brazing wire, is not smooth (Figure 6.16a), whereas the one brazed with the faster feed speed of brazing wire (Figure 6.16b) is smooth. Due to the increased feed speed of brazing wire, the height (h) of the spherical cap increased from 383.460 μm (Figure 6.16a) to 436.13 μm (Figure 6.16b) forming a smooth spherical cap. The spread diameter (2A) of both brazed joints was determined to 2780.167 μm (Figure 6.16a) and 2767.886 μm (Figure 6.16b) respectively. This results in a theoretical contact angle of 30.84° (Figure 6.16a) and 34.98° (Figure 6.16b) respectively, using equation (3.15). The measured contact angles for the joint brazed with a brazing wire feed speed of 109.2 $\frac{mm}{min}$ are: 25.102° (left) and 25.280° (right). For the joint brazed with a brazing wire feed speed of 138.4 $\frac{mm}{min}$, the measured contact angles correspond to 33.230° (left) and 26.090° (right). Although the wetting of the brazing wire onto the base material was sufficient with respect to the obtained contact angles, the joints brazed were still insufficient. This was because ablation of the base material still occurred.

Figure 6.17 shows the joints brazed with feed speeds of base material in the range of

76.00 $\frac{mm}{min}$ up to 79.80 $\frac{mm}{min}$.

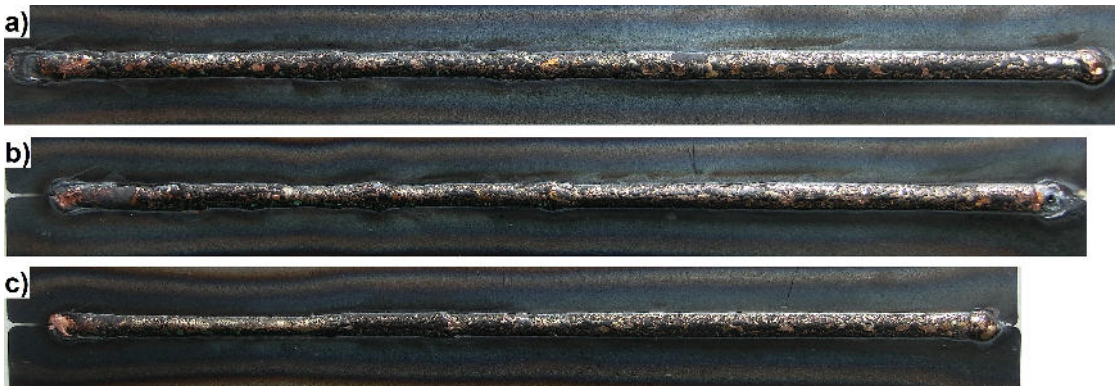

Figure 6.17.: Ratio of feed speeds without shielding gas: brazed joints of test number (B) with the following feed speeds of the base material a) 76.00 $\frac{mm}{min}$; b) 77.90 $\frac{mm}{min}$; c) 79.80 $\frac{mm}{min}$; Parameters for brazing: P_{av} = 150 W, F = +5 mm, v_b = 138.4 $\frac{mm}{min}$, d_{gap} = 0.4 mm, WZL = 5.5 s, WZD = 4.7 s

By visual inspection of these joints (see Figure 6.17), no clear base material ablation was recognised. However, by inspecting the rear side of these joints, it could be seen that the existing gap was not completely filled anymore. Figure 6.18 shows a typical example of rear sides of these brazed joints.

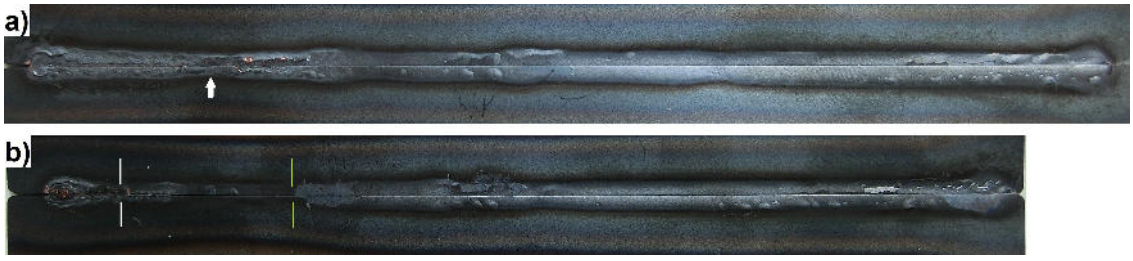

Figure 6.18.: Ratio of feed speeds without shielding gas: brazed joints of test number (B): typical rear sides of the above joints brazed exemplified on the joints brazed with a feed speed of a) 76.00 $\frac{mm}{min}$ b) 79.80 $\frac{mm}{min}$; Parameters for brazing: P_{av} = 150 W, F = +5 mm, v_b = 138.4 $\frac{mm}{min}$, d_{gap} = 0.4 mm, WZL = 5.5 s, WZD = 4.7 s

The white arrow in Figure 6.18 a) indicates the location of the gap where it is not filled by the brazing wire, which is approximately 5 mm long. The green mark in Figure 6.18 b) indicates the location where the existing gap is not recognisable anymore by visual inspection and the white mark indicates where the gap stopped being filled by the

brazing wire. Therefore, the laser brazing process itself is too fast for these tested feed speeds, since the gap is not filled anymore.

With regard to the visual inspection, these tests showed that sufficient brazed joints are achieved for a brazing wire feed speed of 138.4 $\frac{mm}{min}$ and feed speeds of base material in the range of 70.3 $\frac{mm}{min}$ up to 74.10 $\frac{mm}{min}$. This corresponds to a ratio in the range of 1.87:1 up to 1.97:1. These ratios are still close to the rule of thumb of 2:1.
Next to the investigation of the ratios of feed speeds, the joints brazed with a feed speed of base material of 74.10 $\frac{mm}{min}$ and a feed speed of brazing wire of 138.4 $\frac{mm}{min}$ has the best appearance with regard to wetting, gap filling and smoothness of the spherical cap. Therefore this was further investigated by carrying out a polished micrograph section in order to check if base material ablation still took place. For this the joint was cut at 15 mm. Figure 6.19 shows this polished micrograph section. There, it can be seen that ablation of the base material still takes place, but this ablation is decreased compared to the polished micrograph sections presented in Figure 6.16. Furthermore, the wetting onto the base material is sufficient, since the contact angles are measured to 22.875 ° (left) and 29.278 ° (right).

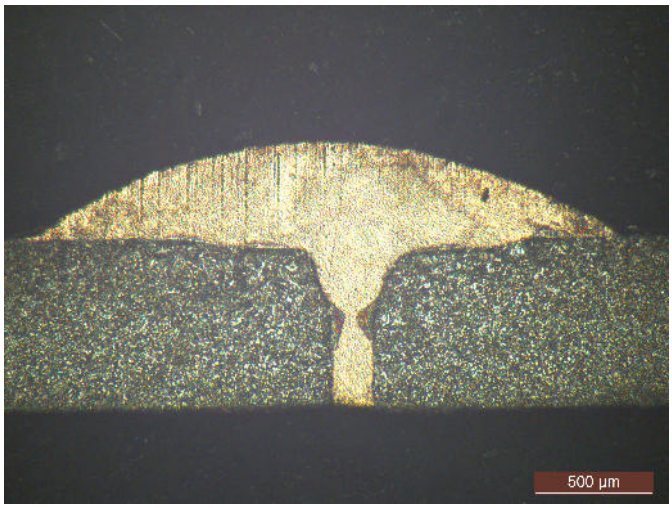

Figure 6.19.: Polished micrograph section of the joint brazed with with a feed speed of 74.10 $\frac{mm}{min}$ for the base material and 138.4 $\frac{mm}{min}$ for the brazing wire (see Figure 6.14 c)); The width of the joint corresponds to 2628.555 μm and the height is 423.983 μm, which results in a theoretical contact angle of 35.79° by using equation 3.15. The contact angles are measured to 22.875 ° (left) and 29.278 ° (right); Parameters for brazing: P_{av} = 150 W, F = +5 mm, v_b = 138.4 $\frac{mm}{min}$, d_{gap} = 0.4 mm, WZL = 5.5 s, WZD = 4.7 s

For this reason, these respective feed speeds are further used throughout this research.

6.3.3. Comparison of the ratios of feed speeds with and without shielding gas

These tests carried out with and without shielding gas showed that feasible ratios of feed speeds correspond approximately to the rule of thumb of 2:1. Only for the tests carried out without shielding gas, the ratio of feed speeds was a bit less (1.87:1), which led to an acceptable brazing result.
Based on these results the rule of thumb with regard to the ratio of feed speeds of 2:1 seems to be valid for brazing butt joints.
The most significant difference observed between these tests was the achievable process speed itself. As mentioned in section 6.3.1, the observed temperature, while brazing with shielding gas, was approx. 100° C to 250° C less, for the same initial position of the thermocouples, compared to the temperatures measured for the Nd:YAG laser parameter studies. That is why only a feasible feed speed of base material of 55.10 $\frac{mm}{min}$ was reached for brazing with shielding gas, as the usage of shielding gas cools down the brazing process. This is in contrast to the achieved feed speed of base material of 74.10 $\frac{mm}{min}$, for brazing without shielding gas. Figure 6.20 shows as an example the two temperature profiles measured for joints brazed once with shielding gas and once without by using the feed speeds of 109.2 $\frac{mm}{min}$ for the brazing wire and 55.10 $\frac{mm}{min}$ for the base material.

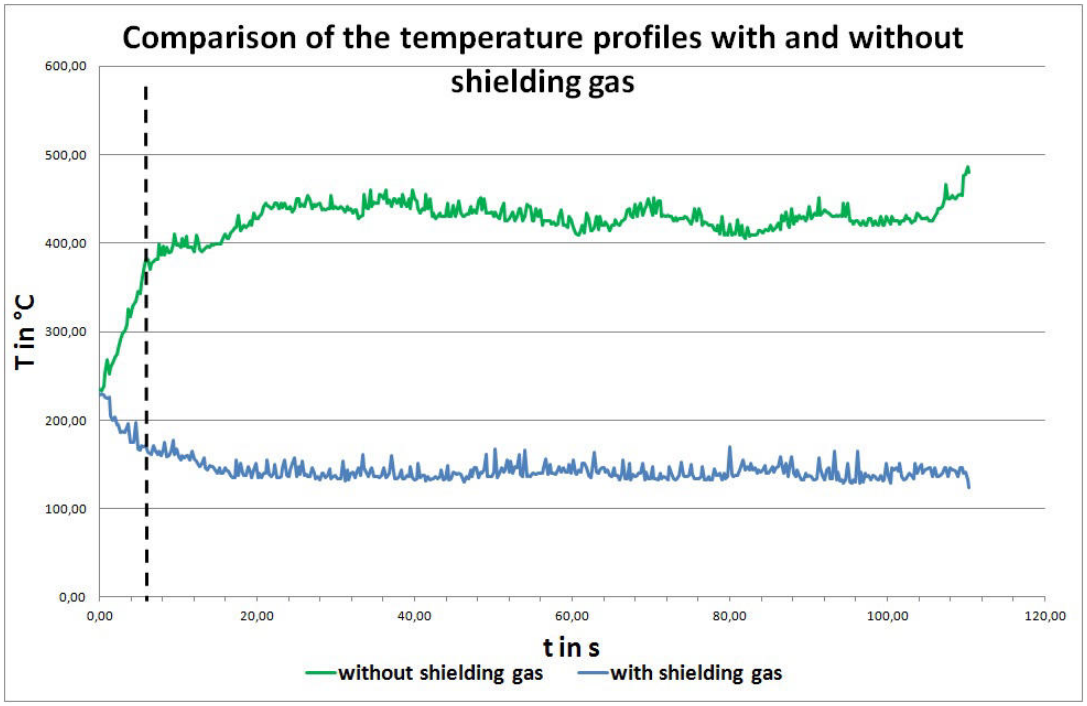

Figure 6.20.: Comparison of temperature profiles of joints brazed with and without using shielding gas exemplified on the joints brazed with a feed speed of 55.10 $\frac{mm}{min}$ by taking the respective data from the thermocouple positioned in front of the laser head. The thermocouples are approximately positioned 2.5 mm apart from the joint; Parameters for brazing: P_{av} = 150 W, F = +5 mm, v_b = 109.2 $\frac{mm}{min}$, d_{gap} = 0.4 mm, WZL = 5.5 s, WZD = 4.7 s

The dashed line in Figure 6.20 indicates when the delay time (WZL) ended. The temperature profile of the joint, brazed with shielding gas, decreases in the beginning to an almost steady value, since the shielding gas is automatically switched on via the program after the delay time (WZL) ended. With the joint, brazed without shielding gas, here the temperature increases during the delay time (WZL) up to an approximately steady value.

For this reason, the further parameter studies with the diode laser are carried out without using shielding gas, because of the significant decrease in achievable process speeds.

6.4. Pre-heating

The pre-heating is determined by the two delay times (WZL) and (WZD) (see section 3.1.2.3). During the initial experiments carried out with the Nd:YAG laser, it was demonstrated that pre-heating is needed in order to achieve a good quality brazed joint (see section 4.4.1). This aspect is further investigated in the following with regard

to the quality of brazed joints.
For this, the delay time (WZL) was set to the values stated in Table 6.4 and the delay time (WZD) was adapted accordingly (see Table 6.4).

Table 6.4.: Pre-heating: Tested delay times (WZL) and their correspondent delay times (WZD)

WZL s	WZD s
5.0	4.3
4.5	3.9
4.0	3.5
3.5	3.0
3.0	2.6

For each pre-heating set, stated in Table 6.4, at least three joints were brazed and subsequently investigated. The parameters for brazing are presented in Table 6.5.

Table 6.5.: Pre-heating: parameters used for laser brazing

P (W)	F (mm)	d_{gap} (mm)	v_b ($\frac{mm}{min}$)	v ($\frac{mm}{min}$)
150	+5	0.4	138.4	74.10

Figure 6.21 shows brazed joints, one for each tested delay time, set in the range of 5.0 s to 3.0 s for (WZL).

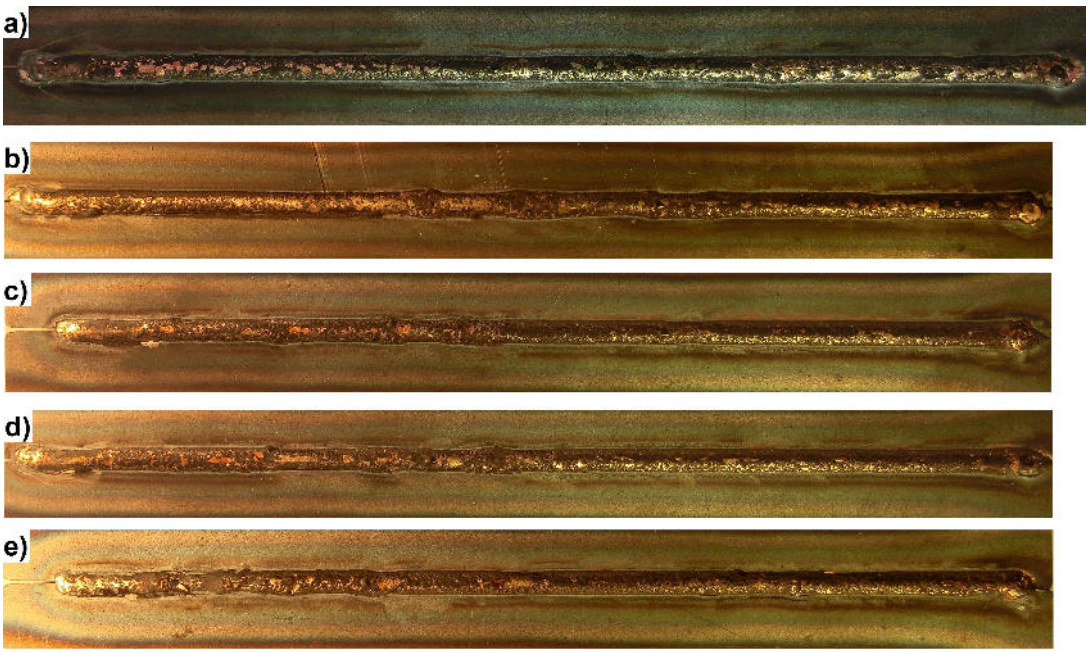

Figure 6.21.: Pre-heating: joints brazed with the delay time (WZL) in the range of 5.0 s to 3.5 s: a) WZL = 5.0 s, WZD = 4.3 s; b) WZL = 4.5 s, WZD = 3.9 s; c) WZL = 4.0 s, WZD = 3.5 s d) WZL = 3.5 s, WZD = 3.0 s; e) WZL = 3.0 s, WZD = 2.6 s; Parameters for brazing: P_{av} = 150 W, F = +5 mm, v_b = 138.4 $\frac{mm}{min}$, v = 74.10 $\frac{mm}{min}$, d_{gap} = 0.4 mm

As it can be seen in Figure 6.21 a), the joint, by visual examination, is smooth and consistent across the width. In Figure 6.21 b) to d), the decrease in pre-heating is recognisable, because the consistency of the joint width disappears. Especially in Figure 6.19 c) and d), where it can be seen that the height of the joint increased at the beginning.

It could be recognised, in addition, a width increase over the length of the joint. Both mentioned aspects indicate that the pre-heating is insufficient at the beginning of the brazing process. This observation corresponds to the occurrence of the oxidation marks. If an appropriate operating temperature for brazing is reached during the pre-heating phase, the oxidation marks remain parallel to the brazed joint, see Figure 6.22 (top). The white line indicates the edge of the oxidation marks. If an appropriate operating temperature is not reached during the pre-heating phase, the oxidation marks diverge over the length of the joint, as Figure 6.22 (bottom) shows.

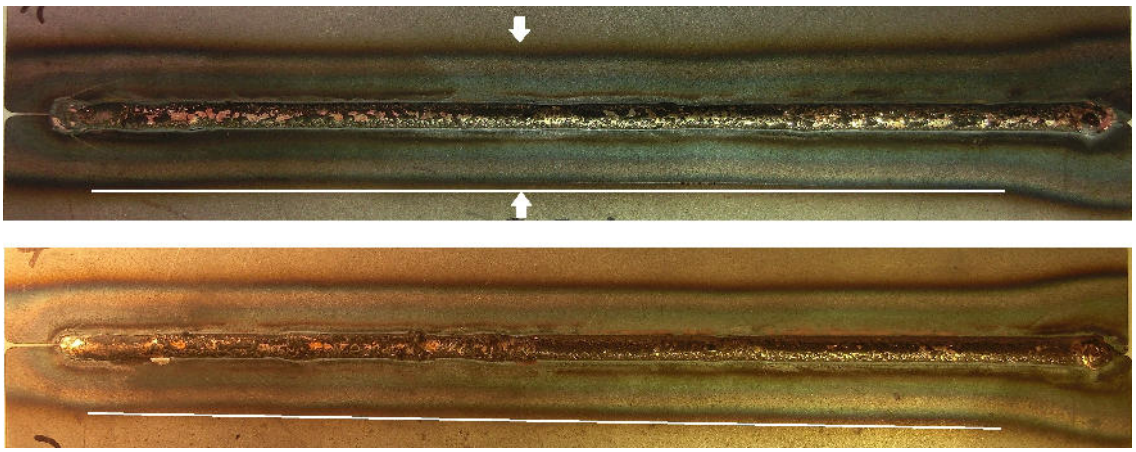

Figure 6.22.: Pre-heating: oxidation marks show consistency in maintaining a proper operating temperature throughout the process (top); Top: joint brazed with WZL = 5.0 s, WZD = 4.3 s;; Bottom: joint brazed with WZL = 4.0 s, WZD = 3.5 s; Parameters for brazing: P_{av} = 150 W, F = +5 mm, v_b = 138.4 $\frac{mm}{min}$, v = 74.10 $\frac{mm}{min}$, d_{gap} = 0.4 mm

Furthermore, the joints, brazed with WZL = 3.0 s, have an additional characteristic, the brazing wire sank almost completely into the gap and formed a partial joint at the rear side of the base material (see Figure 6.21 (e)). This is caused by the decrease of the pre-heating phase, as the base material expands less during this period, which leads to gap widths that are not within the optimal range for laser brazing (see section 3.2.1.1 and 5.2.1 respectively). This characteristic can be clarified when comparing joints brazed with WZL = 3.5 s [10] and WZL = 5.0 s. Figure 6.23 shows an enlarged view of the respective rear sides of the joints brazed. The respective gap widths are determined at a distance of 7 mm, from the beginning, which is indicated by the white lines in Figure 6.23.

[10] A joint brazed with WZL = 3.5 s was chosen for comparison, since all joints brazed with WZL = 3.0 s formed a partial joint on the rear side, so that no gap could be recognised

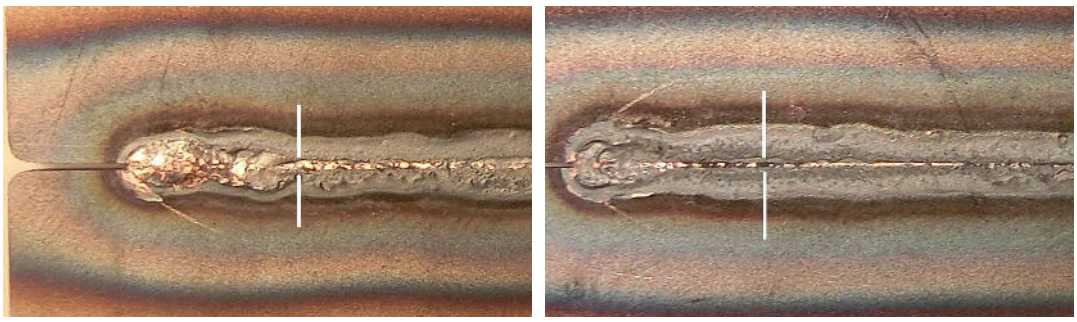

(a) Enlarged view of the rear side of a joint brazed with WZL = 3.5 s

(b) Enlarged view of the rear side of a joint brazed with WZL = 5.0 s

Figure 6.23.: Comparison of gap width of brazed joints in dependence on the delay time (WZL) used: a) WZL = 3.5 s, WZD = 3.0 s; gap width measured at the location of 7 mm: 0.40 mm; b) WZL = 5.0 s, WZD = 4.3 s; gap width measured at the location of 7 mm: 0.26 mm; the location where the gap width is measured is indicated by the white lines; Parameters for brazing: P_{av} = 150 W, F = +5 mm, v_b = 138.4 $\frac{mm}{min}$, v = 74.10 $\frac{mm}{min}$, d_{gap} = 0.4 mm

Thus, the gap width for the joint brazed with WZL = 3.5 s corresponds to approximately 0.40 mm, whereas the gap width of the joint brazed with WZL = 5.0 s is approximately 0.26 mm.[11]

The improper heating can also be recognised by the respective temperature profiles of the brazed joints. For this, the measured temperature profiles of the tested delay time sets (see Table 6.4) are split into two graphs for clearer investigation.

At this point it should be noted that the temperature profiles differ depending on the operating temperature reached. This is caused by the manual positioning of the thermocouples, because setting them the same distance from the joint could not always be achieved. However, for this investigation, it is of minor importance, since the curve progression of the temperature profiles at the beginning is the important fact.

Figure 6.24 shows the respective temperature profiles of the joints brazed with the delay time (WZL) ranging from 5.5 s to 4.5 s. A temperature profile of a joint brazed with a (WZL) of 5.5 s is included in Figure 6.24, as this delay was used for the previous experiments. This profile corresponds to the joint brazed using the parameter set stated in Table 6.5, which is shown in Figure 6.14 c).

[11] The gap widths were determined as described in section 5.2.1

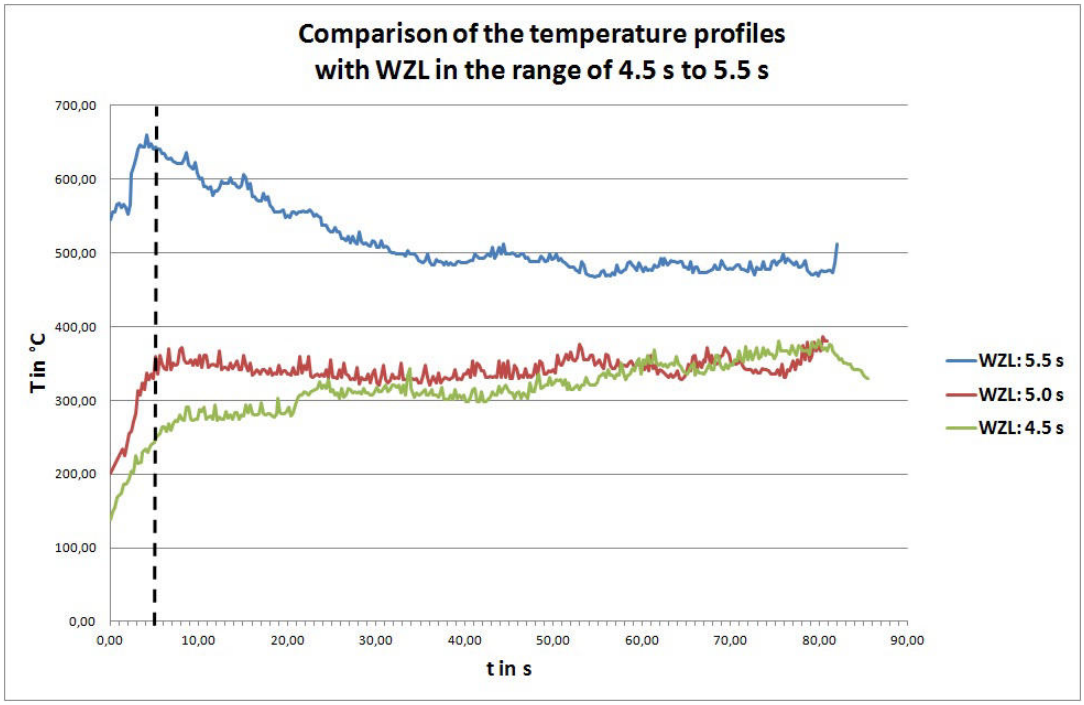

Figure 6.24.: Comparison of temperature profiles of joints brazed with delay times (WZL) in the range of 5.5 s to 4.5 s; the respective delay times (WZD) are stated in Table 6.4; the black dashed line is positioned at the time t of 5 s to easier recognise when the respective delay time (WZL) ends; Parameters for brazing: P_{av} = 150 W, F = +5 mm, v_b = 138.4 $\frac{mm}{min}$, v = 74.10 $\frac{mm}{min}$, d_{gap} = 0.4 mm

The black dashed line in Figure 6.24 is positioned at time t = 5.0 s for easier recognition when the respective delay time (WZL) ends. For WZL = 5.5 s, it can be seen that the temperature increases fast during the pre-heating period (t = 4.0 s). Then the temperature drops slightly, since the wire feed started after the delay of 4.7 s for (WZD). Comparing this temperature profile to the one with WZL = 5.0 s, it can be seen that the operating temperature is just reached when the delay time (WZL) ended and not earlier as for WZL = 5.5 s. Furthermore, a slight decrease in slope can be recognised for the temperature profile WZL = 5.0 s (approx. t = 4.0 s). This can be reasoned by the start of the wire feed (WZD = 4.3 s). The temperature profile of WZL = 4.5 s shows that an adequate operating temperature is not reached during the pre-heating period, since the temperature increases until t = 9.0 s, where an acceptable operating temperature is reached. Converting this time difference of 4.5 s into unit length, this corresponds to a length of 5.56 mm joint brazed with insufficient operating temperature. This behaviour can be seen in Figure 6.21 b), because the joint starts to take on an almost consistent joint width at this location of 5.56 mm.

Figure 6.25 shows the respective temperature profiles for the joints brazed with a delay

of (WZL) in the range of 4.0 s to 3.0 s. The black dashed line is positioned at t = 3.5 s for easier recognition when the respective (WZL) ends.

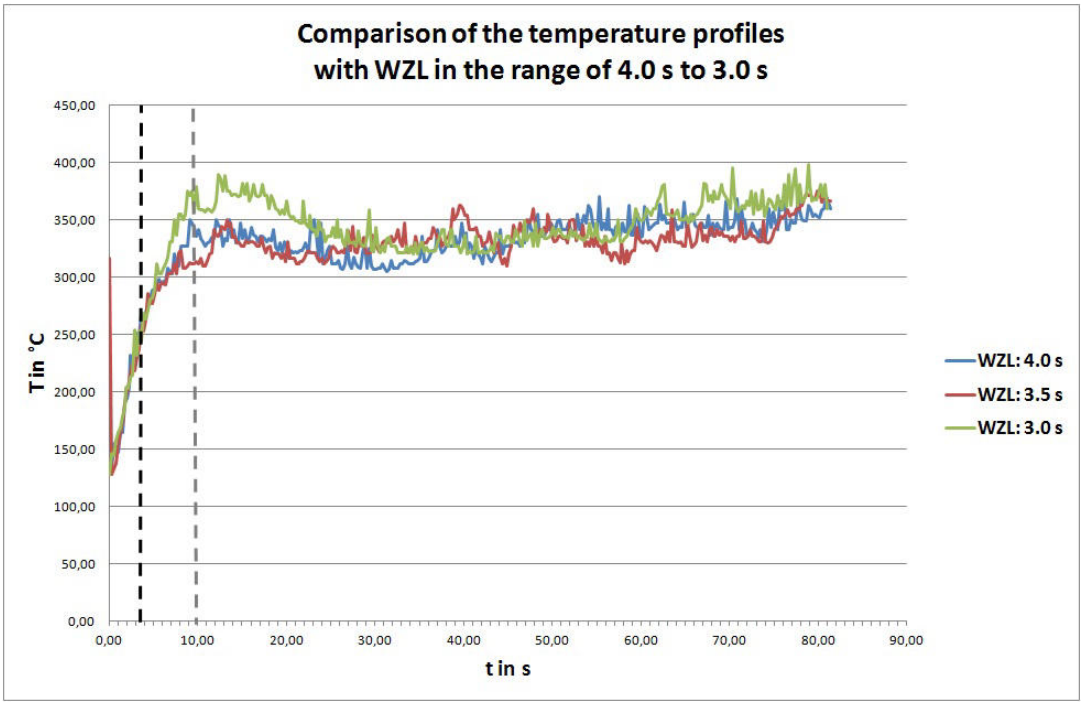

Figure 6.25.: Comparison of temperature profiles of joints brazed with delay times (WZL) in the range of 4.0 s to 3.0 s; the respective delay times (WZD) are stated in Table 6.4; the black dashed line is positioned at the time t of 3.5 s to easier recognise when the respective delay time (WZL) ends; the grey dashed line indicates when an almost steady operating temperature is reached; Parameters for brazing: P_{av} = 150 W, F = +5 mm, v_b = 138.4 $\frac{mm}{min}$, v = 74.10 $\frac{mm}{min}$, d_{gap} = 0.4 mm

As it can be seen in Figure 6.25, none of the temperature profiles reached an appropriate operating temperature during the pre-heating phase. A proper operating temperature is reached approximately at t = 10 s for WZL = 4.0 s which is indicated by the grey dashed line. This corresponds to a length of 7.41 mm brazed joint with insufficient operating temperature by considering the (WZL). The other temperature profiles reach a sufficient operating temperature at approximately t = 11.0 s for WZL = 3.5 s and at t = 12 s for WZL = 3.0 s. Their correspondent lengths of insufficient brazed joints are 9.26 mm and 11.12 mm respectively.

As demonstrated a decrease in (WZL) results in an increase in time when an appropriate operating temperature is reached. Hence, an appropriate pre-heating phase is essential for achieving qualitatively good brazed joints. Within this section the successful implementation of an appropriate pre-heating phase was demonstrated and veri-

fied by the respective temperature profiles and oxidation marks. Moreover, these tests showed that the pre-heating phase can be reduced by 0.5 s, as for WZL = 5.0 s and WZD = 4.3 s also a sufficient operating temperature is reached during the pre-heating phase (see Figure 6.24). For this reason, this pre-heating is used in the following.

6.5. Heat input

The heat input is dependent on the laser power and the feed speed of the base material (see section 6.1) along with the wavelength dependent absorption behaviour of the materials used (see section 4.3). The parameter studies carried out so far showed on the one hand that the ratio of feed speeds has to be approximately 2:1 for brazing butt joints (see section 6.3). On the other hand they showed that pre-heating is needed to obtain a good quality joint (see section 6.4 and 4.4.2 respectively). Although appropriate feed speeds for both base material and brazing wire were identified for laser brazing with the diode laser in section 6.3, the heat input was not optimal as base material ablation still took place (see Figure 6.19). Therefore, experiments were carried out to investigate the influence of the heat input to the brazing result by changing the laser power.
The occurrence of material ablation indicates that the laser power is too high for the given feed speed. Hence, the laser power is gradually decreased from 150 W down to 144 W in 2 W steps. The joints were brazed with the parameters stated in Table 6.6 and with the following laser powers: 150.0 W, 148 W, 146.0 W, 144.0 W.

Table 6.6.: Parameters used for the heat input investigation

WZD (s)	WZL (s)	F (mm)	d_{gap} (mm)	v_b ($\frac{mm}{min}$)	v ($\frac{mm}{min}$)
4.3	5.0	+5	0.4	138.4	74.10

Each joint was repeated 5 times. Figure 6.26 and Figure 6.27 show the brazed joints as well as their reverse sides at the respective power levels.

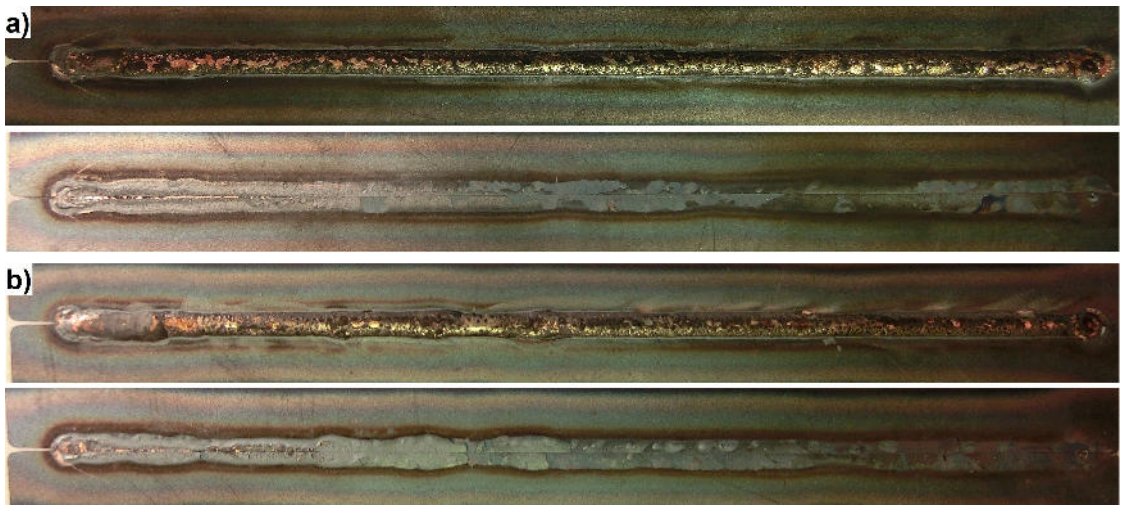

Figure 6.26.: Joints brazed with laser powers of a) P = 150 W and b) P = 148 W; Parameters for brazing: F = +5 mm, v = 74.10 $\frac{mm}{min}$, v_b = 138.4 $\frac{mm}{min}$, d_{gap} = 0.4 mm, WZL = 5.0 s, WZD = 4.3 s

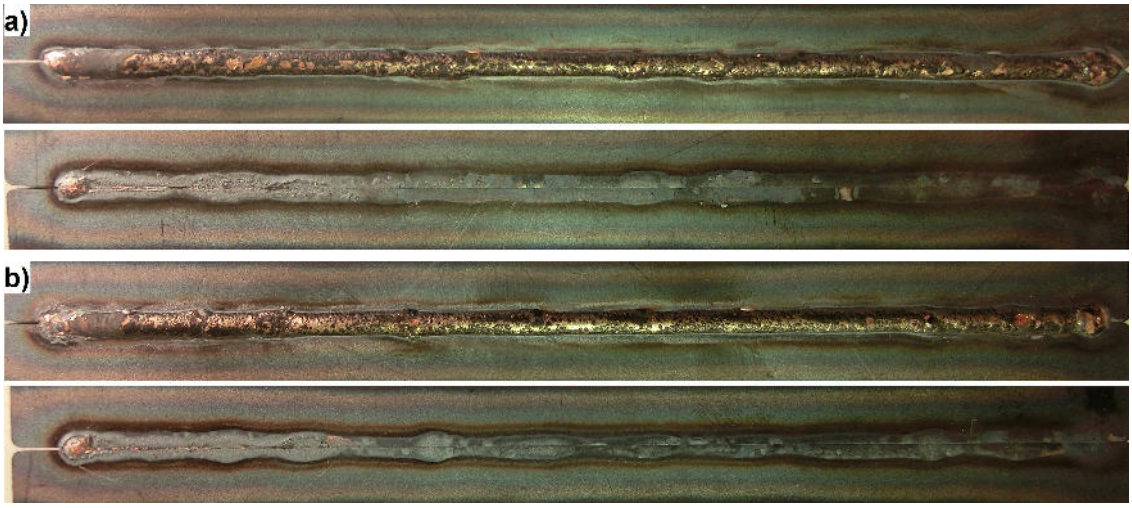

Figure 6.27.: Joints brazed with laser powers of a) P = 146 W and b) P = 144 W; Parameters for brazing: F = +5 mm, v = 74.10 $\frac{mm}{min}$, v_b = 138.4 $\frac{mm}{min}$, d_{gap} = 0.4 mm, WZL = 5.0 s, WZD = 4.3 s

There, it can be seen that the base material does not seem to be affected at the surface, with regard to ablation, and that all existing gaps are completely filled by the brazing wire. To investigate if base material ablation still occurs within the brazed joints, polished micrograph sections were carried out. For this, the brazed joints were cut at the length of 15 mm measured from the beginning of the joint. The respective polished micrograph sections are presented in Figure 6.28 and Figure 6.29.

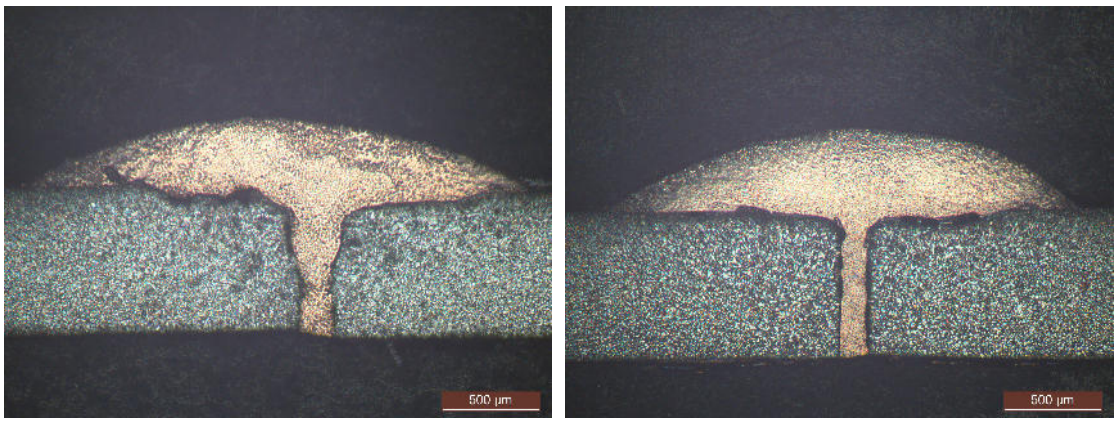

(a) Polished micrograph section of the joint brazed with P = 150 W

(b) Polished micrograph section of the joint brazed with P = 148 W

Figure 6.28.: Polished micrograph sections of the joints brazed with a) P = 150 W and b) P = 148 W; Parameters for brazing: F = +5 mm, v = 74.10 $\frac{mm}{min}$, v_b = 138.4 $\frac{mm}{min}$, d_{gap} = 0.4 mm, WZL = 5.0 s, WZD = 4.3 s

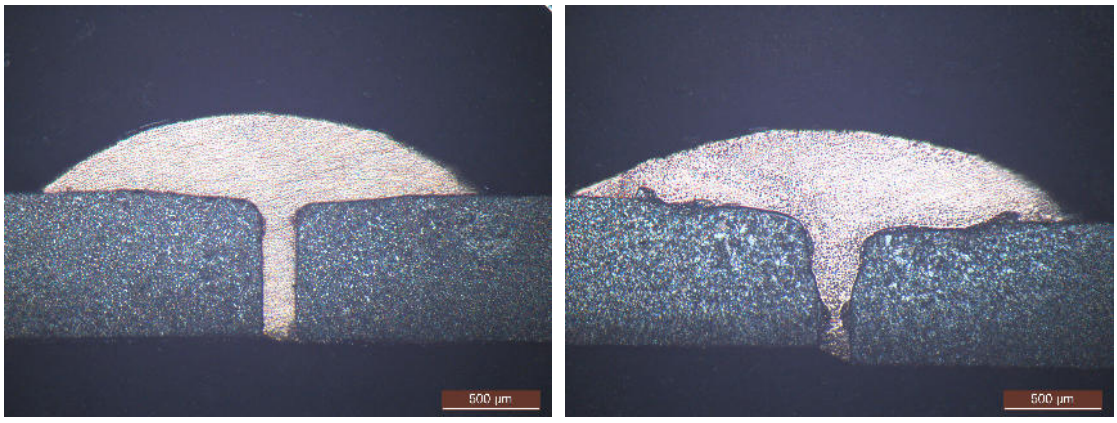

(a) Polished micrograph section of the joint brazed with P = 146 W

(b) Polished micrograph section of the joint brazed with P = 144.0 W

Figure 6.29.: Polished micrograph sections of the joints brazed with a) P = 146 W and b) P = 144 W; Parameters for brazing: F = +5 mm, v = 74.10 $\frac{mm}{min}$, v_b = 138.4 $\frac{mm}{min}$, d_{gap} = 0.4 mm, WZL = 5.0 s, WZD = 4.3 s

As it can be seen in both Figures 6.28 and 6.29 , a decrease in ablation of the base material is recognisable with a decrease in laser power. The significant material ablation in Figure 6.28a resulted from the not centered positioning of the laser spot across the gap. If the laser spot is positioned correctly, the material ablation still occurs, but it is less as shown in Figure 6.19.

The joint brazed with a laser power of P = 144 W differs from the expectations with re-

gard to the base material ablation as well as the wetting onto the base material. It was expected that the base material ablation disappears and that the wetting onto the base material worsens with a decrease in laser power. However, these tests showed that the material ablation decreases from the joints brazed with P = 150 W to P = 146 W and for P = 144 W it increases again. This behaviour is caused by the decrease in laser power. This decrease leads to a lesser thermal expansion during pre-heating, which results in a larger gap width. Thus the gap width is not in the optimal range for laser brazing and therefore the brazing wire sags into the gap. Due to this, lesser brazing wire covers the base material which results in ablation of the base material and in a maintained wetting. The same behaviour was observed during the studies with regard to pre-heating as demonstrated in section 6.4. At this point it should be noted that the above mentioned behaviour only accounts for the beginning of the brazed joints (approximately the first 25 mm), since within this length a gap can be recognised by visual inspection. The rest of the joint shows the expected decrease in wetting as it can be seen in Figure 6.26 and 6.27 respectively with regard to its width.
The joints brazed with P = 144 W showed all this described behaviour except for the one presented in Figure 6.27 b). There, the existing gap is completely filled and none of the brazing wire is sagged through in the beginning of the joint. This characteristic might be reasoned by human error due to the manual start of the laser and the wire feed. In general those joints brazed have an appearance at the beginning of the joint as shown in Figure 6.30.

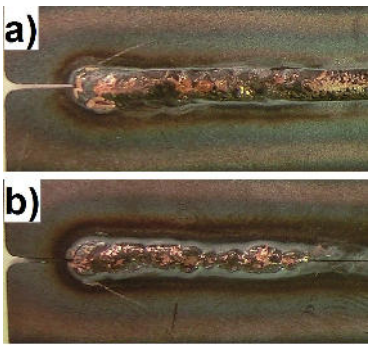

Figure 6.30.: Typical enlarged view of the beginning of a joint brazed with P = 144 W (approx. the first 26 mm): a) Beginning of the joint; b) Its respective rear side; Parameters for brazing: F = +5 mm, v = 74.10 $\frac{mm}{min}$, v_b = 138.4 $\frac{mm}{min}$, d_{gap} = 0.4 mm, WZL = 5.0 s, WZD = 4.3 s

All other joints brazed with the different powers tested were reproducible as presented in Figure 6.26 and Figure 6.27 a) respectively.

The polished micrograph sections of the joints are further investigated with regard to their width, height and the respective contact angles. Moreover, the gap width is measured in center of the thickness of the base material. The results are presented in Table 6.7. Furthermore, the theoretical contact angle is calculated by using equation 3.15 and also stated in Table 6.7.

Table 6.7.: Measurement results from the investigation of the respective polished micrograph section with regard to width, height, contact angle and gap width; ($\theta_{theoretical}$) is determined by using equation 3.15

P (W)	width (μm)	height (μm)	$\theta_{theoretical}$ ($^\circ$)	θ_{left} ($^\circ$)	θ_{right} ($^\circ$)	d_{gap} (μm)
150	2690.467	386.663	32.073	30.355	35.529	171.943
148	2458.474	451.535	40.339	41.009	39.170	143.493
146	2402.808	460.864	41.974	33.762	29.264	179.377
144	2755.554	482.427	38.595	29.531	27.951	154.626

Considering the results obtained with regard to material ablation and contact angle, the joints brazed with a power of 146 W are the best to be obtained. Since its contact angles are within the optimal range (see Table 6.7) and a base material ablation is scarcely recognisable (see Figure 6.29a).
The heat input can be estimated by using equation (4.4). Therefore, the reduction of the heat input from 121.46 $\frac{J}{mm}$ (P = 150 W) down to 118.23 $\frac{J}{mm}$ (P = 146 W) led to good quality brazed joints by using the parameter set stated in Table 6.6.

6.6. Quality investigations

The brazed joints of the experiments carried out with regard to heat input (see section 6.5) are further investigated with regard to their quality, as these joints were brazed with the appropriate parameters identified within these parameter studies with the diode laser (see Table 6.8). For these joints the Vickers hardness testing was carried out.

Table 6.8.: Appropriate parameters for diode laser brazing

WZD (s)	WZL (s)	F (mm)	d_{gap} (mm)	v_b ($\frac{mm}{min}$)	v ($\frac{mm}{min}$)
4.3	5.0	+5	0.4	138.4	74.10

Especially the joint brazed with P = 146 W and the parameters stated in Table 6.8 is further investigated, as this joint was the most appropriate one with regard to achieved quality (see section 6.5). Therefore, tensile testing was carried out with these joints.
The results of both Vickers hardness and tensile testing for the joint brazed with 146 W are presented in the following.
As mention in section 4.4, the alloy zone could be clearly identified by the optical inspection via a microscope. Only a thin black line was visible in all polished micrograph sections carried out. For this reason, the alloy zone was further investigated by the aid of a SEM. For this, the polished micrograph section of the joint brazed with shielding gas was used (see Figure 6.9). The results of this analysis are also presented within this section.

6.6.1. Vickers hardness

The polished micrograph sections, presented in Figure 6.28 and 6.29 respectively, were used for Vickers hardness testing to investigate the hardness changes over the cross-sectional area of the brazed joint. Each polished micrograph section is approximately 20 mm long with regard to the sample. Therefore, the Vickers hardness measurement was started centered and 2 mm away from the left edge of the base material for each polished micrograph section. This distance of 2 mm was selected to ensure that the interface of the base material and embedding material does not influence the hardness measurement (see section 3.2.2.2). For a distance of 5 mm the measurement interval was set to 1 mm. Then the measurement interval was decreased to 0.5 mm, since there the area of the Heat Affected Zone (HAZ), including the gap, was reached, where a significant hardness change was expected. The interval of 0.5 mm was selected to avoid any influence of the previous hardness measurement (see section 3.2.2.2). It was kept constant for 5 mm. Leaving the area of the HAZ, the measurement interval was increased back to 1 mm for the rest of the length of the polished micrograph section. The last measurement was carried out 2 mm away from the right edge of the base material. This just described measurement approach is visualised in Figure 6.31.

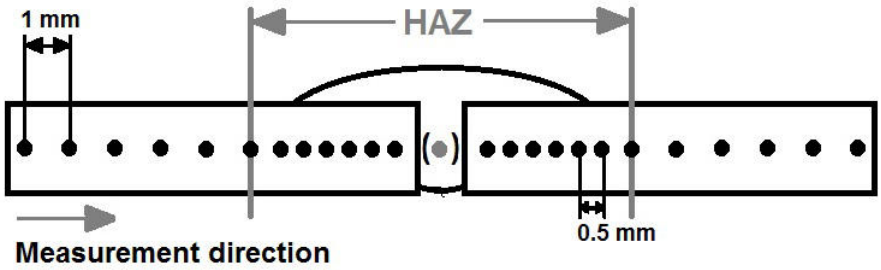

Figure 6.31.: Principle of Vickers hardness measurement approach; the measurement is started centered and 2 mm away from the left edge of the base material; hardness is measured in 1 mm steps until the region of the HAZ is approximately reached; within the region of the HAZ the hardness is measured in 0.5 mm steps. The measurement point in the gap (indicated in grey) is not always measured, because the gap was sometimes to small

Each hardness measurement was carried out as described in section 3.2.2.2, i.e. the indenter was applied onto the surface with 1 kgf (9.807 N) for 15 s.

The hardness change over the cross-sectional area is exemplified on the the joint brazed with P = 146.0 W (see Figure 6.32). The respective measurement results of the diagonals, the correspondent hardness values as well as the hardness changes over the cross-sectional area for the other polished micrograph sections tested can be found in Appendix C.1.

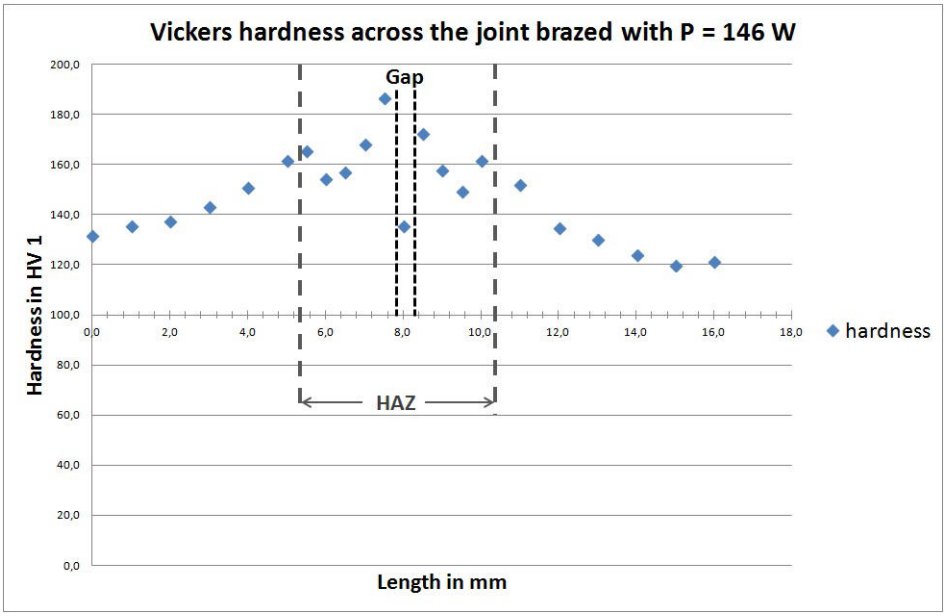

Figure 6.32.: Vickers hardness measurement across the polished micrograph section of the joint brazed with P = 146.0 W; Parameters for brazing: F = +5 mm, v = 74.10 $\frac{mm}{min}$, v_b = 138.4 $\frac{mm}{min}$, d_{gap} = 0.4 mm, WZL = 5.0 s, WZD = 4.3 s

The gap of the brazed joint is located at 8.0 mm in Figure 6.32. Its correspondent hardness value belongs to the brazing wire. That is why this hardness value of 135.5 HV 1 is less compared to the adjacent hardness values, which belong to the base material. However, this hardness value of the brazing wire has to be taken with care, because the gap width of this polished micrograph section corresponds to 179.377 μm (see Table 6.7) and the diagonals of the respective indentation are in the range of 116.0 μm to 118.0μm (see Table C.2). Thus, the base materials have an influence on this measurement, since the minimum required measurement distance was not fulfilled (see section 3.2.2.2).
Furthermore, the expected increase in hardness in the area of the Heat Affected Zone (HAZ) is clearly visible in Figure 6.32, having its peak values directly at the gap. This behaviour is caused by the fast heating due to the incident laser radiation and the subsequent cooling (Higgins, 1983).
The other brazed joints tested show the same behaviour with regard to the hardness change (see Appendix C.1). The hardness measurements taken at the beginning and at the end of the total measurement distance should correspond to the original hardness of the base material. The original hardness of the base material is in the range of 90 - 120 HB (see section 4.3). However, its hardness is given in Brinell hardness. Since an unalloyed steel is used as the base material (Higgins, 1983), the Vickers hardness is allowed to be converted to Brinell hardness according to DIN EN ISO 18265 via the following relation (Bargel and Schulze, 2012):

$$HB = 0.95 * HV. \tag{6.1}$$

Converting the Vickers hardness values, located at the very left and at the very right of the brazed joint, results in a Brinell hardness of 125.02 HB and 115.33 HB respectively (see Table C.2). By considering measurement tolerances, such as the reading of the diagonals as well as the manual adjustment of the polished micrograph section parallel to the linear axes of the Vickers testing machine, the converted value of the very right Vickers hardness can be accepted to be within the stated hardness range of the base material used. The hardness value at the very left is slightly increased, which could be caused by the not exact positioning of the laser spot at the center of the gap (see Figure 6.28 and 6.29 respectively). The laser spot was slightly shifted to the left for all polished micrograph sections.
As mentioned above, the joints brazed with P = 146.0 W are further investigated with

regard to tensile testing (see section 3.2.2.3). The tests as well as the respective results are presented in the following.

6.6.2. Tensile testing

The joints brazed with P = 146.0 W are used for tensile testing, as these joints were the most appropriate ones obtained with regard to quality. For testing, the tensile testing machine Instron 3367 was used (see section 3.2.2.3). Its crossheads have a width of 25 mm. For this reason, the joints brazed with P = 146.0 W have to be prepared, so that the tension tests can be carried out, since the base materials have a total length of 110 mm.

Each joint was cut at 15 mm, 40 mm, 65 mm and 90 mm measured from the beginning of the base material. The cutting at the length of 15 mm was already carried out for the preparation of the polished micrograph section. An example of a brazed joint with the respective cutting marks is shown in Figure 6.33. Only the pieces of the joint (in the following named samples), marked with the encircled numbers (2) to (4), were used for testing (see Figure 6.33).

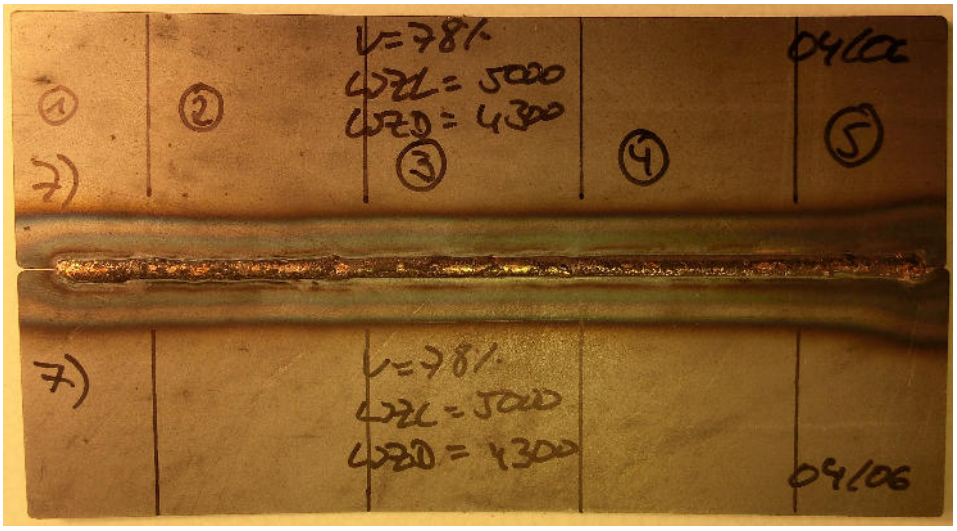

Figure 6.33.: Example of sample preparation for tensile testing: each joint is cut at 15 mm, 40 mm, 65 mm and 90 mm resulting in 5 samples; only samples (2) to (4), indicated by the respective encircled numbers, were used for tensile testing

These samples (2) to (4) correspond to

- The beginning of the joint with gap existence (2)
- The middle of the joint, having no gap (3)
- The end of the joint, with increased thermal expansion due to heat conduction and no gap (4)

Since the 5 joints brazed were cut as stated above, 5 samples per area of interest were obtained, so they are referred to in the following as:

- Sample set (A) corresponds to samples (2)
- Sample set (B) corresponds to samples (3)
- Sample set (C) corresponds to samples (4).

The width of each sample corresponds to the clamping area width of the crossheads, which is 25 mm and each sample is approximately 59.9 mm to 60.2 mm long, depending on the location of the width measurement. Due to the dimensions of the samples, it should be noted that these tension tests only account for a relative analysis of the joint behaviour, because it was not possible to produce the samples in a standard dog bone shape (as used in standard tensile testing) (Fischer, 2008).
To ensure a reproducible clamping of each sample, the oxidation marks were used as guidance (see red arrows in Figure 6.34a). After clamping the first sample, as shown in Figure 6.34a, the distance between the crossheads was measured, which corresponded to 13 mm (see Figure 6.34). Subsequently, a mark was set at the crosshead travel scale, so that this distance could be set for all samples tested.

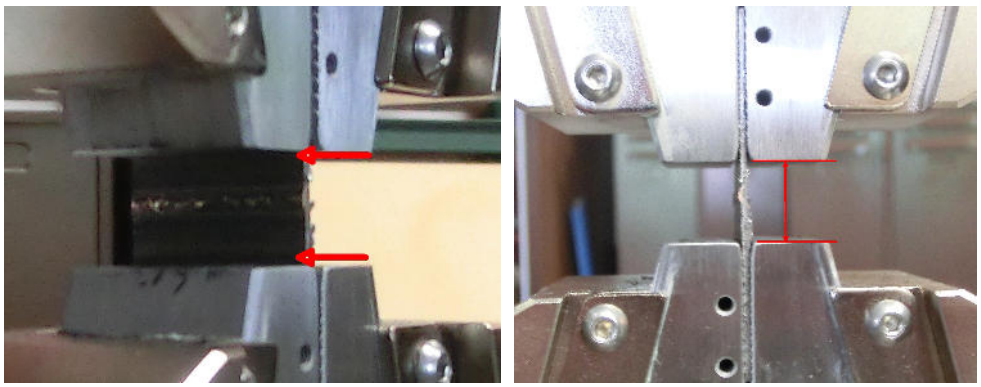

(a) The width of the oxidation marks was used as orientation

(b) The distance between crossheads corresponds to 13 mm

Figure 6.34.: Clamping of the samples via the crossheads: a) The width of the oxidation marks was used as orientation for clamping which is indicated by the red arrows; b) The distance between crossheads corresponds to 13 mm

The following parameters were set for tensile testing:

- Preliminary test:
  - Crosshead travel speed: 10 $\frac{mm}{min}$
  - Force: 200 N
- Actual test:
  - Crosshead travel speed: 5 $\frac{mm}{min}$
  - Condition for stopping the measurement: 40 % of force

The preliminary test for each measurement was needed to ensure proper clamping and no slip of the sample during the actual measurement. Figure 6.35 to 6.36 show the force-displacement curves of the respective sample set. An enlarged view of these curves can be found in Appendix C.2.

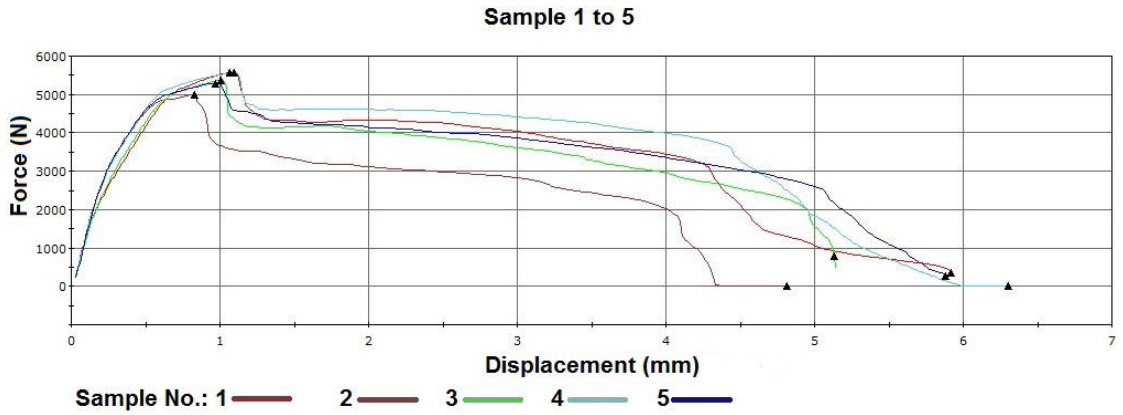

Figure 6.35.: Force-displacement curve of sample set (A); Tensile testing parameters: crosshead travel speed: 5 $\frac{mm}{min}$, condition for stopping the measurement: 40 % of force; Parameters for brazing: P = 146 W, F = +5 mm, v = 74.10 $\frac{mm}{min}$, v_b = 138.4 $\frac{mm}{min}$, d_{gap} = 0.4 mm, WZL = 5.0 s, WZD = 4.3 s

As it can be seen in Figure 6.35 to 6.36, the force against displacement was measured, where the displacement is equal to the extension of the sample being tested. Due to this fact, the measurements are dependent on the dimensions of the sample tested. In general, stress-strain curves are used, which are independent on the geometry of sample tested due to their respective definition (Bargel and Schulze, 2012). However, these force-displacement curves are appropriate for a relative evaluation of the behaviour of the brazed joints with applied force.

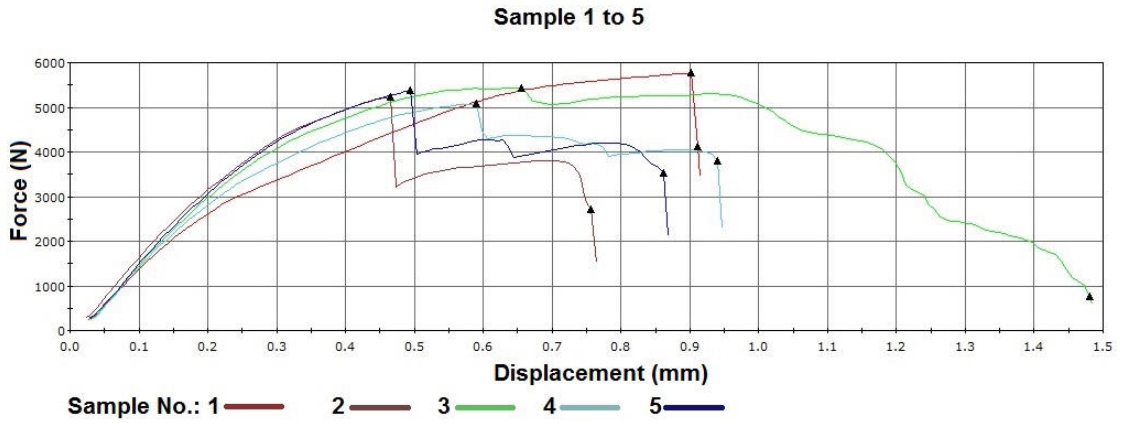

Figure 6.36.: Force-displacement curve of sample set (B); Tensile testing parameters: crosshead travel speed: 5 $\frac{mm}{min}$, condition for stopping the measurement: 40 % of force; Parameters for brazing: P = 146 W, F = +5 mm, v = 74.10 $\frac{mm}{min}$, v_b = 138.4 $\frac{mm}{min}$, d_{gap} = 0.4 mm, WZL = 5.0 s, WZD = 4.3 s

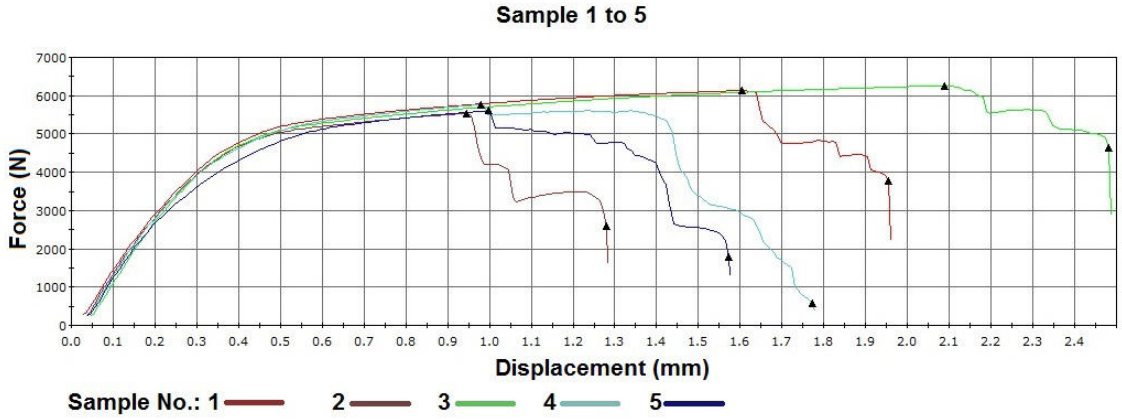

Figure 6.37.: Force-displacement curve of sample set (C); Tensile testing parameters: crosshead travel speed: 5 $\frac{mm}{min}$, condition for stopping the measurement: 40 % of force; Parameters for brazing: P = 146 W, F = +5 mm, v = 74.10 $\frac{mm}{min}$, v_b = 138.4 $\frac{mm}{min}$, d_{gap} = 0.4 mm, WZL = 5.0 s, WZD = 4.3 s

Comparing the force-displacement curves from sample set (A) to (B) (see Figure 6.35 to 6.37), it can be seen that all curves show a smooth and gradual behaviour from linear elastic to gradual deformation up to their respective point of ultimate force. The respective characteristics of each sample with regard to e.g. ultimate force, Young's modulus, were averaged for each sample set and are shown in Table 6.9. The detailed measurement results of each sample set can be found in Appendix C.2. These characteristics were automatically determined by the tensile-testing-machine's software program.

Table 6.9.: Measurement results from tensile testing of sample sets (A) to (C)

Sample set	Average force at fracture (N)	Average crosshead travel at fracture (mm)	Average ultimate Force (N)	Average tensile extension (crosshead travel) at ultimate force $\frac{mm}{mm}$	Average tensile stress (MPa)	Average Young's modulus (MPa)
A	285.86 ±328.04	5.61 ±0.62	5,361.39 ±235.13	0.010 ±0.001	536.14 ±23.51	152,268.96 ±7,526.39
B	2,982.83 ±1,342.73	0.99 ±0.28	5,376.64 ±259.57	0.006 ±0.002	537.66 ±25.96	172,206.61 ±8,744.46
C	2,672.52 ±1,595.62	1.81 ±0.45	5,858.16 ±317.86	0.013 ±0.005	585.82 ±31.79	171,150.08 ±4,359.01

Investigation of the fractured samples was carried out and is exemplified on the sam-

ple (1) from each sample set. Figure 6.38 presents an overview of the fractured samples as well as the initial state of the base materials.

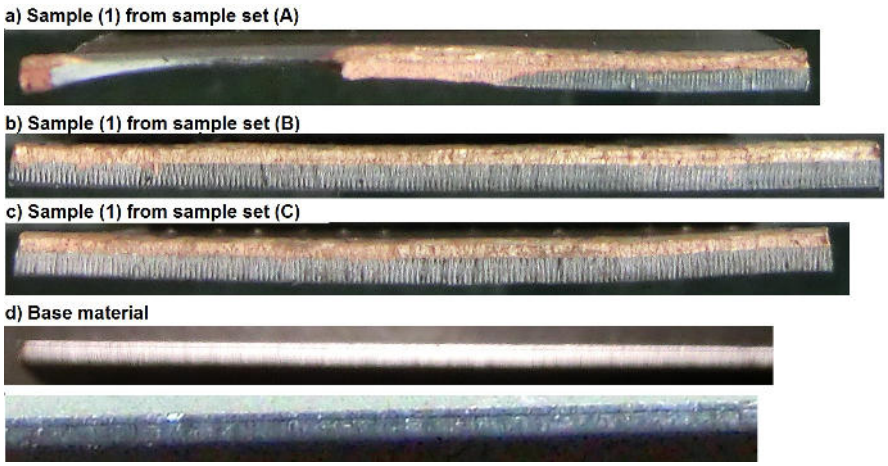

Figure 6.38.: Overview of fractured samples (2) to (4) exemplified on sample (1) of each sample set and initial surface condition of base material; Tensile testing parameters: crosshead travel speed: 5 $\frac{mm}{min}$, condition for stopping the measurement: 40 % of force; Parameters for brazing: P = 146 W, F = +5 mm, v = 74.10 $\frac{mm}{min}$, v_b = 138.4 $\frac{mm}{min}$, d_{gap} = 0.4 mm, WZL = 5.0 s, WZD = 4.3 s

There it can be seen that the gap disappeared over the length of the joint due to thermal expansion of the base materials (see section 5.2.1), as brazing wire only covers the surface of base material (see Figure 6.38 (b) and (c) respectively). In contrast to the sample of sample set (A) in Figure 6.38 a), where the gap was partially filled by the brazing wire. The gap existence as well as its complete filling is the required condition for brazing to obtain a good quality joint (Jacobson and Humpston, 2005). For instance, the gap is needed, so that possible vapors can escape while brazing and do not lead to pores and it also tends to improve the mechanical properties with regard to load-bearing capability (Jacobson and Humpston, 2005).
Although the gap filling is a requirement for brazing, the results from tensile testing do not support this, as they all show the same behaviour. This could be reasoned by the wetting of the brazing wire onto the base material in combination with the applied load in one direction for tensile testing. It is assumed that if multiaxial loading tests or loading tests in another direction would be carried out, the behaviour of the sample sets (A) to (C) would differ due to the gap disappearance over the length of the joint.

6.6.3. Investigation of the alloy zone

During the work carried out so far with regard to polished micrograph sections, an alloy zone could not be clearly recognised. Instead in all polished micrograph sections a thin black line was visible between the base material and the brazing wire. For this reason, it has to be clarified what this thin black line is.
Therefore the Scanning Electron Microscope (SEM) EVO MA10 from Zeiss was used to further investigate the presence of the thin black line with regard to diffusion and alloy zone formation, as it is capable of performing element analysis, which can be subsequently mapped onto the captured image. For this the polished micrograph section presented in section 6.3.1 (see Figure 6.9) was used for investigating this aspect, as this micrograph section shows the same characteristic of a thin black line as all the previous carried out polished micrograph sections. To investigate this micrograph section via the SEM, it was cleaned and sputtered with gold.
Figure 6.39 shows an image of this polished micrograph section captured via the SEM.

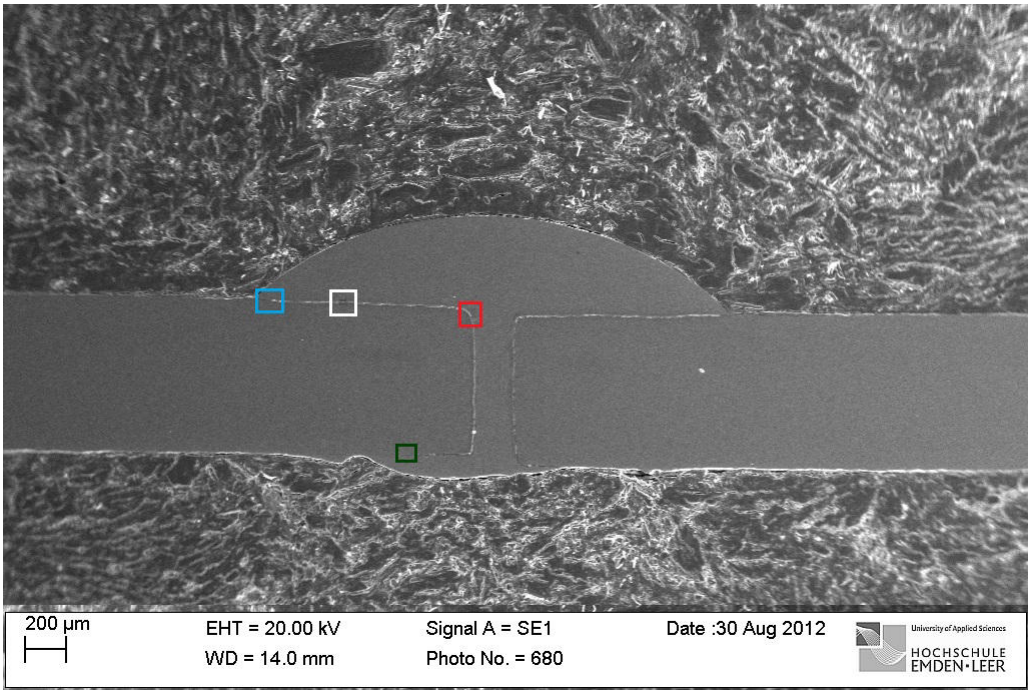

Figure 6.39.: SEM image of the joint brazed with: $P_{av} = 150\,W$, $F = +5\,mm$, $v = 55.10\,\frac{mm}{min}$, $v_b = 109.2\,\frac{mm}{min}$, $d_{gap} = 0.4\,mm$, $WZL = 5.5\,s$, $WZD = 4.7\,s$; the rectangles indicate where a higher resolution image is taken

A close-up picture was taken at different locations on the polished micrograph sec-

tion, indicated by the coloured rectangles in Figure 6.39, and an element analysis performed on each location for copper and iron. The enlarged image of the white rectangle and its correspondent element analysis are presented in Figure 6.40. The enlarged images of the other rectangles as well as their respective element analysis can be found in Appendix C.3, as their results are comparable to the one presented in Figure 6.40.

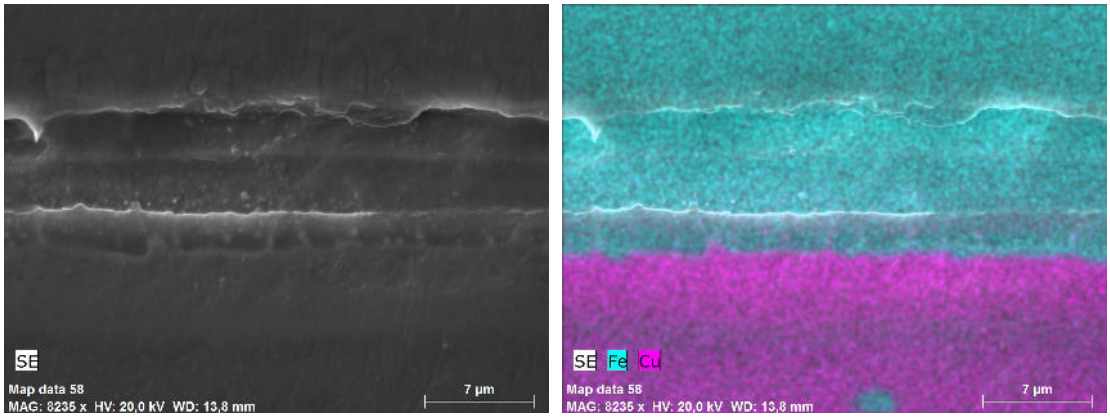

(a) SEM image: enlarged view of the ditch **(b)** SEM: element analysis of the enlarged view of the ditch

Figure 6.40.: SEM images: a) Enlarged view of the white rectangle indicated in Figure 6.39 showing a ditch; b) Mapped information of the element analysis (Fe and Cu) onto the enlarged view

The thin black line, which is recognisable between brazing wire and base material in Figure 6.9 can also be seen in Figure 6.39, but there it is obvious that it has to be a difference in height. Figure 6.40a shows the enlarged view of the white rectangle. There, it can be clearly seen that the line is a ditch of a few microns in width. To determine where this ditch is located with respect to braze or base material or at their interface, the element analysis carried out for copper and iron is mapped onto the respective image (see Figure 6.40b). The single elements mapped onto the image shown in Figure 6.40a can be found in the Appendix in Figure C.6.

It can be seen in Figure 6.40b that the ditch is located within the base material and not directly at the interface between brazing wire and base material. Furthermore, in contrary to expectations, no alloy zone can be determined by this analysis. To ensure that this ditch does not occur due to the preparation of the polished micrograph

sections concerning e.g. ultrasonic bath and etching, this polished micrograph section is ground and polished again without etching once as well as once without using the ultrasonic bath and then subsequently investigated via the SEM. But the result remained the same as presented in Figure 6.40 and in Appendix C.3. For this reason, the influence of the preparation of the polished micrograph section can be neglected as possible reason for the ditch occurrence.
Koltsov et al. observed the same phenomena of crack occurrence for laser brazing with $CuSi_3$ and bare steel in their studies regarding the wetting behaviour. According to Koltsov et al., the bare steel has a passive oxide layer. If the de-oxidation is not completed when the surface of the bare steel reacts with the brazing wire, interfacial cracks develop indicating that the formed interface is mechanically weak (Koltsov et al., 2010). These cracks, Koltsov observed, correspond to those presented in Figure 6.40b and they are also located in the base material steel.
Hence, the thin black line corresponds to a crack that is originated by an incomplete de-oxidation of the base material when the brazing wire reacts to it. Due to this fact, the alloy zone cannot be investigated.

6.7. Summary

The investigations concerning the wire positioning itself led to the same results as the investigations carried out the with Nd:YAG laser (see section 5.1). However, they differ with regard to the wire positioning within the laser spot. It was observed that the wire positioning within the laser spot of the diode laser is not as crucial as for the Nd:YAG laser. This can be reasoned by the top hat profile of the diode laser beam in direction of brazing (see section 3.1.1.2).
As mentioned in section 2.2.2.2, opinions differ in literature with regard to the ratio of feed speeds for the same joint geometry (see Table 2.1). For this reason experiments were carried out concerning this aspect with and without shielding gas. For the initial tests as well as for the parameter studies carried out with the Nd:YAG laser, a ratio between feed speed of brazing wire and feed speed of base material of 2:1 was selected, as a rule of thumb for brazing butt joints. This ratio has been verified, as both experiments carried out with and without shielding gas resulted in a ratio of approximately 2:1. The ratio achieved for brazing without shielding gas corresponded to 1.87:1. Furthermore, it was observed that the usage of shielding gas cools down

the brazing process significantly. This results in slow feed speed of base material. Appropriate joints were brazed with a feed speed of base material of 55.10 $\frac{mm}{min}$. This is in contrast to the joints brazed without using shielding gas. There, good quality brazed joints were obtained with a feed speed of base material of 74.10 $\frac{mm}{min}$. Due to these results, the usage of shielding gas was neglected for the further experiments.
The initial experiments, carried out with the Nd:YAG laser, showed that pre-heating is essential for laser brazing in order to obtain good quality brazed joints (see section 4.4). For this reason, the influence of pre-heating to the brazing process was closely examined. Experiments demonstrated that pre-heating is required to reach an appropriate operating temperature at the beginning of the laser brazing process. The pre-heating process could be verified by the presence of oxidation marks. If an appropriate operating temperature was reached at the beginning of the laser brazing process, these oxidation marks were symmetric around the brazed joint and their distance remained parallel to the joint. Whereas the oxidation marks diverge over the length of the joint, if an insufficient pre-heating phase took place.
Furthermore, the influence of the change in heat input was investigated to the brazing result. These experiments were carried out, as the material ablation still occurred for parameter set used. The heat input depends on the laser power and the feed speed of the base material. Since appropriate feed speeds were determined during the investigations regarding the ratio of feed speeds, the laser power was varied to change the heat input. Results showed that good quality brazed joints were obtained if a laser power of 146 W is used. Table 6.10 summarises the appropriate parameters for diode laser brazing.

Table 6.10.: Appropriate parameters for diode laser brazing

WZD (s)	WZL (s)	F (mm)	d_{gap} (mm)	v_b ($\frac{mm}{min}$)	v ($\frac{mm}{min}$)	P W
4.3	5.0	+5	0.4	138.4	74.10	146

The brazed joints, from the experiments carried out concerning heat input, were further investigated with regard to Vickers hardness and tensile testing. The Vickers hardness measurements showed the expected hardness increase within the area of the HAZ by having its peak value close to the gap. This can be explained by the fast heating due to the incident laser radiation and the subsequent cooling (Higgins, 1983).
For tensile testing, the brazed joints were cut, so that the beginning, middle and end

of the joint could be investigated. This was done in order to compare their different behaviour due to the disappearing gap width. However, results showed the same behaviour for all regions of the joint tested, although gap existence and filling is a requirement for brazing (Jacobson and Humpston, 2005). This could be reasoned by the wetting of the brazing wire onto the base material in combination with the applied load in one direction for tensile testing. It is assumed that if multiaxial loading tests or loading tests in another direction would be carried out, the behaviour of the samples would differ due to the gap disappearance over the length of the joint.

During the optical examination of each polished micrograph section with the aid of a microscope, an alloy zone could not be recognised. Instead, only a thin black line was visible. Therefore, it had to be clarified what this black line is. Hence a polished micrograph section was investigated by using a SEM. Observations showed that this line corresponds to a crack that is originated by an incomplete de-oxidation of the base material when the brazing wire reacts to it. Due to this fact, the alloy zone cannot be investigated.

Chapter 7.

Discussion

7.1. Influencing parameters

As presented in section 2.2.2.2, literature agrees that laser power, the feed speed of base material and brazing wire are important quality influencing parameters (LI et al., 2008, Heitmanek et al., 2014, Kai et al., 2015, Rong et al., 2015). Within this research more quality influencing parameters were identified. These parameters can be subdivided into laser, process parameters and material characteristics (see section 3.1), which are explained and related to the observations made during the parameter studies in the following.

7.1.1. Laser parameters

The laser power is one parameter, which has an influence on the brazing result. Furthermore, the focal position, which influences the spot size of the laser, is another important parameter. Since this spot size determines the area of material to be heated and melted respectively (see section 3.1.1.1.4 and 3.1.1.2.2). During the initial experiments, carried out with the Nd:YAG laser, it was shown that the spot size has an influence on the wetting behaviour of the brazing wire (see section 4.4). If the spot size is too small, improper wetting of the brazing wire onto the base material occurs, due to the temperature gradient between them (Jacobson and Humpston, 2005).
The term laser power has to be differentiated between the type of laser used: pulsed or cw. For a pulsed laser, the laser power is understood as the average laser power, which depends on the peak power, the pulse length and the repetition rate. Hence,

variation of these parameters that determine the average laser power has also an influence on the brazing result. This was presented within the initial experiments carried out with the Nd:YAG laser (see section 4.4). There it was observed, that too high peak powers lead to base material ablation (see Figure 4.14 and 4.15 respectively), although the average laser power was within an acceptable range.
Furthermore, the repetition rate has an influence on the surface condition of the brazed joint. Tests with the Nd:YAG laser showed that a decrease in repetition rate leads to a decrease in surface roughness by maintaining the average laser power. The optimal value for the repetition rate was determined to f = 20 Hz with regard to surface roughness. This characteristic can be reasoned by the low repetition rates in combination with large pulse lengths, which approximate a quasi-continuous behaviour (see section 5.3).

7.1.2. Process parameters

As mentioned above, literature identifies the feed speeds of base material and brazing wire as important quality influencing parameters. However, opinions, found in literature, deviate with regard to the ratio between feed speed of brazing wire and feed speed of base material for the same joint geometry (see Table 2.1 in section 2.2.2.2). The data presented in Table 2.1, summarises the ratio of feed speeds of different literature sources by using the same materials, laser power and joint geometry (flanged seam). There it can be seen that the ratio of feed speeds varies in the range of 1 up to 3.25 (LI et al., 2008, Heitmanek et al., 2014, Kai et al., 2015, Rong et al., 2015).
Literature research was carried out with regard to the ratios of feed speeds for brazing butt joints, albeit not found. For this reason the ratio was set to 2:1, as a rule of thumb. This rule of thumb has been verified by the experiments carried out with the diode laser (see section 6.3). There the ratio of feed speeds was investigated with and without using shielding gas. Results showed, on the one hand that the achievable feed speeds of base material and brazing wire are 55.10 $\frac{mm}{min}$ and 109.10 $\frac{mm}{min}$ respectively for brazing with shielding gas. This corresponds to a ratio of feed speeds of 1.98:1, which fits quite well to the rule of thumb. On the other hand, the ratio of feed speeds is determined to 1.87:1 for brazing without shielding gas. There the achievable feed speeds of the brazing wire and base material are 138.4 $\frac{mm}{min}$ and 74.10 $\frac{mm}{min}$ respectively. As it can be seen, the achievable feed speeds of the experiments carried out with and without shielding gas differ. The slow feed speeds are initiated by the cooling down by the

shielding gas. During the experiments it was observed that the usage of shielding gas cools down the process by 100 °C up to 250 °C (see Figure 6.20). For this reason, shielding gas was used no further.
Furthermore, it was identified during the initial experiments, carried out with the Nd:YAG laser, that a pre-heating is essential in order to obtain good quality brazed joints. Pre-heating is defined by two delay times (WZL) and (WZD) that introduce a delay between starting the process including the laser and starting to braze (see section 3.1.2.3). This aspect is further discussed in section 7.2.

7.1.3. Material characteristics

The selection of materials used for brazing have an influence on the brazing result, as the physical properties of the base material and brazing wire determine the operating temperature for brazing. The operating temperature range is defined by the liquidus temperature of the brazing wire and the solidus temperature of the base material. Within this research, $CuSi_3$ was used as brazing wire, which has a liquidus temperature of 1,025 °C (see Table 4.3 in section 4.3.2). The mild cold rolled steel DC01 was used as base material (see section 4.3.1). As this steel consists mainly of iron, the solidus temperature of iron is used for a Carbon content of 0.12 %, which is approx. 1,490 °C (see Figure A.12). Hence, the operating range corresponds to 1,025 °C - 1,490 °C.
Furthermore, the absorption behaviour of the materials depends on the wavelength used. This behaviour was approximated for the brazing wire by using copper. The absorption of copper for both wavelength used (808 nm and 1,064 nm) corresponds approximately 4 % (see section 4.3.2). Whereas, the absorption of the base material corresponds to approximately 40 % for 1,064 nm and to 50 % for 808 nm (see section 4.3.1).
Next to the wavelength dependent absorption behaviour, the surface condition has also an influence on the brazing result. It was found in literature that oxide layers increase the absorption (Poprawe, 2005). Furthermore the surface roughness influences the absorption positively (see Figure 3.4) (Poprawe, 2005).
This information presented within this section is needed to estimate the required heat input for brazing.

7.1.4. Heat input

The heat input depends on the laser power and the feed speed of the base material. Therefore, it can be seen as a derived value of the influencing parameters. Furthermore, the material characteristics have an influence on the heat input due to their absorption behaviour and surface condition (see section 7.1.3). Experiments showed that the estimation of the heat input did not lead to satisfactory results (see section 4.4, 6.1 and 6.5). The heat input was estimated to 75 $\frac{J}{mm}$ for the initial experiments carried out with the Nd:YAG laser. These experiments showed that a heat input of 90.95 $\frac{J}{mm}$ is required (see section 4.4). The same accounts for the experiments carried out with the diode laser. There the heat input was estimated to 94.74 $\frac{J}{mm}$ (see section 6.1). As the investigation of the ratio of feed speeds determined suitable feed speeds for the brazing wire and the base material (see section 6.3 and 7.1.2), experiments were carried out by using these suitable feed speeds and changing the laser power and therefore the heat input (see section 6.5). Results showed that a good quality brazed joint is achieved, when the heat input corresponds to 118.23 $\frac{J}{mm}$.
The deviation between the estimations and the determined heat input could be reasoned by neglecting the losses regarding heat transport in the estimations.
As mentioned in section 3.2.2.1, the heat input and therefore the heating and fast cooling of the material influences the microstructure or grain size of both materials brazing wire and base materials (Fritz and Schulze, 2006). This change in microstructure results in a hardness change in the region of the Heat Affected Zone (HAZ) across the brazed joint (Higgins, 1983). For this reason this hardness change was measured (see section 6.6.1). The results showed the expected behaviour. The hardness of the base material increases in the region of the HAZ by having its peak value at the gap of the joint (see Figure 6.32).

7.2. Pre-heating

During the initial experiments (see section 4.4), it was observed that the temperature increases, while brazing, over the length of the joint (see Figure 4.16). This behaviour demonstrates that an appropriate operating temperature was not reached at the beginning of the brazing process. For this reason, a pre-heating phase was introduced to obtain a sufficient operating temperature at the beginning of the laser brazing process. This pre-heating phase is defined by two delay times (WZL) and (WZD) that intro-

duce a delay between starting the process including the laser and starting to braze (see section 3.1.2.3). Results of these initial experiments showed that pre-heating is essential in order to obtain good quality brazed joints. A sufficient pre-heating was obtained if (WZL) and (WZD) were set to 3.5 s and 2.8 s respectively for Nd:YAG laser brazing.

For this reason, this aspect was further investigated during the parameter studies, carried out with the diode laser (see section 6.4). For these experiments the delay time (WZL) was varied and (WZD) was adapted accordingly. The results showed that if an appropriate operating temperature is reached at the beginning of the brazing process, the oxidation marks were symmetric around the brazed joint and their distance remained parallel to the joint. Whereas the oxidation marks diverge over the length of the joint, if an insufficient pre-heating phase took place (see Figure 6.22).

Next to the oxidation marks, also the brazed joint itself indicates if an appropriate temperature is reached at the beginning of the brazing process, as the width of the joint is consistent over its length (see Figure 6.21 (a)). Furthermore, the experiments showed that a good quality brazed joint is obtained, if (WZL) and (WZD) were set to 5.0 s and 4.3 s respectively for diode laser brazing. The difference between the two delay times (WZL) and (WZD) is caused by the human error. As both the laser and the wire feed have to be started manually and both are supposed to start at the same time. Hence a human error of approximately 0.7 s is considered.

Based on these results, the successful implementation of a pre-heating phase was demonstrated and confirmed by the oxidation marks as well as the consistency in width of the brazed joints.

Comparing these results with literature, an approach was found with regard to pre-heating. However, it was limited to the electric resistive pre-heating of the brazing wire in order to obtain a better surface quality of the joints (Mathieu et al., 2006b). Furthermore, pre-heating was also identified by Heitmanek et al. as an important aspect for the process stability and joint quality of laser brazing (Heitmanek et al., 2014). However, they used a different approach. Their approach was to manipulate the beam shape by using the dynamic beam shaping system LASSY from Fraunhofer IWS, which is based on scanning mirror optics. They changed the beam shape from circular to elliptical in the direction of brazing to obtain a pre-heating of the base material (Heitmanek et al., 2014). These literature sources indicate that obtaining a sufficient operating temperature and minimising the temperature gradient between brazing wire and base material are important to the brazing result, which corresponds to the findings

presented within this work.

7.3. Wire positioning also within the laser spot

During the initial experiments, carried out with the Nd:YAG laser (see section 4.4), it was observed that the wire positioning seems to have an influence on the brazing result. Therefore this aspect was further investigated with both lasers, as their beam profiles differ from each other (see section 3.1.1).
The investigations revealed that the wire positioning itself as well as within the laser spot has a significant influence on the brazing result. For large incidence angles of the brazing wire ($> 47^{\circ}$), it was observed that if the wire was loosely placed onto the base material, it resulted in visibly wavy brazed joints (see section 5.1.1 and 6.2). This waviness could be caused by improper heating as well as oscillations of the brazing wire (see section 5.1.1). The oscillations of the wire can be decreased if the incidence angle is decreased. However, to completely eliminate the oscillations, the brazing wire has to be positioned onto the base material as shown in Figure 5.2 (Right). There, the wire is slightly pressed onto the base material, which ensures a small incidence angle of the wire and sufficient contact between brazing wire and base material within the laser spot. Furthermore, the wire is guided by the gap, which eliminates the occurrence of oscillations.
Furthermore, the wire positioning within the laser spot was investigated. The trailing, center and leading position were tested (see section 5.1.2). Experiments, carried out with the Nd:YAG laser, showed that only good quality brazed joints were achieved, if the wire is placed in the center of the laser spot (see section 5.1.2). The other positions tested led to an improper heating and therefore to an insufficient brazing result.
The same experiments were also carried out with the diode laser (see section 6.2). With regard to the wire positioning itself the same observations were made. Only the wire positioning within the laser spot was not as crucial as for the Nd:YAG laser. This can be explained by the different beam profiles of the lasers. The Nd:YAG laser has a circular laser spot with a Gaussian distribution having its highest intensity in the center of the laser spot (see section 3.1.1.1). Whereas, the diode laser has a rectangular laser spot with a top hat profile in the direction of brazing (see section 3.1.1.2).
Literature research was carried out regarding this aspect, albeit not found.

7.4. Characteristics of disappearing gap width and deformation

During the initial experiments (see section 4.4), it was observed that the initial gap of 0.1 mm disappeared over the length of the joint. Therefore, this aspect was further investigated within the parameter studies carried out with the Nd:YAG laser (see section 5.2.1), as this initial gap was supposed to be within the optimal range for laser brazing (see section 3.2.1.1). The investigations showed that the gap decreases linearly over the length of the brazed joint (see Figure 5.10). This behaviour can be reasoned by the thermal expansion of the base materials due to heat conduction (Hornbogen, 1983). Furthermore, it was demonstrated that the correspondent measurements agree well with the theory of linear expansion with regard to a uniform temperature change (see Figure 5.11).

The gap existence as well as its complete filling is a required condition for brazing to obtain a good quality joint (Jacobson and Humpston, 2005). Therefore, the disappearance of the gap over the length of the joint is a unfavourable condition.

Although the tensile testing experiments, carried out on joints brazed with the diode laser, do not support this (see section 6.6.2). For these experiments, the joints were cut at the beginning, middle and end to investigate the influence of disappearing gap to the tensile testing. It was observed that the all samples tested show the same behaviour, whether a gap exists or not. This could be reasoned by the wetting of the brazing wire onto the base material in combination with the applied load in one direction for tensile testing. It is assumed that if multiaxial loading tests or loading tests in another direction would be carried out, the behaviour of the samples would differ due to the gap disappearance over the length of the joint.

Furthermore tests were carried out to maintain the gap width over the length of the joint, e.g. using spring steel of respective thickness as a spacer, tacking of base materials prior to the brazing process and leaving space between the clamping bracket and base material. However, non of them led to a satisfactory result (see section 5.2.2).

As mentioned in section 4.3.1, the automotive industry uses zinc galvanised steel as base material for laser brazing. The liquidus temperature of zinc corresponds to 419.58 °C and its evaporating temperature is 907 °C (Stöcker, 2000). As it can be seen, the evaporating temperature of zinc is below the liquidus temperature of the brazing wire of 1,025 °C (see Table 4.3 in section 4.3.2). Hence, pores can form out while brazing, if

the zinc vapour cannot escape. For this reason, the gap is a required condition for brazing, so that possible vapours can escape (Jacobson and Humpston, 2005).
To overcome this characteristic of disappearing gap width, it is assumed that faster process speeds in combination with a laser within the kW power range are needed. As this should lead to a decrease in heat conduction and therefore to a decrease in thermal expansion of the base materials.
Along with the observations made regarding the disappearance of gap width, deformations of the brazed joint were also observed during all experiments carried out. The deformation occurs in the form of deflection over the length of the brazed joints (see Figure 5.17 in section 5.2.3). This deflection is caused by heating induced thermal expansion strains (Usmani et al., 2001). The direction of curvature (see Figure 5.17) indicates a uniform temperature gradient over the thickness of the joint. As the uniform temperature rise within the base material was proven for the gap disappearance over the length of the joint (see Figure 5.11), the deflection could be theoretically approximated to 2.13 mm. To verify this approximation measurements were carried out that confirmed this estimated value, as the deflection was measured to $2.25\,\text{mm} \pm 0.14\,\text{mm}$ (see section 5.2.3).

7.5. Alloy zone

During the optical examination of each polished micrograph section with the aid of a microscope, an alloy zone could not be recognised. Instead, only a thin black line was visible. Therefore, it had to be clarified what this black line is. Hence a polished micrograph section was investigated by using a SEM. Observations showed that this line corresponds to a crack (see section 6.6.3) that is located in the base material. The same phenomenon, of crack occurrence for laser brazing with $CuSi_3$ and bare steel, was also observed by Koltsov et al. (Koltsov et al., 2010). According to Koltsov et al., the crack is originated by an incomplete de-oxidation of the base material when the brazing wire reacts to it. Due to this fact, the alloy zone could not be investigated.

Chapter 8.

Conclusion

Several conclusions can be drawn from the work presented in the previous chapters. Chapter 3 identified the parameters that have an influence on the brazing result. These influencing parameters can be subdivided into material characteristics, laser and process parameters. Chapter 4, 5 and 6 are the main body of this work, where the investigations and the results of the initial tests as well as of the parameter studies with both lasers used are presented. These results led to several interesting conclusions, where the major ones are presented in the following.

As presented in section 2.2.2.2, literature agrees that laser power, the feed speed of base material and brazing wire are important quality influencing parameters (LI et al., 2008, Heitmanek et al., 2014, Kai et al., 2015, Rong et al., 2015). However, further influencing parameters were identified within this work, which are presented in the following. It was determined that the laser spot size has a significant influence on the brazing result, as it influences the area to be heated and melted respectively. Therefore, the spot size should be selected large enough, so that the base material is heated properly and the brazing wire melted. This leads to a proper wetting of the brazing wire onto the base material resulting in good quality brazed joints with regard to the quality measure contact angle. If a pulsed laser is used for brazing, the average laser power is determined by the peak power, pulse length and repetition rate. Experiments showed that if the repetition rate is kept constant, the average laser power should be obtained by decreasing the peak power and increasing pulse length. Otherwise base material ablation occurs due to the high peak powers. Furthermore, investigations demonstrated that the repetition rate of a pulsed laser has an influence on the surface condition of brazed joints. For the experiments the average laser power was kept constant and

only the repetition rate was changed and the pulse length adapted accordingly. Results showed that a decrease in repetition rate leads to a decrease in surface roughness of the brazed joint by having its optimal value at f = 20 Hz. Moreover, the ratio between feed speed of brazing wire and feed speed of base material was investigated for brazing butt joints. For initial testing the ratio was set to 2:1, as a rule of thumb. This rule of thumb was verified, as the achievable ratio of feed speeds were in the range of 1.87:1 for diode laser brazing without shielding gas and 1.99:1 for Nd:YAG laser brazing.

Furthermore, two key aspects were identified and presented within this work that have a significant influence on the quality of brazed joints. These key aspects represent the novelty of this work.

The first key aspect is the understanding of the importance of the wire positioning itself as well as within the laser spot. In this work, it was shown that if the wire itself is not placed correctly onto the base material, this will lead to low quality brazed joints. This low quality of the brazed joints is caused by oscillations of the brazing wire in combination with improper heating of the base material. To eliminate this behaviour, the wire has to be slightly pressed onto the base material, so that it bends a little. This way, the wire is guided by the gap, which prevents the wire from oscillating. Furthermore, the wire has sufficient contact with the base material within the laser spot, which leads to a proper heating of the base material and therefore to a good quality brazed joint. The wire positioning within the laser spot is crucial for laser beams that have a Gaussian intensity distribution. There it was found, that only the wire positioning at the center of the laser spot led to good quality joints with regard to the contact angle. For the wire positioning at the leading or trailing edge of the laser spot, low quality joints were obtained. Whereas the wire positioning within the laser spot was not that crucial for laser beams that have a top hat intensity profile in the direction of brazing. Variations of wire positioning within this laser spot resulted still in good quality joints with regard to contact angle.

The second key aspect, presented in this work, is the successful implementation of a pre-heating phase prior to the actual brazing process. During the experiments, it was observed that the temperature increases over the length of the joint, while brazing. This leads to insufficient brazed joints until an appropriate operating temperature is reached. For this reason, a pre-heating phase was implemented, which is defined by two delay times (WZD) and (WZL) that introduce a delay between starting the process including the laser and starting to braze. This pre-heating phase ensures an appropri-

ate operating temperature for brazing at the beginning of the laser brazing process. The successful implementation of the pre-heating phase was verified by the symmetry of the oxidation marks around the brazed joint, where their distance remained parallel to the joint. Next to the oxidation marks, also the brazed joint itself was an indicator for successful pre-heating, as the width of the joint was consistent over its length, if an appropriate temperature was reached at the beginning of the brazing process.

Chapter 9.

Future work

Further investigations could be carried out with regard to the observed characteristics of disappearing gap width over the length of the joint and deformation (see section 5.2). Since, it is assumed that these characteristics would disappear, if faster laser brazing process speeds are obtained by using a laser in the kW power range. If this assumptions proves to be correct, then the verified ratio of feed speeds for brazing butt joints of 2:1 should be investigated again in terms of how the existence of a gap would affect it, if at all. With regard to this assumption, further investigations can be carried out how the presence of a zinc layer influences the brazing result.

Throughout this work, the base materials were cleaned prior to brazing. For this reason, it can be further investigated how the surface condition in terms of dirt and oil residuals will affect the brazing result, as the base components might not be cleaned in industry prior to brazing. Next to this surface condition, investigations can be carried out in terms of how the surface roughness of the base material influences the wetting behaviour of the melted brazing wire.

Furthermore, the information, gained by the empirical research carried out within this thesis, can be used to develop a simulation model by the aid of Finite Element Method (FEM). As laser brazing is a very complex process, it can be divided into smaller portions as a first step. These portions correspond to the various parameters and processes that need to be considered for the model development. For instance, the laser radiation itself is a parameter that has to be considered with regard to its beam shape, intensity distribution as well as wavelength. Furthermore, the absorption behaviour of the materials used has to be defined, depending on the wavelength used. As described in section 4.2.1.1, the absorption behaviour of the materials

changes with increasing temperature, which also has to be considered. Another aspect is the change of physical state from solid to liquid of the brazing wire, which needs to be considered as well. Along with this physical state change, the wetting of the melted brazing wire onto the base material has also to be considered. If a gap is supposed to be considered within the Finite Element model, which is supposed to be filled by the melted brazing wire, the capillary filling pressure has to also be described for the model. Furthermore, the heat conduction of the materials used should also be considered. These processes and parameters mentioned above are the most significant ones that need to be considered for modelling the laser brazing process. Therefore, the suggestion is to develop a model for each process first and then combine these single models into a complete Finite Element model.

Bibliography

M. Alavi, M. Lorenz, and S. Buettgenbach. *Microstructure and composition of laser soldered joints: investigation of intermetallic layers by high sensitive surface analysis: Proceedings of the International Conference on Interconnection Technology in Electronics*, volume 129. DVS - Verlag, Duesseldorf, 1990.

M. Apter. High power diode lasers offer efficient answer: High-power diode bars that are highly efficient and boast output powers of hundreds of watts are now, 2005. URL http://www.nlight.net/nlight-files/file/articles/HP_May05_OLE.pdf. 2013-01-03.

F. Bachmann. Industrial applications of high power diode lasers in materials processing. *Applied Surface Science*, (208-209):125–136, 2003. 2014-05-29.

Hans Dieter Baehr and Karl Stephan. *Wärme- und Stoffübertragung*. Springer, Berlin, 6 edition, 2009. ISBN 9783540876885. URL http://dx.doi.org/10.1007/978-3-540-87689-2.

Bahaa E. A., Malvin Saleh, and Carl Teich. Fundamentals of photonics: Chapter 3: Beam optics, 1991.

H.-J. Bargel and G. Schulze. *Werkstoffkunde*. Springer-Lehrbuch. Springer, Berlin and Heidelberg, 11., bearb. aufl. 2012 edition, 2012. ISBN 9783642177163. URL http://dx.doi.org/10.1007/978-3-642-17717-0.

R. Beach and et. al. Modular microchannel cooled heatsinks for high average power laser diode arrays. *Journal of quantum electronics*, 4(28):966–975, 1992. doi: 10.1109/3.135215. 0214-01-22.

Becker Stahl Service GmbH. Elektrolytisch verzinktes feinblech, 2008. URL http://www.becker-stahl-service.de/pdf/Elektrolytisch_verzinktes_Feinblech.pdf. 2008-10-08.

D. Bergström, A. Kaplan, and J. Powell. Mathmatical modelling of laser absorption mechanisms in metals: A review: presented at m4pl16 workshop in igls, austria in january 20-24, 2003, 2003.

M. Berke. Ultrasonic imaging in automatic and manual testing: Aipnd (associazione italiana prove non distruttive), 2006. URL http://www.ndt.net/article/ecndt2006/doc/We.3.1.5.pdf. 2014-03-03.

J. Bliedtner, H. Mueller, D. Wolff, T. Heyse, and G. Michel. Diode lasers weld deep. *Eur. Prod. Engng*, (7):32–38, 2000. URL http://www.ifw-jena.de/www/ifw/oeffentlichkeit/publikationen/archiv.htm?index=70.

S. Bonss. Tailored blank schweissen mit hldl: 2. workshop: Anwendung von hochleistungsdiodenlasern, 14 / 15. October 1999.

M. Brandner, G. Seibold, and M. Haag. Effektive umsetzung der spezifischen strahleigenschaften von hldl zur materialbearbeitung. *LaserOpto*, 31(1):71, 1999.

Michael Brandner. *Steigerung der Prozesseffizienz beim Löten und Kleben mit Hochleistungsdiodenlasern*. Laser in der Materialbearbeitung. Utz, Wiss., München, 2003. ISBN 3-8316-0288-3.

Britannica. Definition: welding, 2009. URL http://www.britannica.com/EBchecked/topic/639223/welding. 2009-05-31.

Frank Buchmüller. *Diplomarbeit: Automatisierte Oberflaechenmessung mit Lasersensoren*. PhD thesis, Fachhochschule Emden, Emden, 2005.

William D. Callister. *Fundamentals of materials science and engineering: An interactive e.text*. Wiley, New York, 5. ed edition, 2001. ISBN 0555118924. URL http://www.loc.gov/catdir/description/wiley035/00050455.html.

P. Chaudhuri, P. Santa, S. Yoele, A. Prakash, D. Chenna Reddy, L. T. Lachhvani, J. Govindarajan, and Y. C. Saxena. Non-destructive evaluation of brazed joints between cooling tube and heat sink by ir thermography and its verification using fe analysis. *NDT&E International*, (39):88–95, 2006.

Peter K. Cheo. *Handbook of solid-state lasers*, volume v. 18 of *Optical engineering*. M. Dekker, New York, 1989. ISBN 9780824778576.

M. Dahmen and S. Kaierle. Continuous process monitoring during laser welding of thin aluminium sheet: Fraunhofer ilt annual report, 2006. URL http://www.ilt.fraunhofer.de/content/dam/ilt/en/documents/annual_reports/JB2006-eng.pdf. 2014-03-15.

P. Das. *Lasers and optical engineering*. Springer, New York, 1991. ISBN 9783540971085. URL http://www.loc.gov/catdir/enhancements/fy0815/89026312-d.html.

DILAS Diodenlaser GmbH and Osram Opto Semiconductors GmbH & Co, editors. *High-brightness high-power kW-system with tapered diode laser bars*, 2005. ISBN doi:10.1117/12.589044.

DIN EN ISO 11146-1. Laser und laseranlagen - prüfverfahren für laserstrahlabmessungen, divergenzwinkel und beugungsmaßzahlen - teil 1: Stigmatische und einfach astigmatische strahlen, 2005-04. URL http://www.beuth.de/de/norm/din-en-iso-11146-1/74054387?SearchID=688251528. 2014-06-01.

DIN ISO 857-2. Teil 2: Schweißen und verwandte prozesse - begriffe - teil 2: Weichlöten, hartlöten und verwandte begriffe, 2007-3. URL http://www.beuth.de/de/norm/din-iso-857-2/94230389. 2010-03-13.

Dip Braze Inc. What is dip brazing?, 2009. URL http://www.dipbraze.com/whatis.htm. 2009-05-03.

W. Doeldisson. Halbleiterlaser fuer die optische nachrichtentechnik. *Laser Magazin*, (3):8–18, 1999.

L. Dorn, H. Grutzek, and S. Jafari. *Schweissen und Loeten mit Festkoerperlasern*. Springer, Berlin and Heidelberg and New York and London and Paris and Tokyo and Hong Kong and Barcelona and Budapest, 1992. ISBN 3540555439. URL http://www.worldcat.org/title/schweissen-und-loten-mit-festkorperlasern/oclc/75271829?ap=citavi.

L. Dorn, S. Jafari, and F. Hofmann. Untersuchungen der verbindungseigenschaften an laserstrahlgefuegten brillengestellen. *Materialwissenschaft und Werkstofftechnik*, 29: 281–291, 1998.

F. Dorsch, P. Hennig, and M. Nickel. High - brightness fibre - coupled diode laser module: Fabrication, testing, reliability and applications of semiconductor lasers iii (proc. spie). volume 3285, pages 192–198. doi: 10.1117/

12.307606. URL http://proceedings.spiedigitallibrary.org/proceeding.aspx?articleid=935477.

P. Du, P. Shi, D. Li, A. Schell, P. Hu, and R. Haas. Innoslab lasers with tailored beam profiles for applications in photovoltaics, 20. / 21. September 2007.

I. Dueckminor and M. Frede. Effiziente groesse. *Laser Magazin*, (2):7–11, 2006.

J. Dutta Majumdar and I. Manna. Laser processing of materials. *Sadhana*, 28(3 & 4): 495–562, 2003.

J. Eichler and H.-J. Eichler. *Laser: Bauformen, Strahlführung, Anwendungen*. Laser in Technik und Forschung. Springer, Berlin, 3., völlig neubearb. und erw. aufl edition, 1998. ISBN 9783540639169.

G. Erbert. Physik und technologie von hochleistungs - diodenlasern hoher brillianz, 14./15. September 2000.

Ulrich Fischer. *Tabellenbuch Metall*. Europa-Fachbuchreihe für Metallberufe. Verl. Europa-Lehrmittel, Haan-Gruiten, 44., neu bearb. aufl edition, 2008. ISBN 3808517247.

Flir Systems Inc. Benutzerhandbuch thermacamtm sc640: Publ.no.: 1558548 rev.a174, 2006. URL http://www.flir.com/uploadedFiles/Thermography_APAC/Products/Product_Literture/SC640_Datasheet%20APAC.pdf.

Franz Gysi AG. Gebraeuchliche werkstoffe, 2008. URL http://www.fgysi.ch/pdf/1164695511-keta2-d.pdf. 2014-06-08.

A.-H. Fritz and G. Schulze, editors. *Fertigungstechnik: Mit 62 Tabellen*. VDI-Buch. Springer, Berlin, 7., neu bearb. aufl edition, 2006. ISBN 9783540256236.

R. Gedney. Tensile testing basics, tips and trends, 2005. URL http://www.admet.com/assets/Tensile_Testing_Basics_Quality_Magazine.pdf. 2009-04-04.

M. Geiger, H. Hanebuth, and P. Hoffmann. Laserstrahlhartloeten in der automobilindustrie. *Blech Rohre Profile*, 41(12):825–828, 1994.

R. J. Geusic, Marcos H. W., and L. G. van Uitert. Laser oscillations in nd - doped yttrium aluminium, yttrium gallium, and gandolinium garnets. *Appl. Phys. Lett.*, (4):182–201, 1964.

G. Gilbert. Laser soldering with high power laser diodes. *Proceedings of the Institute of Physics Quantum Group Meeting Direct Applications of High Power Laser Diodes*, 1(8):102–112, 1995.

Heinrich Gobrecht, Ludwig Bergmann, and Clemens Schaefer. *Mechanik, Akustik, Wärme: Mit einem Anhang über die Weltraumfahrt*, volume zum Gebrauch bei akademischen Vorlesungen und zum Selbststudium / von L. Bergmann und Cl. Schaefer ; Bd. 1 of *Lehrbuch der Experimentalphysik*. de Gruyter, Berlin, 9., verb. aufl edition, 1975. ISBN 3110048612.

K. E. Goodson, K. Kurabayashi, and R.F.W. Pease. Improved heat sinking for laser-diode arrays using microchannels in cvd diamond: Proc. of the 30th national heat transfer conference, portland (usa). *IEEE Transactions on Components, Packaging, and Manufacturing Technology: Part B*, 20(1):104–109, 1997. ISSN 10709894. doi: 10.1109/96.554536.

M.s Graudenz and M. Heitmanek. Laser tools in the manufacturing process. *Laser Technik Journal*, 9(4):24–27, 2012. ISSN 16137728. doi: 10.1002/latj.201290049.

M. Haag. *Systemtechnische Optimierungen der Strahlqualität von Hochleistungsdiodenlasern*. Laser in der Materialbearbeitung. Utz, Wiss., München, 2000. ISBN 9783896758408.

Matthias Haag, Thomas Rudlaff, and Beckmann,Leo H. J. F. ¡title¿assessment of different high-power diode lasers for material processing¡/title¿. In *Lasers and Optics in Manufacturing III*, SPIE Proceedings, pages 583–591. SPIE, 1997. doi: 10.1117/12.281120. URL http://spie.org/Publications/Proceedings/Paper/10.1117/12.281120.

D. Haensch, D. Haaf, H. Putz, H. G. Treusch, A. Gillner, and R. Poprawe. Welding of plastics with diode laser: Icaleo'98, 16-19.11.1998.

H. Haferkamp, M. Marquering, and K. Kreutzburg. Laser beam brazing of car body components for the automotive industry: 26th international symposium on automotive technology and automation, isata'93 aachen. In *ISATA International Symposium on Automotive Technology and Automation, 26th. Proceedings of the Dedicated Conference on the Motor Vehicle and the Environment: Demands of the Nineties and Beyond*, pages 81–88. Automotive Automation Limited, Croydon, England, 1993.

R. N. Hall, G. E. Fenner, J. D. Kingsley, T. J. Saltz, and R. N. Calson. Stimulated emission of radiation from a semiconductor (gaas). *Phys. Rev. Lett.*, 9:366/9, 1962.

H. Hanebuth. *Laserstrahlhartlöten mit Zweistrahltechnik*, volume 55 of *Fertigungstechnik - Erlangen*. Meisenbach, Bamberg, 1996. ISBN 9783875250749.

I. Hayashi, M. B. Panish, P. W. Foy, and S. Sumski. Junction lasers which operate continuously at room temperature. *Appl. Phys. Lett.*, 17:109, 1970.

E. Hecht. *Optik*. Oldenbourg Wissenschaftsverlag, München, 4., überarb. aufl edition, 2005. ISBN 3486273590.

M. Heitmanek, M. Dobler, M. Graudenz, W. Perret, G. Göbel, M. Schmidt, and E. Beyer. Laser brazing with beam scanning: Experimental and simulative analysis. *Physics Procedia*, 56:689–698, 2014. ISSN 18753892. doi: 10.1016/j.phpro.2014.08.076.

B. Heutling. Eddy current inspection of pipes by means of wire - guided crawlers: Lrucm - seminar, 2008.

R. A. Higgins. *Engineering Metallurgy: Part 1: Applied physical metallurgy*. Hodder and Stoughten, Great Britain, 5th edition edition, 1983. ISBN 0340285249.

N. Hiller. Halbleiterlaserdioden: Grundlagen, strukturen, eigenschaften, anwendungen. *Laser: Technologien und Anwendungen*, (2):58–61, 1990.

Hochschule Hof. Reverse engineering - lasertriangulation, 2009. URL `http://www.hof-university.de/Reverse-Engineering-Lasertri.3585.0.html`. 03.17.2009.

N. Holonyak and S. F. Bevacqua. Coherent (visible) light emission from ga (as1-xpx) junctions. *Appl. Phys. Lett.*, 1(4):82/3, 1962.

Erhard Hornbogen. *Werkstoffe: Aufbau und Eigenschaften von Keramik, Metallen, Kunststoffen und Verbundwerkstoffen*. Springer, Berlin (u.a.), 3 edition, 1983. ISBN 3540117024.

H. Hornig. Laserunterstuetztes fuegen im fahrzeugbau: Proceedings zur tagung : Lasertechnologien im automobilbau 29.2. - 1.3.2000 fellbach. In Tagung Lasertechnologien im Automobilbau, editor, *Lasertechnologien im Automobilbau : Multitool Laser in der Praxis ; Stuttgart-Fellbach, 29. Februar und 1. Maerz 2000*. Landsberg, 2000.

H. Hornig. Praxis des laserstrahlhartlötens im fahrzeugbau (bmw group): Proceedings of 5. laser - anwenderforum bremen. In Frank Vollertsen, editor, *Laserstrahlfügen*, volume Bd. 28 of *Strahltechnik*, pages 124–137. BIAS-Verl, Bremen, 2006. ISBN 3933762189.

H. Huegel. *Strahlwerkzeug Laser - eine Einfuehrung: (Teubner Studienbuecher Maschinenbau)*. Teubner Studienbücher Technik. Vieweg+Teubner Verlag, Wiesbaden, 1992. ISBN 3663115356. URL http://www.worldcat.org/title/strahlwerkzeug-laser-eine-einfuhrung/oclc/857987360?ap=citavi.

C. Ibarra-Castanedo, J. M Piau, S. Guibert, X. P. Maldague, and A. Bendada. Ultrasonic and advanced methods for nondestructive testing and material characterization: Chapter 14. active infraredthermography techniques for the nondestructive testing of materials, 2006. URL http://vision.gel.ulaval.ca/~bendada/publications/Id663.pdf. 2010-02-18.

C. Ibarra-Castanedo, E. Grinzato, S. Marinetti, P. Bison, M. Genest, M. Grenier, J. M. Piau, A. Bendada, and X. Maldague. Recent progresses in the inspection of aerospace components by infrared thermography: 17th world conference on nondestructive testing shanghai, china, 2008.

R. Iffländer. *Festkörperlaser zur Materialbearbeitung*. Springer - Verlag, Berlin, 1990. ISBN 354052150X.

M. B. Ignatiev, I. Y. U. Smurov, G. Flamant, and V. N. Senchenko. Surface temperature measurements during pulsed laser action on metallic and ceramic materials. *Applied Surface Science*, 96-98:505–512, 1996.

David M. Jacobson and Giles Humpston. *Principles of brazing*. ASM International, Materials Park and Ohio, 2005. ISBN 9780871708120.

Jingwei Wang, Zhenbang Yuan, Lijun Kang, Kai Yang, Yanxin Zhang, and Xingsheng Liu. Study of the mechanism of "smile" in high power diode laser arrays and strategies in improving near-field linearity. In *59th Electronic Components and Technology Conference, 2009*, pages 837–842, Piscataway and NJ, 2009. IEEE. ISBN 9781424444755. doi: 10.1109/ECTC.2009.5074109. URL http://www.focuslight.com.cn/administrator/img/20125141743449977.pdf.

Ma Kai, Yu Zhishui, Zhang Peilei, Lu Yunlong, Yan Hua, Li Chonggui, and Liu Xiaopeng. Influence of wire feeding speed on laser brazing zinc-coated steel with cu-based

filler metal. *The International Journal of Advanced Manufacturing Technology*, 76 (5-8):1333–1342, 2015. ISSN 0268-3768. doi: 10.1007/s00170-014-6347-9.

S. Keitel and H. Orlick. Laserstrahl - hartloeten mit hoeheren festkoerperlaser - leistungen unter besonderer berücksichtigung der fuegegeometrie: Praezisionsbearbeitung mit festkoerperlasern (fuegen), broschuere zur abschlusspraesentation des bmbf gefoerderten verbundprojekts, 20.03.1996, 1996.

K. Kincade and S. G. Anderson. Laser marketplace 2008: Innovation opens the door for next wave of success. *LaserFocusWorld*, page 44, 2008.

R. Klein and L. Abram. Flussmittelarmes laserhartloeten von karosseriewerkstoffen: Praezisionsbearbeitung mit festkoerperlasern (fuegen), broschuere zur abschlusspraesentation des bmbf gefoerderten verbundprojekts 20.03.1996, 1996.

R. J. Klein Wassink. *Weichloeten in der Elektronik: Eine ausführliche Abhandlung über das Löten oberflächenmontierter und bedrahteter Bauteile*. Leuz Verlag, Saulgau/Württ., 2.auflage edition, 1991. ISBN 3874800660.

W. Koechner. *Solid - State Laser Engineering*, volume v. 1 of *Springer Series in Optical Sciences*. Springer, Berlin, 2nd completely rev. and updated ed edition, 1988. ISBN 9783540187479. URL http://www.worldcat.org/title/solid-state-laser-engineering/oclc/18463556?ap=citavi.

C. J. Koester and E. Snitzer. Amplification in a fiber laser. *Appl. Opt.*, 3(10):1182, 1964.

A. Koltsov, N. Bailly, and L. Cretteur. Wetting and laser brazing of zn-coated steel products by cu–si filler metal. *Journal of Materials Science*, 45(8):2118–2125, 2010. ISSN 0022-2461. doi: 10.1007/s10853-009-3949-y.

V. Krause and et. al. *Microchannel coolers for high power laser diodes in copper technology: Proc. of Laser Diode Technology and Applications VI (Proc. of SPIE)*, volume 2048. Fraunhofer Inst. for Laser Technology, Aachen, 1994.

V. Krause and H. G. Treusch. Potential von laserdioden fuer loetanwendungen in der smd - technologie: Proceedings of the 6th international conference on interconnection technology in electronics fellbach, germany, 1992.

V. Krause, H. G. Treusch, E. Beyer, and P. Loosen. High power laser diodes as a beam source for materials processing: 4th european conference onlaser treatment of materials, eclat'92 goettingen, 1992.

P. Kubik. Härteprüfung nach brinell/ vickers/ rockwell, 2010. URL http://www.kubixxx.de/.data/Haertepruefung_-_Brinell_Vickers_Rockwell.pdf. 2020-03-15.

Ltd Kyowa Interface Science Co. Contact angle, 2008. URL http://face-kyowa.com/en/learning/learning1.html. 04.16.2008.

J. K. Larsson. Lasers for various materials processing - a review of the latest laser applications in automative manufacturing: Proc. of the 7th nordic conference in laser processing of materials, nolamp, 1999.

Laserline GmbH. Handbuch diodenlaser: Lasertyp: LdI 40 - 150: Seriennummer: 223311, 2003. URL http://www.laserline.de/laserline-diodenlaser.html.

Laserline GmbH. Direct diode lasers – direct power, 2009. URL http://www.laserline.de/diode_laser/high_power_diode_lasers_direct_diode_lasers.html. 2009-06-05.

Layertec GmbH. Metallic coatings, 2014. URL http://www.layertec.de/en/capabilities/coatings/metallic. 2014-05-11.

Li-qun LI, Xiao-song FENG, and Yan-bin CHEN. Influence of laser energy input mode on joint interface characteristics in laser brazing with cu-base filler metal. *Transactions of Nonferrous Metals Society of China*, 18(5):1065–1070, 2008. ISSN 10036326. doi: 10.1016/S1003-6326(08)60182-X.

Li Lin. The advances and characteristics of high-power diode laser materials processing. *Optics and Lasers in Engineering*, (34):231–253, 2000.

E. F. Lish. Laser microsoldering adresses surface mount technology: Proceedings of the 36th electronic components conference seattle, usa, 1986.

Wei Liu, Shuang Liu, Junjie Ma, and Radovan Kovacevic. Real-time monitoring of the laser hot-wire welding process. *Optics & Laser technology*, 57:66–76, 2014. doi: 10.1016/j.optlastec.2013.09.026.

P. Loosen, L. Beckmann, and H. J. F. Advanced concepts of using diode lasers in materials processing. In *Lasers and Optics in Manufacturing III*, SPIE Proceedings, pages 480–485. SPIE, 1997. doi: 10.1117/12.281118. URL http://proceedings.spiedigitallibrary.org/proceeding.aspx?articleid=928112.

Peter Loosen, Hans-Georg Treusch, C. R. Haas, U. Gardenier, Manfred Weck, V. Sinnhoff, S. Kasperowski, vor dem Esche, R., Kurt J. Linden, and Prasad R. Akkapeddi. High - power diode - lasers and their direct industrial applications. In *Photonics West '95*, volume SPIE Proceedings, pages 78–88. SPIE, 1995. doi: 10.1117/12.208435. URL http://proceedings.spiedigitallibrary.org/proceeding.aspx?articleid=986936.

Howard H. Manko. *Solders and soldering: Materials, design, production, and analysis for reliable bonding*. McGraw-Hill, New York, 4th ed edition, 2001. ISBN 9780071382960.

S. Mann. Application of model based predictive control in laser beam welding, 2001.

A. Mathieu, S. Mattei, A. Deschamps, B. Martin, and D. Grevey. Temperature control in laser brazing of a steel / aluminium assembly using thermographic measurements. *NDT&E International*, 39:272–276, 2006a.

Alexandre Mathieu, Sébastien Pontevicci, Jean-claude Viala, Eugen Cicala, Simone Matteï, and Dominique Grevey. Laser brazing of a steel/aluminium assembly with hot filler wire (88% al, 12% si). *Materials Science and Engineering: A*, 435-436:19–28, 2006b. ISSN 09215093. doi: 10.1016/j.msea.2006.07.099.

Donald A. McQuarrie. *Mathematical methods for scientists and engineers*. University Science Books, Sausalito and Calif, 2003. ISBN 9781891389290.

Melles Griot. Product catalogue, 1996. URL http://www.mellesgriot.com/.

Melles Griot. Catalogue: Introduction to laser technology, 2005. URL http://www.mellesgriot.com/.

Dieter Meschede. *Optik, Licht und Laser*. Teubner Studienbücher Physik. Teubner, Wiesbaden, 2., überarb. und erw. aufl edition, 2005. ISBN 9783519132486.

metalinfo. Young's modulus, 2009. URL http://metals.about.com/od/metalterminology/l/bldefyoungsmodu.htm. 2009-05-13.

Metall Svetsmaterial KB. Material properties of cusi3, 2008. URL http://www.svetsmaterial.se/cusi3.html. 04.17.2008.

U. Muessigmann, J. Schwarz, and J. Kubon. Qualitaetspruefung an laserloet- und laserschweißnaehten. *Horizonte*, (23):20–22, 2003.

Wolfgang Müller and Jörg-Uwe Müller. *Löttechnik: Leitfaden für die Praxis*, volume 127 of *Fachbuchreihe Schweißtechnik*. Dt. Verl. für Schweisstechnik, Düsseldorf, 1995. ISBN 387155149X.

C. Murner and J. P. Hansen. Buried corrosion detection in multi-layer airframe structures using pulsed eddy current, 25-28 Oct. URL `http://www.ndt.net/article/wcndt2008/index.htm`.

M. I. Nathan, W. P. Dumke, G. Burns, F. H. Dill, and G. Lasher. Stimulated emission of radiation from gaas p-n junction. *Appl. Phys. Lett.*, 1(2):62/4, 1962.

C. Naumer, N. Lichtenstein, B. Schmidt, P. Bruns, F. Kubacki, P. Harten, and O. Lissotschenko. Brightness required! - more efficient laser diodes with refractive micro - optics. *Laser + Photonik*, (3):26–29, 2007.

Bert John Neubert and Wolf-Dieter Scharfe. Laser systems beam characteristics, metrology, and standards. In Friedrich Bachmann, Peter Loosen, and Reinhart Poprawe, editors, *High Power Diode Lasers*, volume 128 of *Springer Series in Optical Sciences*, pages 181–215. Springer, New York and NY and Berlin and Heidelberg, 2007. ISBN 9780387344539.

Norwalk, CT : Reed Exhibition Companies, editor. *Proceedings of the technical program: NEPCON West '97 : conference: February 23-February 27, 1997 : exhibition: February 25-February 27, 1997, Anaheim Convention Center, Anaheim, California. The new world of electronics manufacturing: Proceedings of the technical program, National Electronic Packaging and Production Conference NEPCON West'97*, 1997.

Osram Opto Semiconductors GmbH. Data sheet spl mn81x2: Passively cooled diode laser bar, 40w cw at 808 nm, 2007. URL `http://html.alldatasheet.com/html-pdf/218709/OSRAM/SPLMN81X2/626/4/SPLMN81X2.html`. 2010-01-14.

G. Overton and S. G. Anderson. Laser marketplace 2009: Photonics enters a period of high anxiety. *LaserFocusWorld*, 2009. URL `http://www.laserfocusworld.com/articles/print/volume-45/issue-1/features/laser-marketplace-2009-photonics-enters-a-period-of-high-anxiety.html`.

B. Perrin. The basics of thermocouples. *Circuit Cellar*, (12):1–5, 1999.

A. V. Polijanczuk and D. G. Whitehead. Semiconductor lasers for microsoldering: Ieee: Advances in interconnection technology, 18.04.1991. URL http://ieeexplore.ieee.org/xpl/articleDetails.jsp?arnumber=181464.

R. Poprawe. *Lasertechnik fuer die Fertigung: Grundlagen, Perspektiven und Beispiele fuer den innovativen Ingenieur*. Springer, Berlin, 2005. ISBN 978-3-540-26435-4.

Aleksandr M. Prokhorov, V. I. Konov, I. Ursu, and Mihailescu, I., N. *Laser Heating of metals*. The Adam Hilger Series on optics and optoelectronics. Hilger, Bristol, 1990. ISBN 075030040X. URL http://www.loc.gov/catdir/enhancements/fy0745/91183693-d.html.

Prometec GmbH. User manual: Laserscope uff 100: Version: Pda.223.106ge, 1996. URL prometec.de. 2013-03-26.

A. Ribolla, G. L. Damoulis, and G. F. Batalha. The use of nd: Yag laser weld for large scale volume assembly of automotive body in white. *Journal of Materials Processing Technology*, (164-165):1120–1127, 2005.

H. Riedelsberger. Laser brazing in automotive industry: Session 3: Applied technology, 30th October 2006. URL http://aws.org/conferences/abstracts/2006/018.pdf.

S. Rivas, R. Servent, and J. Belda. Automated spot weld inspection in the automotive industry, 2005. URL http://www.ndt.net/article/wcndt2004/html/automotive/408_rivas/408_rivas.htm.

Youmin Rong, Zhen Zhang, Guojun Zhang, Chen Yue, Yafei Gu, Yu Huang, Chunming Wang, and Xinyu Shao. Parameters optimization of laser brazing in crimping butt using taguchi and bpnn-ga. *Optics and Lasers in Engineering*, 67:94–104, 2015. doi: 10.1016/j.optlaseng.2014.10.009.

RP Photonics Consulting GmbH. Beam parameter product, 2008. URL http://www.rp-photonics.com/beam_parameter_product.html. 2008-10-08.

H.-G Rubahn. *Laseranwendungen in der Oberflächenphysik und Materialbearbeitung*. Teubner B.G. GmbH, Stuttgart, 1996.

B. Samson, J. Biesenbach, and G. Treusch. Fiber-laser pumping: Diode technology advances fiber-laser pumping. *LaserFocusWorld*, (Sep), 2008.

F. Schneider. Diodenlaser - pumplichtquellen fuer festkoerperlaser. *Laser: Technologien und Anwendungen*, (1):60, 1988.

B. Schuermann, G. Vitr, and K. Wissenbach. Randschichtbehandlung mit hochleistungs - diodenlasern. *LaserOpto*, 31(1):80–83, 1999.

E. Semerad, L. Musiejovsky, and J. Nicolics. Laser soldering of surface-mounted devices for high-reliability applications. *Journal of Material Science*, 28:5065–5069, 1993.

A. E. Siegman. *Lasers*. University Science Books, Mill Valley and Calif, 1986. ISBN 9780685055953.

M. Simon, I. Tiseanu, C. Sauerwein, H. Waelischmiller, M. Sindel, M. Brodmann, and M. Schmuecker. Advanced computed tomography system for the inspection of large aluminium car bodies: European conference on nondestructive testing ecndt berlin, 2006.

Jochen Speiser. Handout: High brightness thin - disk laser, 2008. URL `http://www.dlr.de/dlr/desktopdefault.aspx/tabid-10002/`.

R. V. Steele and Strategies unlimited. Laser marketplace 2007: Diode-laser market takes a breather. *LaserFocusWorld*, 2007.

William M. Steen. *Laser material processing*. Springer, London, 2 edition, 1998. ISBN 3540761748.

Horst Stöcker. *Taschenbuch der Physik: Formeln, Tabellen, Übersichten*. Deutsch, Thun, 4 edition, 2000. ISBN 3817116276.

J. Stone and C. A. Burrus. Neodymium - doped fiber lasers: room temperature cw operation with an injection laser pump. *Appl. Opt.*, 13(6):1256, 1974.

B. Struve. *Laser: Grundlagen, Komponenten, Technik*. Verlag Technik, Berlin, 2001. ISBN 9783341012598.

Svarkainfo. Arc brazing - innovative, safe and economical, 2009. URL `http://www.svarkainfo.ru/rus/info/news/2007/09/02/68`. 2009-05-03.

K. Toenshoff, A. H. Berndt, and M. Stuermer. Halbleiterlaser bieten vorteile im industriellen einsatz. *TR Transfer*, (50):30, 1993.

D. Triantafyllidis, M. J. J. Schmidt, and L. Li. Diode laser welding of thermocouples: Icaleo'99, 1999. URL http://www.worldcat.org/title/icaleo-99-proceedings-of-the-laser-microfabrication-conference/oclc/47191071.

TRINOS Vakuum-Systeme GmbH. Thermoelemente, 2008. URL http://shop.trinos.de/vakuum_s/trinos-thermoelemente.html. 2008-08-28.

TRUMPF GmbH + Co. KG (Holding). HI cw laser, 2009. URL http://www.de.trumpf.com/produkte/lasertechnik/produkte/festkoerperlaser/stablaser/hl-cw.html. 2009-06-05.

TWI Ltd. Induction brazing, 2009. URL http://www.twi.co.uk/content/kssbd001.html. 2009-05-03.

M. Ungers, R. Rolser, and P. Abels. Hardware based analysis and process control for laser brazing applications. *Physics Procedia*, 41:524–530, 2013. ISSN 18753892. doi: 10.1016/j.phpro.2013.03.111.

University of Tennessee. Iron-carbon phase diagram, 2008. URL http://www.aytacbicer.com/TR/DersNotlari/metal/FeC.pdf. 04.16.2008.

A. S. Usmani, J. M. Rotter, S. Lamont, A. M. Sanad, and M. Gillie. Fundamental principles of structural behaviour under thermal effects. *Fire Safety Journal*, 36(8):721–744, 2001. ISSN 03797112. doi: 10.1016/S0379-7112(01)00037-6.

F. Vacher, C. Gilles-Pascaud, J. M. Decitre, C. Fermon, M. Pannetier, and G. Cattiaux. Non destructive testing with gmr magnetic sensor arrays: European conference of non - destructive testing (ecndt) berlin, 2006. URL http://scholar.google.de/scholar_url?hl=de&q=http://www-ist.cea.fr/publicea/exl-doc/200600007545.doc&sa=X&scisig=AAGBfm0Av67KWgM5QldXsf0pHfLUUMQojw&oi=scholarr&ei=OaasU6GoNuaJ0AXN6IHoCw&ved=0CB8QgAMoADAA.

VDI Technologiezentrum Physikalische Technologien. Fuegen mit festkoerperlasern - laser in der materialbearbeitung, 1996. URL http://www.vditz.de/.

M. M. F. Verguld. New developments and trends in soldering technology for miniaturized assemblies: National electronic packaging and production conference nep-

con west '92, 1992. URL http://books.google.de/books/about/NEPCON_West_92.html?id=I4lJmgEACAAJ&redir_esc=y.

Vitronic. 3d-soldering seam inspection, 2008a. URL http://www.vitronic.de/de/startseite.html.

Vitronic. Recognizing faults and optimizing production, 2008b. URL http://www.vitronic.de/de/startseite.html.

J. Wallace. High-power diode lasers: Direct-diode lasers combine to form powerful, high-brightness beam. *LaserFocusWorld*, 2009.

WEKA FACHMEDIEN GmbH. Lebensdauer von laserdioden, 2009. URL http://www.elektroniknet.de/home/laser/wissenschaft-und-forschung/news/d/lebensdauer-von-laserdioden/. 2009-06-04.

G. H. Winstel and C. Weyrich. *Optoelektronik: Luminiszenz- und Laserdioden*, volume 1. Springer, Berlin, 1981. URL http://www.worldcat.org/title/optoelektronik/oclc/646197020?ap=citavi.

K. Wissenbach. *Dissertation: Umwandlungshärten mit CO2- Laserstrahlung*. PhD thesis, TH Darmstadt, 1985. URL http://www.worldcat.org/title/umwandlungsharten-mit-co-laserstrahlung/oclc/50438122?referer=di&ht=edition.

C. E. Witherell. Laser micro - brazing to join small parts. *Laser Focus*, pages 73–80, 1981.

W. Wuich. *Löten: Lötverfahren, Lote, Flussmittel, Anwendungstechniken*. Kamprath-Reihe. kurz und bundig. Vogel-Verlag, Würzburg, 1972. ISBN 9783802300578.

G. Württemberger. *Fachkunde Metall*. Europa - Lehrmittel, 36th edition edition, 1987. ISBN 9783808510285.

A. Yashan, W. Bisle, and T. Meier. Inspection of hidden defects in metal-metal joints of aircraft structures using eddy current technique with gmr sensor array: European conference of non - destructive testing ecndt berlin, 2006. URL http://www.ndt.net/article/ecndt2006/doc/Tu.4.4.4.pdf.

B.S Yilbas, Z. Yilbas, and Akcakoyun. Investigation into absorption of the incident laser beam during nd : Yag laser processing of metals. *Optics & Laser technology*, 28(7): 503–511, 1996.

P. Zaremba. *Hart- und Hochtemperaturlöten*, volume 20 of *Die schweißtechnische Praxis*. DVS-Verl., Düsseldorf, 1988. ISBN 9783871555268.

S. Zhouping, L. Qihong, D. Jingxing, Z. Jun, and W. Runrong. Beam quality improvement of laser diode array by using off-axis external cavity: Optical society of america(osa). *Optics Express*, 19(15), 2007.

A. Appendix for the chapter "Quality influencing parameters"

A.1. Verification of the calculated HL204P Nd:YAG laser beam characteristics

To verify the calculated laser beam characteristics of the used Nd:YAG laser the beam profiler Laserscope UFF 100 from Prometec GmbH is used. The respective data sheet of this device can be found in Appendix D.7. In total 24 measurements of the laser spot at different z-positions are carried out to determine the caustic of the laser beam with its respective characteristics.
For the caustic measurement the lens with a focal length of 150 mm is used. Since the laser used operates in pulsed mode and the Laserscope UFF 100 has a certain sampling rate, a suitable parameter set for the Nd:YAG laser has to be determined to avoid or at least diminish any kind of interferences. For this, testing is carried out to find a sufficient parameter set prior to the actual measurement. The determined parameter set is as follows:

- power P (W): 357
- pulse length t_p (ms): 17.7
- repetition rate f (Hz): 12.5
- average power P_{av} (W): 80.7
- number of averaging: 10

The Laserscope UFF 100 is placed within the Nd:YAG laser work station (see section 4.1). Subsequently the laser is focused and positioned on the measurement window of the Laserscope. For the measurement only the z-position is changed and the amplification of the measurement signal is adapted accordingly. The start position for the measurement is z = -56.75 mm. The results of the caustic measurement can be found in Appendix A.2.

Figure A.1 shows an example of a false colour image of the laser spot at the respective z-position (A.1a) as well as the measured caustic (A.1b). The provided analysis software of the Laserscope UFF 100 calculates the beam characteristics beam waist, divergence and Rayleigh length based on the method of second-order moments as well as the 86 % method. The results are shown in Table A.1.

Furthermore, Table A.1 includes the theoretically determined or provided values for the respective parameters. More detailed information regarding the measurements and their results can be found in Appendix A.2.

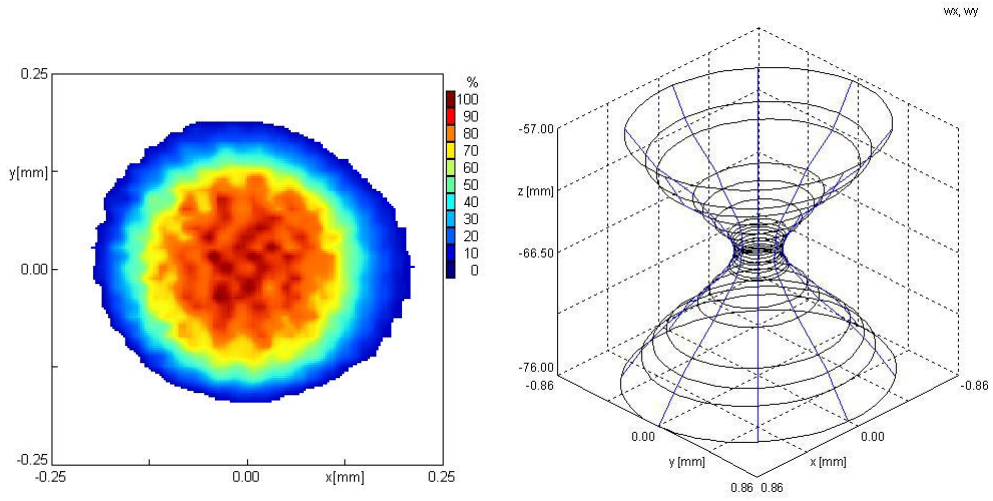

(a) Example of a measured false colour image of the laser spot for caustic determination

(b) Measured caustic of the Nd:YAG laser beam

Figure A.1.: a) Example of a measured false colour image of the laser spot for caustic determination at z-position -65.700 mm with a fill factor of the measurement window of 59 % and with a beam radius w: 0.147 mm (86 % method) determined by the provided Laserscope UFF 100 software ; b) Measured caustic of the Nd:YAG laser beam

As it can be seen in Table A.1 the experimentally determined parameters, beam waist radius (w_0), divergence ($\frac{\theta}{2}$) as well as the (BPP) are smaller compared to the theoret-

Table A.1.: Determined Nd:YAG laser beam characteristics via the Laserscope UFF 100 by using the 86 % method and the method of second-order moments as well as the theoretical determined and given values (see Table 3.1) for comparison

Laser beam characteristics	86 % method	Method of second-order moments	Theoretical
Beam waist radius w_0 (mm)	0.138	0.149	0.150
Rayleigh length z_R (mm)	1.603	1.683	1.401
Divergence angle $\frac{\theta}{2}$ (rad)	0.086	0.0885	0.107
Determined BPP (mm*mrad)	11.868	13,187	16

ically determined values and the Rayleigh length (z_R) is respectively larger due to its definition (see equation 3.6). The experimentally determined values are influenced by positioning of the laser spot within the measurement window, amplification of the measurement signal, selection of the size of the measurement window with regard to the fill factor, the operation mode of the laser as well as the repeatability of the measurement device.

The correct positioning of the laser spot within the measurement is important for the calculation of the power density distribution. For all measurements the whole laser spot is covered within the measurement window only a marginal displacement of x = 0.136 mm and y = -0.420 mm with regard to the center of the power density distribution could not be avoided.

The fill factor should be in the range of 50 % to 75 %, i.e. that the area of the laser spot should cover at least 50 % and up to 75 % of the measurement window (e.g. see Figure A.1a) (Prometec GmbH, 1996).

This provided range should not be exceeded, since then the asymptotic decreasing parts at the edge of the laser spot are neglected. If the fill factor is below this range the total measurement signal is predominated by the noise component. For all measurements the fill factor is kept within this range. However, the manual of the Laserscope indicates that the measurement error is minimal for a fill factor of approximately 55% (Prometec GmbH, 1996). But this value could not always be obtained due to laser spot size versus size of measurement window with respect to fill factor.

As mentioned, the laser spot is not perfectly aligned to the point of origin of the measurement window. For this reason the real point of origin deviates from the calculated one. This difference is added to the measurement signal for each point at the distribution. Depending on the fill factor this difference can have a significant influence on the calculation of the volume of the power density distribution. The influence increases with a decrease in the fill factor (Prometec GmbH, 1996).

The amplification of the measurement signal also influences the result. For instance, if the amplification is too small, information is lost and therefore the determined parameters might be inaccurate. The same occurs, if the signal is amplified too much. As it seems an optimal amplification is not always maintained with regard to determined parameters.

The beam radius (w) according to the 86 % method is determined by at first adding all measurement points of the power density distribution that in sum correspond to 86 % of the total sum of all measurement points. This is carried out, since the volume of the power density distribution is proportional to the laser power. Subsequently, the cross-sectional area of the laser spot is determined by counting the respective measurement points and multiplying each of these points with the corresponding measurement window dependent fractional area. This obtained area is assumed to be circular and the beam radius is calculated respectively (Prometec GmbH, 1996).

Since the laser used operates in pulsed mode and the Laserscope has a certain sampling rate for each size of the measurement window, interference can occur. As mentioned above, a sufficient set of laser parameters was determined and each measurement result is the average of 10 measurements to diminish the influence of interference.

However, sometimes the interference could not be totally avoided as it can be seen in Figure A.2 which also has an influence on the measurement results.

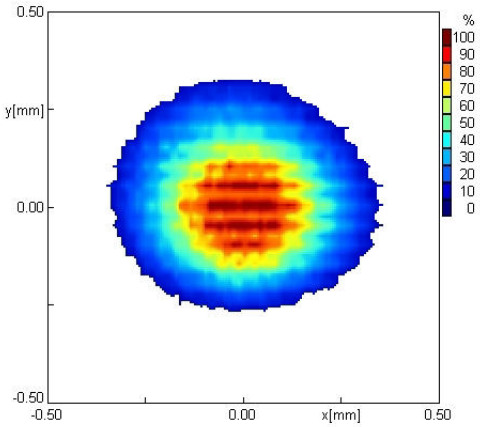

Figure A.2.: Example of a measured false colour image of the laser spot used for caustic determination with recognisable interference at z-position -64.000 mm with a beam radius w of 0.250 mm (86 % method) and a fill factor of 50 %

Considering all these previous mentioned influences as well as the mechanical repeatability of this device of $\pm$ 0.05 mm in y and $\pm$ 2 μm in x-direction, the relative deviation of 8.00 % (86 % method) and 0.67 % (method of second-order moments) for the beam waist radius (w_0), 12.60 % (86 % method) and 16.76 % (method of second-order moments) for the Rayleigh length (z_R) and 19.38 % (86 % method) and 17.03 % (method of second-order moments) for the divergence ($\frac{\theta}{2}$) between the experimentally determined and theoretical parameters can be reasoned.

A.2. Results of the caustic measurements of the HL204P Nd:YAG laser

PROMETEC PROLAS Caustic results

Parameter		Value		Unit
PROLAS-Version				
Device		UFF 100		
Ser.-No.		UFF100-374		
Laser power	P		0	W
Company		HS-EL		
Laser		HL 204P		
Beam shape				
Optics				
Location				
Comment 1				
Comment 2				
Operator				
z assigned to ext.		ze		
ext. Reference position	zeref	0.000		mm
Wavelength			1.060	µm
z-Offset	zOff		-66.276	mm
Rotate angle			45	°
View angle			30	°

Result		Value		Unit
Beam waste radius	w0(r86%)	0.138		mm
Rayleigh length	zR(r86%)		1.603	mm
Focus position	z0(r86%)		-66.276	mm
ext. Focus position	ze0(r86%)		-66.276	mm
Divergence angle	theta(r86%)	0.172		rad
Beam propagation factor	K(r86%)	0.028		
Time limit defraction factor	M^2(r86%)		35.220	
Coefficient	a(r86%)		2,97E+02	1/mm
Coefficient	b(r86%)		3,93E+04	
Coefficient	c(r86%)		1,30E+06	mm
Beam waste radius	w0(w)	0.149		mm
Rayleigh length	zR(w)		1.683	mm
Focus position	z0(w)		-66.246	mm
ext. Focus position	ze0(w)		-66.246	mm
Divergence angle	theta(w)	0.177		rad
Beam propagation factor	K(w)	0.026		
Time limit defraction factor	M^2(w)		39.121	
Coefficient	a(w)		3,14E+02	1/mm
Coefficient	b(w)		4,16E+04	
Coefficient	c(w)		1,38E+06	mm
Beam waste radius	w0(wx)	0.156		mm
Rayleigh length	zR(wx)		1.648	mm
Focus position	z0(wx)		-66.249	mm

ext. Focus position	ze0(wx)		-66.249	mm
Divergence angle	theta(wx)	0.189		rad
Beam propagation factor	K(wx)	0.023		
Time limit defraction factor	M^2(wx)		43.546	
Coefficient	a(wx)		3,57E+02	1/mm
Coefficient	b(wx)		4,73E+04	
Coefficient	c(wx)		1,57E+06	mm
Beam waste radius	w0(wy)	0.142		mm
Rayleigh length	zR(wy)		1.729	mm
Focus position	z0(wy)		-66.241	mm
ext. Focus position	ze0(wy)		-66.241	mm
Divergence angle	theta(wy)	0.164		rad
Beam propagation factor	K(wy)	0.029		
Time limit defraction factor	M^2(wy)		34.634	
Coefficient	a(wy)		2,70E+02	1/mm
Coefficient	b(wy)		3,58E+04	
Coefficient	c(wy)		1,19E+06	mm

Fitting parameter definition: w(z)= 0.5 * SQRT(a*z*z+b*z+c)

Diagram files used in caustic

Filename	z-Position	Radius (86%)	Beam radius	x-Beam radius	y-Beam radius	Rotate angle	Ellipticity	Area (86%)	abs. Beam position	abs. Beam position
*.pms	z	r(86%)	w	wx	wy	psi	epsilon	A(86%)	x0	y0
	mm	mm	mm	mm	mm	°		mm²	mm	mm
SWO_f150_F-0002.pmd	-57.000	0.748	0.783	0.835	0.726	-23	1.150	1.760	0.065	-0.384
SWO_f150_F-0064.pmd	-59.000	0.655	0.672	0.710	0.631	-17	1.126	1.346	0.076	-0.352
SWO_f150_F-0006.pmd	-60.000	0.593	0.608	0.649	0.566	-13	1.147	1.104	0.123	-0.381
SWO_f150_F-0057.pmd	-62.000	0.380	0.390	0.418	0.360	-16	1.162	0.4547	0.116	-0.388
SWO_f150_F-0055.pmd	-63.000	0.329	0.334	0.359	0.308	-13	1.165	0.3409	0.142	-0.399
SWO_f150_F-0053.pmd	-64.000	0.250	0.261	0.281	0.241	-8	1.166	0.1966	0.127	-0.409
SWO_f150_F-0050.pmd	-65.000	0.179	0.184	0.192	0.174	-15	1.102	0.1005	0.143	-0.423
SWO_f150_F-0086.pmd	-65.300	0.163	0.170	0.178	0.162	-9	1.103	0.08368	0.143	-0.423
SWO_f150_F-0085.pmd	-65.500	0.154	0.162	0.169	0.154	-9	1.098	0.07491	0.135	-0.422
SWO_f150_F-0084.pmd	-65.700	0.147	0.156	0.163	0.149	-9	1.093	0.06790	0.130	-0.423
SWO_f150_F-0018.pmd	-66.000	0.137	0.149	0.156	0.143	-4	1.090	0.05939	0.150	-0.439
SWO_f150_F-0080.pmd	-66.300	0.136	0.149	0.156	0.141	-7	1.105	0.05769	0.123	-0.424
SWO_f150_F-0083.pmd	-66.300	0.135	0.150	0.156	0.143	-3	1.088	0.05718	0.126	-0.423
SWO_f150_F-0066.pmd	-66.500	0.137	0.151	0.158	0.142	-6	1.111	0.05914	0.145	-0.425
SWO_f150_F-0069.pmd	-66.800	0.142	0.157	0.163	0.150	-8	1.089	0.06292	0.152	-0.422
SWO_f150_F-0019.pmd	-67.000	0.154	0.162	0.170	0.155	-6	1.094	0.07433	0.156	-0.437
SWO_f150_F-0078.pmd	-67.300	0.170	0.178	0.187	0.168	-8	1.112	0.09078	0.125	-0.426
SWO_f150_F-0070.pmd	-67.500	0.180	0.185	0.194	0.174	-10	1.113	0.1015	0.122	-0.425
SWO_f150_F-0029.pmd	-69.000	0.279	0.293	0.317	0.266	-10	1.191	0.2442	0.153	-0.446
SWO_f150_F-0033.pmd	-70.000	0.361	0.367	0.391	0.341	-10	1.148	0.4102	0.177	-0.446
SWO_f150_F-0037.pmd	-72.000	0.497	0.551	0.583	0.518	-11	1.125	0.7762	0.122	-0.459
SWO_f150_F-0038.pmd	-73.000	0.605	0.635	0.669	0.599	-11	1.116	1.151	0.139	-0.486
SWO_f150_F-0040.pmd	-74.000	0.680	0.700	0.740	0.657	-14	1.126	1.453	0.131	-0.489
SWO_f150_F-0045.pmd	-76.000	0.810	0.822	0.870	0.771	-14	1.128	2.061	0.157	-0.482

A.3. LDL 40-150 output power dependency on driving current

Figure A.3.: Diode laser LDL 40-150 output power dependency on driving current(Laserline GmbH, 2003)

A.4. Verification of simple astigmatic beam

To ensure that the beam is simple astigmatic, several measurements of the laser spot are carried out with the beam profiler Laserscope UFF 100 from PROMETEC GmbH. Even if this device is specified for CO_2 as well as Nd:YAG laser radiation, it can be used to estimate the respective beam classification (Prometec GmbH, 1996).

Figure A.4 shows as an example two beam profiles, each captured at different z-positions. These profiles clearly indicate that the laser beam of the diode laser is simple astigmatic, since the principal axis of the beam does not rotate while propagating (Neubert and Scharfe, 2007).

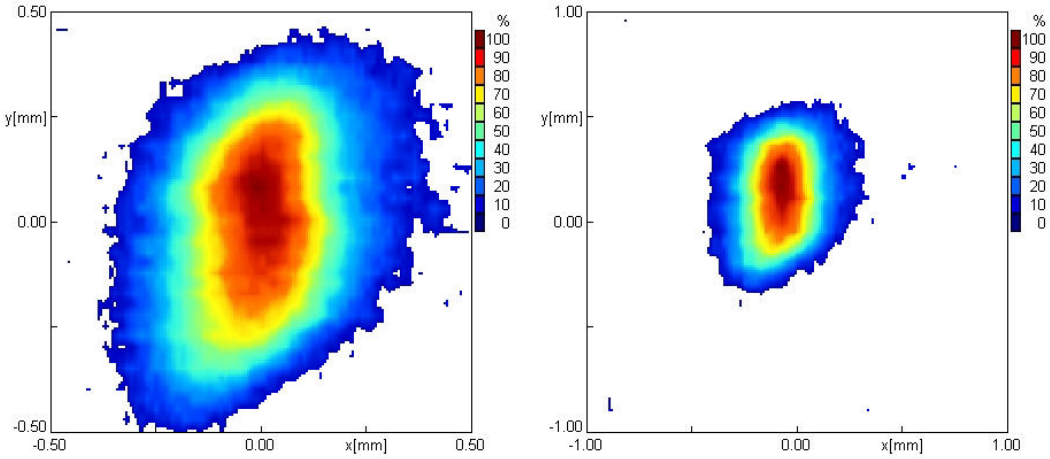

(a) Beam profile of the diode laser spot at the focal position z = 0 mm (beam waist)

(b) Beam profile of the defocused diode laser spot (z = -26.01 mm)

Figure A.4.: Images of the diode laser spot captured with the beam profiler Laserscope UFF 100 from PROMETEC GmbH. The sensitivity of the Laserscope is not linear for the diode laser wavelength used. a) Beam profile of the diode laser spot at the focal position (z = 0 mm); b) Beam profile of the defocused diode laser spot (z = -26.01 mm)

A.5. Verification of the theoretically determined diode laser spot sizes

During orientation control of the laser spot within the work station, it is observed for the laser spot at the focal position (F) = + 5 mm (Figure A.5 (c)) that the diameters correspond approximately to the half of theoretical estimated ones by measuring the ablated part of the paper.

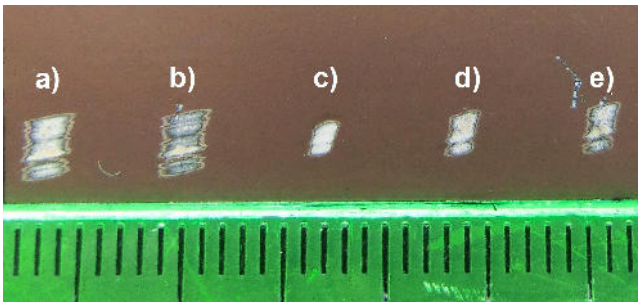

Figure A.5.: Orientation of the diode laser spot within the work station: a) z = +10 mm, P = 85 W; b) z = +10 mm, P = 85 W; c) z = +5 mm, P = 45 W; d) z = +7 mm, P = 45 W; e) z = +8 mm, P = 65 W;

The diameters determined for the other focal positions is in general smaller than the theoretical estimated ones via the equation (3.8), since the power used was not sufficient to completely ablate the photo-sensitive paper. It is assumed that the ablated part of the paper corresponds only to the half of the theoretical diameter, since the other 50 % of the laser spot (see Figure 3.3) are too weak to cause any reaction at the photo-sensitive paper (or to say it in different terms: for the other 50 % of the laser spot the photo-sensitive paper is too insensitive).

To validate this assumption the measurement is carried out again for the focal positions (F) [12] $+4\,\text{mm}$, $+5\,\text{mm}$, $+6\,\text{mm}$, $+7\,\text{mm}$ and $+10\,\text{mm}$. For each focal position a single laser pulse is emitted onto the photo-sensitive paper and repeated at least 15 times with different powers used. The powers are varied to ensure that this observation does not only account for a single focal position in combination with a specific power used. From each measurement a picture is taken with the Casio Exilim Ex-ZR100 12.1 MPixel camera and the respective diameters (d_x(F)) and (d_y(F)) are measured. The measurement approach is exemplified on the focal position (F) = $+5\,\text{mm}$. All other measurement results can be found in Appendix A.6. Table A.2 shows the number of emitted laser pulses and the respective power used for each pulse. Figure A.6 shows

Table A.2.: Powers used for verification of spot diameters estimation of the diode laser at the focal position (F) $= +5\,\text{mm}$

No.	P in W
1	45
2	45
3	45
4	45
5	45
6	45
7	45
8	50
9	50
10	50
11	50
12	50
13	48
14	48
15	48
16	48
17	48

the result of the measurement with the focal position (F) $= +5\,\text{mm}$. To measure the re-

[12] "+" sign for the focal positions indicates that the focal position is above the surface

spective diameters, the pixels have to be correlated to unit length. For this, a ruler with a 0.5 mm scale is used, which can be seen in Figure A.6 at the bottom. Subsequently, for each spot the diameters (d_x) and (d_y) are measured as indicated in Figure A.6. For all the measurements a tolerance of ± 15 pixels is taken into account that corresponds to $\pm$ 0.288 mm for the focal position (F) = +5 mm.

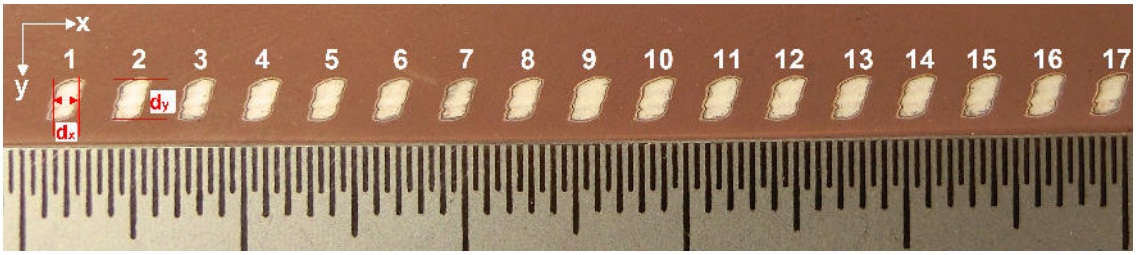

Figure A.6.: Measurement result of diode laser spot diameters for the focal position (F) = +5 mm; the measurement approach of (d_x) and (d_y) is presented at laser spot number 1 and 2 respectively

Table A.3 shows the measurement results for the focal position (F) = + 5 mm.

Table A.3.: Measurement results for the laser spot diameters (d_x) and (d_y) at the focal position (F) = +5 mm. The determined diameters correspond to twice the measured ones

Number	Power in W	measured dx in mm	measured dy in mm	determined dx in mm	determined dy in mm
1	45	1.154	1.788	2.308 $\pm$ 0.288	3.577 $\pm$ 0.288
2	45	1.173	1.865	2.346 $\pm$ 0.288	3.731 $\pm$ 0.288
3	45	1.154	1.827	2.308 $\pm$ 0.288	3.654 $\pm$ 0.288
4	45	1.192	1.865	2.385 $\pm$ 0.288	3.731 $\pm$ 0.288
5	45	1.173	1.885	2.346 $\pm$ 0.288	3.769 $\pm$ 0.288
6	45	1.173	1.923	2.346 $\pm$ 0.288	3.846 $\pm$ 0.288
7	45	1.154	1.865	2.308 $\pm$ 0.288	3.731 $\pm$ 0.288
8	50	1.173	1.904	2.346 $\pm$ 0.288	3.808 $\pm$ 0.288
9	50	1.212	1.942	2.423 $\pm$ 0.288	3.885 $\pm$ 0.288
10	50	1.212	1.923	2.423 $\pm$ 0.288	3.846 $\pm$ 0.288
11	50	1.231	1.923	2.462 $\pm$ 0.288	3.846 $\pm$ 0.288
12	50	1.212	1.923	2.423 $\pm$ 0.288	3.846 $\pm$ 0.288
13	48	1.212	1.904	2.423 $\pm$ 0.288	3.808 $\pm$ 0.288
14	48	1.212	1.923	2.423 $\pm$ 0.288	3.846 $\pm$ 0.288
15	48	1.231	1.923	2.462 $\pm$ 0.288	3.846 $\pm$ 0.288
16	48	1.231	1.923	2.462 $\pm$ 0.288	3.846 $\pm$ 0.288
17	48	1.154	1.885	2.308 $\pm$ 0.288	3.769 $\pm$ 0.288

Comparing the determined diameters (d_x(5)) and (d_x(5)) respectively with the theoretical determined ones (d_x(5) = 2.43 mm and d_y(5) = 3.68 mm (see section 3.1.1.2.2)), it can be said that the theoretical ones are within the measurement tolerance of the determined diameters. These measurements are also carried out for the other focal positions mentioned. The results are presented in Figure A.7. Figure A.7 shows on the one hand the theoretical propagation of the beam diameters, which are determined by using equation 3.8, and on the other hand the mean of the determined diameters at the respective focal positions.

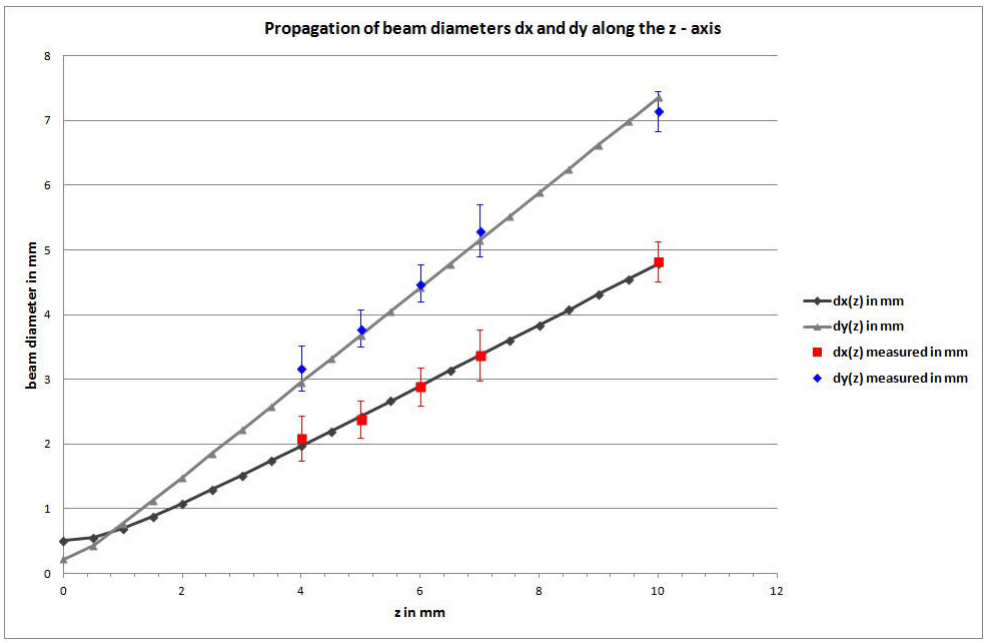

Figure A.7.: Propagation of laser beam diameters along the z-axis: measured and theoretical diameters

A.6. Verification of the calculated diode laser spot diameters (d_x(z)) and (d_y(z))

In Figure A.8 to A.11 the measurement results for the respective focal position are presented. In Table A.4 to A.7 the measured and determined spot diameters (d_x(z)) and (d_y(z) are shown. For each spot diameter measurement a measurement tolerance of $\pm$15 pixels is taken into account.

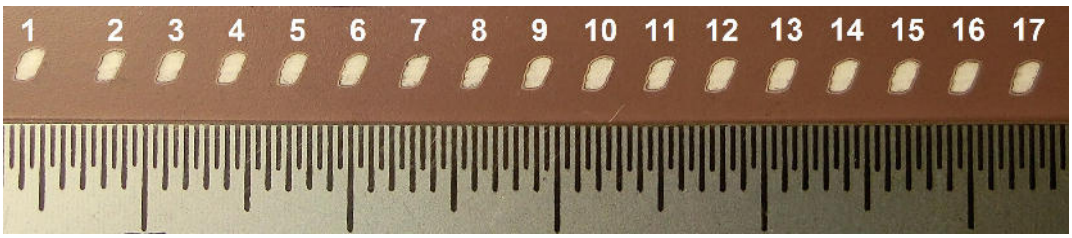

Figure A.8.: Measurement result of diode laser spot diameters for the focal position (F) $= +4$ mm

Table A.4.: Measurement results for the laser spot diameters(d_x) and (d_y) at the focal position (F) = $+4$ mm. The determined diameters correspond to twice the measured ones

Number	Power in W	measured dx in mm	measured dy in mm	determined dx in mm	determined dy in mm
1	40	1.093	1.581	2.186 ± 0.349	3.163 ± 0.349
2	38	1.023	1.558	2.047 ± 0.349	3.116 ± 0.349
3	35	1.047	1.558	2.093 ± 0.349	3.116 ± 0.349
4	30	1.047	1.558	2.093 ± 0.349	3.116 ± 0.349
5	30	1.023	1.558	2.047 ± 0.349	3.116 ± 0.349
6	30	1.047	1.535	2.093 ± 0.349	3.070 ± 0.349
7	30	1.047	1.581	2.093 ± 0.349	3.163 ± 0.349
8	30	1.047	1.581	2.093 ± 0.349	3.163 ± 0.349
9	30	1.023	1.581	2.047 ± 0.349	3.163 ± 0.349
10	35	1.070	1.605	2.140 ± 0.349	3.209 ± 0.349
11	35	1.023	1.605	2.047 ± 0.349	3.209 ± 0.349
12	35	1.047	1.605	2.093 ± 0.349	3.209 ± 0.349
13	35	1.047	1.605	2.093 ± 0.349	3.209 ± 0.349
14	38	1.070	1.628	2.140 ± 0.349	3.256 ± 0.349
15	38	1.047	1.628	2.093 ± 0.349	3.256 ± 0.349
16	38	1.047	1.628	2.093 ± 0.349	3.256 ± 0.349
17	38	1.047	1.605	2.093 ± 0.349	3.209 ± 0.349

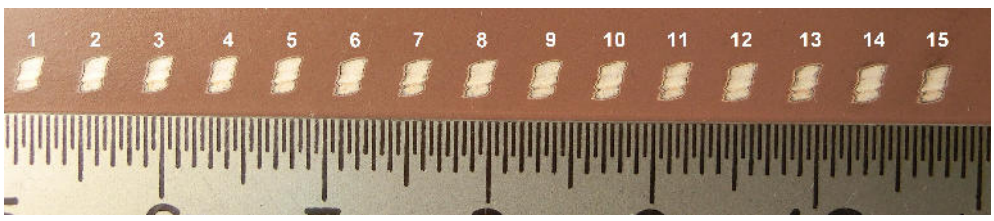

Figure A.9.: Measurement result of diode laser spot diameters for the focal position (F) $= +6$ mm

Table A.5.: Measurement results for the laser spot diameters (d_x) and (d_y) at the focal position (F) = +6 mm. The determined diameters correspond to twice the measured ones

Number	Power in W	measured dx in mm	measured dy in mm	determined dx in mm	determined dy in mm
1	55	1.371	2.162	2.741 ± 0.290	4.324 ± 0.290
2	55	1.390	2.162	2.780 ± 0.290	4.324 ± 0.290
3	55	1.448	2.181	2.896 ± 0.290	4.363 ± 0.290
4	55	1.429	2.220	2.857 ± 0.290	4.440 ± 0.290
5	55	1.429	2.220	2.857 ± 0.290	4.440 ± 0.290
6	58	1.467	2.259	2.934 ± 0.290	4.517 ± 0.290
7	58	1.448	2.220	2.896 ± 0.290	4.440 ± 0.290
8	58	1.467	2.278	2.934 ± 0.290	4.556 ± 0.290
9	58	1.486	2.278	2.973 ± 0.290	4.556 ± 0.290
10	58	1.448	2.297	2.896 ± 0.290	4.595 ± 0.290
11	60	1.467	2.239	2.934 ± 0.290	4.479 ± 0.290
12	60	1.448	2.297	2.896 ± 0.290	4.595 ± 0.290
13	60	1.448	2.259	2.896 ± 0.290	4.517 ± 0.290
14	60	1.467	2.297	2.934 ± 0.290	4.595 ± 0.290
15	60	1.448	2.259	2.896 ± 0.290	4.517 ± 0.290

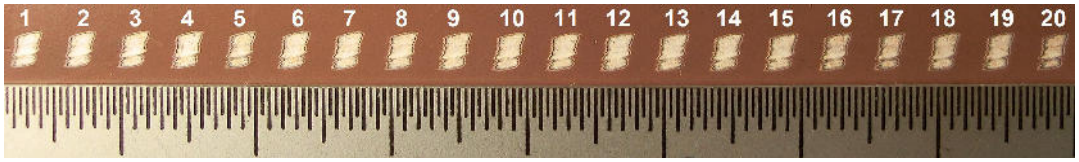

Figure A.10.: Measurement result of diode laser spot diameters for the focal position (F) = +7 mm

Table A.6.: Measurement results for the laser spot diameters (d_x) and (d_y) at the focal position (F) = +7 mm. The determined diameters correspond to twice the measured ones

Number	Power in W	measured dx in mm	measured dy in mm	determined dx in mm	determined dy in mm
1	65	1.676	2.500	3.351 ± 0.399	5.000 ± 0.399
2	65	1.676	2.527	3.351 ± 0.399	5.053 ± 0.399
3	65	1.702	2.580	3.404 ± 0.399	5.160 ± 0.399
4	65	1.702	2.633	3.404 ± 0.399	5.266 ± 0.399
5	65	1.676	2.580	3.351 ± 0.399	5.160 ± 0.399
6	68	1.702	2.686	3.404 ± 0.399	5.372 ± 0.399
7	68	1.702	2.660	3.404 ± 0.399	5.319 ± 0.399
8	68	1.702	2.660	3.404 ± 0.399	5.319 ± 0.399
9	68	1.729	2.660	3.457 ± 0.399	5.319 ± 0.399
10	68	1.729	2.686	3.457 ± 0.399	5.372 ± 0.399
11	70	1.729	2.686	3.457 ± 0.399	5.372 ± 0.399
12	70	1.729	2.686	3.457 ± 0.399	5.372 ± 0.399
13	70	1.755	2.686	3.511 ± 0.399	5.372 ± 0.399
14	70	1.755	2.686	3.511 ± 0.399	5.372 ± 0.399
15	70	1.755	2.713	3.511 ± 0.399	5.426 ± 0.399
16	60	1.622	2.660	3.245 ± 0.399	5.319 ± 0.399
17	60	1.569	2.660	3.138 ± 0.399	5.319 ± 0.399
18	60	1.622	2.713	3.245 ± 0.399	5.426 ± 0.399
19	60	1.622	2.713	3.245 ± 0.399	5.426 ± 0.399
20	60	1.569	2.606	3.138 ± 0.399	5.213 ± 0.399

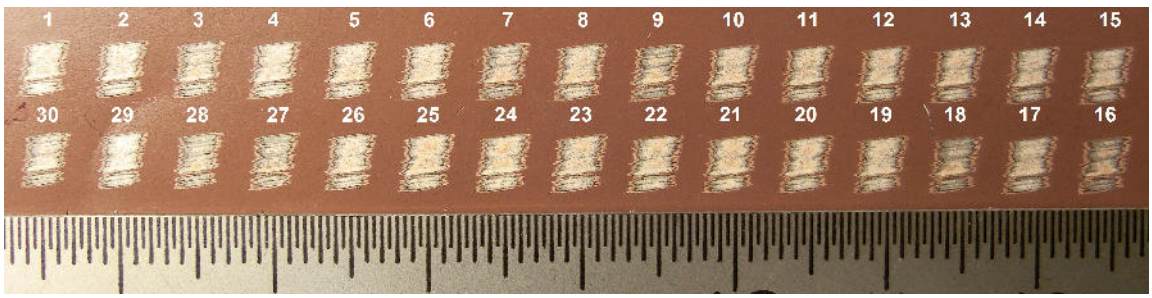

Figure A.11.: Measurement result of diode laser spot diameters for the focal position (F) = +10 mm

Table A.7.: Measurement results for the laser spot diameters (d_x) and (d_y) at the focal position (F) = +10 mm. The determined diameters correspond to twice the measured ones

Number	Power in W	measured dx in mm	measured dy in mm	determined dx in mm	determined dy in mm
1	95	2.387	3.498	4.774 ± 0.309	6.996 ± 0.309
2	95	2.366	3.580	4.733 ± 0.309	7.160 ± 0.309
3	95	2.387	3.539	4.774 ± 0.309	7.078 ± 0.309
4	95	2.407	3.580	4.815 ± 0.309	7.160 ± 0.309
5	95	2.428	3.601	4.856 ± 0.309	7.202 ± 0.309
6	98	2.407	3.601	4.815 ± 0.309	7.202 ± 0.309
7	98	2.325	3.560	4.650 ± 0.309	7.119 ± 0.309
8	98	2.407	3.601	4.815 ± 0.309	7.202 ± 0.309
9	98	2.366	3.519	4.733 ± 0.309	7.037 ± 0.309
10	98	2.407	3.580	4.815 ± 0.309	7.160 ± 0.309
11	100	2.366	3.580	4.733 ± 0.309	7.160 ± 0.309
12	100	2.387	3.601	4.774 ± 0.309	7.202 ± 0.309
13	100	2.387	3.560	4.774 ± 0.309	7.119 ± 0.309
14	100	2.407	3.580	4.815 ± 0.309	7.160 ± 0.309
15	100	2.428	3.580	4.856 ± 0.309	7.160 ± 0.309
16	105	2.366	3.519	4.733 ± 0.309	7.037 ± 0.309
17	105	2.428	3.601	4.856 ± 0.309	7.202 ± 0.309
18	105	2.449	3.580	4.897 ± 0.309	7.160 ± 0.309
19	105	2.469	3.642	4.938 ± 0.309	7.284 ± 0.309
20	105	2.510	3.621	5.021 ± 0.309	7.243 ± 0.309
21	110	2.551	3.642	5.103 ± 0.309	7.284 ± 0.309
22	110	2.551	3.642	5.103 ± 0.309	7.284 ± 0.309
23	110	2.593	3.642	5.185 ± 0.309	7.284 ± 0.309
24	110	2.593	3.663	5.185 ± 0.309	7.325 ± 0.309
25	110	2.551	3.642	5.103 ± 0.309	7.284 ± 0.309
26	90	2.325	3.560	4.650 ± 0.309	7.119 ± 0.309
27	90	2.305	3.498	4.609 ± 0.309	6.996 ± 0.309
28	90	2.243	3.457	4.486 ± 0.309	6.914 ± 0.309
29	90	2.305	3.539	4.609 ± 0.309	7.078 ± 0.309
30	90	2.222	3.416	4.444 ± 0.309	6.831 ± 0.309

A.7. Preparation of polished micrograph sections

The preparation is as follows: a sample is manually cut and embedded. Subsequently, it is ground and polished with the following grain sized: P120, P240, P600 and P1200. Between each step it is cleaned via an ultrasonic bath to get rid of any residuals from the previously used grinding plate. Before polishing, the embedded sample is cleaned with 96 % denatured ethanol. Then the micrograph section is polished by the aid of a 9 μm diamond suspension and subsequently cleaned and etched by using Nital.

A.8. Height and width measurement of the polished micrograph sections

To determine the respective height h as well as the spread diameter 2A of the brazed joint, the microscope or more precisely the camera, which is mounted onto the microscope, has to be calibrated first. For this a stage micrometer with a total scale of 1 mm and a smallest subdivision of 10 μm is placed onto the microscope stage. The camera is set and these settings are saved and always used. For each magnification of the microscope a picture is taken of the stage micrometer. Subsequently, the pixels of the image are related to the displayed distances by averaging over at least 4 subdivisions. Due to this relation the spread diameter as well as the height of the brazed joint can be determined.

A.9. The iron - iron carbide (Fe-Fe_3C) phase diagram

In this section, only the relevant parts of the iron - iron carbide phase diagram are explained for the analysis of the micrograph sections.
A portion of the iron - iron carbide (Fe- Fe_3C) phase diagram is presented in Figure A.12. As it can be seen in Figure A.12, steel ranges up to a carbon content of 2 %. The range of steel is subdivided into hypoeutecoid and hypereutectoid alloys (Callister, 2001).

Figure A.12.: The iron - iron carbide (Fe - Fe3C) phase diagram (Callister, 2001); the red circle indicates the eutectoid and the red highlighted line corresponds to the solidus line

The hypoeuctectoid alloy ranges from 0.022 wt% to 0.76 wt% carbon content (Figure A.12), whereas the hypereutectoid alloy is within the range of 0.76 wt% - 2.14 wt% carbon content. The steel 1.033, which is used as base material, has a carbon content of 0.12 %. Therefore, this steel belongs to the group of hypoeutectoid alloys (see reddish box in Figure A.12). The phase transformations of this type of steel are explained in the following (Callister, 2001).

Hypoeutectoid alloys

The phase transformations, due to a slow cooling of a hypoeutectoid alloy, are explained along the vertical line yy' in Figure A.13. In point **c**, approximately 875 °C, the microstructure will entirely consist of austenite (γ). If the alloy is cooled to point **d**,

approximately 775°C, two phases (α) - ferrite and austenite (γ) will coexist within the microstructure. There, most of the small (α) - particles will form along the original (γ) grain boundaries (Callister, 2001).

Figure A.13.: Microstructure of hypoeutectoid steel (Callister, 2001)

If an alloy is cooled along the line **MN** (Figure A.13), through the coexisting (α) - ferrite and austenite (γ) phases, it becomes slightly richer in carbon. But if an alloy is cooled along the line **MO**, the change is more dramatic, because the carbon content rises considerably.

Cooling from point **d** to **e**, just above the eutectoid temperature (T_e), will produce an increased fraction of (α) - ferrite, as it can be seen in the schematic microstructure in Figure A.13 (Callister, 2001).

If the temperature is lowered just below the eutectoid temperature, to point **f**, all the austenite (γ), which was present in point **e** will transform to pearlite ((α) - ferrite + cementite (Fe_3C)). The (α) - ferrite, which existed in point **e**, will virtually not change while

cooling to point **f**. It will normally be present as a continuous matrix phase that surrounds the isolated pearlite colonies. The microstructure of this point **f** is also shown in Figure A.13 (Callister, 2001).

Therefore, the (α) - ferrite phase will be present in both the pearlite and also as the phase that formed while cooling through point **e**. The ferrite that is present in the pearlite is called eutectoid ferrite, whereas the (α) - ferrite that formed above the eutectoid temperature (T_e) is called proeutectoid ferrite (Figure A.13). In Figure A.14 an enlarged view of the microstructure in point **f** can be seen (Callister, 2001).

Figure A.14.: Microstructure of a hypoeutectoid alloy below the eutectoid temperature (T_e) (Callister, 2001)

In Figure A.15 a polished micrograph section of a hypoeutectoid alloy is shown. For pearlite, the spacing between the (α) - ferrite and cementite layers varies from grain to grain. Some of the pearlite appears dark due to the many close - spaced layers that are unresolved at the magnification of this polished micrograph section (Callister, 2001).

Figure A.15.: Polished micrograph section of a hypoeutectoid alloy (University of Tennessee, 2008); Magnification: 635x

A.10. Vickers hardness measurement

For carrying out such a measurement, the polished micrograph sections are going to be used.

These polished micrograph sections (No.1, Figure A.16) will be placed in the clamping device just below the objective (No.2, Figure A.16). Subsequently, the focus will be set onto the surface of the probe. Then, the indenter, which has a pyramid shape, (No.3, Figure A.16) is applied onto the surface with 1 kgf (corresponds to 9.807 N) for 15 sec.

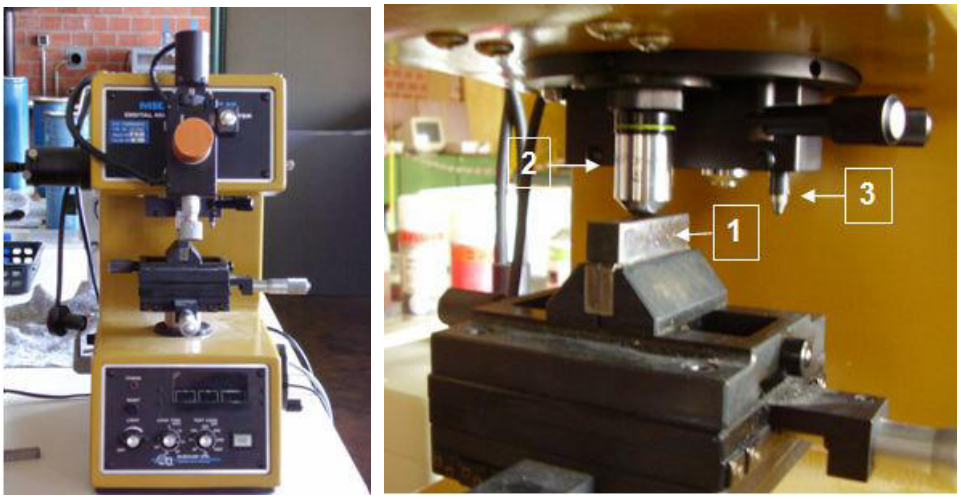

(a) Vickers hardness testing machine **(b)** Enlarged view of the Vickers hardness testing machine;1) Probe; 2) Objective; 3) Indenter

Figure A.16.: a) Vickers hardness testing machine; b) Enlarged view of the Vickers hardness testing machine;1) Probe; 2) Objective; 3) Indenter

B. Appendix for the chapter "Experimental procedures and initial tests"

B.1. Laser brazing setup

B.1.1. Clamping device

The design and realisation of the clamping device can be seen in Figure B.1. The respective technical drawings can found in Appendix E.1.1.

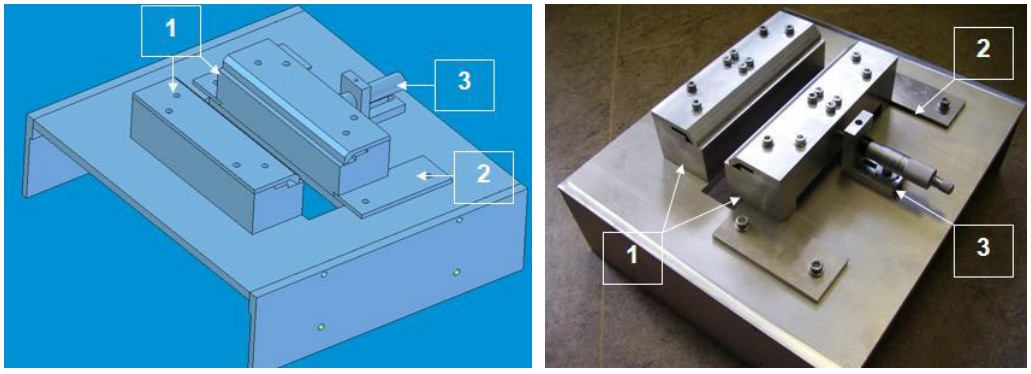

(a) Design of the clamping device **(b)** Realisation of the clamping device

Figure B.1.: Design (a) and realisation (b) of the clamping device; 1) Clamping brackets; 2) Dovetail; 3) Micrometer gauge

To enable clamping for different sizes of metal plates, the clamping brackets (No.1; Figure B.1) have a length of 180 mm. Furthermore, one clamping bracket is mounted

on a dovetail (No.2; Figure B.1), so that the width of the plates can also be varied by moving this clamping bracket. Even clamping over the full plate length is obtained by the design and mounting of the upper part of the clamping brackets. To realise an easy adjustment of the gap width between the base materials, which are going to be joined, a micrometer gauge is placed in front of the movable clamping bracket (No. 3; Figure B.1).

B.1.2. Wire feeder

The design and realisation of the wire feeder are shown in Figure B.2. The respective technical drawings can found in Appendix E.1.2.

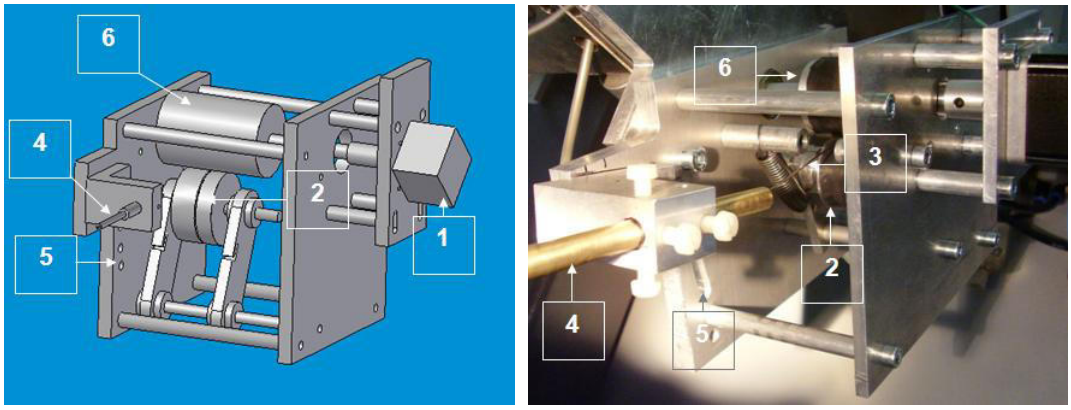

(a) Design of the wire feeder **(b)** Realisation of the wire feeder

Figure B.2.: Design (a) and realisation (b) of the wire feeder; 1) Stepper motor; 2) Tensioner with guidance groove; 3) Wire; 4) Wire guidance; 5) Adjustment of the incidence angle of the wire; 6) Drive roll

For defined guidance of the wire (No.3; Figure B.2b) through the wire feeder, the tensioner is provided with a guidance groove (No.2; Figure B.2a). Above the tensioner is the drive roll, which is pivoted via a grooved ball bearing (No.6; Figure B.2a). The drive roll is mounted onto the axis of the stepper motor. To improve the grip for pulling the wire a rubber sleeve was attached to this roll.

For adjusting the incidence angle of the wire, a curved slot hole is used (No.5; Figure B.2a). The holder of the wire guidance and therefore, the incidence angle of the wire can be directed by moving the holder within this slot hole. The wire feed is driven

by a stepper motor (No. 1; Figure B.2a). This stepper motor SM 42051 is controlled by a LabView© designed software program via the stepper motor card SMC 800. The motor and the card are both from the company Emis GmbH. The designed LabView© program is described in section 4.2.3.
The wire guidance (No.4, Figure B.2a) is important as early test showed (see Figure 4.1). Therefore, the wire is guided from the wire reel to the tensioner by using three tubes, where one is smaller than the other. These tubes are put into each other, so that the inner diameter of the whole wire guidance is about 0.1 mm larger than the used wire to prevent oscillation of the wire (see Figure B.3a). From the tensioner to the actual brazing process, the brazing wire is also guided via a tube. This final wire guidance has a small clearance (see Figure B.3).

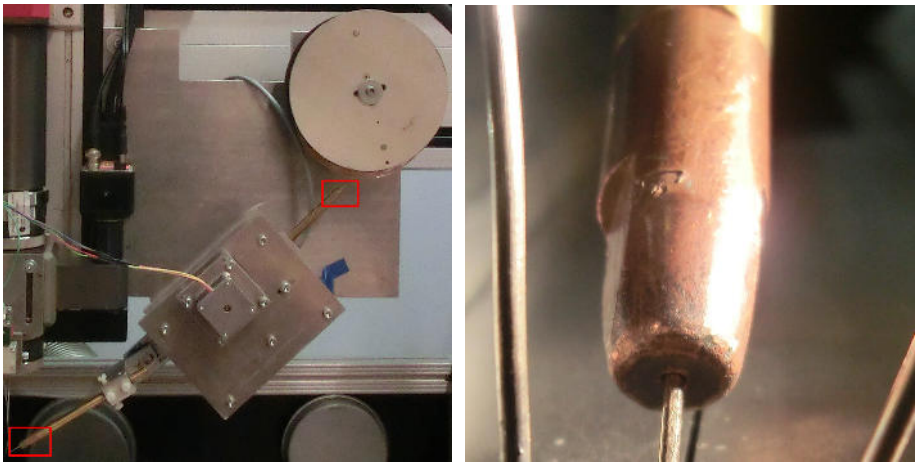

(a) Implemented wire guidance

(b) Enlarged front view of the lower red rectangle in B.3a

Figure B.3.: a) Implemented wire guidance; b) Enlarged view of the lower red rectangle in a) showing the tube

B.2. Measurement equipment

B.2.1. Testing of the optimised temperature measurement setup

The optimised temperature measurement setup is implemented into the Nd:YAG laser work station, as described in section 4.2.1.2.

The testing of the optimised temperature measurement setup was carried out for laser welding, since at this time the wire feeder, described in section 4.1 was manufactured, which is an optimisation of the first one designed with regard to wire feed control.
However, for testing the temperature measurement setup, the process taking place plays a minor role.
Before carrying out the tests, two metal samples consisting of mild cold - rolled constructional steel 1.0330 are prepared as follows:

- Cleaning of the samples with 96 % denatured ethanol
- Ultrasonic bath in distilled water to get rid of possible dirt or grease
- Cleaning of the samples with 96 % denatured ethanol

Subsequently, these samples are put into the clamping device and the process parameters of the laser work station are set as follows:

- Peak Power (P) = 2500 W
- Repetition rate (f) = 50 Hz
- Pulse length (t_p) = 1.3 ms
- Focal position (F) = -15 mm below the surface of the sample
- Feed speed (v) = 250 mm/min

Since the thermocouples are manually placed, the displacement between measurement tip of the thermocouples and the joint is determined for each measurement. A third thermocouple is used for triggering, i.e. to automatically start the measurement. However, the measurement is still manually stopped. Four measurements are carried out with this set of parameters to compare the application of this setup.
Within all displayed measurement signals in the following subsections the red graph corresponds to the signal of the thermocouple used as a trigger, the green graph corresponds to the one behind the laser head and the black graph corresponds to the one in front of the laser head.

B.2.1.1. First measurement

For this measurement the thermocouple behind the laser head (green graph) is displaced by approx. 3 mm from the joint, whereas the one in front of the laser head (black graph) is positioned about 2 mm away from the joint. The measurement results are shown in Figure B.4.

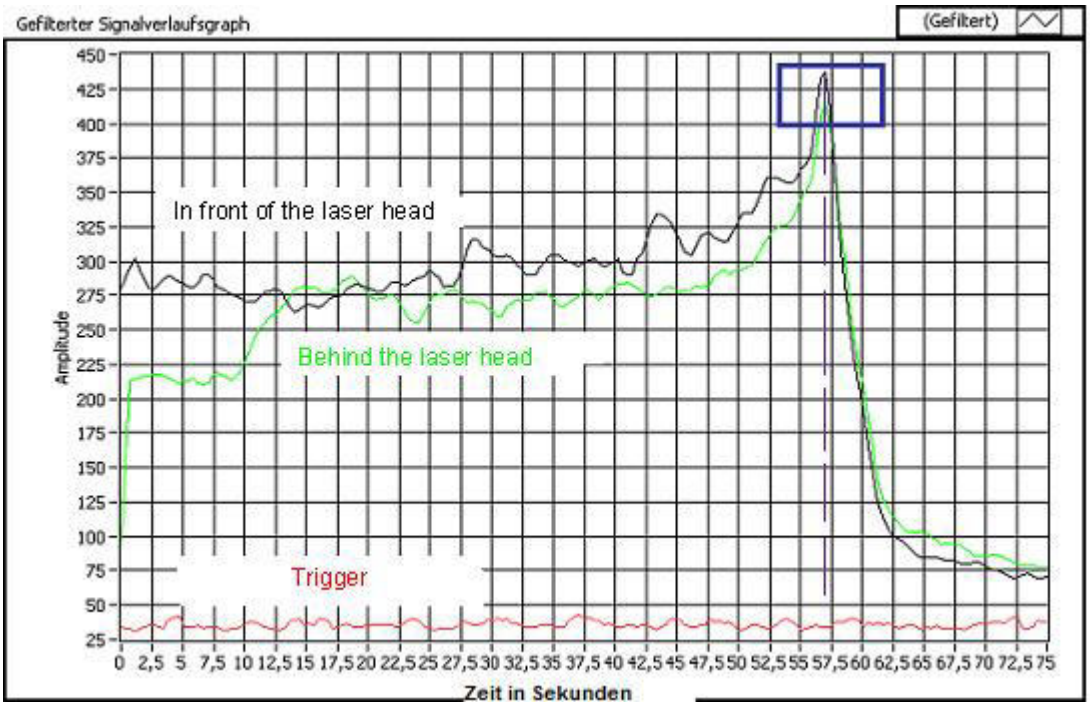

Figure B.4.: First measurement result showing the temperature profile against time; the black graph corresponds to the measurement signal of the thermocouple in front of the laser head, the green one corresponds to the signal of the one behind the laser head and the red graph is the signal of the trigger

There, the unequal positioning of the thermocouples can be seen since the thermocouple in front of the laser head measures higher temperatures compared to the other one. The contact between the thermocouple and base material is given during the whole measurement. The relatively small variations in temperature result from lodging of the measurement tip of the thermocouples onto tiny unevenness of the surface of the base material, during the time the sample is moving beneath the laser head with the mounted thermocouples. While lodged, the thermocouples remain in one position for a bit longer which results in temperature increase.

Furthermore, a continuous increase in temperature can be seen in both graphs neglecting the small temperature variations. The reason for this is the heat conduction of the base material. At the end of the samples the temperature increases drastically (blue rectangle) due to heat accumulation since laser radiation impacted on base material over its whole length.

B.2.1.2. Second measurement

The thermocouple behind the laser head is displaced by approx. 3 mm and the one in front of the laser head by approximately the same value. In Figure B.5 the measurement results are shown. Both temperature profiles do not show an even temperature distribution. However, both maintain contact to base material during the whole measurement.
The measurement result of the thermocouple in front of the laser head increases very fast in temperature until 2.5 s. Then the slope of temperature rise decreases till 5 s. At this point in time a drastic rise in temperature is measured (purple rectangle), due to lodging of the measurement tip of the thermocouples onto tiny unevenness of the surface of base material, while the sample is moving beneath the laser head with the mounted thermocouples. Therefore, the thermocouples remain in one position for a bit longer which results in temperature increase. After this temperature peak, the slope of temperature rise is back to that of the beginning of about 4 s. The small temperature variations until the end of measurement result from lodging or from little displacement of the measurement tip away or in direction of the heat input. At 40 s a temperature increase occurs due to heat accumulation.
The measurement result of the thermocouple behind the laser head has also a very fast increase in temperature until about 2.5 s. Then, the temperature drops suddenly due to moving away of the measurement tip from the heat input. The same situation occurred at the second temperature rise at approximately 8 s. The drastic increase (blue rectangle) is caused by lodging of the measurement tip onto some unevenness of the surface of base material. This measurement result of the thermocouple behind the laser head does not show the expected temperature increase at the end of the samples due to heat accumulation since the measurement tip was lodged first and then displaced away from the heat input.

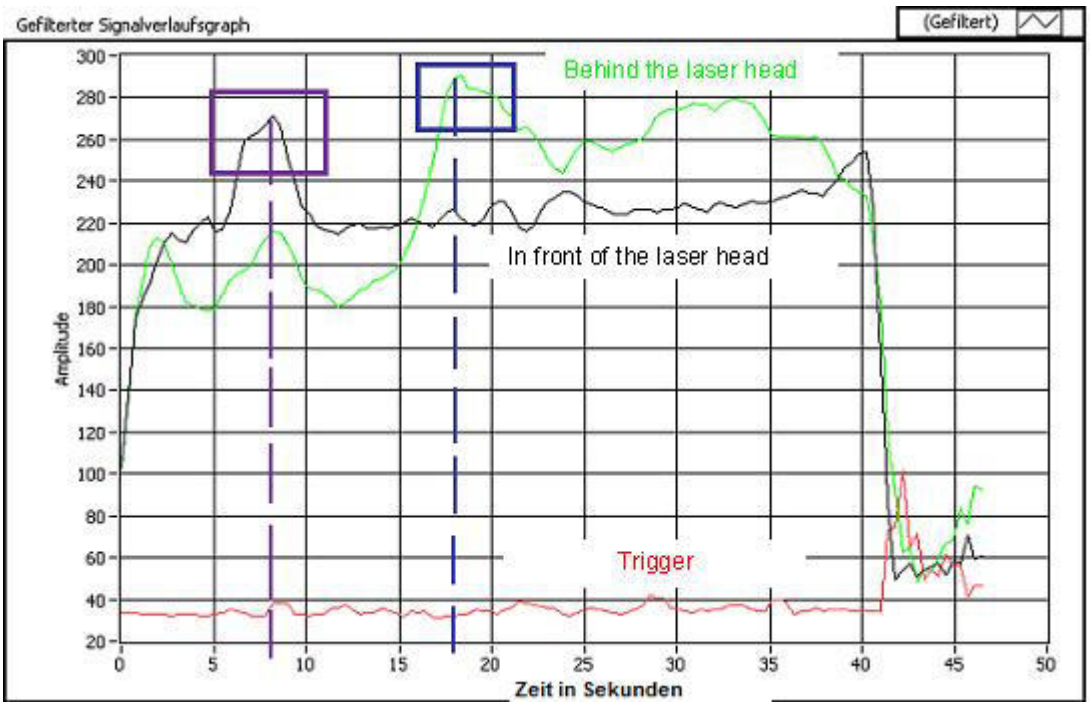

Figure B.5.: Second measurement result showing the temperature profile against time; the black graph corresponds to the measurement signal of the thermocouple in front of the laser head, the green one corresponds to the signal of the one behind the laser head and the red graph is the signal of the trigger

B.2.1.3. Third measurement

Within this measurement the thermocouple in front of the laser head was positioned about 0.5 mm away from the joint and the one behind the laser head about 1.5 mm away. The measurement results are shown in Figure B.6.

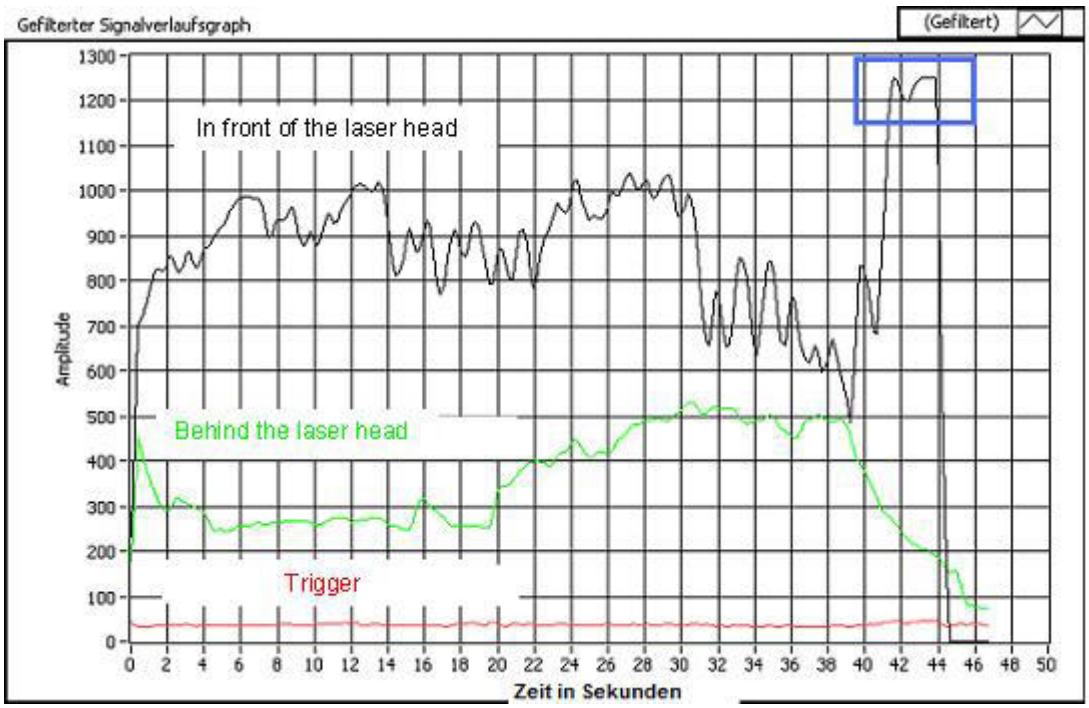

Figure B.6.: Third measurement result showing the temperature profile against time; the black graph corresponds to the measurement signal of the thermocouple in front of the laser head, the green one corresponds to the signal of the one behind the laser head and the red graph is the signal of the trigger

The measurement signal of the thermocouple in front of the laser head (black graph) shows persistent changes in temperature. These changes result from wedging of the measurement tip with the surface of the base material while moving over it. After wedging the measurement tip jumps to the actual position of the brazing process. During this jumping the temperature decreases (black graph). Furthermore, this causes a variation in displacement of the measurement tip regarding to the joint, which can be seen, since the temperature decreases in the range of 30 s - 40 s.

However, the wedging at 40 s leads to a displacement closer to the joint, which results in a drastic temperature rise in conjunction with the heat accumulation at the end of the base material. As the temperature exceeds 1200 °C (blue rectangle) the thermocouple is destroyed since it can only cope with a maximum temperature of 1200 °C. It was exchanged by a thermocouple of the same type and manufacturer.

The measurement signal of the thermocouple behind the laser head is smoother compared to the one in front of the laser head. Due to having a larger displacement from the joint the temperature is significantly less than the one of the other thermocouple. Within the time of 2 s - 20 s the temperature decreases steadily due to the moving away of the measurement tip from the joint. However, at 20 s the temperature starts

to increase until 39 s since the measurement tip moves towards the joint. After that the temperature continuously decreases and the expected heat accumulation is not seen because of departing of the measurement tip from the joint.

B.2.1.4. Fourth measurement

For this measurement the thermocouple behind the laser head was positioned ca. 3.5 mm away from the joint and the other one about 4 mm away. The measurement results are shown in Figure B.7.

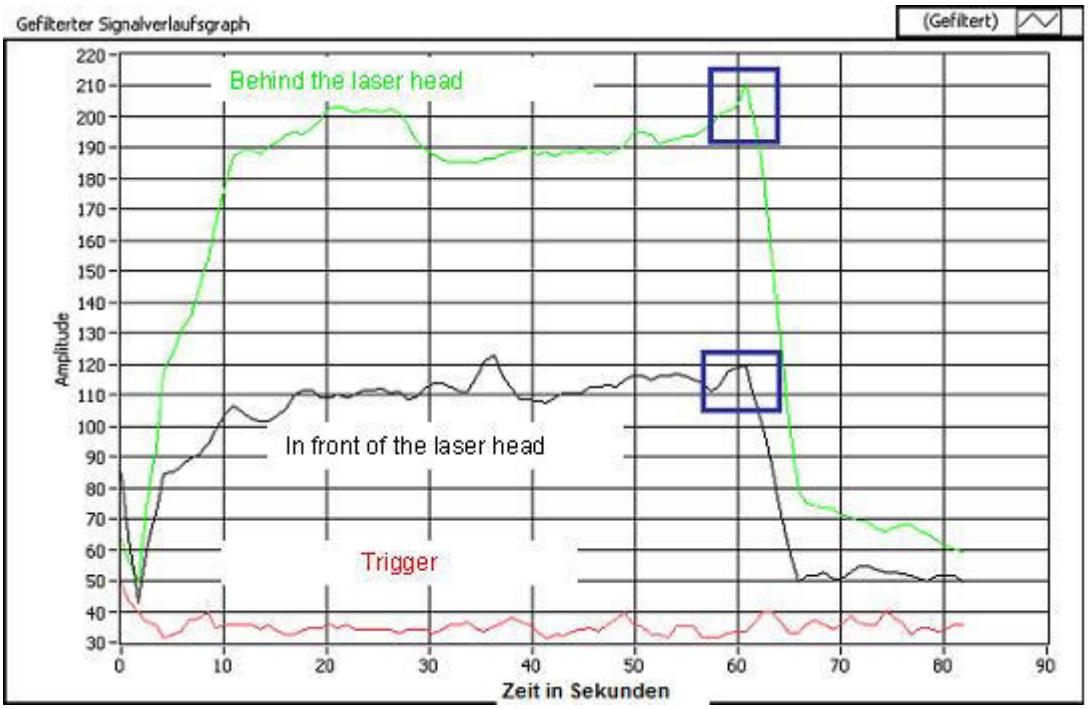

Figure B.7.: Fourth measurement result showing the temperature profile against time; the black graph corresponds to the measurement signal of the thermocouple in front of the laser head, the green one corresponds to the signal of the one behind the laser head and the red graph is the signal of the trigger

The unequal positioning of the thermocouples can be directly seen due to the different temperature ranges of the measurement signals. Both graphs show a relatively smooth signal without any huge variations in temperature compared to the third measurement. Furthermore, they both clearly indicate the heat accumulation at the end of the base materials due to an increase in temperature (blue rectangles).

B.2.1.5. Discussion

The first measurement setup has to be optimised due to not maintaining contact with the surface of the base materials throughout the measurement.
For this a new positioner and holder for the thermocouples was designed, manufactured and subsequently implemented into the Nd:YAG laser work station.
Several limitations due to lack of space have to be regarded for designing since it was determined during testing of the first setup that incidence angles of the thermocouples between 70 ° - 90 ° obtain a contact throughout the whole measurement. To realise those incidence angles the thermocouples have to be directly mounted to the laser head. The new setup enables measurements up to 10 mm away from each side of the joint. Furthermore, a height adjustment was implemented, so that the thermocouples can easily be adjusted to changing focal positions or to adapt the height depending on the incidence angle.
First tests with the new setup showed that the contact throughout the whole measurement is maintained. However, variations in temperature have been recognised during the measurement. These variations can be caused by departing of the measurement tip of the thermocouple from its primary position regarding the displacement from the joint due to the ductility of the thermocouple.
Furthermore, it can result from wedging of the measurement tip with the surface of the base material, which leads to jumps of the measurement tip to the actual position of the brazing process. The danger of wedging increases either with an increased pressure to the measurement tip caused by a not sufficient height adjustment or with increasing the contact area of the measurement tip.
For this a compromise between maintaining the contact throughout the measurement and the incidence angle has to be found, which is approximately at 70 ° to minimise the danger of wedging.
The repeated measurements showed that they are not reproducible due to manual positioning, departing from the primary position while moving and wedging.
However, a better estimation of the temperature range can be gained as without this setup and with more experience in positioning of the thermocouples the estimation can be advanced.

B.2.2. Verification of the optimised temperature measurement setup

B.2.2.1. Approach for verification

For verification of the temperature measurement setup the SC640 IR camera from FLIR Systems was used. The verification was carried out using the diode laser work station. For this setup two base material samples consisting of mild cold-rolled constructional steel 1.0330 were used. These were cleaned via an ultrasonic bath and ethanol. These samples were put into the clamping device and the process parameters for the laser brazing process were set according to table B.1. Since the thermocouples have to be manually placed, the displacement between center of the laser spot and position of the thermocouple is measured. In this case the thermocouple in front of the laser and the one behind are approximately displaced by 3 mm and 2 mm respectively (Figure B.8a).

Table B.1.: Parameters of the brazing process for thermocouple verification at the diode laser work station

Parameter	
Power (W)	150
Delay time wire feed WZD (ms)	4700
Delay time laser WZL (ms)	3500
Wire feed (steps/s)	4
Feed speed of the base material (mm/min)[13]	60.8
Focal position F[14] (mm)	-5
Gap (mm)	0.4

Before the actual verification via the IR camera can take place, measurements have to be carried out to do the IR camera settings correctly in order to obtain valid measurement results. For this reason the ambient temperature as well as the relative humidity have to be determined, which is done by using the hand-held measurement device 605-H1 from Testo AG. The datasheet of this device can be found in the Appendix D.6.

Furthermore the emissivity of the used base materials is a required parameter. However, the emissivity (ε) is not known and cannot be sufficiently determined for the given

[13]The feed speed for the diode laser work station has to be entered in (μm/s), however it was converted to (mm/min), which is used for the Nd:YAG laser work station

[14]the "-" indicates that the focal position is below the surface of the sample

material, so that the used value for the emissivity is taken from the provided emissivity tables from FLIR Systems. These emissivity tables provided by FLIR Systems only contain general material names, such as "steel" and information about either its surface condition or type of manufacture. No exact material types are stated. For this reason, the value $\varepsilon = 0.56$ at a temperature of 50 °C is chosen which corresponds closest to the used material "rolled steel sheet" (Flir Systems Inc., 2006, S. 260).
To achieve a sufficient resolution for the infrared images a 76 mm objective is used for the IR camera. Subsequently, the IR camera is positioned as shown in Figure B.8b and the distance between camera and laser spot position (object distance) is measured. This position, the set temperature range and the respective incidence angle of the camera to the laser brazing process were found best due to prior testing.

(a) Positioning of the thermocouples

(b) Positioning of the used IR camera SC640 from FLIR Systems for verification of the temperature measurement setup

Figure B.8.: a) Positioning of the thermocouples; b)Position of the used IR camera SC640 for the measurement

Another parameter, required for the IR camera, is the apparent reflected temperature, which is dependent on ambient heat and/or light sources and is determined by following the instructions stated in the manual of the camera (Flir Systems Inc., 2006). All these required parameters for the IR camera settings and their corresponding values are stated in Table B.2. After all parameters are set, the laser brazing process including the temperature measurement is started. During the brazing process IR images are recorded in best possible constant time intervals. The intervals sometimes differ due to

Table B.2.: Parameters used as IR camera SC640 setting for temperature measurement setup verification

Parameter	
Used objective (mm)	76
Emissivity (ε)	0.56
Distance to object d_{obj} (m)	1.1
Ambient temperature (°C)	17.2
Relative humidity (%)	40.0
Apparent reflected temperature (°C)	28.4
Used temperature range (°C)	0-500

storage times as well as obstacles within the view field of the camera, such as screw heads on the clamping device (see Figure B.1b). Both measurement results are shown and discussed within the following subsection.

B.2.2.2. Results and discussion of temperature measurement setup verification

Over the whole length of the brazed joint a total of 9 IR images are recorded and subsequently analysed by using the spot meter tool of the provided software analysis program from FLIR Systems.
To identify the thermocouple, especially the region of contact between thermocouple and base material, in the IR image correctly for spot meter analysis the temperature range which is supposed to be displayed in the image is adjusted accordingly via this program.
For example, Figure B.9 shows the difference in display of the first recorded IR image depending on the temperature range.

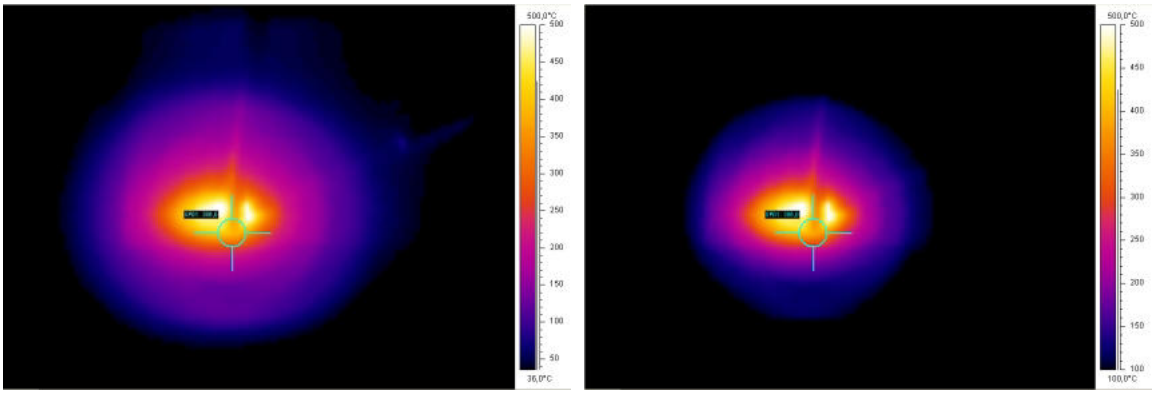

(a) Temperature range: 36°C - 500°C **(b)** Temperature range: 100°C - 500°C

Figure B.9.: a) and b): First IR-image of the laser brazing process with the spot meter result of 386.0°C for the thermocouple in front of the laser with two different temperature ranges: a) 36°C - 500°C; b) 100°C - 500°C

Figure B.10 presents an enlarged view of the first recorded IR image including the analysis result of the spot meter. As it can be seen in Figure B.10 only the thermocouple in front of the laser can be clearly recognised due to diffuse reflection of the incident laser beam as well as the exact placement of the thermocouple in front of the laser in line with the one behind the laser. As already mentioned in subsection B.2.2.1 several incidence angles of the camera were tested prior to the actual measurement to significantly minimise the influence of the diffuse reflection. It was found that the flatter the incidence angle, the less diffuse the reflection. For this reason an incidence angle of approximately 35° was chosen (see Figure B.8b).

All recorded IR images were analysed as described above. The correspondent spot meter analysis results including the measurement uncertainty of 2% from the camera itself for each IR image can be found in Table B.3.

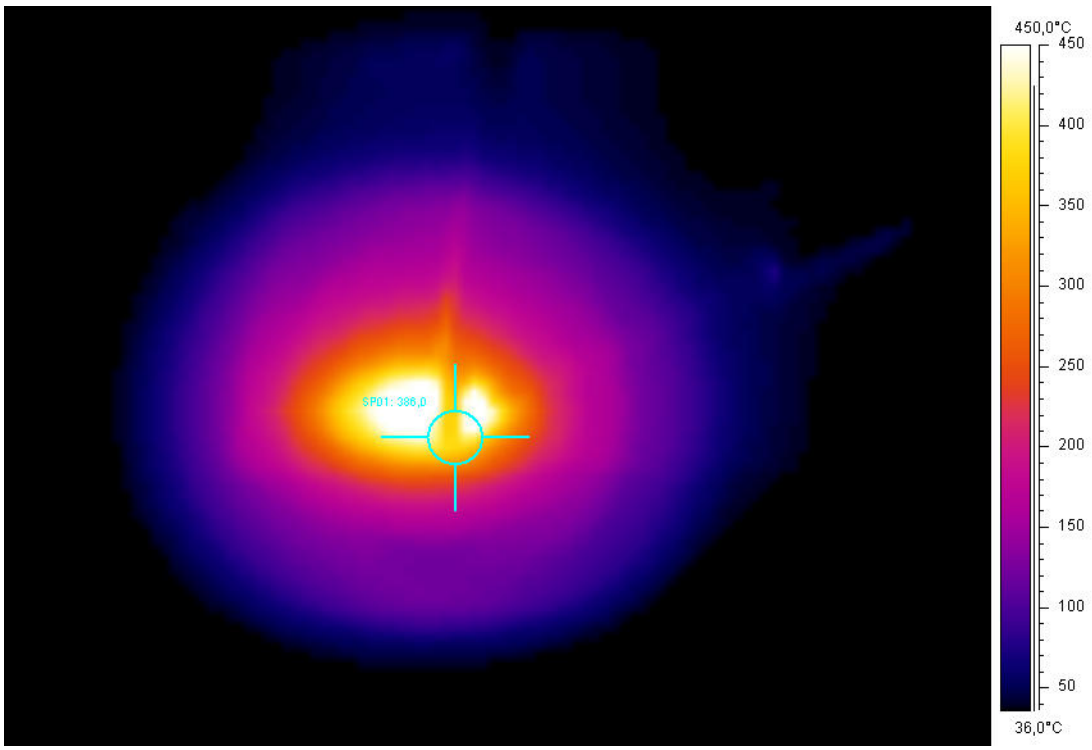

Figure B.10.: First IR-image of the laser brazing process with the spot meter result of 386.0 °C for the thermocouple in front of the laser

Table B.3.: Results of the IR spot meter analysis for the thermocouple in front of the laser

No.	Spotmeter result of thermocouple (°C)
1	386.0 ± 7.7
2	326.3 ± 6.5
3	362.3 ± 7.2
4	364.1 ± 7.3
5	344.4 ± 6.9
6	352.6 ± 7.1
7	308.7 ± 6.2
8	346.5 ± 6.9
9	389.4 ± 7.8

Figure B.11 shows the temperature measurement signals of the thermocouples for the brazed joint, where the black signal corresponds to the thermocouple behind the laser and the red signal to the one in front of the laser. The green signal is from the former third thermocouple which is only used for testing purpose if required. In this case it is a dummy signal, because it was not used.

Furthermore the displacement of the thermocouples with regard to the brazing process can be seen in Figure B.11, since the thermocouple behind the laser has a higher signal than the one in front of the laser. The temperature measurement signals are not

smooth due to not always maintaining contact while e.g. scratching over the surface of the base materials. This circumstance has already been recognised and reasoned in section B.2.1.

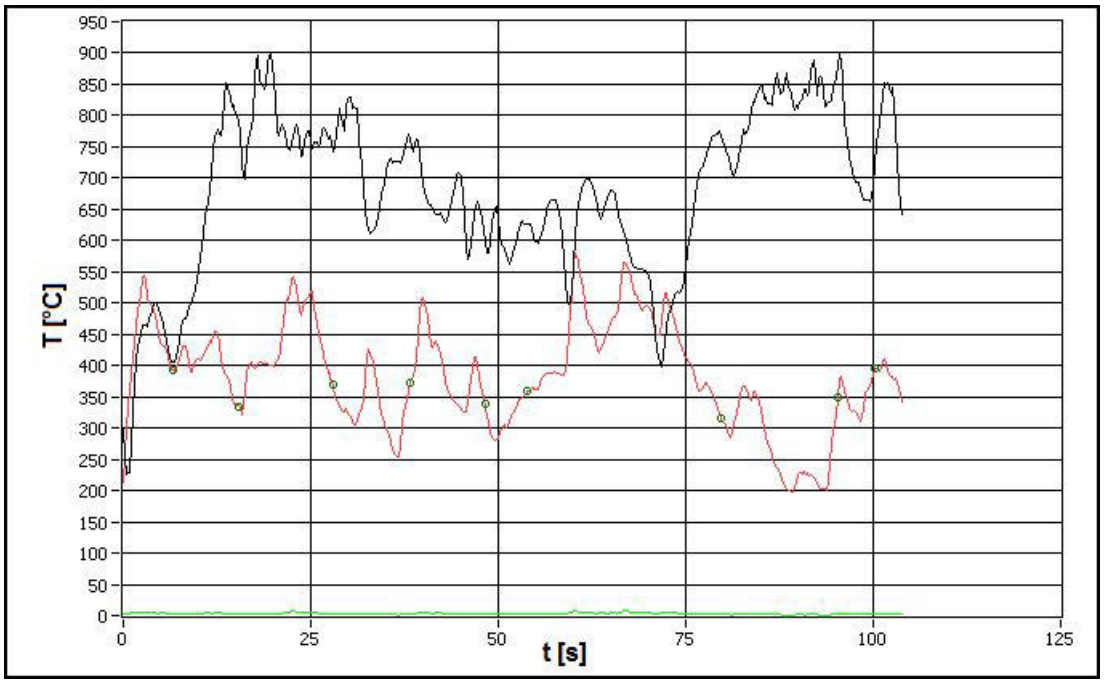

Figure B.11.: Measurement result of the thermocouples (the red graph corresponds to the measurement signal of the thermocouple in front of the laser and the black graph to the one behind the laser) ; The green circles indicate when and with which result the IR pictures were taken

In Figure B.11 green circles along the red measurement signal indicate when the IR images were recorded as well as the result of the respective spot meter analysis. As it can be seen both measurement results approximate each other considering the measurement uncertainty of the camera as well as the uncertainty of the thermocouples which is stated as $\pm 2.5^{\circ}C$ within the designated temperature range. Due to this result it is verified that the optimised temperature measurement setup operates correctly.

B.2.3. Verification of the wire feed control

To verify the encoder, the transmission ratio between the encoder and the stepper motor has to be determined first. This is done as follows:

$$transmission\,ratio = \frac{counts\,of\,encoder\,per\,revolution}{steps\,of\,the\,motor\,per\,revolution} = \frac{512}{200} = 2.56 \tag{B.1}$$

Subsequently the circumference of the tensioner has to be determined. Since the tensioner has a diameter of 30 mm the circumference corresponds to 94.25 mm. The stepper motor does 200 steps per revolution, so that one step of the stepper motor theoretically corresponds to 0.47 mm fed wire. The wire feed control was tested for different velocities of the wire feed, but only the results of the most commonly used velocity (7 steps per second) for the parameter studies are presented. The measurement results of the other velocities tested can be found in Appendix B.2.4. At a speed of 7 steps per second for the duration of one minute 197.4 mm of wire are fed in theory. Testing was done by feeding the wire for one minute and subsequently measuring the length of the fed wire as well as saving the counts of the encoder. This test was repeated five times and the results are shown in table B.4. The average encoder count

Table B.4.: Results from testing the encoder at a feed speed of 7 steps per second for a duration of one minute

	Counts of encoder	fed wire (mm)
	2215	190
	2172	190
	2105	189
	2063	187
	2094	190
Average	2129.8 ± 62.1	189.2 ± 1.3

corresponds to 2129.8 ± 62. Within one minute the stepper motor carries out 420 steps at a speed of 7 steps per second. To receive the result of how many counts does the encoder do per step of the motor, the average encoder count has to be divided by 420. Furthermore the transmission ratio of 2.56 has to be considered which results in 1.98 counts of the encoder per step of the motor. This means that the encoder almost carries out two counts every time the motor does a step. A reason for this result could be that the motor swings a little between the steps so that the encoder receives two signals.

As already explained in the previous section, the second channel cannot be implemented due to cost reasons to overcome this problem. However, within a good estimation it can be said that the result of the encoder has to be halved to obtain the total steps carried out by the stepper motor with regard to the transmission ratio.
To also have a manual control of the fed wire, marks were set on the wire in defined distances as a further control possibility.

B.2.4. Verification of wire feed control for different velocities

Table B.5.: Results from testing the encoder at a feed speed of 2 steps per second for a duration of one minute

	Counts of encoder	fed wire (mm)	total steps of stepper motor
	577	55	120
	562	55	120
	578	55	120
	545	53	120
	578	54	120
Average	568 ± 14.54	54.4 ± 0.89	120

Table B.6.: Results from testing the encoder at a feed speed of 3 steps per second for a duration of one minute

	Counts of encoder	fed wire (mm)	total steps of stepper motor
	862	83	180
	864	83	180
	842	82	180
	873	82	180
	880	81	180
Average	864.2 ± 14.36	82.2 ± 0.84	180

Table B.7.: Results from testing the encoder at a feed speed of 4 steps per second for a duration of one minute

	Counts of encoder	fed wire (mm)	total steps of stepper motor
	1210	110	240
	1151	110	240
	1155	108	240
	1157	108	240
	1152	110	240
Average	1165 ± 25.27	109.2 ± 1.09	240

Table B.8.: Results from testing the encoder at a feed speed of 5 steps per second for a duration of one minute

	Counts of encoder	fed wire (mm)	total steps of stepper motor
	1421	135	300
	1516	140	300
	1551	140	300
	1514	139	300
	1529	138	300
Average	1506.2 $\pm$ 49.87	138.4 $\pm$ 2.07	300

Table B.9.: Results from testing the encoder at a feed speed of 6 steps per second for a duration of one minute

	Counts of encoder	fed wire (mm)	total steps of stepper motor
	1823	161	360
	1836	163	360
	1824	160	360
	1830	162	360
	1808	161	360
Average	1824.2 $\pm$ 10.45	161.4 $\pm$ 1.14	360

Table B.10.: Results from testing the encoder at a feed speed of 8 steps per second for a duration of one minute

	Counts of encoder	fed wire (mm)	total steps of stepper motor
	2461	215	480
	2683	220	480
	2468	218	480
	2484	216	480
	2613	218	480
Average	2541.8 $\pm$ 100.40	217.4 $\pm$ 1.95	480

Table B.11.: Results from testing the encoder at a feed speed of 9 steps per second for a duration of one minute

	Counts of encoder	fed wire (mm)	total steps of stepper motor
	2639	240	540
	2681	243	540
	2591	244	540
	2700	244	540
	2611	247	540
Average	2644.4 $\pm$ 45.90	243.6 $\pm$ 2.51	540

B.3. Surface roughness (R_z) of the base material

To determine the surface roughness (R_z) of the base material, the roughness was measured on 4 base materials at 10 locations as shown in Figure B.12. There, it can be seen that 5 measurements were carried out over the length of the base material (measurement locations (a) - (e)) and 5 across the base material (measurement locations (f) - (j)). The first measurement point is located 10 mm away from the edge of the base material. The distance between the other measurement locations corresponds

to 20 mm.

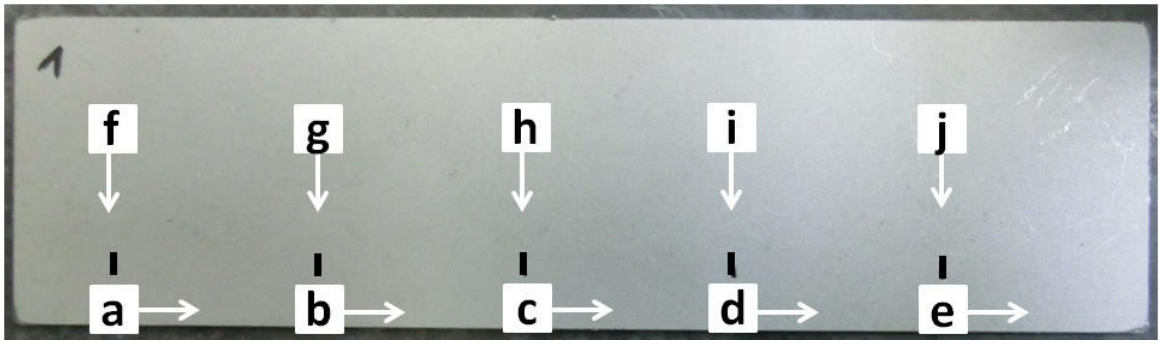

Figure B.12.: Surface roughness measurement approach of base material; a) - e) measurement over the length of the base material; f) - j) measurement across the base material

The surface roughness of the base material was measured with the stylus instrument Perthometer S5P from Perthen GmbH. This instrument has a measurement range of 50 μm and the radius of the measurement tip corresponds to 5 μm. The measurement distance is set to 4.8 mm, whereas the distance of 0.8 mm corresponds to the forward measurement distance, which is not included in the actual measurement.
From all measurements carried out the mean of the surface roughness (R_z) was calculated for each location. The results are presented in Table B.12.

Table B.12.: Mean values of R_z mean for respective location

Over the length	R_z mean (μm)	Across the base material	R_z mean (μm)
a	5.69	f	5.64
b	5.70	g	5.80
c	5.95	h	5.16
d	5.67	i	5.23
e	5.26	j	5.58
Mean:	5.65 ± 0.155		5.48 ± 0.23

B.4. Realised adaptation of the software program "LNS_QS_V2"

The user interface of the adapted program, called "SurfMeas", is shown in Figure B.13. It has two tabs named current measurement (aktuelle Messung) and system messages / Excel (Systemmeldungen / Excel). To the left of these tabs the measurement range for a measurement is determined by the entered lengths. The length in front of the sample (Länge vor), the sample length (Werkstücklänge) and the length behind the sample (Länge nach) can be set in the corresponding edit line (Figure B.13). Out of these entered values the needed measurement time (Gesamtzeit) for internal processing is calculated and displayed in ms. The tab current measurement displays the measurement signal. There, the red lines indicate the sample length.

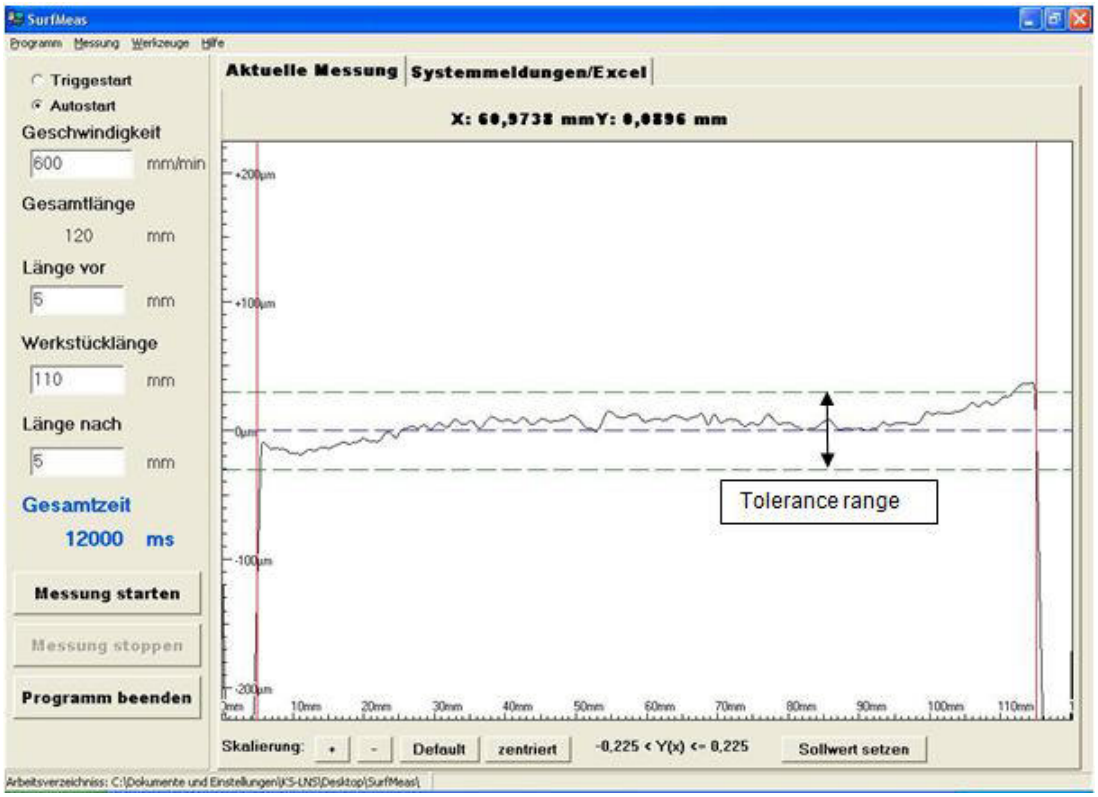

Figure B.13.: Screenshot of the new software program "SurfMeas" showing the tab current measurement (aktuelle Messung) where a measurement signal is displayed

The tab system messages / Excel (Systemmeldungen / Excel) is shown in Figure B.14.

There, the system messages during measurement are displayed. The displayed Excel table shows in column B the entered length. The time needed for the measurement of each entered length is calculated and automatically displayed in column C. This calculated time is needed for the determination of the measurement range, since the number of measurement values can be determined by the set measurement frequency of the sensor and the measurement time. The number of measurement values is needed for allocating them to the measurement length.

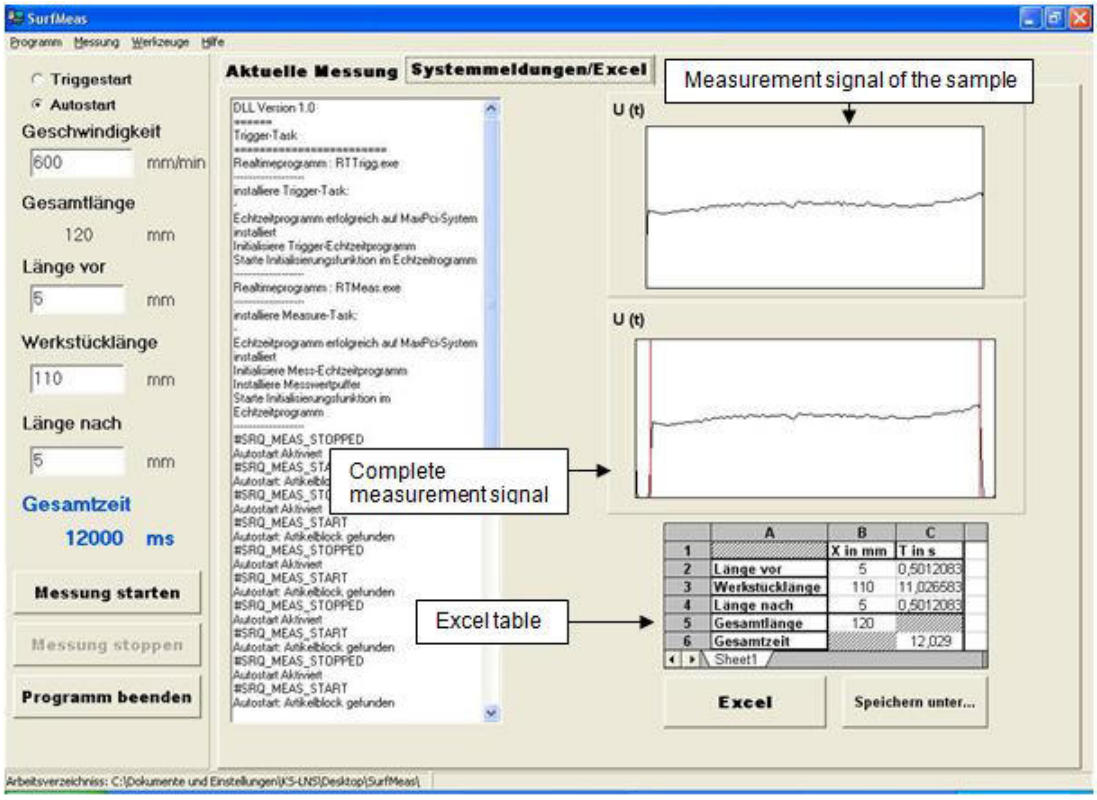

Figure B.14.: Screenshot of the software program "SurfMeas" showing the tab system messages / Excel, where the system messages, the complete measurement signal, the measurement signal of the sample and the Excel table are displayed

The selection between automatic or triggered start of measurement is also realised by selecting the correspondent radio button in the upper left corner (see Figure B.13). However, for the automatic start of measurement additional u - shaped trigger plates are needed that are implemented into setup (see Figure B.15) to have defined edges for starting and stopping the measurement.

Furthermore the red arrows in Figure B.15 indicate the length in front of the sample (Länge vor) and behind the sample (Länge nach) that has to be entered in the corresponding edit line (see Figure B.13).

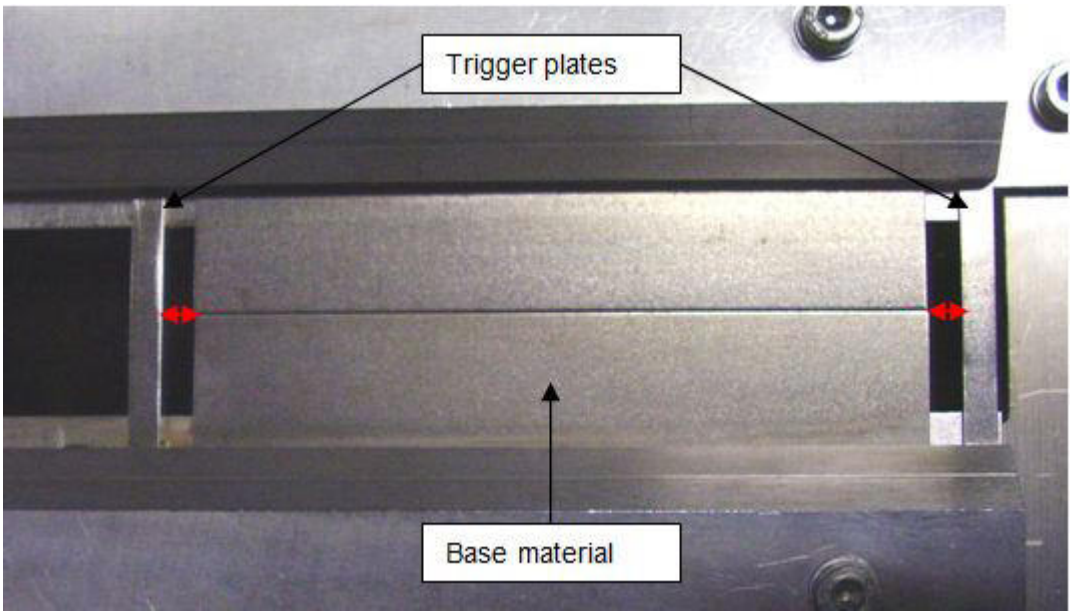

Figure B.15.: Positioning of the trigger plates in front of and behind the base materials

Furthermore, it was required to export the measurement data to Excel and to store its corresponding settings. This is fulfilled by clicking the button "Excel" in the lower right corner (Figure B.14). By clicking this button, the program exports the measurement data and its corresponding settings by generating three worksheets in an Excel file:

1. Table of measurement data
2. Diagram of measurement data
3. Settings for measurement

C. Appendix for the chapter "Parameter studies with the diode laser"

C.1. Vickers hardness measurement of the joints brazed with different powers

Table C.1.: Measurement results of the respective diagonals from the indentation and the correspondent Vickers hardness for P = 150 W

Position in mm	d_1 in μm	d_2 in μm	Hardness in HV1
0.0	118.3	126.0	124.3
1.0	122.7	126.3	119.6
2.0	123.1	121.1	124.4
3.0	117.3	120.4	131.3
4.0	112.6	118.0	139.5
5.0	108.7	113.1	150.8
5.5	107.1	111.2	155.6
6.0	103.4	108.3	165.5
6.5	107.8	110.1	156.2
7.0	104.9	108.8	162.4
7.5	102.1	103.7	175.1
8.0	107.8	110.3	155.9
8.5	106.1	107.2	163.0
9.0	102.4	106.3	170.3
9.5	106.6	110.7	157.1
10.0	104.2	105.2	169.2
11.0	107.2	113.3	152.6
12.0	111.8	113.6	146.0
13.0	114.8	119.2	135.5
14.0	115.4	120.9	132.8
15.0	115.9	119.2	134.2
16.0	116.9	118.7	133.6

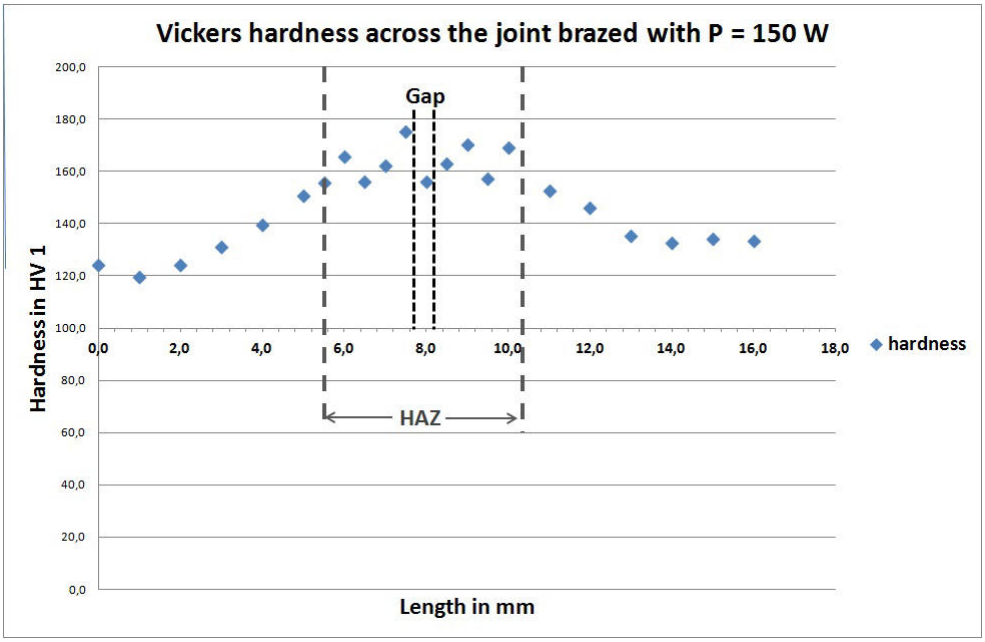

Figure C.1.: Vickers hardness measurement across the polished micrograph section of the joint brazed with P = 150 W

Table C.2.: Measurement results of the respective diagonals from the indentation and the correspondent Vickers hardness for P = 146 W

Position in mm	d_1 in μm	d_2 in μm	Hardness in HV
0.0	114.5	122.9	131.6
1.0	115.9	118.1	135.5
2.0	113.4	118.9	137.4
3.0	109.9	117.7	143.2
4.0	110.5	111.1	151.0
5.0	105.9	108.4	161.5
5.5	104.6	107.1	165.5
6.0	108.4	110.9	154.2
6.5	107.4	109.9	157.1
7.0	105.7	104.3	168.2
7.5	98.7	100.8	186.4
8.0	116.0	118.0	135.5
8.5	103.8	103.6	172.4
9.0	106.0	110.9	157.7
9.5	110.3	112.7	149.2
10.0	104.1	110.0	161.8
11.0	109.4	111.4	152.1
12.0	118.1	116.5	134.8
13.0	117.9	120.8	130.2
14.0	122.8	121.7	124.1
15.0	121.1	127.7	119.8
16.0	122.5	124.7	121.4

Table C.3.: Measurement results of the respective diagonals from the indentation and the correspondent Vickers hardness for P = 148 W

Position in mm	d_1 in μm	d_2 in μm	Hardness in HV1
0.0	122.0	124.5	122.1
1.0	124.9	126.7	117.2
2.0	121.2	120.8	126.7
3.0	117.2	121.5	130.2
4.0	116.5	117.8	135.1
5.0	111.4	112.6	147.8
5.5	112.7	112.4	146.4
6.0	110.9	112.0	149.3
6.5	109.7	111.1	152.1
7.0	108.5	110.4	154.8
7.5	103.1	102.3	175.8
8.0	103.4	106.5	168.4
8.5	103.0	103.0	174.8
9.0	108.0	104.0	165.0
9.5	108.8	108.8	156.6
10.0	110.0	113.1	149.0
11.0	111.0	115.0	145.2
12.0	113.4	113.9	143.6
13.0	114.8	119.5	135.1
14.0	116.8	123.0	129.0
15.0	122.4	125.9	120.3
16.0	122.2	124.9	121.5

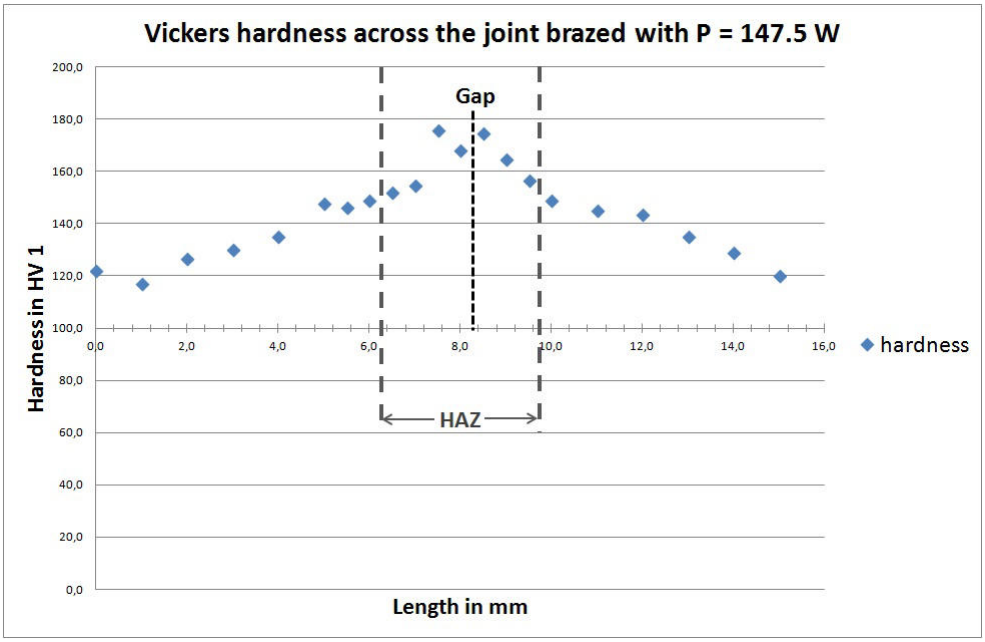

Figure C.2.: Vickers hardness measurement across the polished micrograph section of the joint brazed with P = 148 W

Table C.4.: Measurement results of the respective diagonals from the indentation and the correspondent Vickers hardness for P = 144 W

Position in mm	d_1 in μm	d_2 in μm	Hardness in HV1
0.0	119.7	121.9	127.1
1.0	118.5	120.0	130.4
2.0	116.0	118.6	134.8
3.0	112.1	115.0	143.8
4.0	109.9	112.1	150.5
5.0	110.2	110.7	152.0
5.5	107.9	109.1	157.5
6.0	109.0	109.5	155.4
6.5	104.7	108.3	163.5
7.0	105.2	101.8	173.1
7.5	102.9	101.1	178.2
8.0	113.3	111.6	146.6
8.5	105.5	108.8	161.5
9.0	110.7	112.3	149.2
9.5	117.9	114.1	137.8
10.0	110.9	110.9	150.8
11.0	108.2	109.5	156.5
12.0	109.9	114.6	147.2
13.0	120.5	119.1	129.0
14.0	118.1	121.7	129.0
15.0	123.1	124.3	121.2
16.0	119.4	121.0	128.3

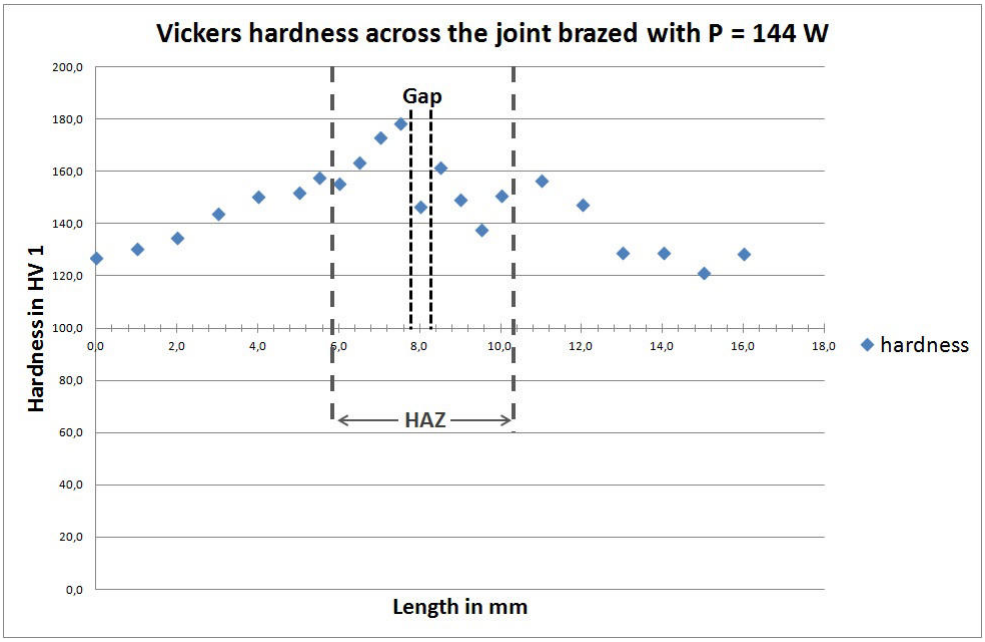

Figure C.3.: Vickers hardness measurement across the polished micrograph section of the joint brazed with P = 144 W

C.2. Tensile testing of the joints brazed with P = 146 W

Table C.5.: Measurement results from tensile testing of sample set (A)

Sample No.	Force at fracture (N)	Crosshead travel at fracture (mm)	Ultimate Force (N)	Tensile extension (crosshead travel) at ultimate force $\frac{mm}{mm}$	Tensile stress (MPa)	Young's modulus (MPa)
1	362.27	5.92	5565.85	0.010	556.58	151622.81
2	0.68	4.81	5000.74	0.008	500.07	156655.60
3	797.34	5.14	5377.27	0.010	537.73	139462.66
4	0.64	6.30	5571.53	0.011	557.15	157758.55
5	268.38	5.88	5291.59	0.009	529.16	155845.17
Arithmetic mean	285.86	5.61	5361.39	0.010	536.14	152268.96
Standard deviation	328.04	0.62	235.13	0.001	23.51	7526.39

Table C.6.: Measurement results from tensile testing of sample set (B)

Sample No.	Force at fracture (N)	Crosshead travel at fracture (mm)	Ultimate Force (N)	Tensile extension (crosshead travel) at ultimate force $\frac{mm}{mm}$	Tensile stress at ultimate force (MPa)	Young's modulus (MPa)
1	4,123.18	0.91	5,767.48	0.009	576.75	157,606.46
2	2,704.77	0.76	5,229.34	0.004	522.93	176,891.13
3	772.18	1.48	5,440.77	0.006	544.08	176,758.83
4	3,794.76	0.94	5,075.14	0.006	507.51	170,666.48
5	3,519.24	0.86	5,370.49	0.005	537.05	179,110.12
Arithmetic mean	2,982.83	0.99	5,376.64	0.006	537.66	172,206.61
Standard deviation	1,342.73	0.28	259.57	0.002	25.96	8,744.46

Table C.7.: Measurement results from tensile testing of sample set (C)

Sample No.	Force at fracture (N)	Crosshead travel at fracture (mm)	Ultimate Force (N)	Tensile extension (crosshead travel) at ultimate force $\frac{mm}{mm}$	Tensile stress at ultimate force (MPa)	Young's modulus (MPa)
1	3,763.21	1.95	6,128.45	0.016	612.85	170,355.58
2	2,579.30	1.28	5,540.63	0.009	554.06	178,295.87
3	4,637.07	2.48	6,254.85	0.020	625.48	168,764.27
4	5,83.47	1.77	5,760.35	0.009	576.04	171,486.35
5	1,799.53	1.57	5,606.51	0.010	560.65	166,848.31
Arithmetic mean	2,672.52	1.81	5,858.16	0.013	585.82	171,150.08
Standard deviation	1,595.62	0.45	317.86	0.005	31.79	4,359.01

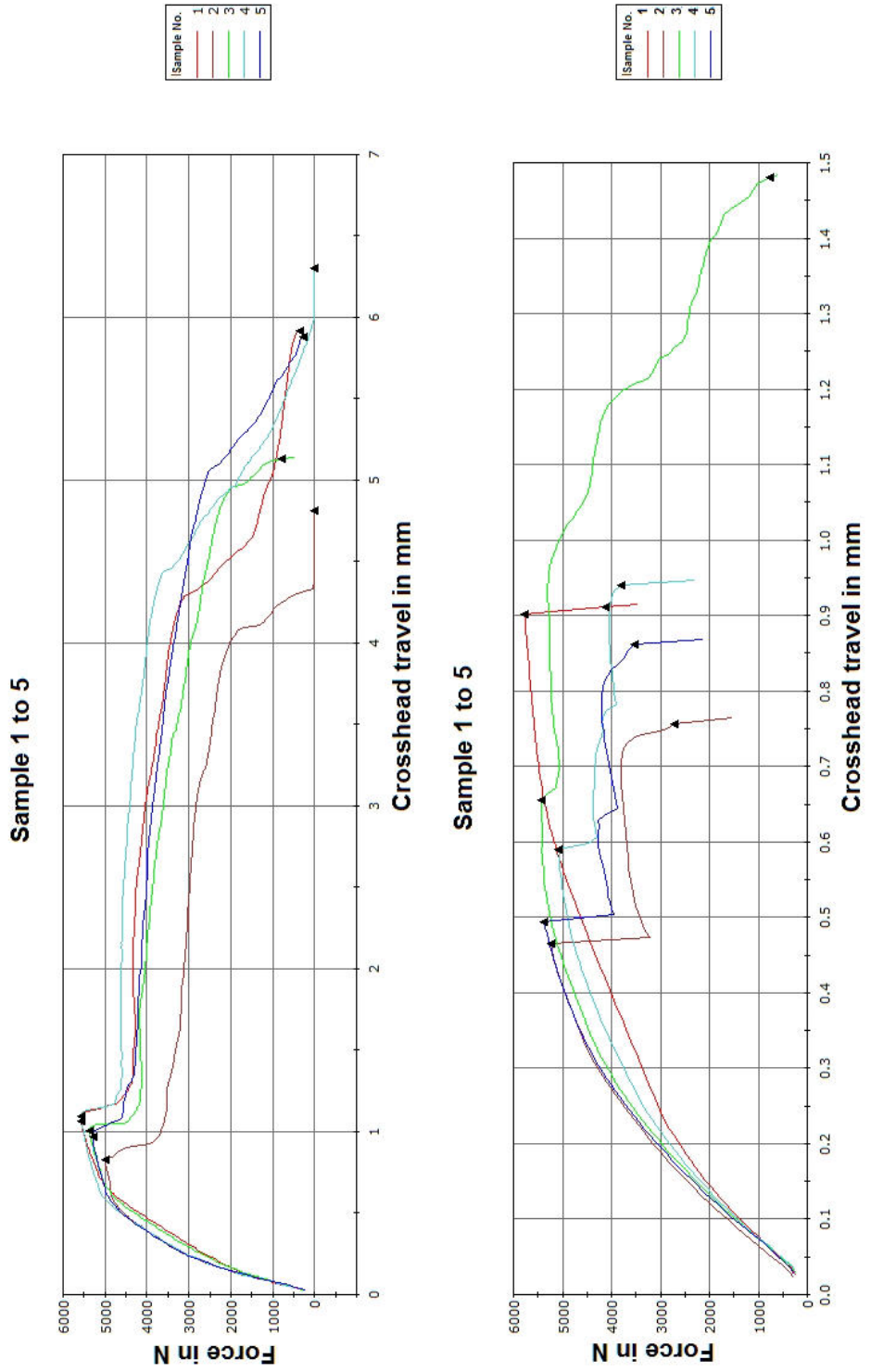

(a) Force-displacement curve of sample set (A) **(b)** Force-displacement curve of sample set (B)

Figure C.4.: Force-displacement curves: a) Force-displacement curve of sample set (A); b) Force-displacement curve of sample set (B); Tensile testing parameters: crosshead travel speed: 5 $\frac{mm}{min}$, condition for stopping the measurement: 40 % of force; Parameters for brazing: P = 146 W, F = +5 mm, v = 74.10 $\frac{mm}{min}$, v_b = 138.4 $\frac{mm}{min}$, d_{gap} = 0.4 mm, WZL = 5.0 s, WZD = 4.3 s

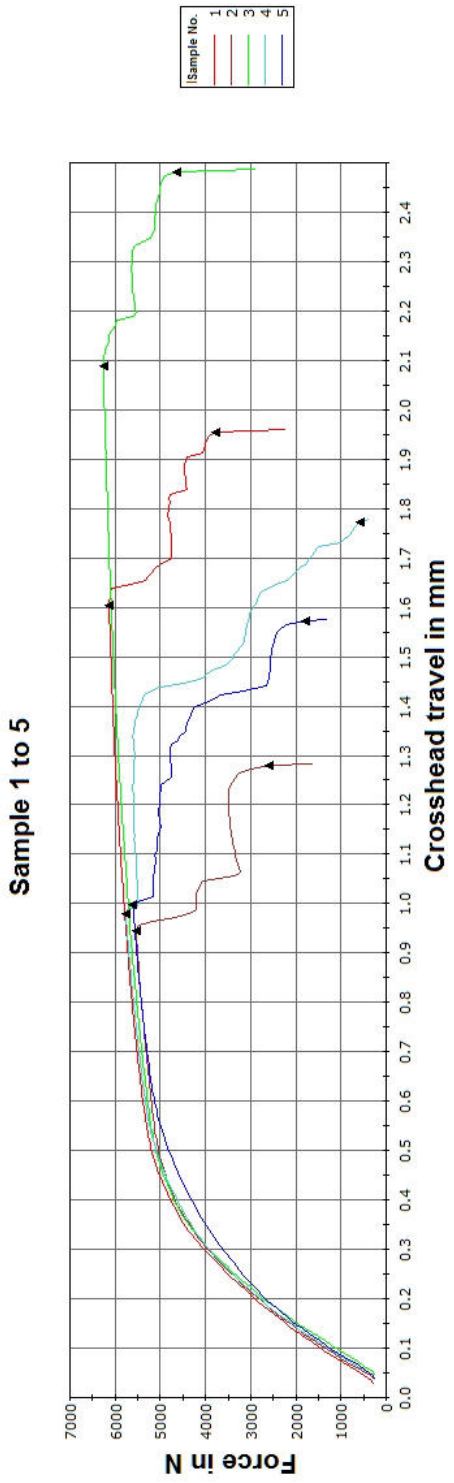

Figure C.5.: Force-displacement curve of sample set (C); Tensile testing parameters: crosshead travel speed: 5 $\frac{mm}{min}$, condition for stopping the measurement: 40 % of force; Parameters for brazing: P = 146 W, F = +5 mm, v = 74.10 $\frac{mm}{min}$, v_b = 138.4 $\frac{mm}{min}$, d_{gap} = 0.4 mm, WZL = 5.0 s, WZD = 4.3 s

C.3. SEM: element analysis mapped onto the respective image

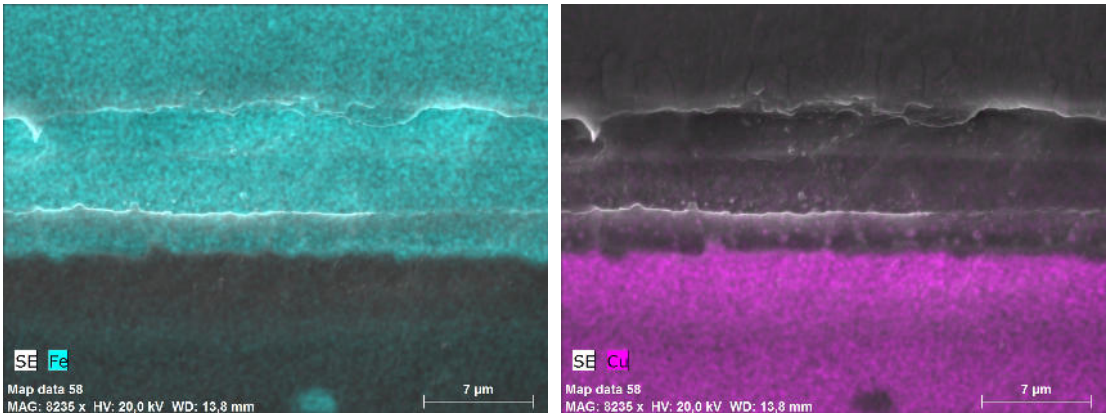

(a) Element analysis regarding iron of Figure 6.40a **(b)** Element analysis regarding copper of Figure 6.40a

Figure C.6.: SEM image of Figure 6.40a with the respective element analysis: a) Iron; b) Copper; Parameters used for brazing: P_{av} = 150 W, F = +5 mm, v = 55.10 $\frac{mm}{min}$, v_b = 109.2 $\frac{mm}{min}$, d_{gap} = 0.4 mm, WZL = 5.5 s, WZD = 4.7 s

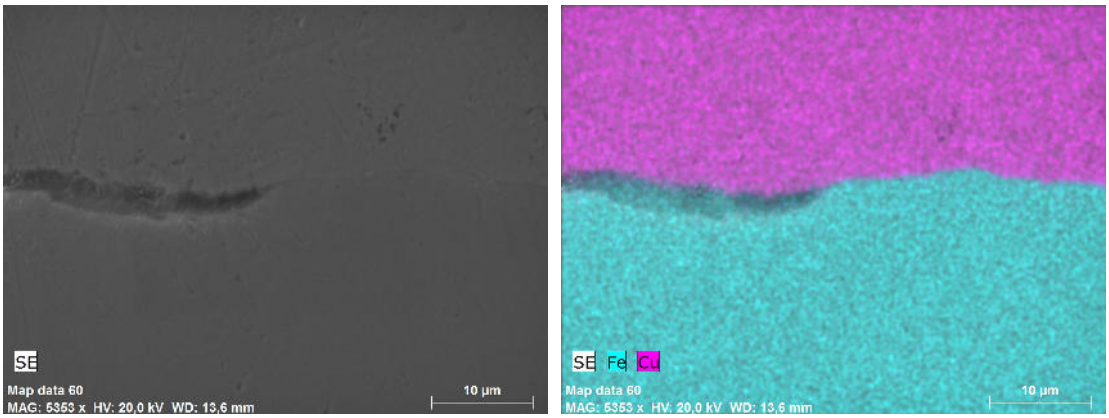

(a) SEM image: enlarged view of the blue rectangle indicated in Figure 6.39 **(b)** SEM: element analysis with regard to copper and iron of the enlarged view of the blue rectangle indicated in Figure 6.39

Figure C.7.: SEM images: a) enlarged view of the blue rectangle indicated in Figure 6.39 showing a partial ditch; b) Mapped information of the element analysis (Fe and Cu) onto the enlarged view; Parameters used for brazing: P_{av} = 150 W, F = +5 mm, v = 55.10 $\frac{mm}{min}$, v_b = 109.2 $\frac{mm}{min}$, d_{gap} = 0.4 mm, WZL = 5.5 s, WZD = 4.7 s

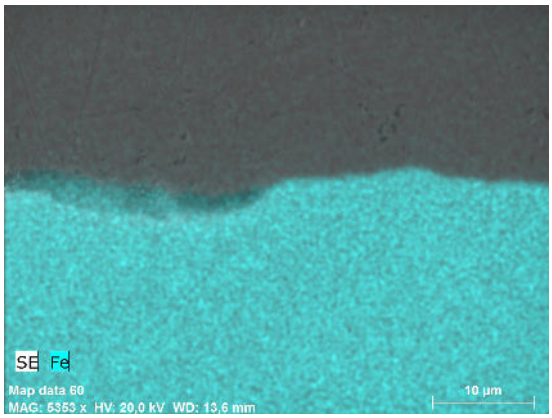

(a) Element analysis regarding iron of Figure C.7a

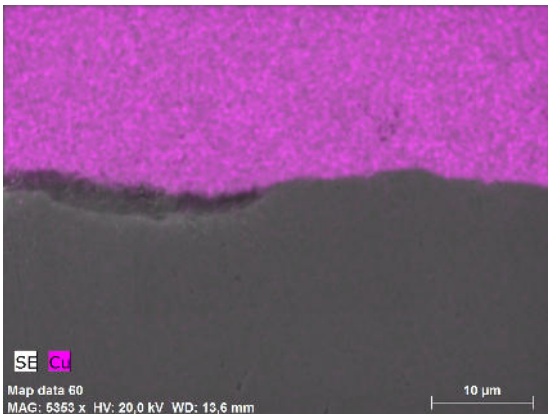

(b) Element analysis regarding copper of Figure C.7a

Figure C.8.: SEM image of Figure C.7a with the respective element analysis: a) Iron; b) Copper; Parameters used for brazing: $P_{av} = 150\,W$, $F = +5\,mm$, $v = 55.10\,\frac{mm}{min}$, $v_b = 109.2\,\frac{mm}{min}$, $d_{gap} = 0.4\,mm$, $WZL = 5.5\,s$, $WZD = 4.7\,s$

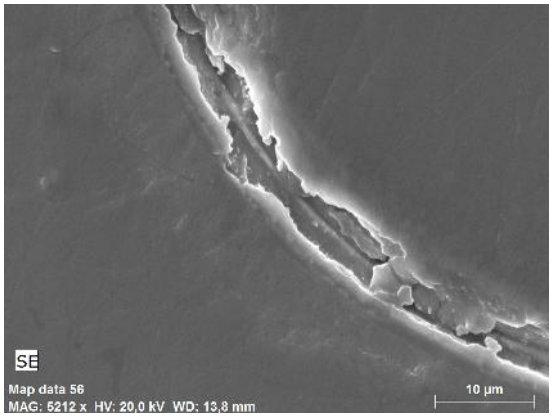

(a) SEM image: enlarged view of the red rectangle indicated in Figure 6.39

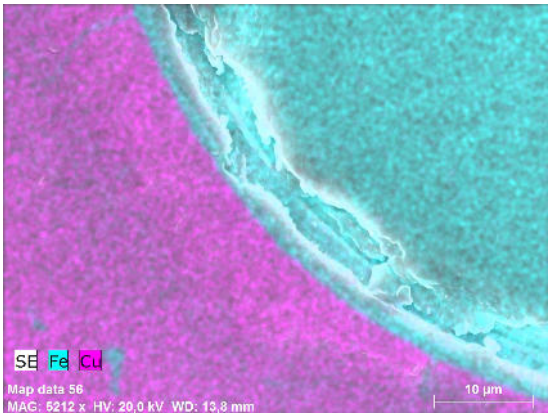

(b) SEM: element analysis with regard to copper and iron of the enlarged view of the red rectangle indicated in Figure 6.39

Figure C.9.: SEM images: a) Enlarged view of the red rectangle indicated in Figure 6.39 showing a ditch at the corner of the base material; b) Mapped information of the element analysis (Fe and Cu) onto the enlarged view; Parameters used for brazing: $P_{av} = 150\,W$, $F = +5\,mm$, $v = 55.10\,\frac{mm}{min}$, $v_b = 109.2\,\frac{mm}{min}$, $d_{gap} = 0.4\,mm$, $WZL = 5.5\,s$, $WZD = 4.7\,s$

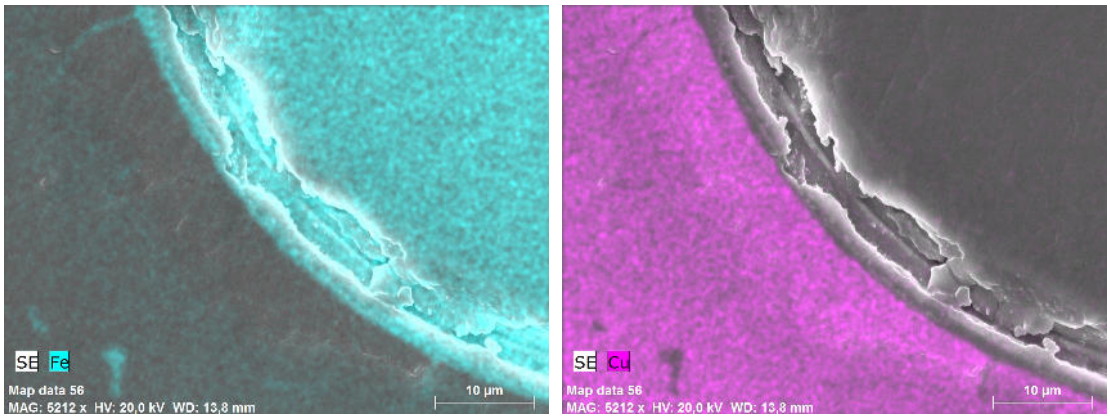

(a) Element analysis regarding iron of Figure C.9a **(b)** Element analysis regarding copper of Figure C.9a

Figure C.10.: SEM image of Figure C.9a with the respective element analysis: a) Iron; b) Copper; Parameters used for brazing: P_{av} = 150 W, F = +5 mm, v = 55.10 $\frac{mm}{min}$, v_b = 109.2 $\frac{mm}{min}$, d_{gap} = 0.4 mm, WZL = 5.5 s, WZD = 4.7 s

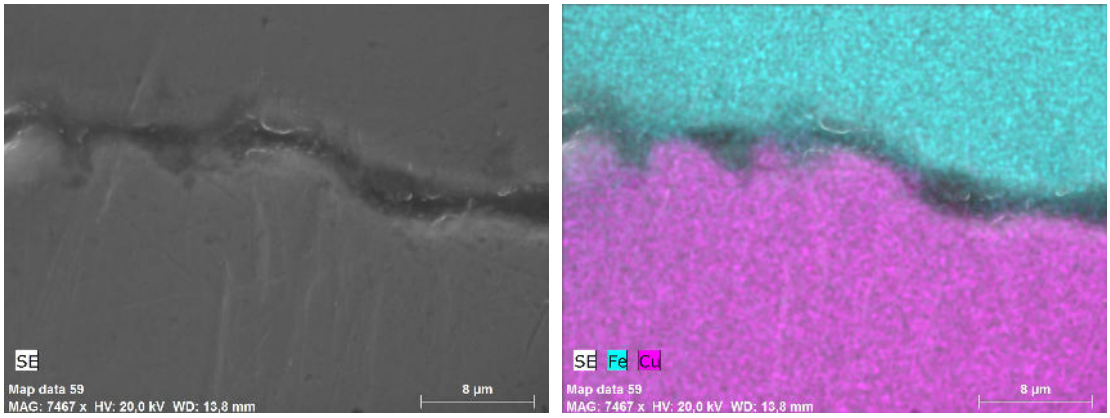

(a) SEM image: enlarged view of the dark green rectangle indicated in Figure 6.39 **(b)** SEM: element analysis with regard to copper and iron of the enlarged view of the dark green rectangle indicated in Figure 6.39

Figure C.11.: SEM images: a) enlarged view of the dark green rectangle indicated in Figure 6.39 showing a partial ditch; b) Mapped information of the element analysis (Fe and Cu) onto the enlarged view; Parameters used for brazing: P_{av} = 150 W, F = +5 mm, v = 55.10 $\frac{mm}{min}$, v_b = 109.2 $\frac{mm}{min}$, d_{gap} = 0.4 mm, WZL = 5.5 s, WZD = 4.7 s

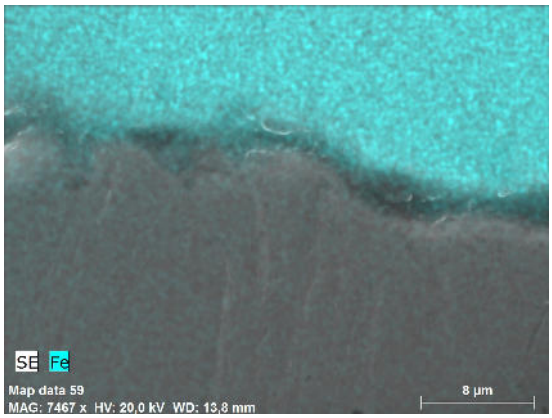

(a) Element analysis regarding iron of Figure C.11a

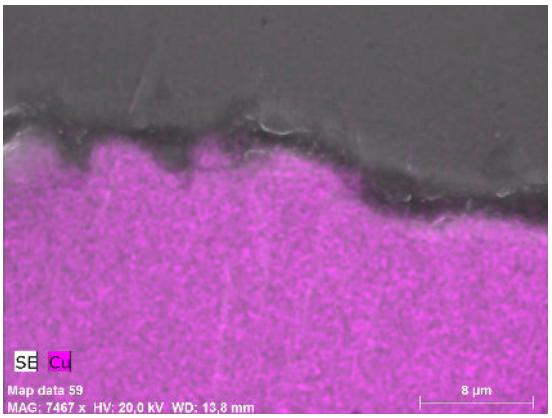

(b) Element analysis regarding copper of Figure C.11a

Figure C.12.: SEM image of Figure C.11a with the respective element analysis: a) Iron; b) Copper; Parameters used for brazing: P_{av} = 150 W, F = +5 mm, v = 55.10 $\frac{mm}{min}$, v_b = 109.2 $\frac{mm}{min}$, d_{gap} = 0.4 mm, WZL = 5.5 s, WZD = 4.7 s

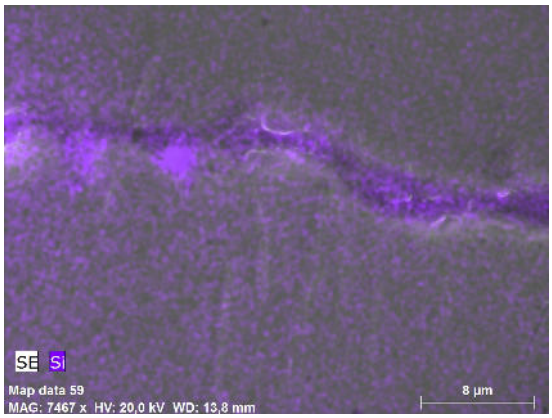

(a) Element analysis regarding silicon of Figure C.11a

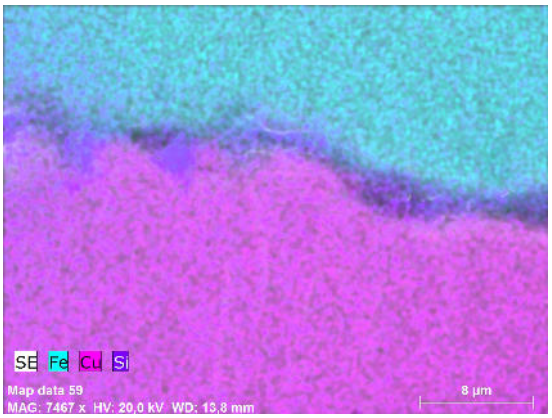

(b) Element analysis regarding iron, copper and silicon of Figure C.11a

Figure C.13.: SEM image of Figure C.11a with the respective element analysis: a) Silicon; b) Mapped information of the element analysis (Fe, Cu and Si) onto the enlarged view; Parameters used for brazing: P_{av} = 150 W, F = +5 mm, v = 55.10 $\frac{mm}{min}$, v_b = 109.2 $\frac{mm}{min}$, d_{gap} = 0.4 mm, WZL = 5.5 s, WZD = 4.7 s

D. Data sheets

D.1. Data sheet of the measurement amplifier AD595


Figure removed
due to
copyright
restrictions


Figure removed
due to
copyright
restrictions


Figure removed
due to
copyright
restrictions


Figure removed
due to
copyright
restrictions


Figure removed
due to
copyright
restrictions


Figure removed
due to
copyright
restrictions


Figure removed
due to
copyright
restrictions


Figure removed
due to
copyright
restrictions

D.2. Data sheet of the 10 bit analogue-digital converter


Figure removed
due to
copyright
restrictions


Figure removed
due to
copyright
restrictions


Figure removed
due to
copyright
restrictions


Figure removed
due to
copyright
restrictions

D.3. Data sheet of the encoder HEDM 5500 B11


Figure removed
due to
copyright
restrictions


Figure removed
due to
copyright
restrictions


Figure removed
due to
copyright
restrictions


Figure removed
due to
copyright
restrictions


Figure removed
due to
copyright
restrictions


Figure removed
due to
copyright
restrictions


Figure removed
due to
copyright
restrictions


Figure removed
due to
copyright
restrictions


Figure removed
due to
copyright
restrictions


Figure removed
due to
copyright
restrictions


Figure removed
due to
copyright
restrictions


Figure removed
due to
copyright
restrictions


Figure removed
due to
copyright
restrictions


Figure removed
due to
copyright
restrictions


Figure removed
due to
copyright
restrictions

D.4. Data sheet of NI Usb 6009 card from National Instruments


Figure removed
due to
copyright
restrictions


Figure removed
due to
copyright
restrictions


Figure removed
due to
copyright
restrictions


Figure removed
due to
copyright
restrictions


Figure removed
due to
copyright
restrictions


Figure removed
due to
copyright
restrictions

D.5. Data sheet of the laser - triangulation sensor M7L/0,5


Figure removed
due to
copyright
restrictions


Figure removed
due to
copyright
restrictions


Figure removed
due to
copyright
restrictions

D.6. Data sheet of the hand-held measurement device testo 605-H1


Figure removed
due to
copyright
restrictions


Figure removed
due to
copyright
restrictions

D.7. Data sheet of the beam profiler laserscope UFF 100 from Prometec


Figure removed
due to
copyright
restrictions


Figure removed
due to
copyright
restrictions


Figure removed
due to
copyright
restrictions


Figure removed
due to
copyright
restrictions

D.8. Specifications of the tensile testing machine 3367 from Instron Corporation


Figure removed
due to
copyright
restrictions


Figure removed
due to
copyright
restrictions


Figure removed
due to
copyright
restrictions


Figure removed
due to
copyright
restrictions

E. Technical drawings

E.1. Technical drawings of the laser brazing setup

E.1.1. Technical drawings of the clamping device

Technical drawings of the clamping brackets

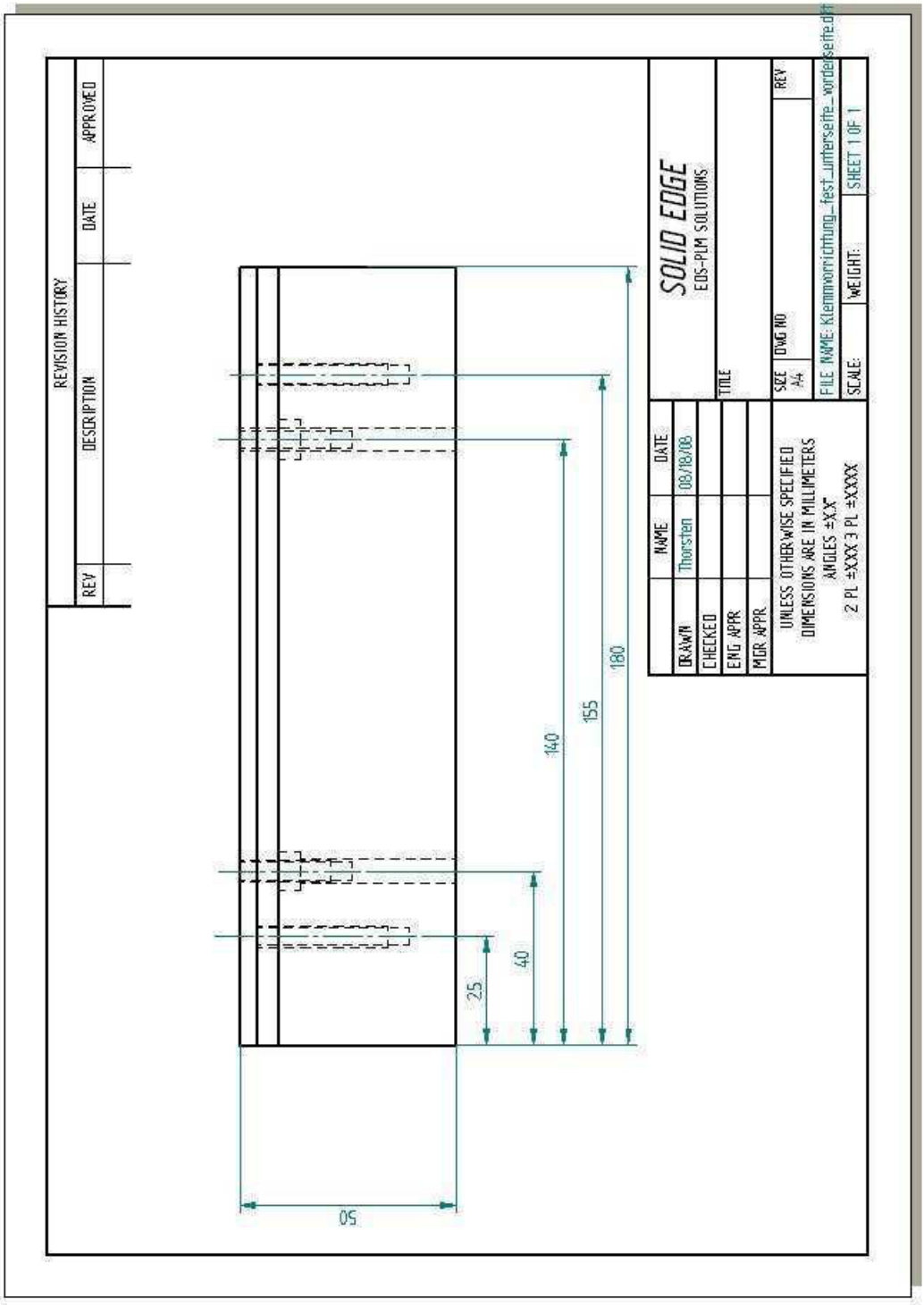
REVISION HISTORY
REV
DESCRIPTION
DATE
APPROVED
SOLID EDGE
EDS-PLM SOLUTIONS
NAME
DATE
DRAWN
Thorsten
08/18/09
CHECKED
ENG APPR.
MGR APPR.
TITLE
SIZE
A4
DWG NO
REV
FILE NAME: Klemmvorrichtung_fest_unterseite_vorderseite.dft
UNLESS OTHERWISE SPECIFIED
DIMENSIONS ARE IN MILLIMETERS
ANGLES ±X.X°
2 PL ±XXX 3 PL ±XXXX
SCALE:
WEIGHT:
SHEET 1 OF 1
180
155
140
40
25
50

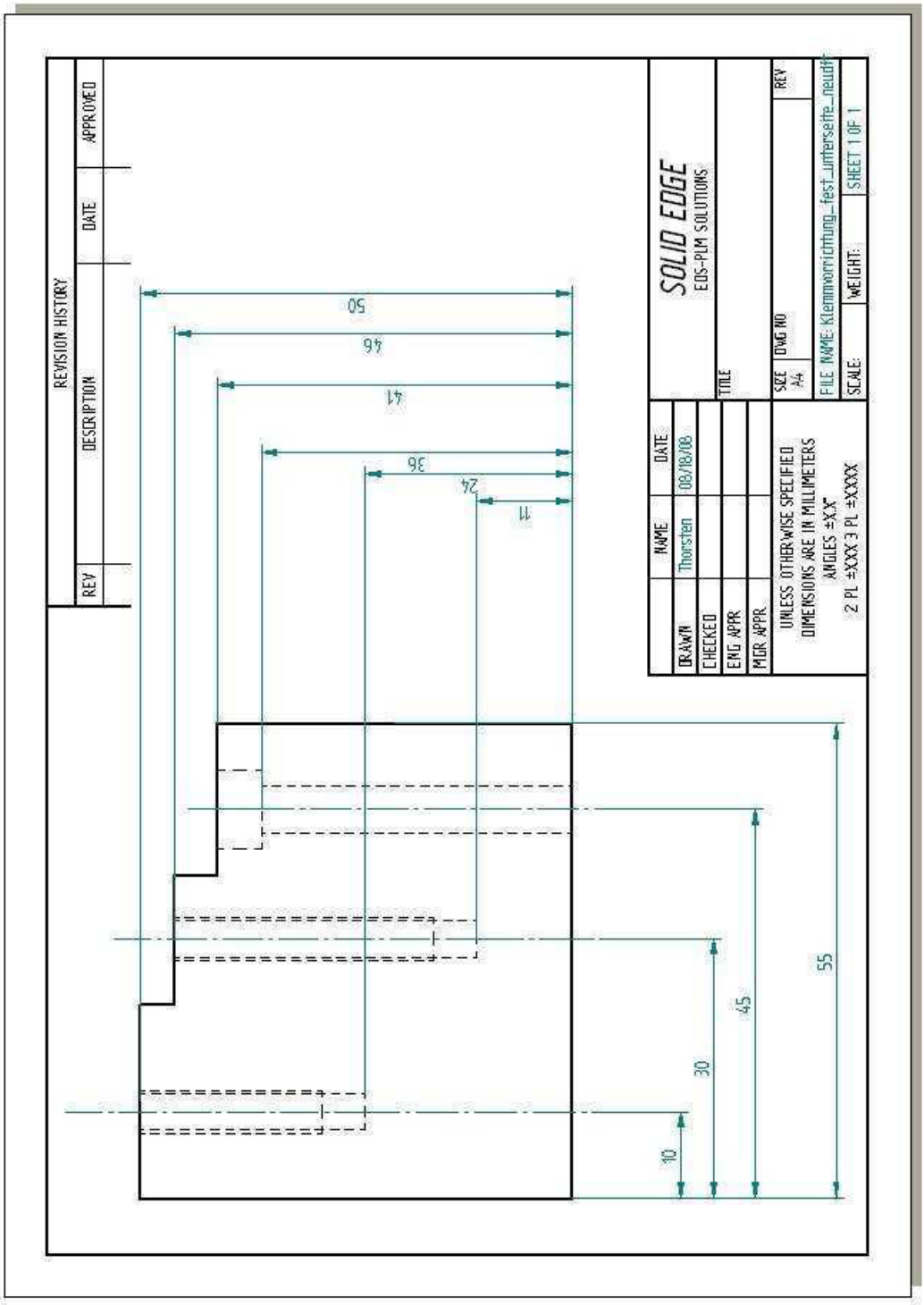
REVISION HISTORY
REV
DESCRIPTION
DATE
APPROVED
SOLID EDGE
EDS-PLM SOLUTIONS
NAME
DATE
DRAWN
Thorsten
08/18/08
CHECKED
ENG APPR.
MGR APPR.
TITLE
SIZE A4
DWG NO
REV
FILE NAME: Klemmvorrichtung_fest_unterseite_neu.dft
SCALE:
WEIGHT:
SHEET 1 OF 1
UNLESS OTHERWISE SPECIFIED
DIMENSIONS ARE IN MILLIMETERS
ANGLES ±X.X°
2 PL ±XXX 3 PL ±XXXX
50
46
41
36
24
11
55
45
30
10

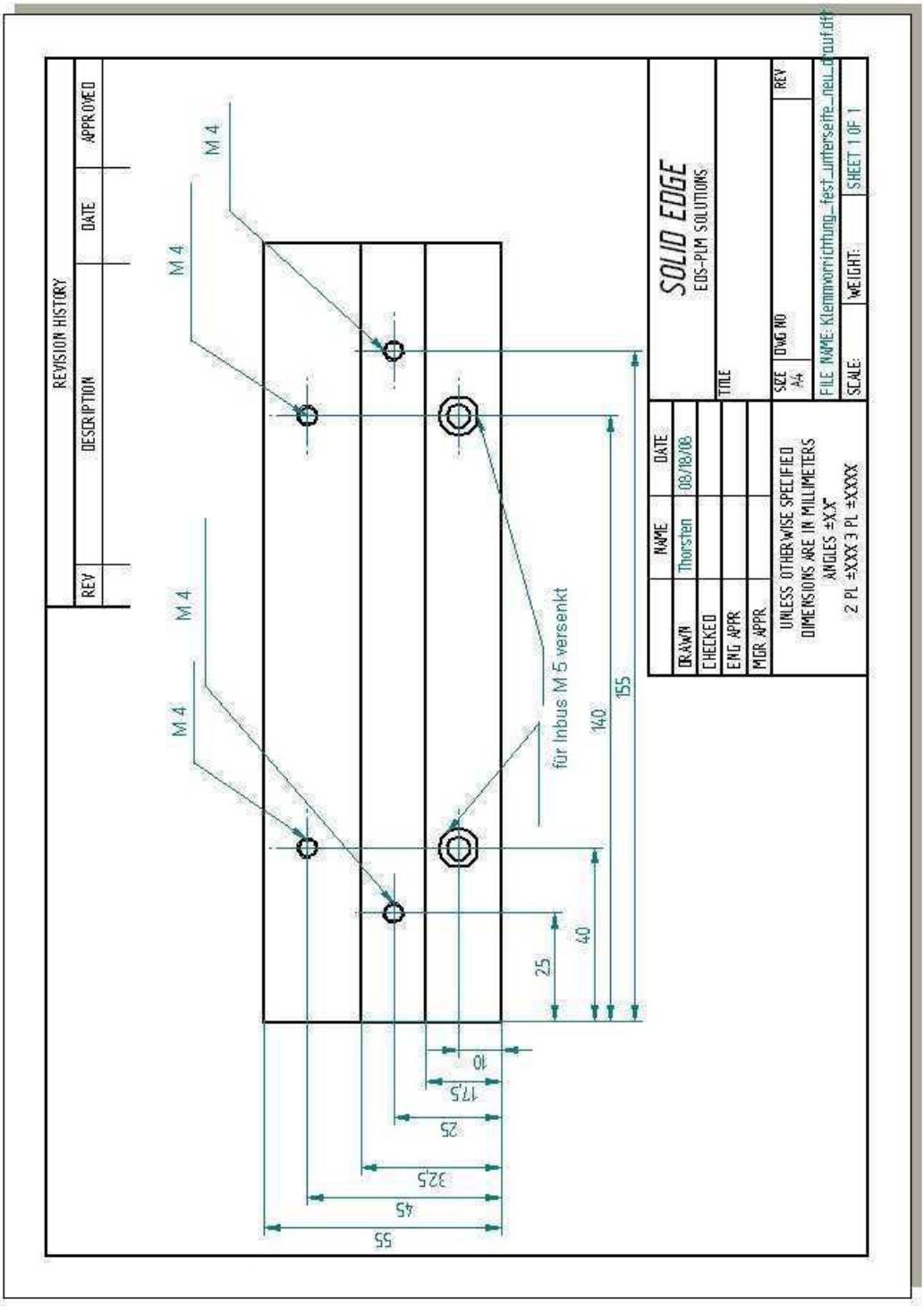
REVISION HISTORY
REV
DESCRIPTION
DATE
APPROVED
M 4
M 4
M 4
M 4
für Inbus M 5 versenkt
155
140
40
25
10
17,5
25
32,5
45
55
SOLID EDGE
EDS-PLM SOLUTIONS
NAME
DATE
DRAWN
Thorsten
08/18/08
CHECKED
ENG APPR.
MGR APPR.
TITLE
UNLESS OTHERWISE SPECIFIED
DIMENSIONS ARE IN MILLIMETERS
ANGLES ±X.X°
2 PL ±XXX 3 PL ±XXXX
SIZE
A4
DWG NO
REV
FILE NAME: Klemmvorrichtung_fest_unterseite_neu_Grauf.dft
SCALE:
WEIGHT:
SHEET 1 OF 1

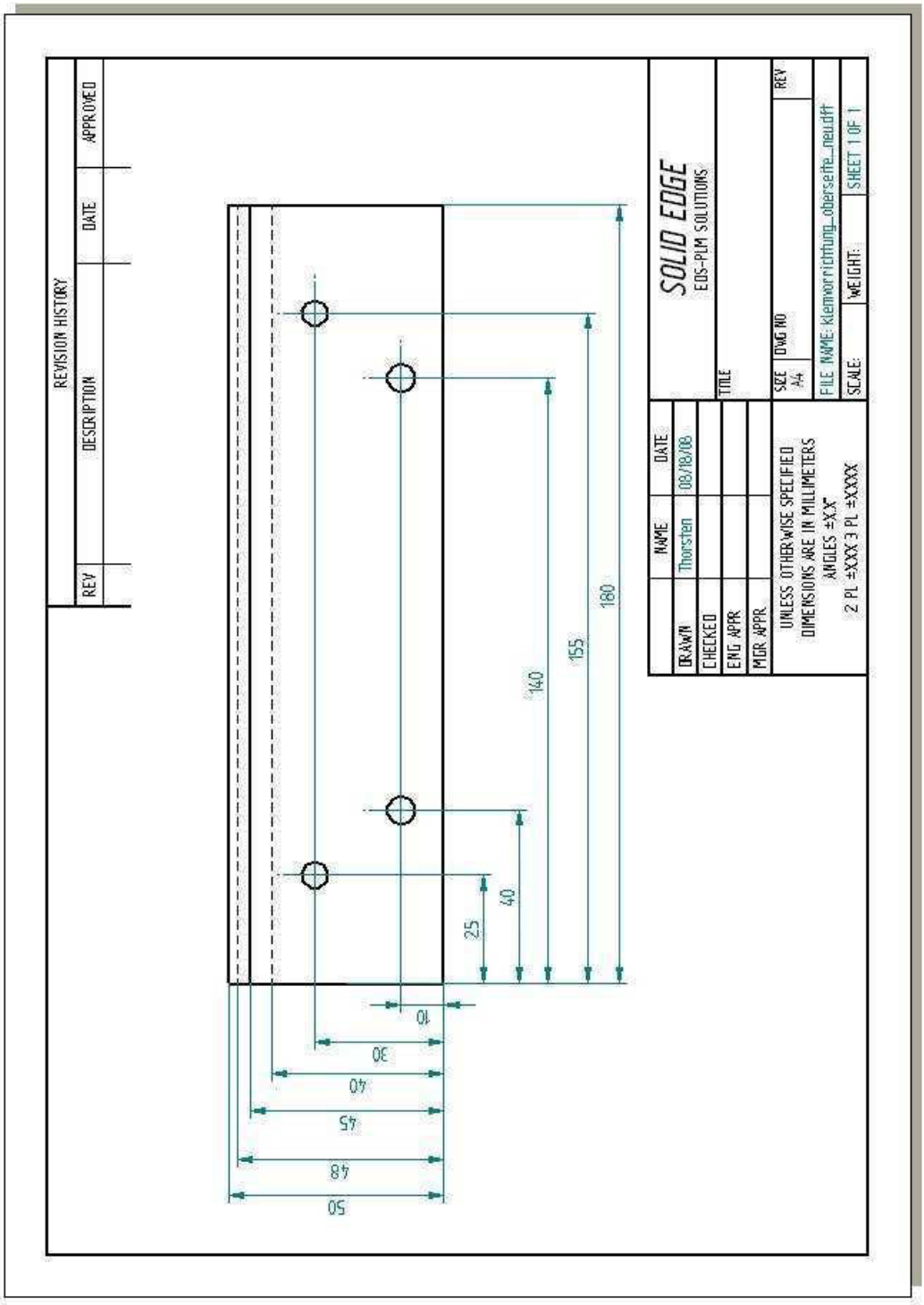
REVISION HISTORY
REV
DESCRIPTION
DATE
APPROVED
SOLID EDGE
EDS-PLM SOLUTIONS
NAME
DATE
DRAWN
Thorsten
08/18/08
CHECKED
ENG APPR.
MGR APPR.
TITLE
SIZE A4
DWG NO
REV
FILE NAME: klemmvorrichtung_oberseite_neu.dft
SCALE:
WEIGHT:
SHEET 1 OF 1
UNLESS OTHERWISE SPECIFIED
DIMENSIONS ARE IN MILLIMETERS
ANGLES ±X.X°
2 PL ±XXX 3 PL ±XXXX
180
155
140
40
25
10
30
40
45
48
50

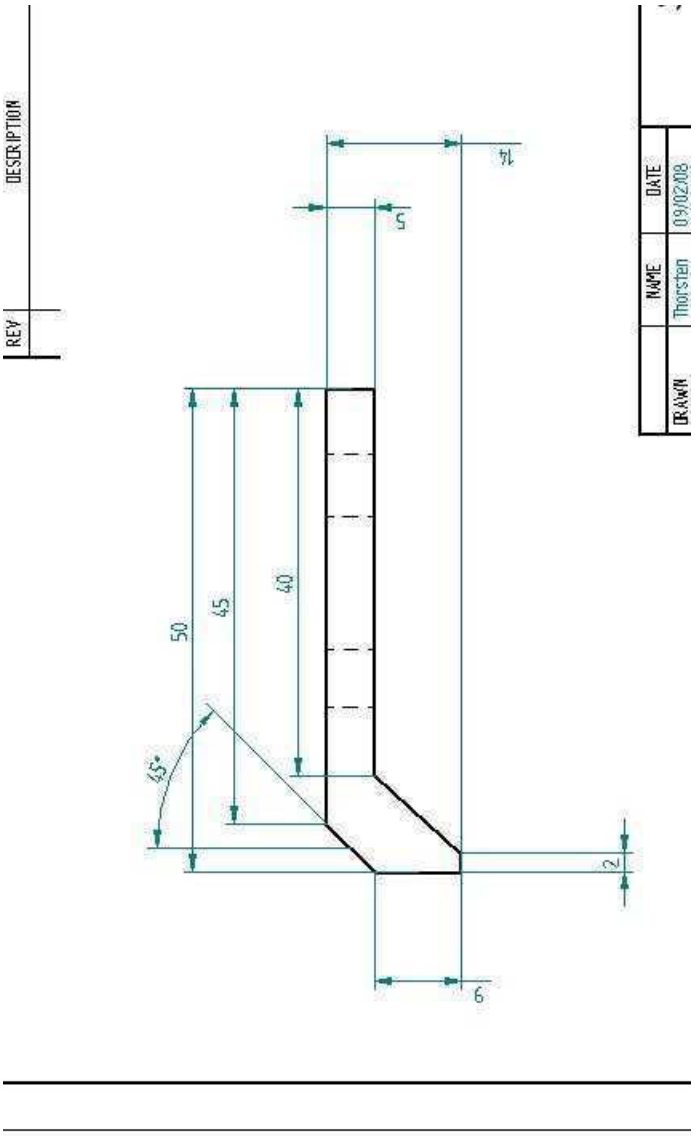
REV
DESCRIPTION
DRAWN
NAME
Thorsten
DATE
09/02/08
14
5
50
45
40
45°
2
6

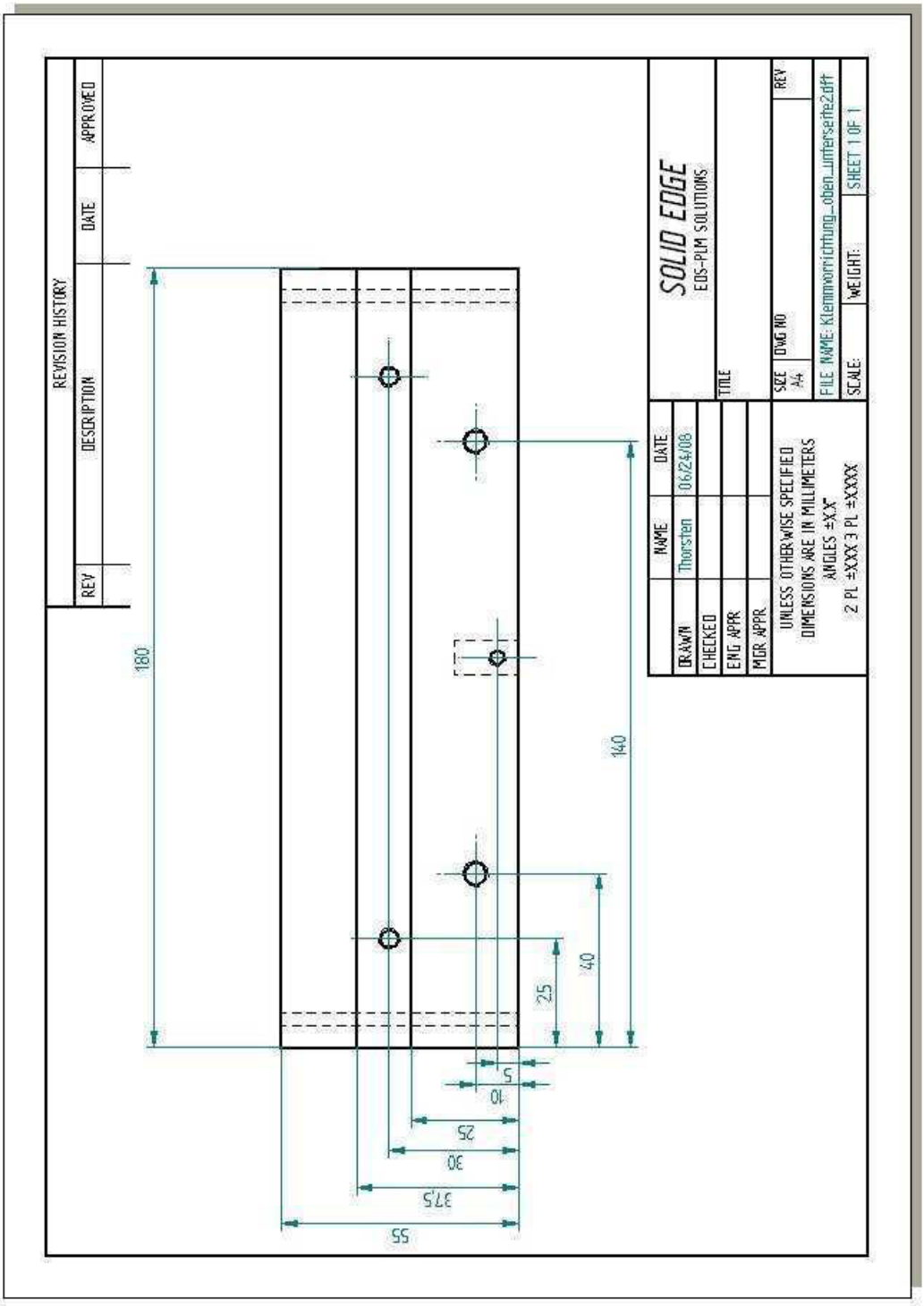
REVISION HISTORY
REV
DESCRIPTION
DATE
APPROVED
180
140
40
25
5
10
25
30
37,5
55
SOLID EDGE
EDS-PLM SOLUTIONS
NAME
DATE
DRAWN
Thorsten
06/24/08
CHECKED
ENG APPR.
MGR APPR.
TITLE
UNLESS OTHERWISE SPECIFIED
DIMENSIONS ARE IN MILLIMETERS
ANGLES ±X.X°
2 PL ±XXX 3 PL ±XXXX
SIZE
A4
DWG NO
REV
FILE NAME: Klemmvorrichtung_oben_umfersatte2.dft
SCALE:
WEIGHT:
SHEET 1 OF 1

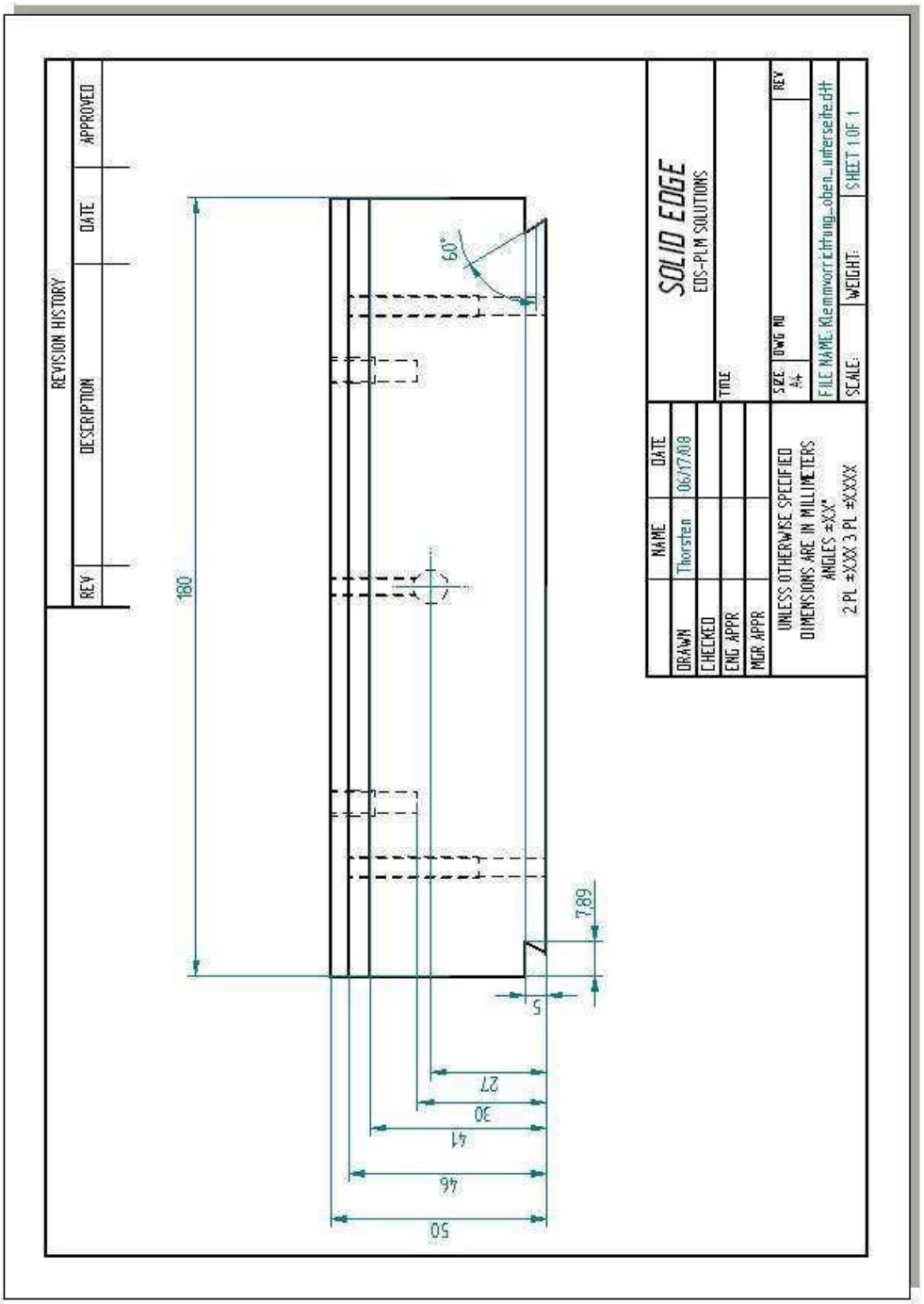
REVISION HISTORY
REV
DESCRIPTION
DATE
APPROVED
SOLID EDGE
EDS-PLM SOLUTIONS
NAME
DATE
DRAWN
Thorsten
06/17/08
CHECKED
ENG APPR
MGR APPR
TITLE
SIZE
A4
DWG NO
REV
FILE NAME: Klemmvorrichtung_oben_unterseite.dft
SCALE:
WEIGHT:
SHEET 1 OF 1
UNLESS OTHERWISE SPECIFIED
DIMENSIONS ARE IN MILLIMETERS
ANGLES ±X.X°
2 PL ±X.XX 3 PL ±X.XXX
180
60°
7.89
5
27
30
41
46
50

Technical drawing of the base plate

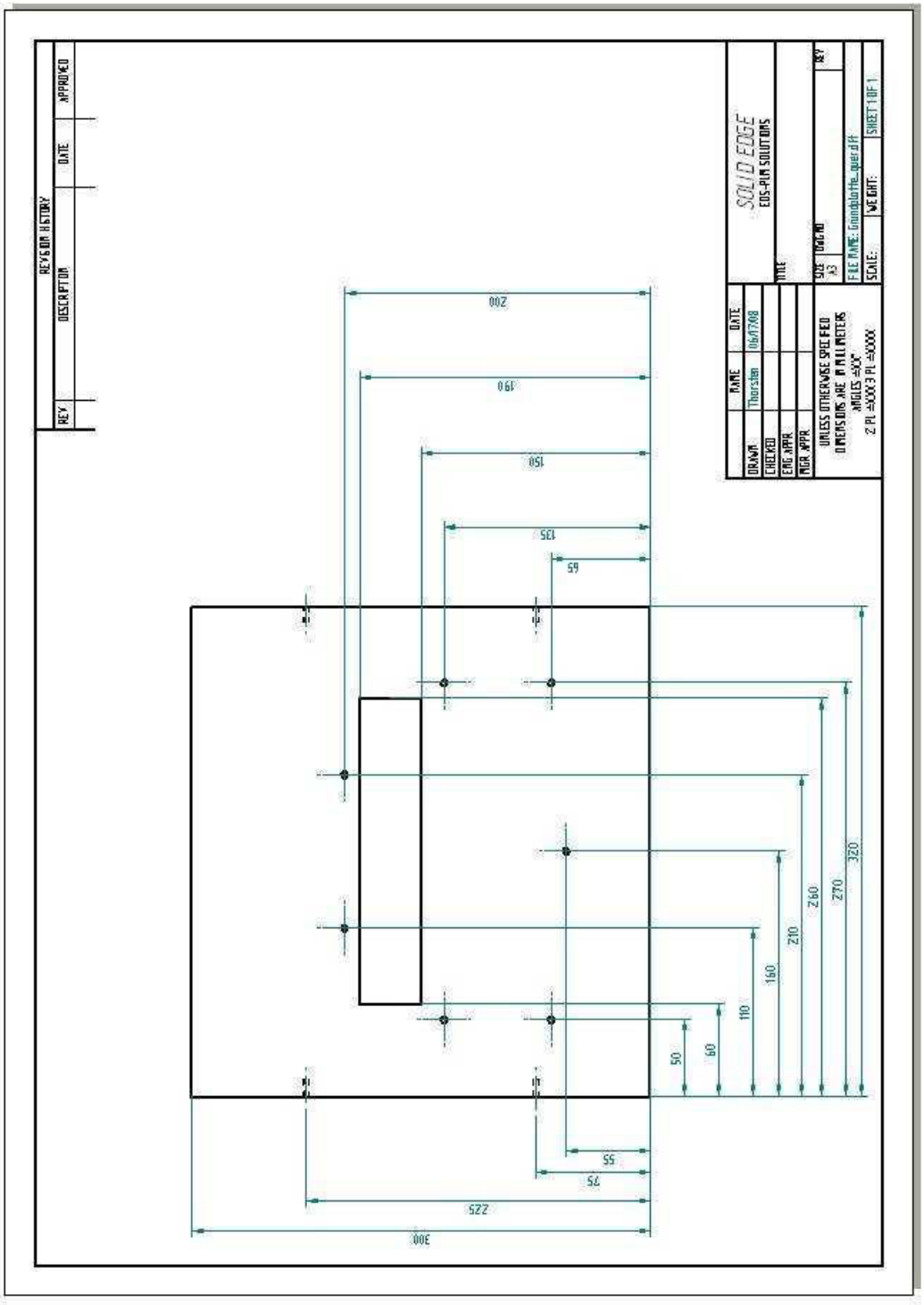
REVISION HISTORY
REV
DESCRIPTION
DATE
APPROVED
SOLID EDGE
EOS-PLM SOLUTIONS
NAME
DATE
DRAWN
Thorsten
06/07/08
CHECKED
ENG APPR.
MFG APPR.
UNLESS OTHERWISE SPECIFIED
DIMENSIONS ARE IN MILLIMETERS
ANGLES ±0.5°
2 PL ±0.000 3 PL ±0.0000
TITLE
SIZE
A3
DWG NO
REV
FILE NAME: Grundplatte_quer.dft
SCALE:
WEIGHT:
SHEET 1 OF 1
200
190
150
135
65
320
270
260
210
160
110
60
50
55
75
225
300

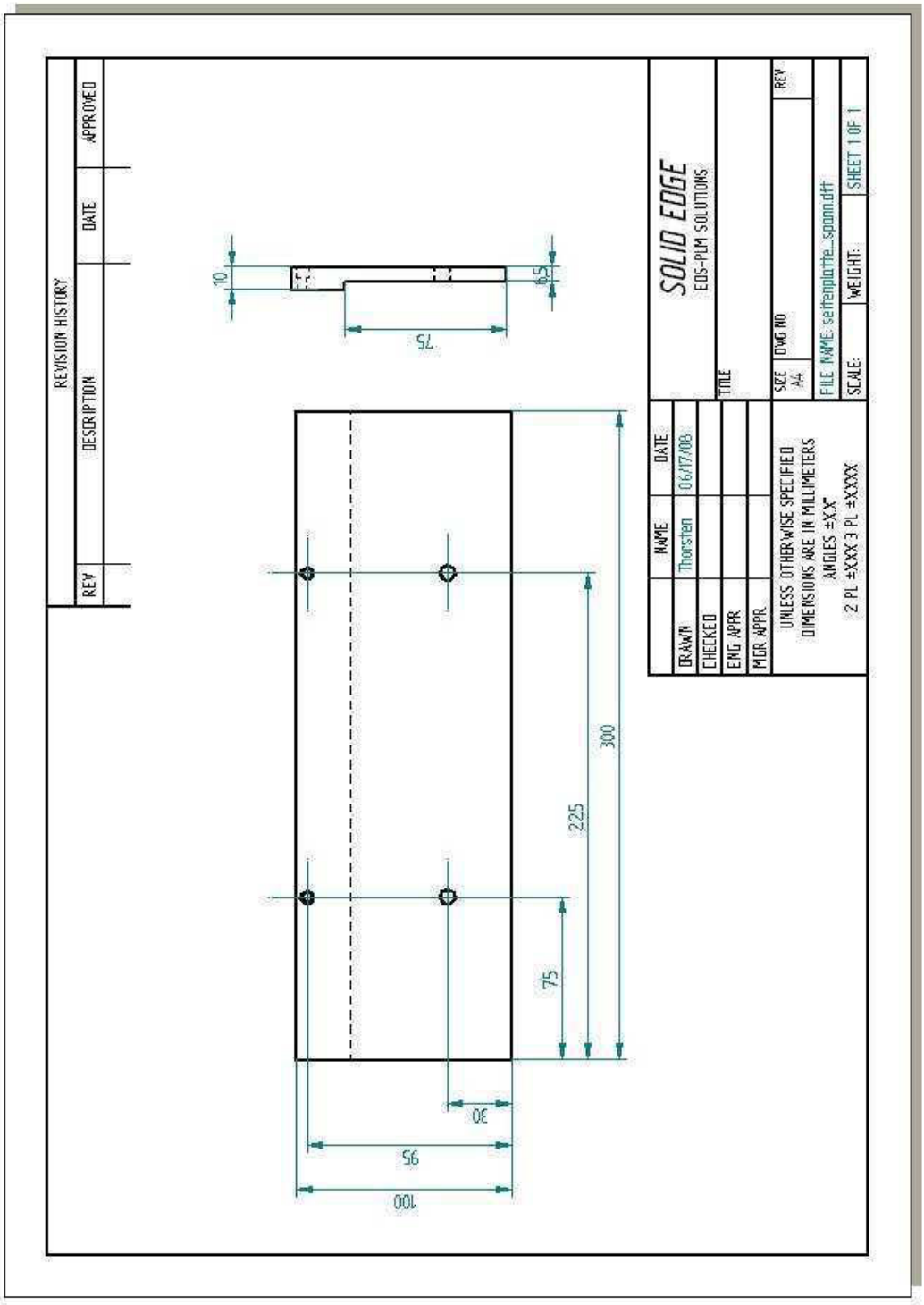
REVISION HISTORY
REV
DESCRIPTION
DATE
APPROVED
10
6,5
75
SOLID EDGE
EDS-PLM SOLUTIONS
NAME
DATE
DRAWN
Thorsten
06/17/08
CHECKED
ENG APPR.
MGR APPR.
TITLE
SIZE
A4
DWG NO
REV
FILE NAME: seitenplatte...spann.dft
UNLESS OTHERWISE SPECIFIED
DIMENSIONS ARE IN MILLIMETERS
ANGLES ±X.X°
2 PL ±XXX 3 PL ±XXXX
SCALE:
WEIGHT:
SHEET 1 OF 1
300
225
75
30
95
100

Technical drawing of the dovetail

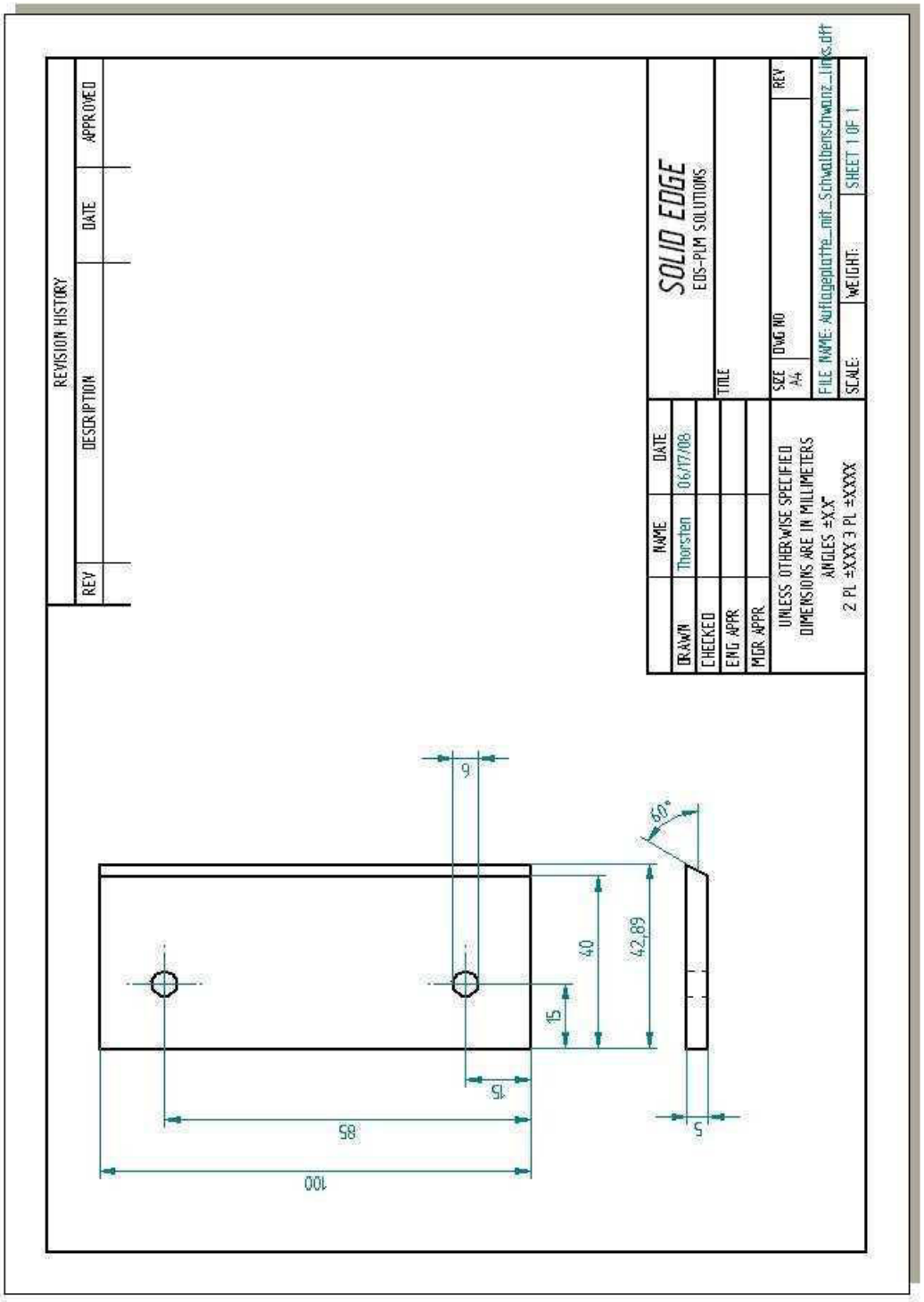
REVISION HISTORY
REV
DESCRIPTION
DATE
APPROVED
SOLID EDGE
EDS-PLM SOLUTIONS
NAME
DATE
DRAWN
Thorsten
06/17/08
CHECKED
ENG APPR.
MGR APPR.
TITLE
SIZE
A4
DWG NO
REV
FILE NAME: Auflageplatte_mit_Schwalbenschwanz_links.dft
UNLESS OTHERWISE SPECIFIED
DIMENSIONS ARE IN MILLIMETERS
ANGLES ±X.X°
2 PL ±XXX 3 PL ±XXXX
SCALE:
WEIGHT:
SHEET 1 OF 1
6
60°
40
42,89
15
15
85
100
5

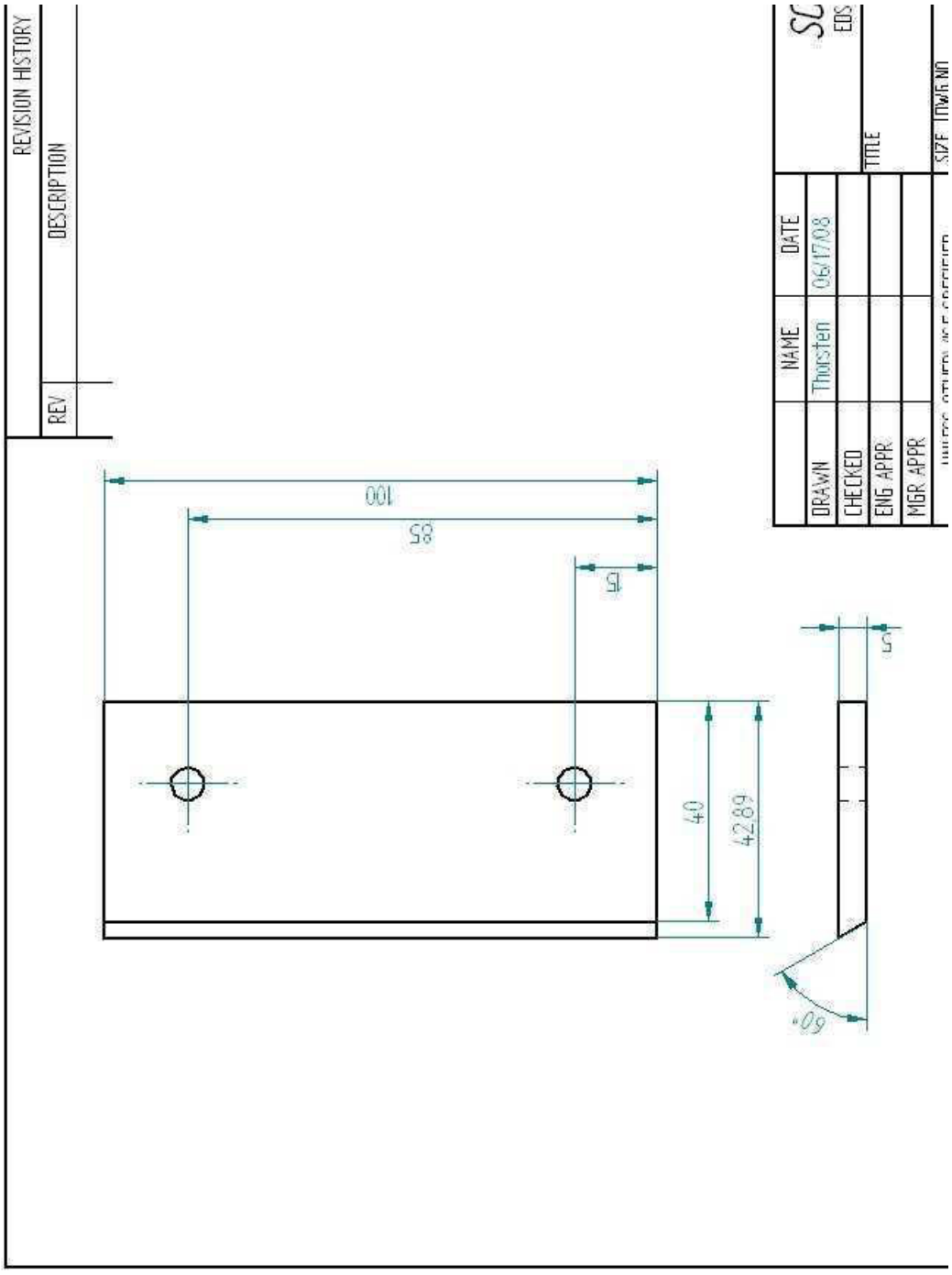
REVISION HISTORY
REV
DESCRIPTION
NAME
DATE
DRAWN
Thorsten
06/17/08
CHECKED
ENG APPR
MGR APPR
EDS
TITLE
100
85
15
40
42.89
5
60°

Technical drawing of the holder for the micrometer gauge

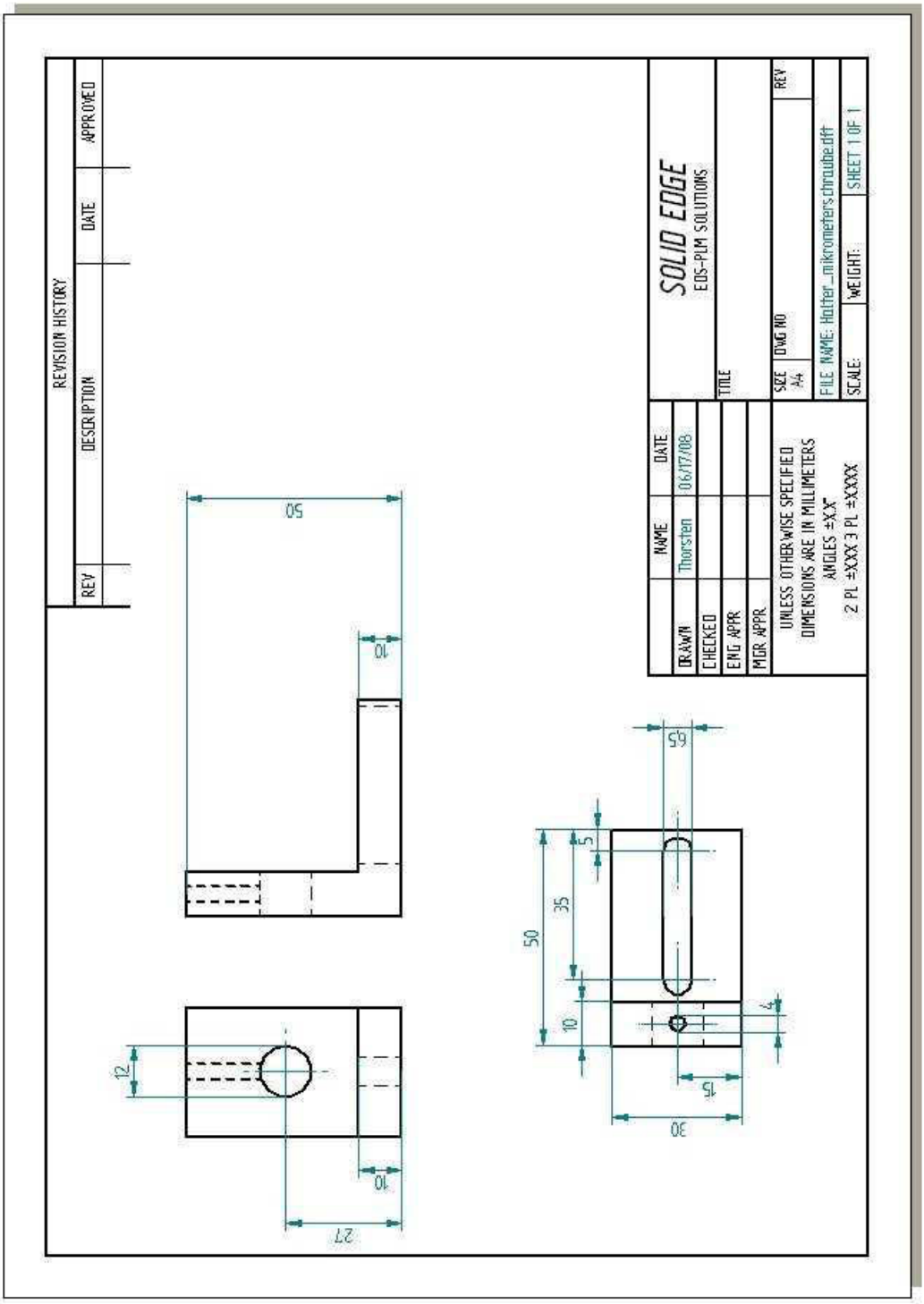
REVISION HISTORY
REV
DESCRIPTION
DATE
APPROVED
SOLID EDGE
EDS-PLM SOLUTIONS
NAME
DATE
DRAWN
Thorsten
06/17/08
CHECKED
ENG APPR.
MGR APPR.
TITLE
SIZE
A4
DWG NO
REV
FILE NAME: Halter_mikrometerschraube.dft
UNLESS OTHERWISE SPECIFIED
DIMENSIONS ARE IN MILLIMETERS
ANGLES ±X.X°
2 PL ±XXX 3 PL ±XXXX
SCALE:
WEIGHT:
SHEET 1 OF 1
50
10
12
10
27
65
5
50
35
10
4
15
30

E.1.2. Technical drawings of the wire feeder

Technical drawing of the base plate

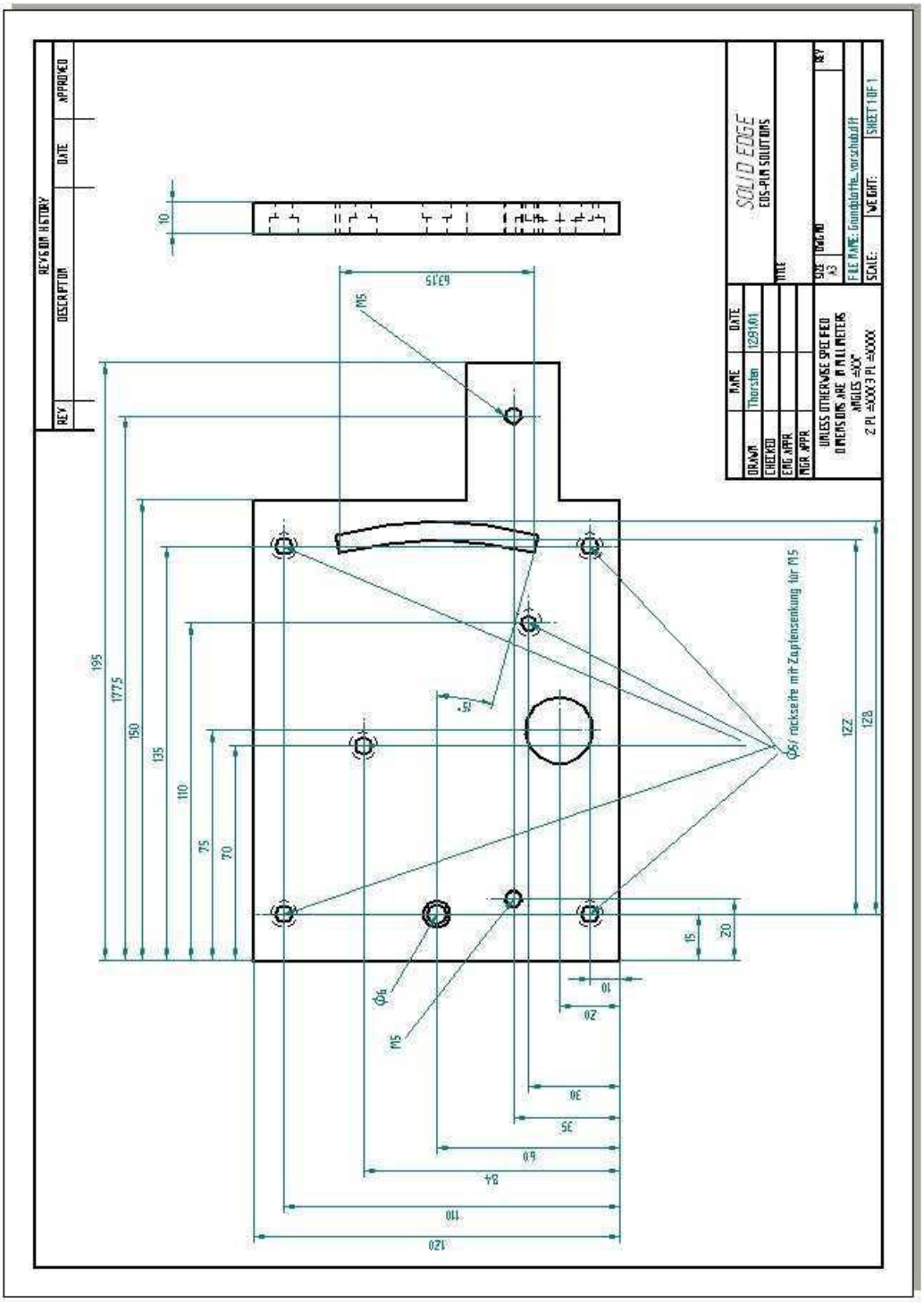
REVISION HISTORY
REV
DESCRIPTION
DATE
APPROVED
SOLID EDGE
EDS-PLM SOLUTIONS
NAME
DATE
DRAWN
Thorsten
12/01/01
CHECKED
ENG APPR.
MFG APPR.
UNLESS OTHERWISE SPECIFIED
DIMENSIONS ARE IN MILLIMETERS
ANGLES ±0.5°
2 PL ±0.03 3 PL ±0.005
SIZE
A3
DWG NO
REV
FILE NAME: Grundplatte_vorschlag1.ft
SCALE:
WEIGHT:
SHEET 1 OF 1
TITLE
M5
63.15
10
195
177.5
150
135
110
75
70
15°
ϕ6
M5
ϕ5 rückseite mit Zapfensenkung für M5
122
128
15
20
10
20
30
35
60
84
110
120

Technical drawing of the base plate for connection to the z-axis of the work station

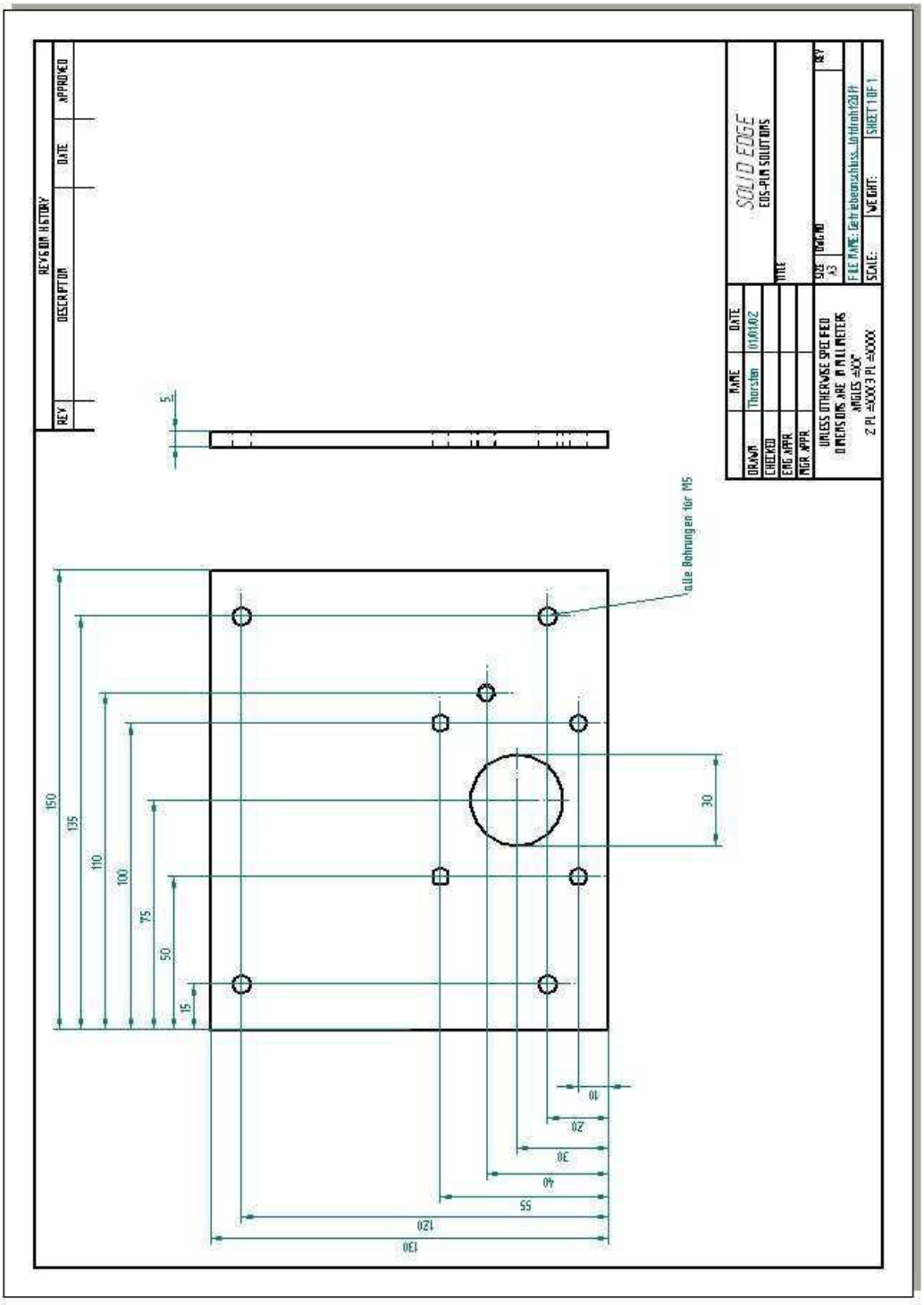
REVISION HISTORY
REV
DESCRIPTION
DATE
APPROVED
SOLID EDGE
EOS-PUM SOLUTIONS
NAME
DATE
DRAWN
Thorsten
01/01/02
CHECKED
ENG APPR.
MGR APPR.
UNLESS OTHERWISE SPECIFIED
DIMENSIONS ARE IN MILLIMETERS
ANGLES ±0.5°
2 PL ±0.03 3 PL ±0.005
TITLE
SIZE
A3
DWG NO
REV
FILE NAME: Lehreaberarschluss_Unterteil.par
SCALE:
WEIGHT:
SHEET 1 OF 1
5
alle Bohrungen für M5
150
135
110
100
75
50
15
30
10
20
30
40
55
120
130

Technical drawing of the tensioner including implementation components

The technical drawings are presented in the following order:

- Tensioner with guidance groove
- Positioner for the folder of the tensioner
- Holder of the tensioner
- Axis of the tensioner

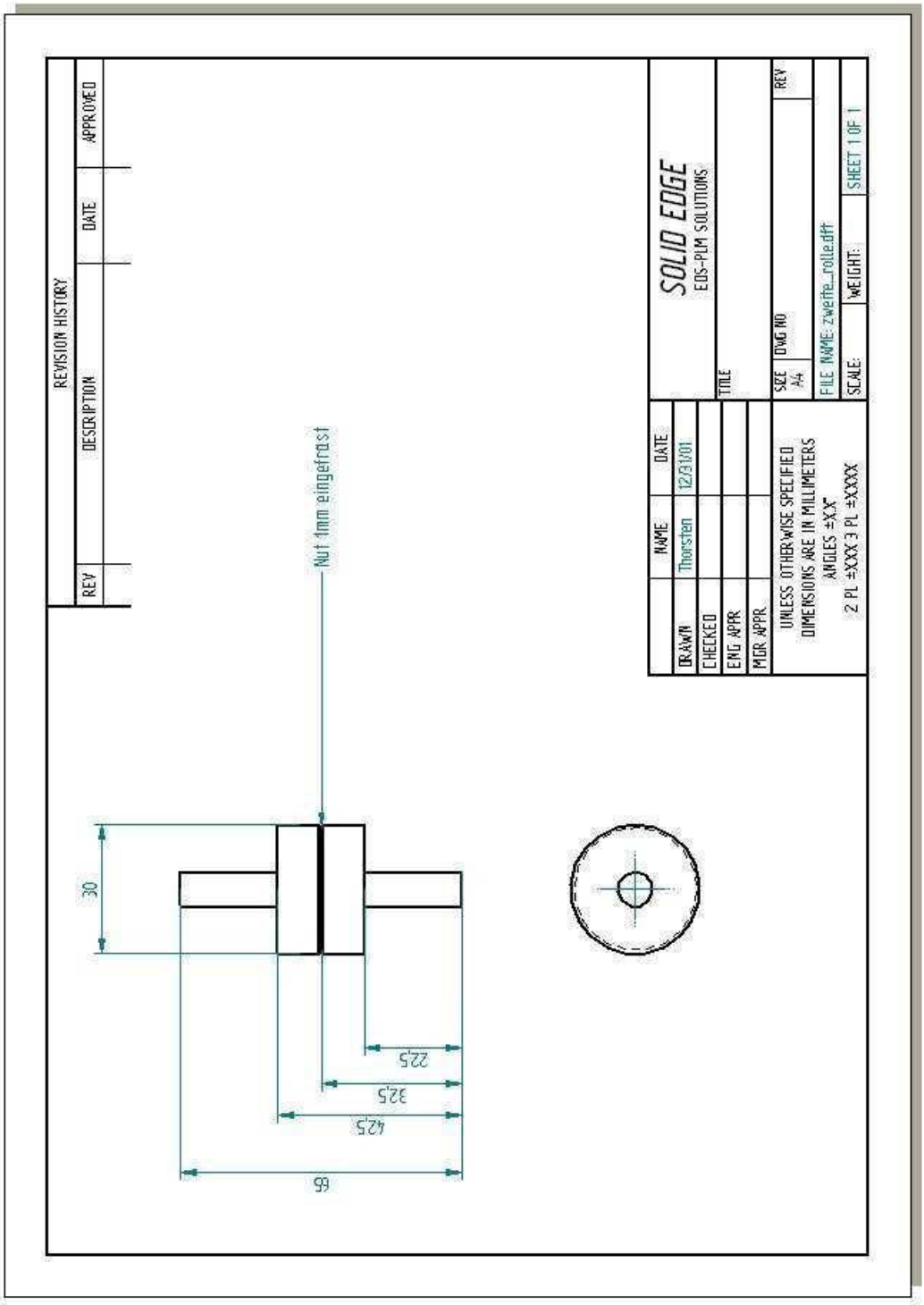
REVISION HISTORY
REV
DESCRIPTION
DATE
APPROVED
SOLID EDGE
EDS-PLM SOLUTIONS
NAME
DATE
DRAWN
Thorsten
12/3/01
CHECKED
ENG APPR.
MGR APPR.
TITLE
SIZE
A4
DWG NO
REV
FILE NAME: zweiffe_rolle.dft
UNLESS OTHERWISE SPECIFIED
DIMENSIONS ARE IN MILLIMETERS
ANGLES ±X.X°
2 PL ±XXX 3 PL ±XXXX
SCALE:
WEIGHT:
SHEET 1 OF 1
Nut 1mm eingefrast
30
22,5
32,5
42,5
65

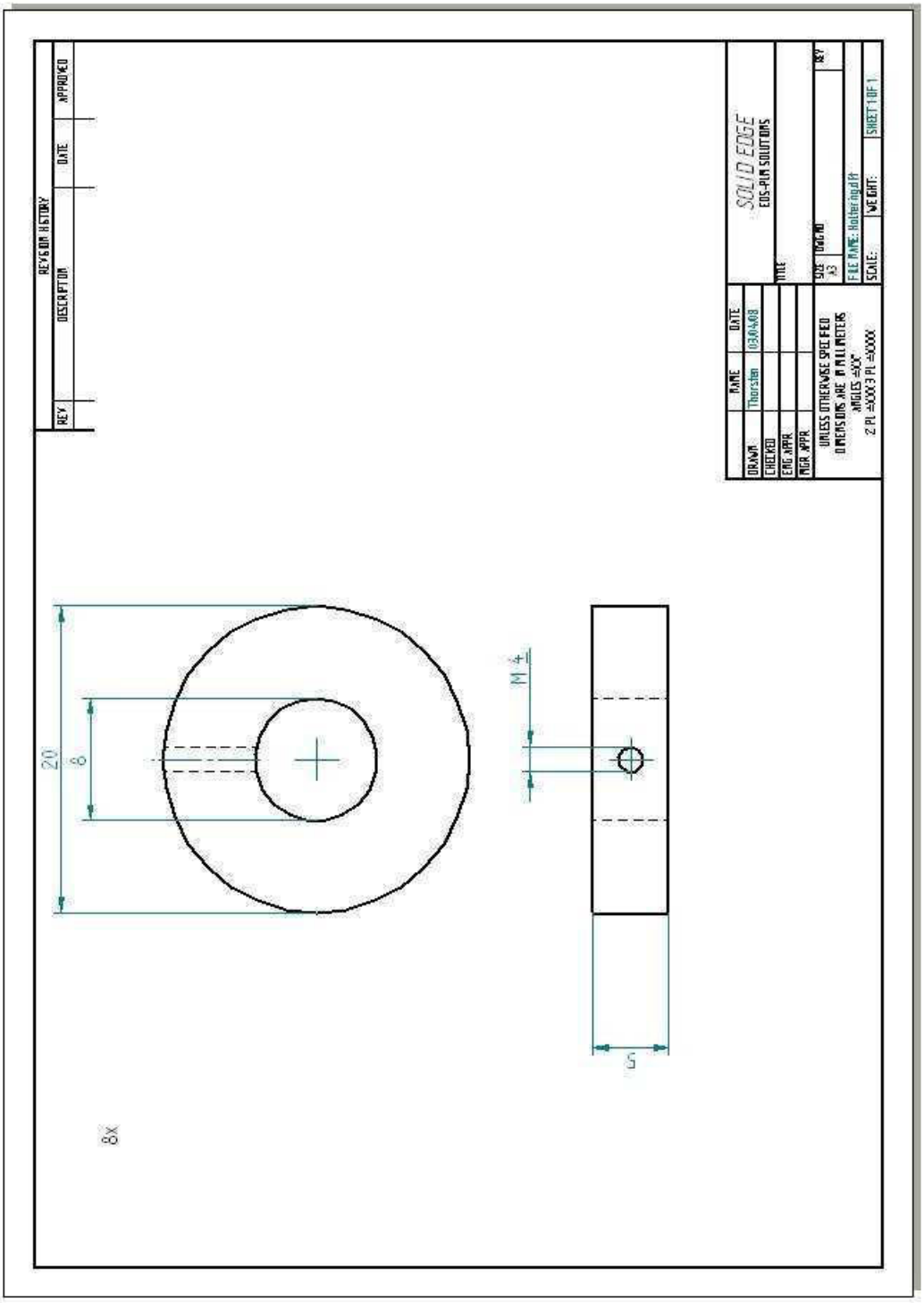
REVISION HISTORY
REV
DESCRIPTION
DATE
APPROVED
SOLID EDGE
EDS-PLM SOLUTIONS
NAME
DATE
DRAWN
Thorsten
03/04/08
CHECKED
ENG APPR.
MGR APPR.
UNLESS OTHERWISE SPECIFIED
DIMENSIONS ARE IN MILLIMETERS
ANGLES ±0.5°
2 PL ±0.03 3 PL ±0.005
TITLE
SIZE
A3
DWG NO
REV
FILE NAME: Halterung.dft
SCALE:
WEIGHT:
SHEET 1 OF 1
20
8
M 4
5
8x

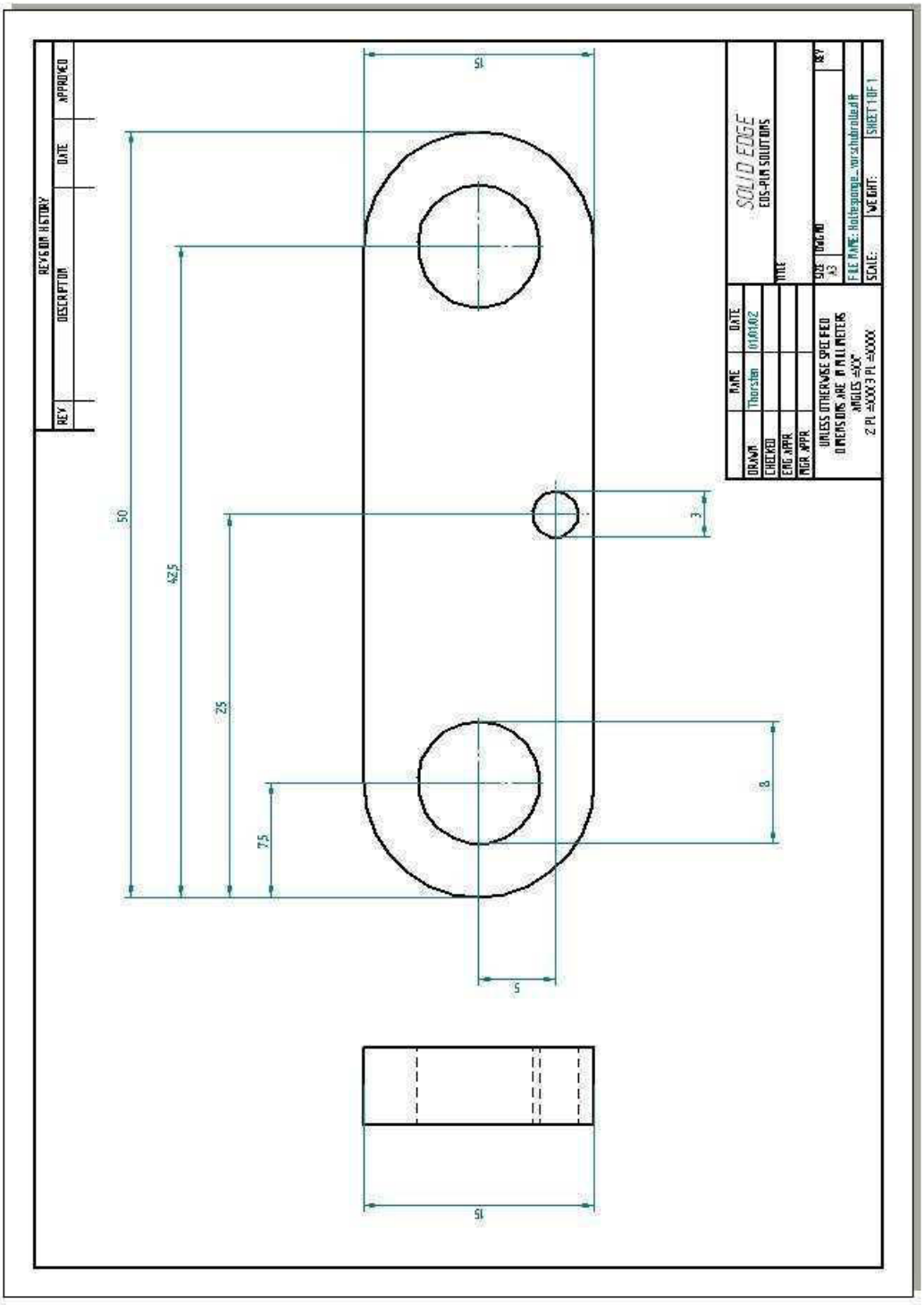
REVISION HISTORY
REV
DESCRIPTION
DATE
APPROVED
51
50
42,5
25
7,5
3
8
5
15
SOLID EDGE
EDS-PLM SOLUTIONS
DRAWN
Thorsten
01/01/02
CHECKED
ENG APPR.
MGR APPR.
UNLESS OTHERWISE SPECIFIED
DIMENSIONS ARE IN MILLIMETERS
ANGLES ±XX°
2 PL ±XXX 3 PL ±XXXX
SIZE
A3
DWG NO
REV
FILE NAME: Halterung_vorschubrolle.ai
SCALE:
WEIGHT:
SHEET 1 OF 1

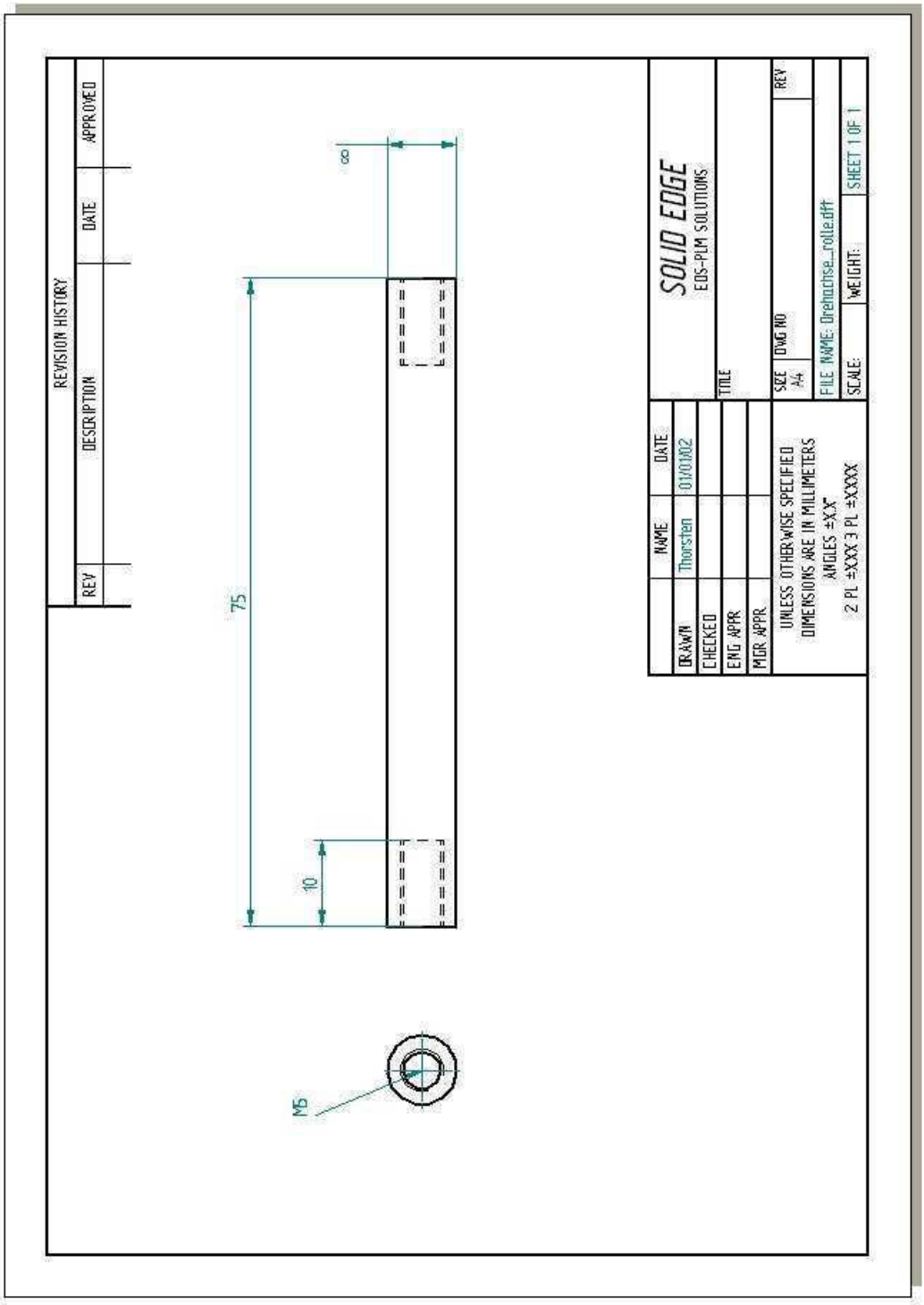
REVISION HISTORY
REV
DESCRIPTION
DATE
APPROVED
SOLID EDGE
EDS-PLM SOLUTIONS
NAME
DATE
DRAWN
Thorsten
01/01/02
CHECKED
ENG APPR.
MGR APPR.
TITLE
SIZE
A4
DWG NO
REV
FILE NAME: Drehachse_rolle.dft
UNLESS OTHERWISE SPECIFIED
DIMENSIONS ARE IN MILLIMETERS
ANGLES ±X.X°
2 PL ±XXX 3 PL ±XXXX
SCALE:
WEIGHT:
SHEET 1 OF 1
8
75
10
M5

Technical drawing of the components needed for stepper motor implementation

The technical drawings are presented in the following order:

- Connection plate for the stepper motor
- Connection between drive roll and tensioner
- Pillar for connection plate of the stepper motor

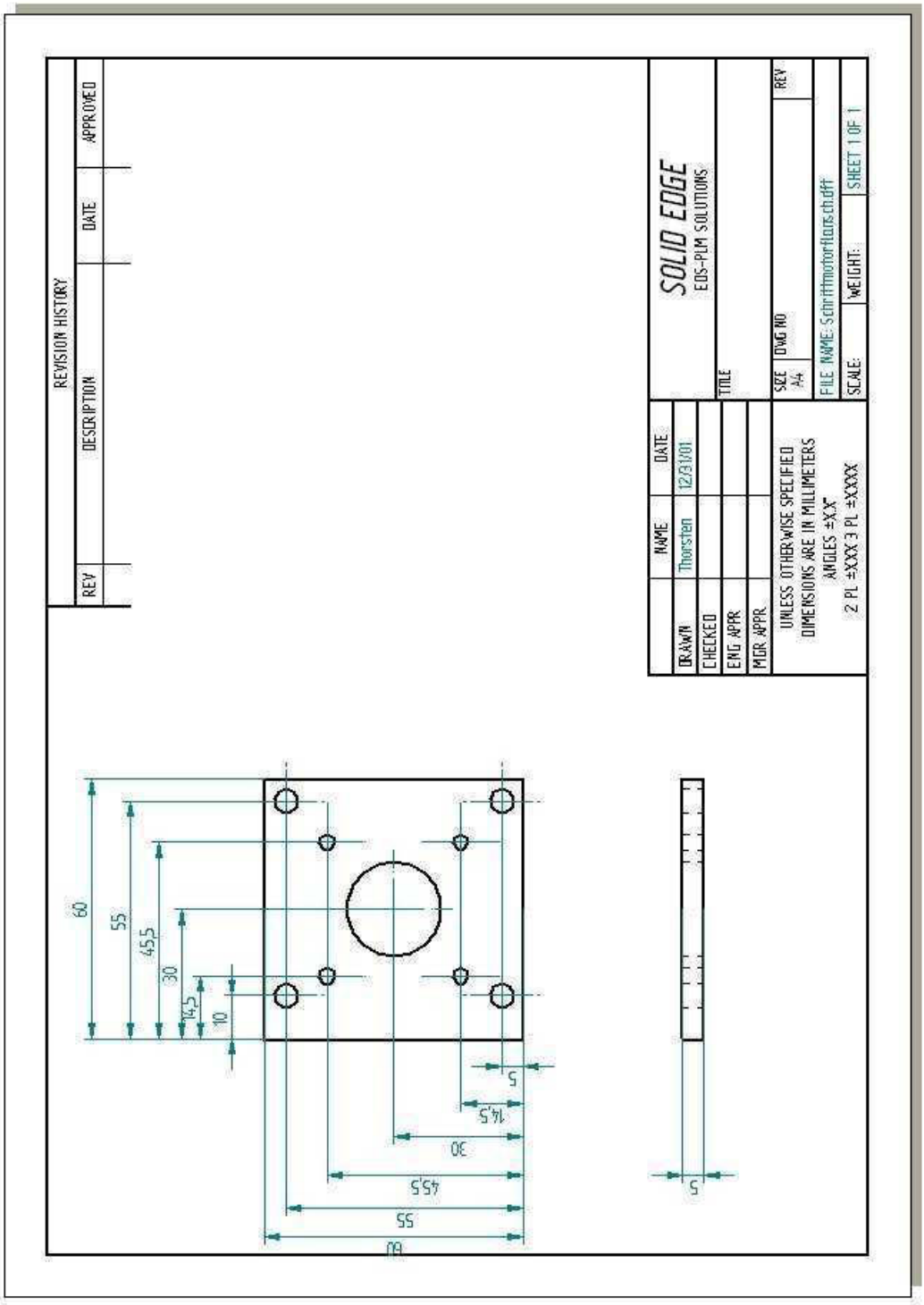
REVISION HISTORY
REV
DESCRIPTION
DATE
APPROVED
SOLID EDGE
EDS-PLM SOLUTIONS
NAME
DATE
DRAWN
Thorsten
12/31/01
CHECKED
ENG APPR.
MGR APPR.
TITLE
UNLESS OTHERWISE SPECIFIED
DIMENSIONS ARE IN MILLIMETERS
ANGLES ±X.X°
2 PL ±XXX 3 PL ±XXXX
SIZE
A4
DWG NO
REV
FILE NAME: Schriftmotorflansch.dft
SCALE:
WEIGHT:
SHEET 1 OF 1
60
55
45,5
30
14,5
10
5
14,5
30
45,5
55
60
5

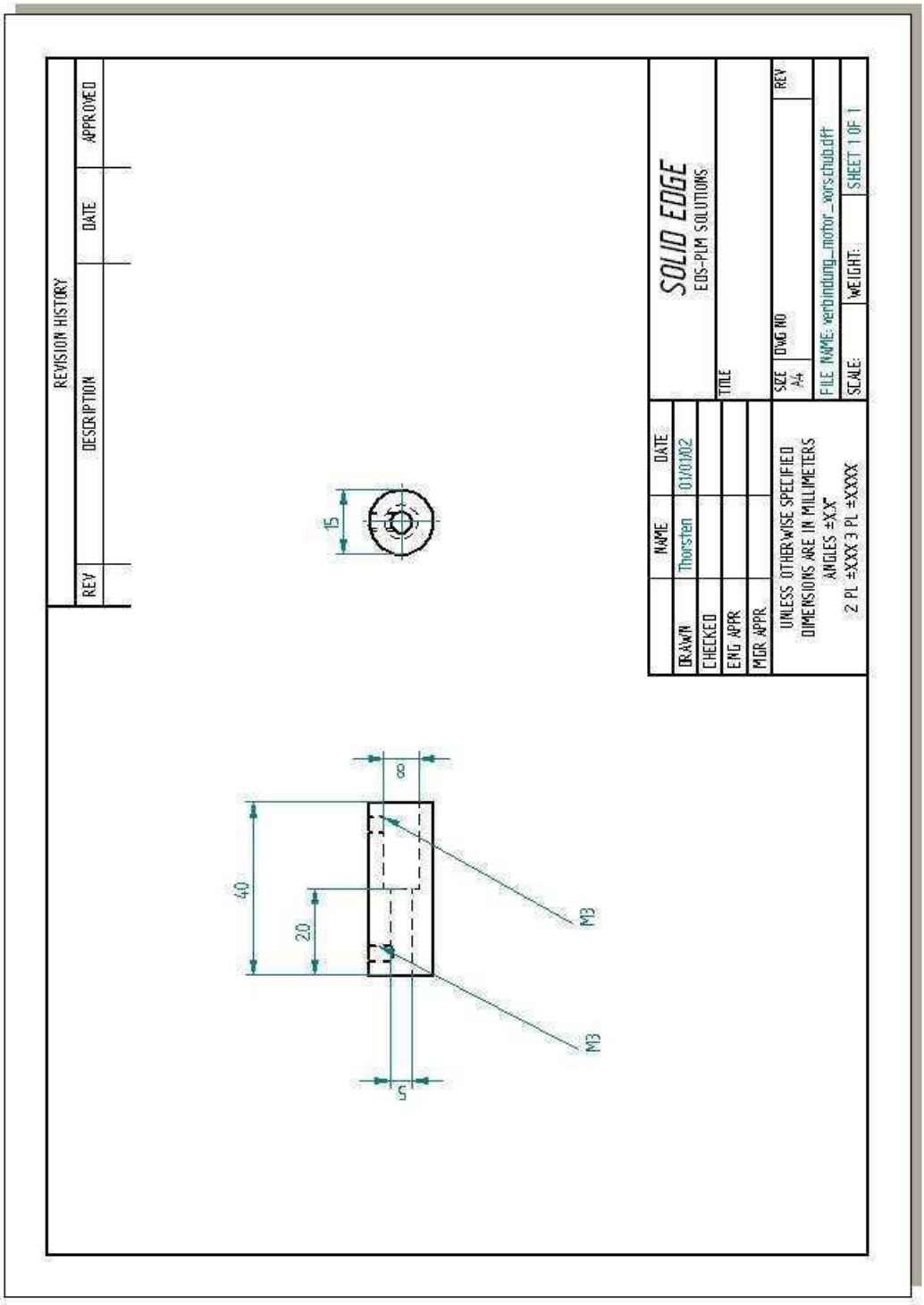
REVISION HISTORY
REV
DESCRIPTION
DATE
APPROVED
15
8
4.0
2.0
M3
M3
5
NAME
DATE
DRAWN
Thorsten
01/01/02
CHECKED
ENG APPR.
MGR APPR.
UNLESS OTHERWISE SPECIFIED
DIMENSIONS ARE IN MILLIMETERS
ANGLES ±X.X°
2 PL ±XXX 3 PL ±XXXX
SOLID EDGE
EDS-PLM SOLUTIONS
TITLE
SIZE
A4
DWG NO
REV
FILE NAME: verbindung_motor_vorschub.dft
SCALE:
WEIGHT:
SHEET 1 OF 1

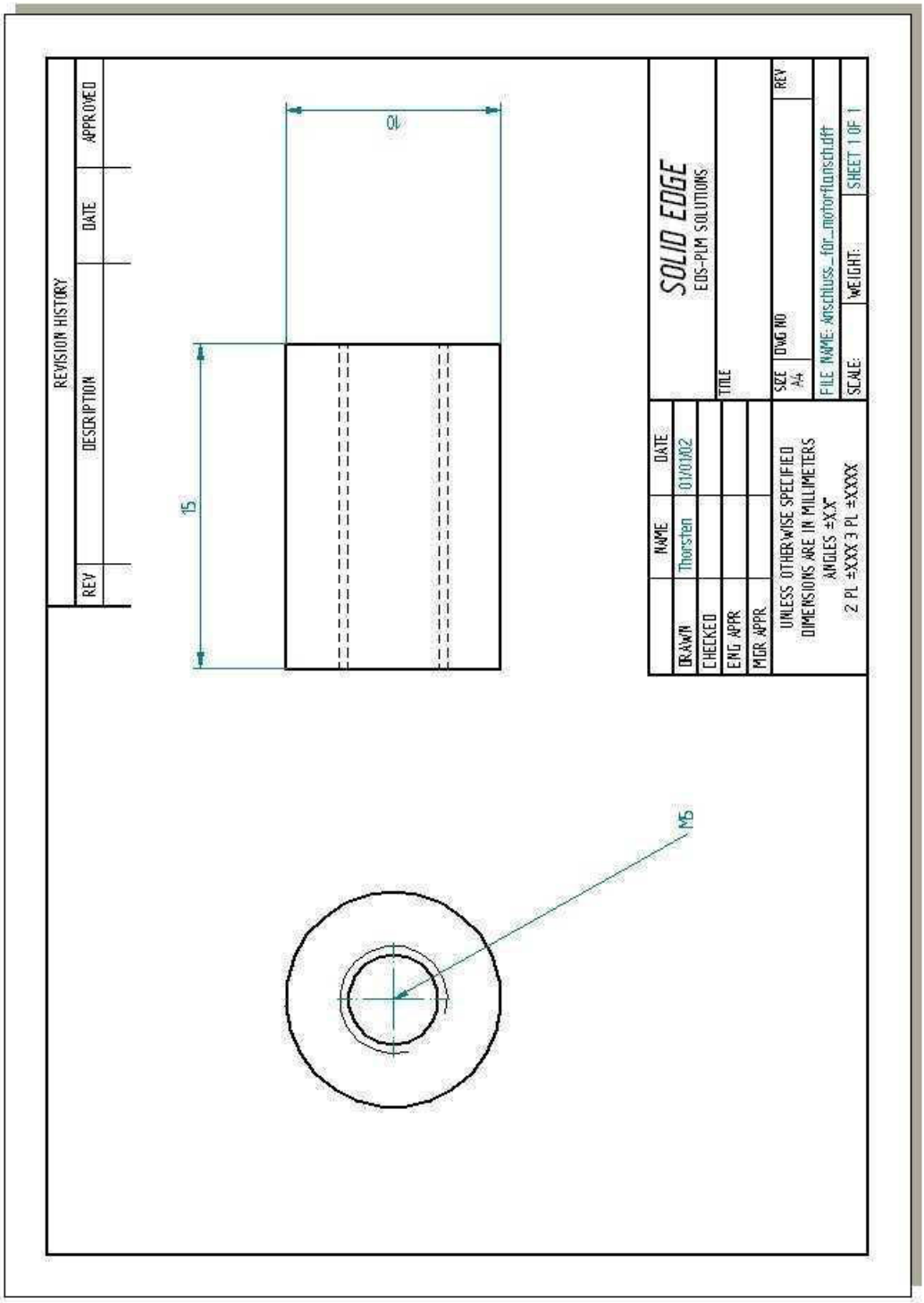
REVISION HISTORY
REV
DESCRIPTION
DATE
APPROVED
10
15
M5
SOLID EDGE
EDS-PLM SOLUTIONS
NAME
DATE
DRAWN
Thorsten
01/01/02
CHECKED
ENG APPR.
MGR APPR.
TITLE
UNLESS OTHERWISE SPECIFIED
DIMENSIONS ARE IN MILLIMETERS
ANGLES ±X.X°
2 PL ±XXX 3 PL ±XXXX
SIZE
A4
DWG NO
REV
FILE NAME: Anschluss_für_motorflansch.dft
SCALE:
WEIGHT:
SHEET 1 OF 1

Technical drawing of the drive roll

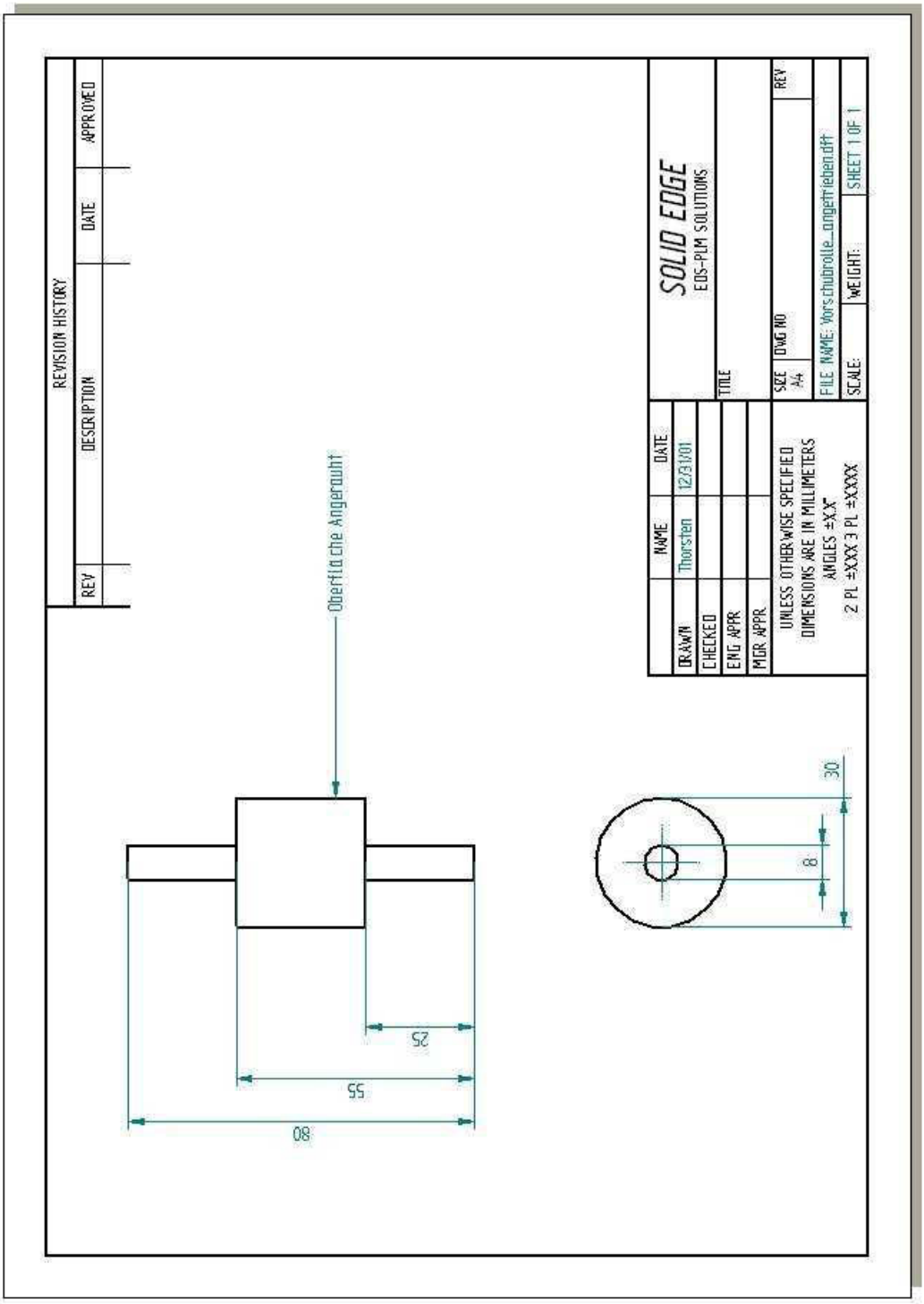
REVISION HISTORY
REV
DESCRIPTION
DATE
APPROVED
Oberfläche Angeraut
80
55
25
30
8
SOLID EDGE
EDS-PLM SOLUTIONS
NAME
DATE
DRAWN
Thorsten
12/31/01
CHECKED
ENG APPR.
MGR APPR.
TITLE
UNLESS OTHERWISE SPECIFIED
DIMENSIONS ARE IN MILLIMETERS
ANGLES ±X.X°
2 PL ±XXX 3 PL ±XXXX
SIZE
A4
DWG NO
REV
FILE NAME: Vorschubrolle_angetrieben.dft
SCALE:
WEIGHT:
SHEET 1 OF 1

Technical drawing of the holder for the wire guidance

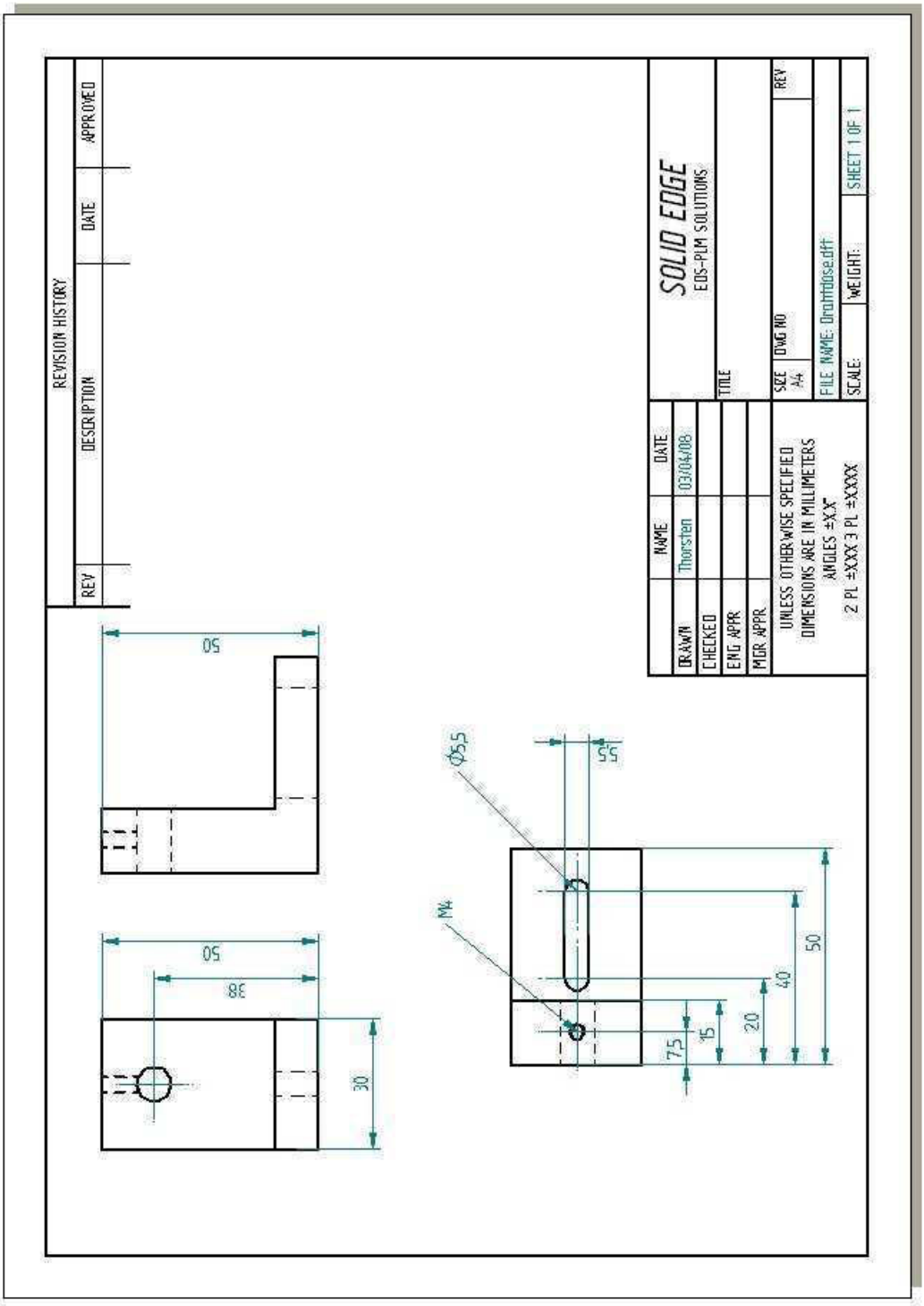
REVISION HISTORY
REV
DESCRIPTION
DATE
APPROVED
SOLID EDGE
EDS-PLM SOLUTIONS
NAME
DATE
DRAWN
Thorsten
03/04/08
CHECKED
ENG APPR.
MGR APPR.
TITLE
SIZE
A4
DWG NO
REV
FILE NAME: Drahtdose.dft
UNLESS OTHERWISE SPECIFIED
DIMENSIONS ARE IN MILLIMETERS
ANGLES ±X.X°
2 PL ±XXX 3 PL ±XXXX
SCALE:
WEIGHT:
SHEET 1 OF 1
50
38
30
Ø5.5
5.5
M4
75
15
20
40
50

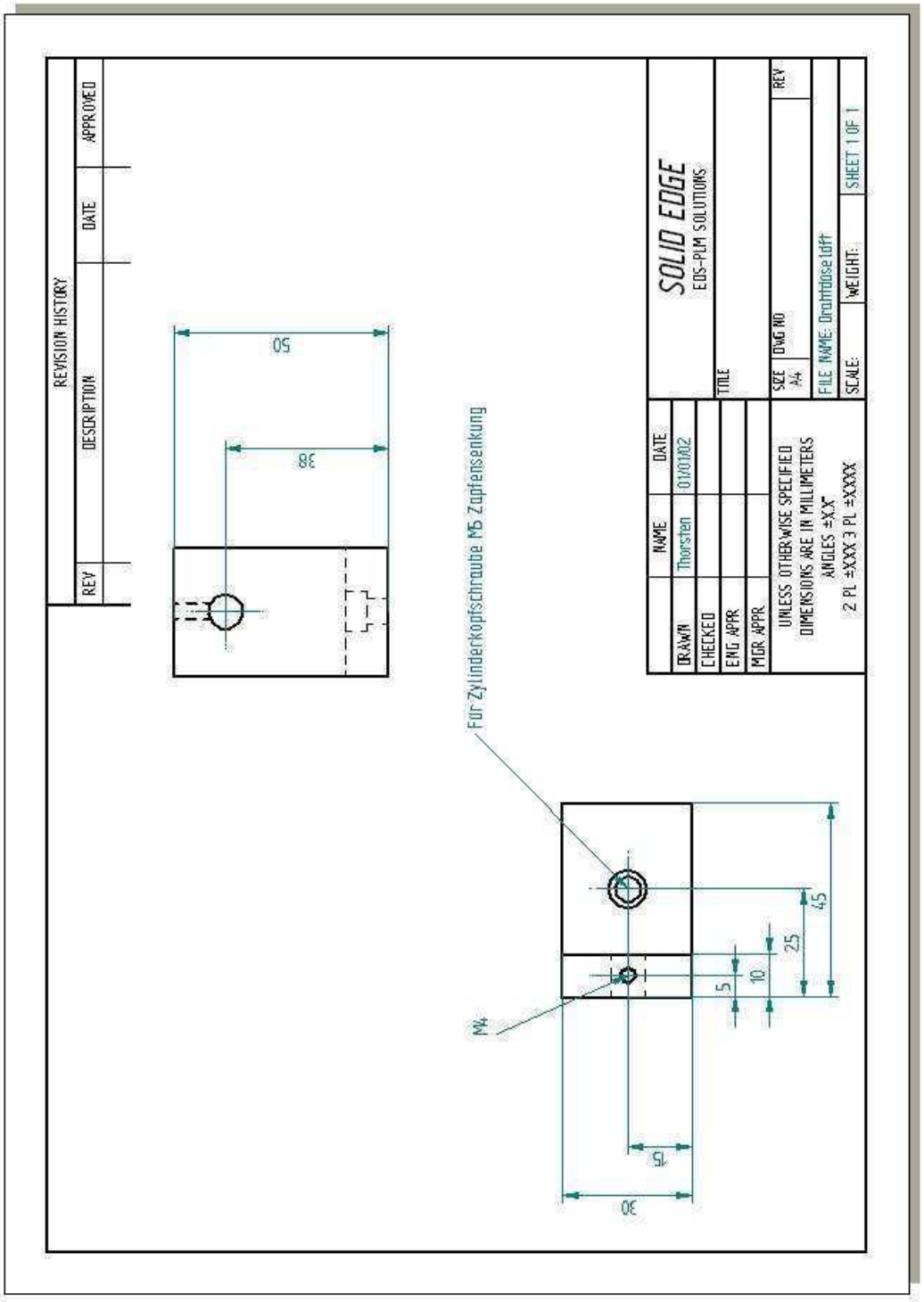
REVISION HISTORY
REV
DESCRIPTION
DATE
APPROVED
50
38
4
Für Zylinderkopfschraube M5 Zapfensenkung
M4
5
10
25
45
15
30
SOLID EDGE
EOS-PLM SOLUTIONS
NAME
DATE
DRAWN
Thorsten
01/01/02
CHECKED
ENG APPR.
MGR APPR.
TITLE
UNLESS OTHERWISE SPECIFIED
DIMENSIONS ARE IN MILLIMETERS
ANGLES ±X.X°
2 PL ±XXX 3 PL ±XXXX
SIZE
A4
DWG NO
REV
FILE NAME: Drahtdose1.dft
SCALE:
WEIGHT:
SHEET 1 OF 1

Technical drawing of the pillar for the wire feeder

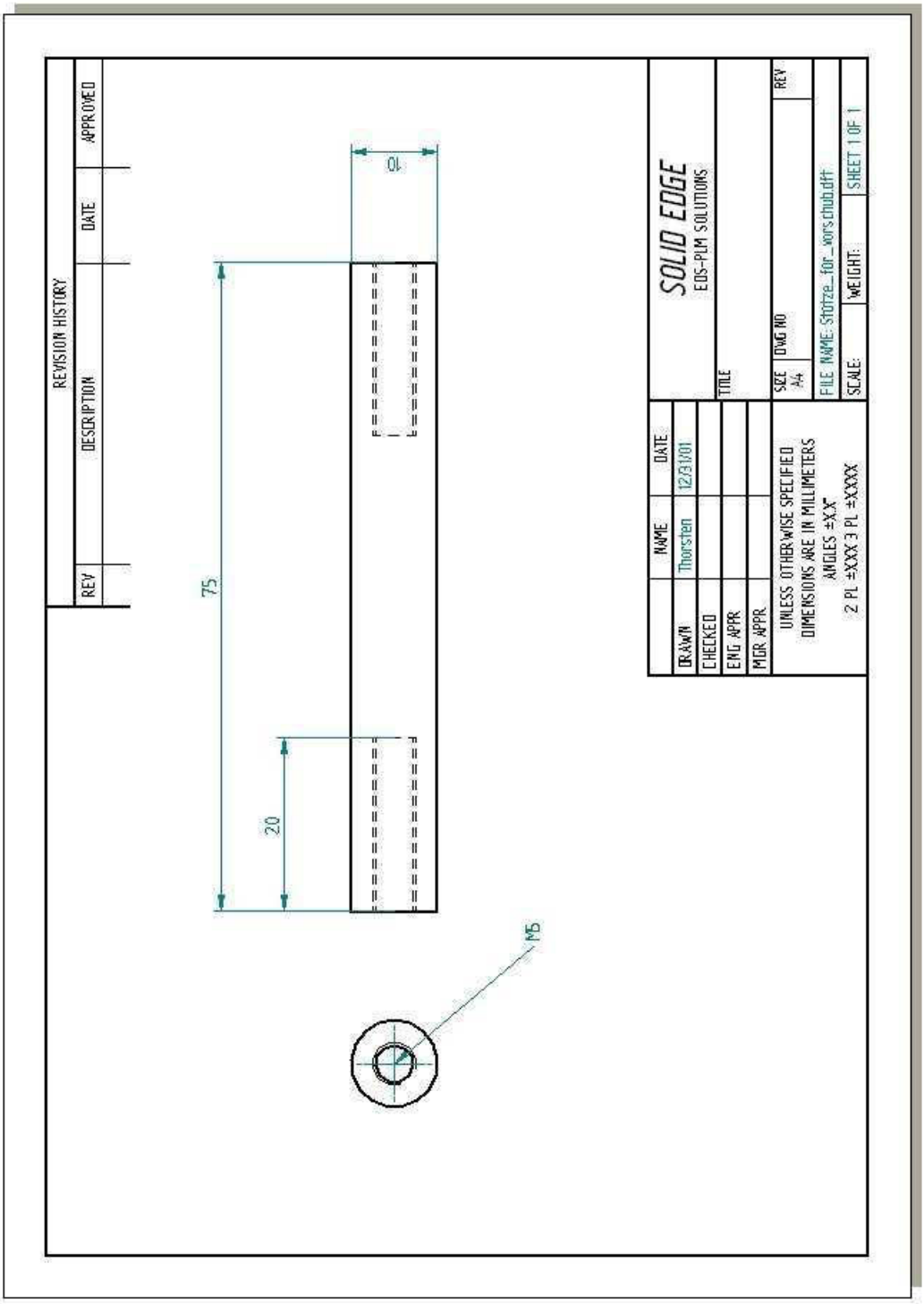
REVISION HISTORY
REV
DESCRIPTION
DATE
APPROVED
10
75
20
M5
SOLID EDGE
EDS-PLM SOLUTIONS
NAME
DATE
DRAWN
Thorsten
12/31/01
CHECKED
ENG APPR.
MGR APPR.
TITLE
UNLESS OTHERWISE SPECIFIED
DIMENSIONS ARE IN MILLIMETERS
ANGLES ±X.X°
2 PL ±XXX 3 PL ±XXXX
SIZE
A4
DWG NO
REV
FILE NAME: Stütze_für_vorschub.dft
SCALE:
WEIGHT:
SHEET 1 OF 1

E.2. Technical drawings of the optimised temperature measurement setup

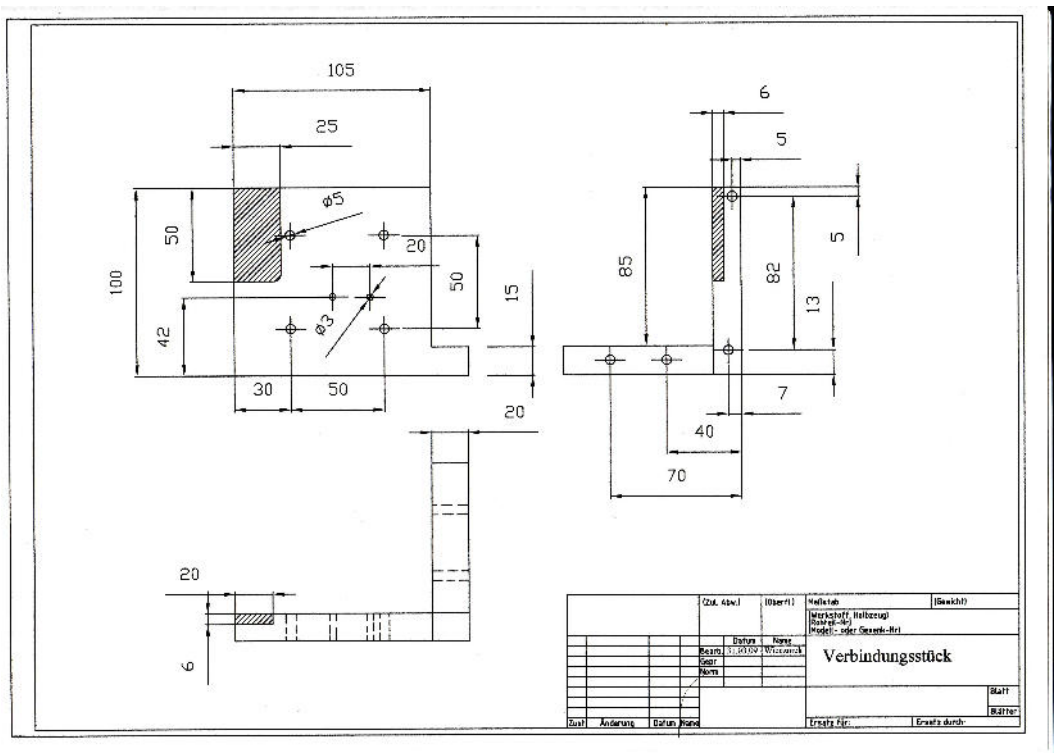

Figure E.1.: Technical drawing of the connection plate

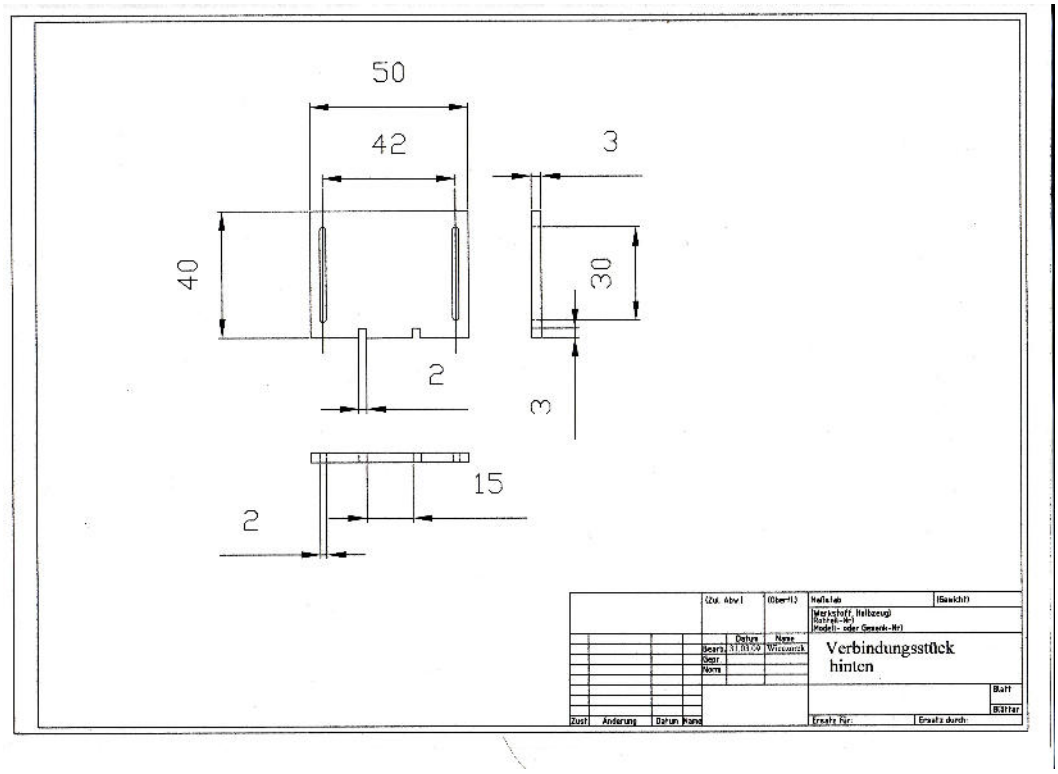

Figure E.2.: Technical drawing of the connection plate for behind the laser head

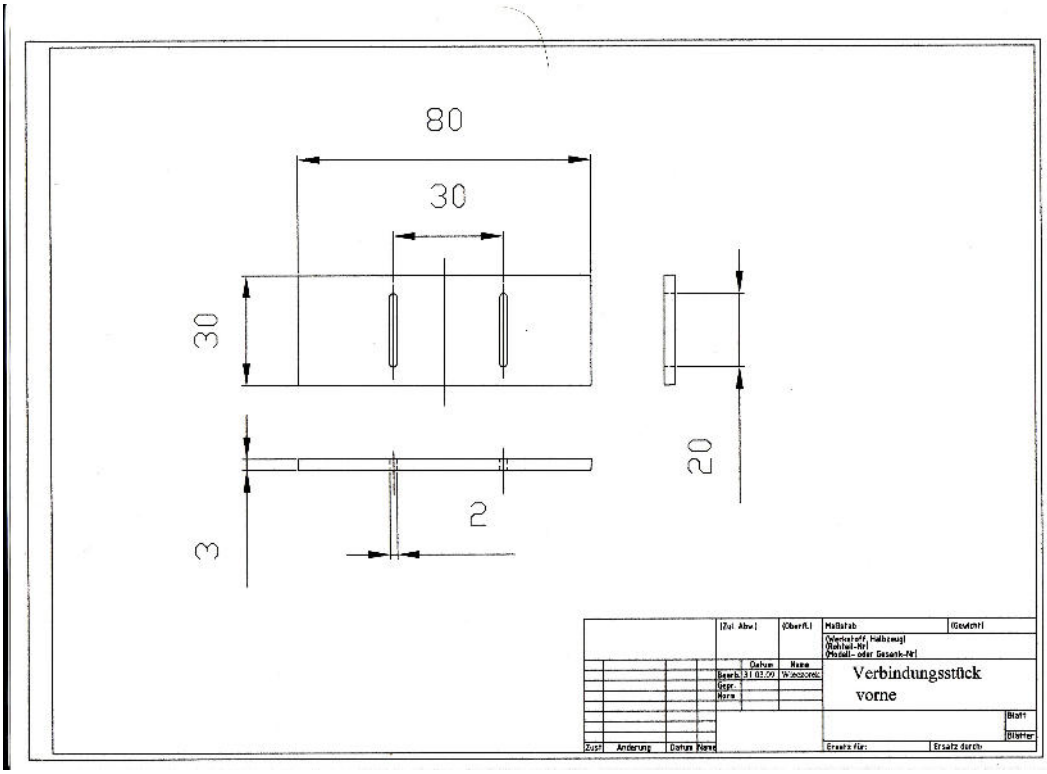

Figure E.3.: Technical drawing of the connection plate for in front of the laser head

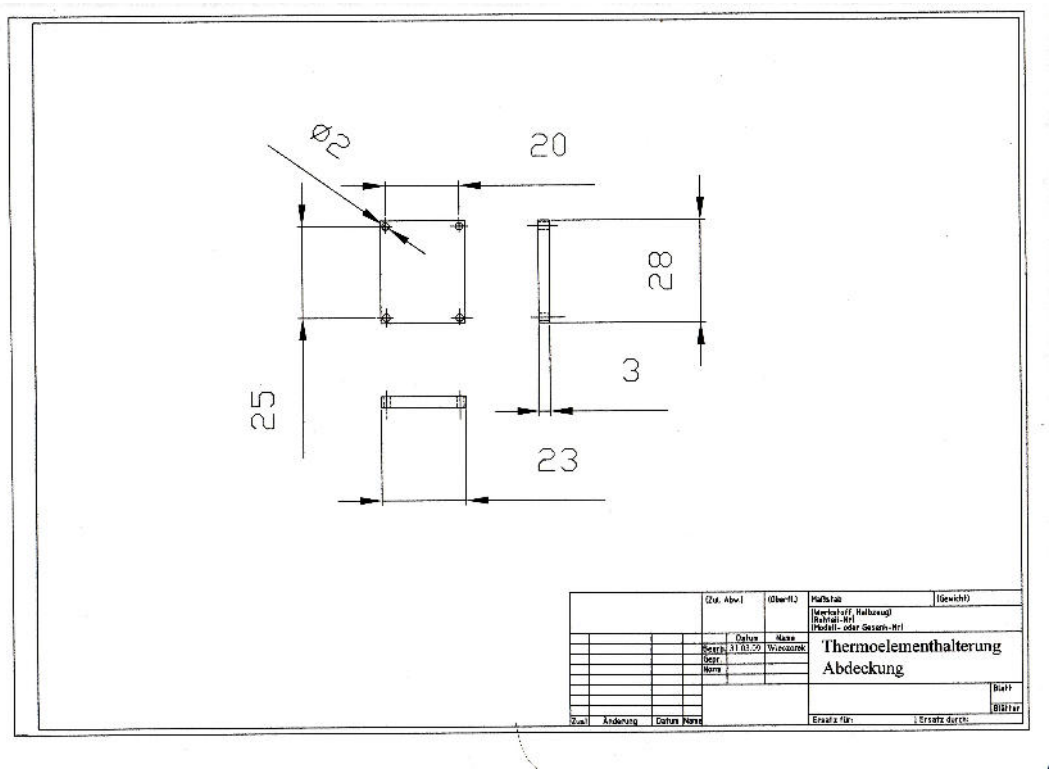

Figure E.4.: Technical drawing of the thermocouple housing

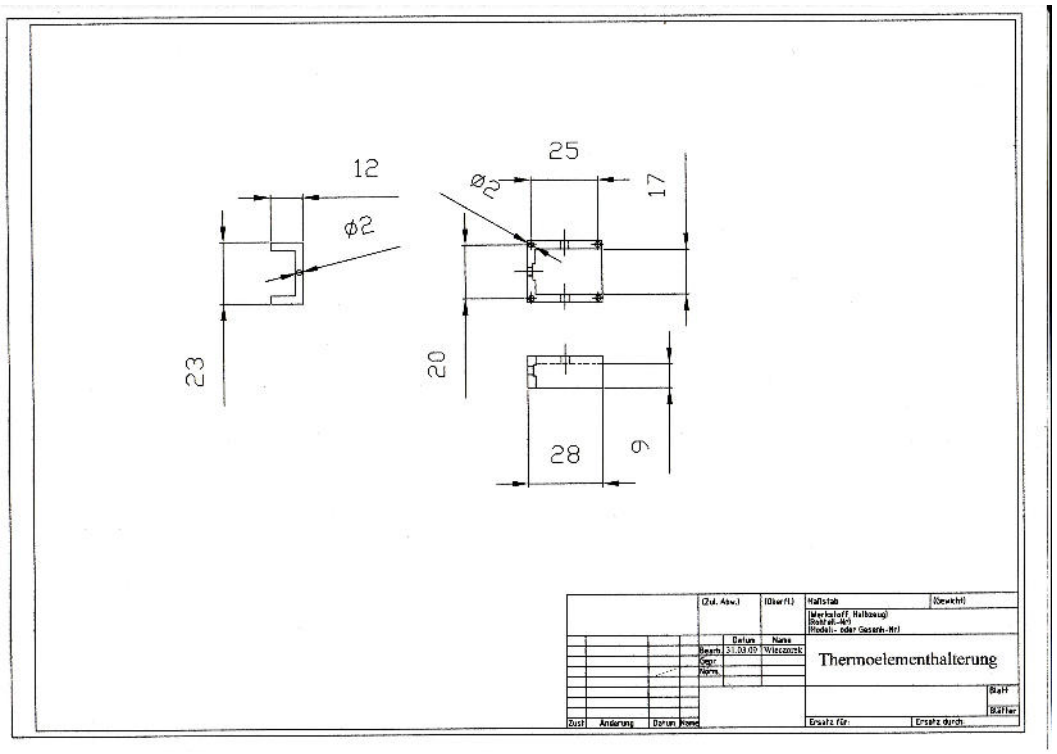

Figure E.5.: Technical drawing of the thermocouple housing

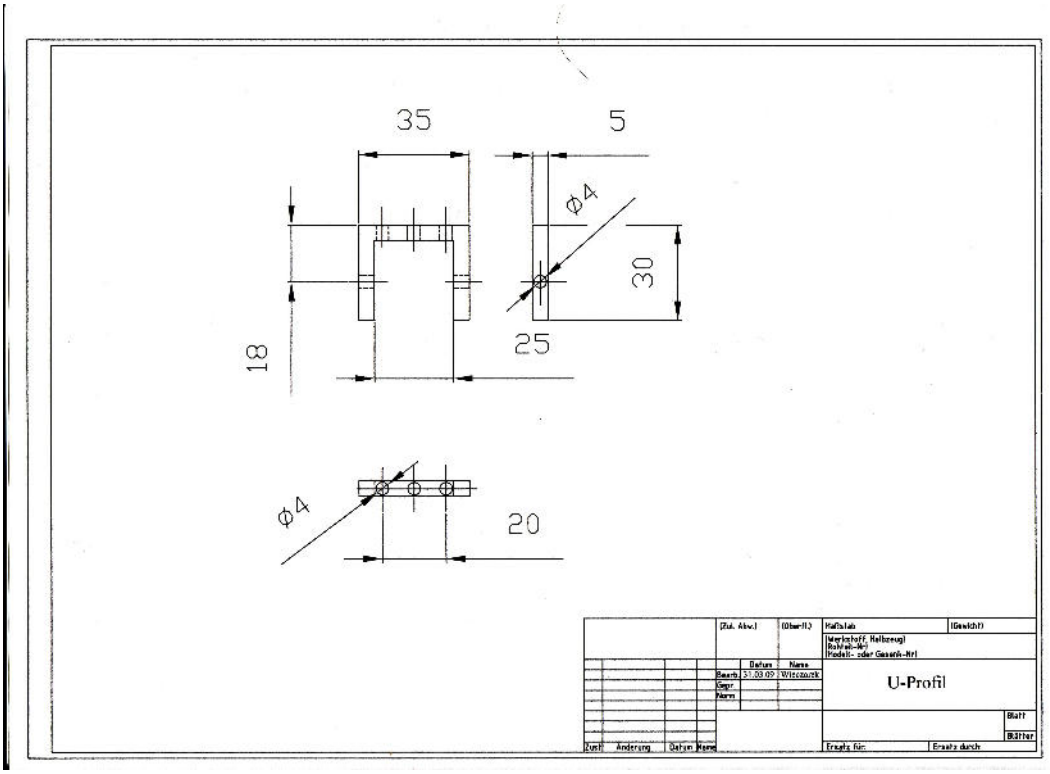

Figure E.6.: Technical drawing of the U - profile

E.3. Technical drawings of the fixture for the laser - triangulation sensor

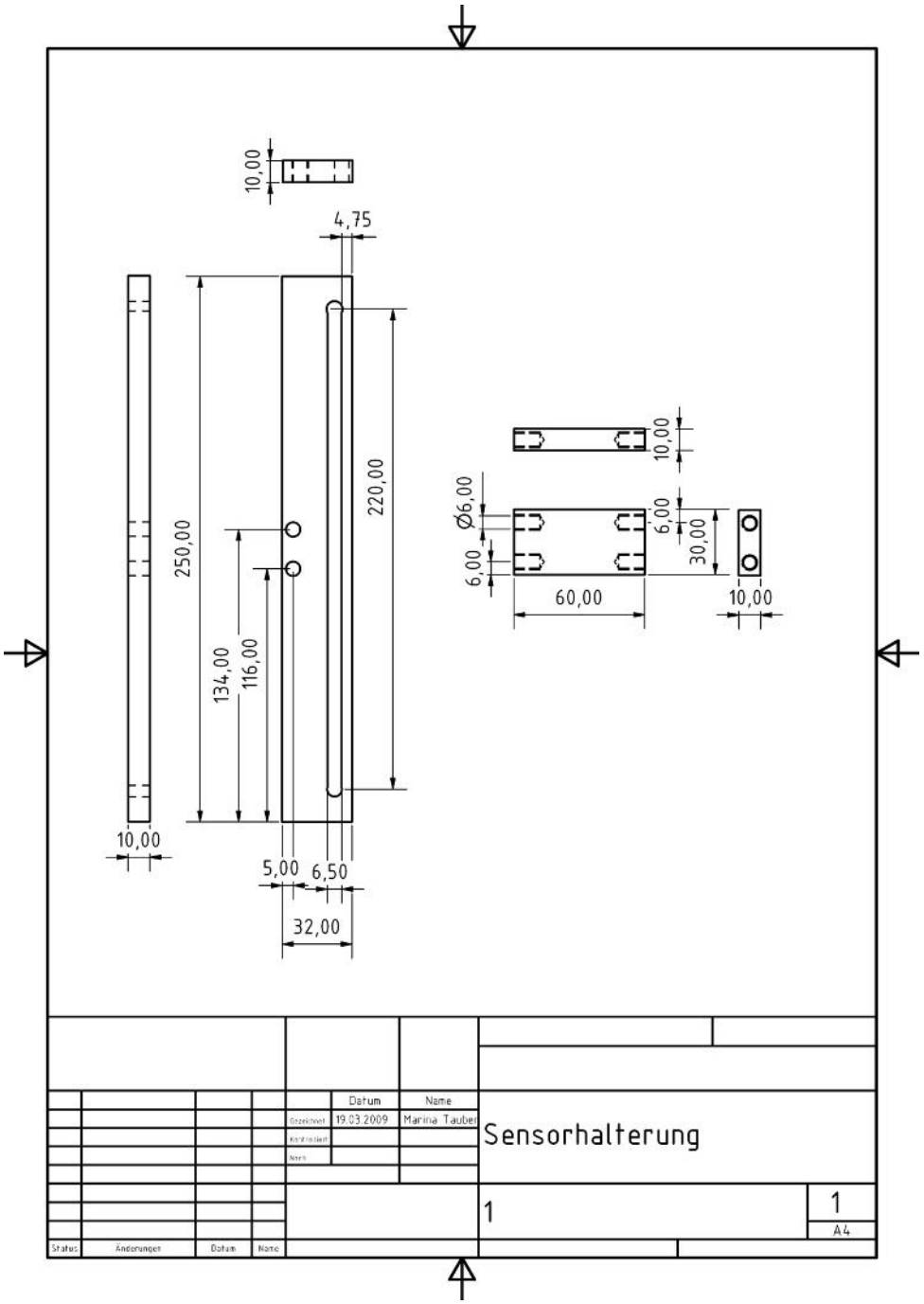
10,00
4,75
250,00
220,00
134,00
116,00
10,00
5,00
6,50
32,00
10,00
Ø6,00
6,00
6,00
30,00
60,00
10,00
Datum
Name
19.03.2009
Marina Tauber
Sensorhalterung
1
1
A4

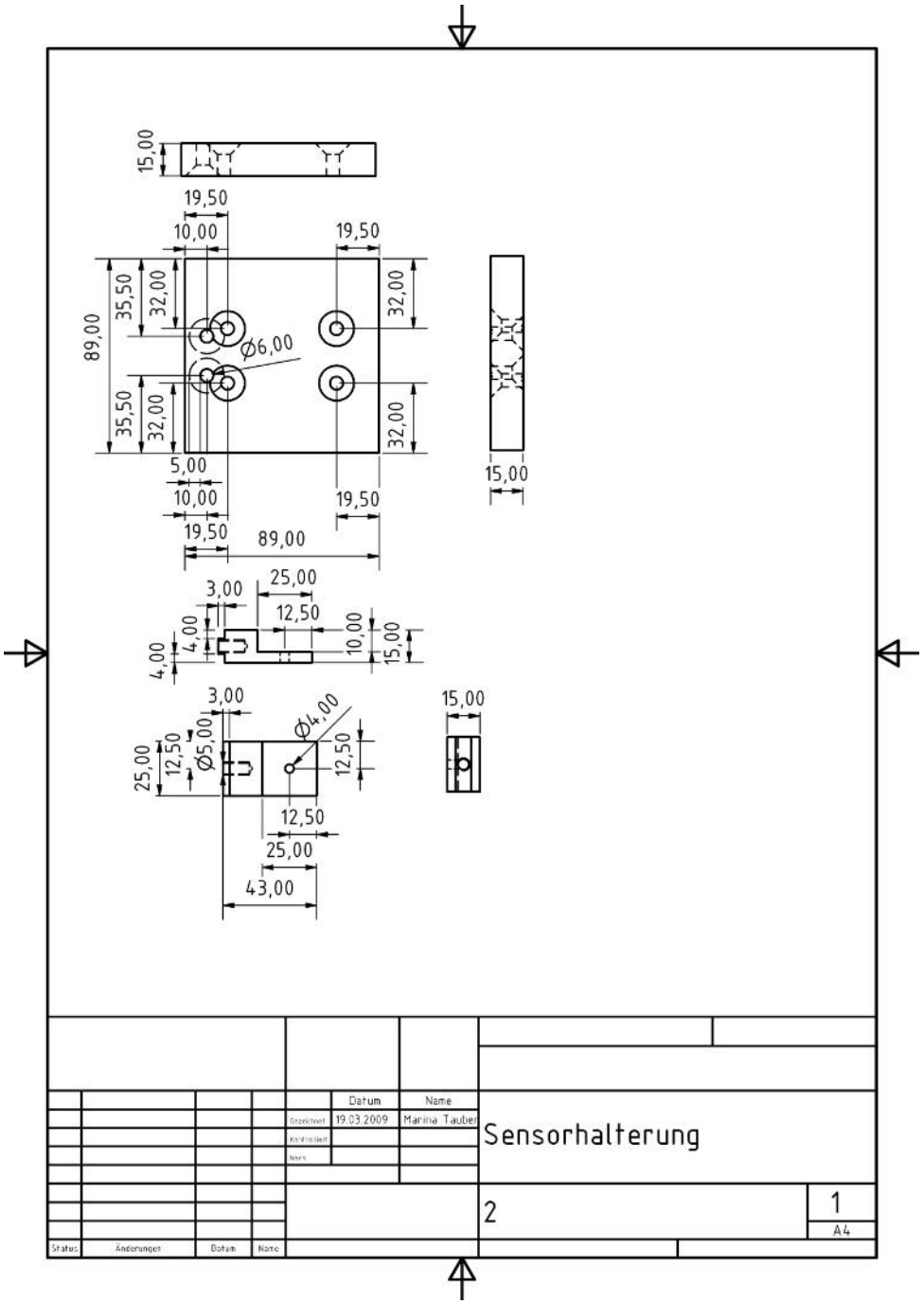
15,00
19,50
10,00
19,50
35,50
32,00
32,00
89,00
Ø6,00
35,50
32,00
32,00
5,00
15,00
10,00
19,50
19,50
89,00
25,00
3,00
12,50
4,00
10,00
15,00
4,00
3,00
15,00
Ø4,00
Ø5,00
25,00
12,50
12,50
12,50
25,00
43,00
Datum
Name
19.03.2009
Marina Tauber
Sensorhalterung
2
1
A4
Status
Änderungen
Datum
Name